2013

# Biological Control of Manganese in Water Supplies in the Presence of Humic Acids

Michael S. Snyder
*University of Kentucky,* runnermss@yahoo.com

## Recommended Citation

**STUDENT AGREEMENT:**

I represent that my thesis or dissertation and abstract are my original work. Proper attribution has been given to all outside sources. I understand that I am solely responsible for obtaining any needed copyright permissions. I have obtained and attached hereto needed written permission statements(s) from the owner(s) of each third-party copyrighted matter to be included in my work, allowing electronic distribution (if such use is not permitted by the fair use doctrine).

I hereby grant to The University of Kentucky and its agents the non-exclusive license to archive and make accessible my work in whole or in part in all forms of media, now or hereafter known. I agree that the document mentioned above may be made available immediately for worldwide access unless a preapproved embargo applies.

I retain all other ownership rights to the copyright of my work. I also retain the right to use in future works (such as articles or books) all or part of my work. I understand that I am free to register the copyright to my work.

**REVIEW, APPROVAL AND ACCEPTANCE**

The document mentioned above has been reviewed and accepted by the student's advisor, on behalf of the advisory committee, and by the Director of Graduate Studies (DGS), on behalf of the program; we verify that this is the final, approved version of the student's dissertation including all changes required by the advisory committee. The undersigned agree to abide by the statements above.

Michael S. Snyder, Student

Dr. Y. T. (Ed) Wang, Major Professor

Dr. Kamyar C. Mahboub, Director of Graduate Studies

BIOLOGICAL CONTROL OF MANGANESE IN WATER SUPPLIES
IN THE PRESENCE OF HUMIC ACIDS

_____

DISSERTATION

_____

A dissertation submitted in partial fulfillment of the
requirements for the degree of Doctor of Philosophy in the
College of Engineering
at the University of Kentucky

By
Michael Snyder

Lexington, Kentucky

Director: Dr. Y.T. (Ed) Wang, Professor of Civil Engineering

Lexington, Kentucky

2013

ABSTRACT OF DISSERTATION

BIOLOGICAL CONTROL OF MANGANESE IN WATER SUPPLIES
IN THE PRESENCE OF HUMIC ACIDS

The main objective of this study was to improve our understanding of biological filtration (biofilm type) treatment for manganese (Mn) removal in drinking water. Biological filtration treatment involves biofilms of Mn(II)-oxidizing microorganisms attached to solid filter material that remove and immobilize dissolved Mn(II) in raw water by conversion to black $MnO_{2(s)}$ precipitates. Mn-biological filtration is an emerging green technology that can serve as an alternative to conventional physicochemical treatments, but its full potential is hindered by various factors. These include lack of understanding the (1) optimal removal conditions for Mn, (2) mechanisms for biofilter Mn releases, and (3) effects of recalcitrant natural organic matter (NOM) on biofiltration. Confounding these issues is the unknown identity of the diverse microbial communities which occupy the biofilms attached to the filter media.

To investigate these issues, biological Mn removal was studied in laboratory bench scale reactors using a new Mn(II)-oxidizing bacterium isolate, *Pseudomonas Putida* EC112. The main research hypothesis formulated that the transition metal catalyst, $MnO_{2(s)}$, can increase the bioavailable carbon and energy from recalcitrant NOM (e.g., humic acids (HA)) in biological filters. Mn and HA can be found in most natural waters, including groundwaters, lakes and streams. To test the hypothesis, the potential for strain EC112 growth and Mn(II) oxidation utilizing the organic substrate products from the oxidation reaction between HA and $MnO_{2(s)}$ was assessed.

Biological Mn(II)-oxidation kinetics were investigated in batch (suspended cell) and continuous flow (biofilm) bioreactors at optimal pH and temperature conditions for strain EC112. Batch kinetics was successfully characterized with the Monod model. Continuous flow steady-state kinetics was modeled with a single, first-order kinetic parameter.

Enhanced Mn(II) removal capacity was observed for strain EC112 in batch and continuous flow reactors in the presence of HA and $MnO_{2(s)}$. The effect of $MnO_{2(s)}$ on HA biodegradability was studied and optimal conditions for biodegradation were identified.

Biofilter Mn(II) releases were observed during the continuous flow bioreactor experiments. Release conditions were identified and releases modeled using pseudo first-order kinetics.

Changes in HA structure induced by $MnO_{2(s)}$ oxidation were studied with Fourier transform infrared (FT-IR) and proton nuclear magnetic spectroscopy ($^1$H-NMR).

KETWORDS: Biological filtration, drinking water, humic acids, manganese, *Pseudomonas Putida*.

Michael Snyder
Student's Signature

April 4, 2013
Date

BIOLOGICAL CONTROL OF MANGANESE IN WATER SUPPLIES
IN THE PRESENCE OF HUMIC ACIDS

By

Michael Snyder

Dr.Y.T. (Ed) Wang
Director of Dissertation

Dr.Kamyar C. Mahboub
Director of Graduate Studies

 April 4, 2013
Date

*Dedicated to the poor
and underprivileged*

I can't believe the end has finally come, after 7 years of constant, uninterrupted labor. No, what a minute, this is just the beginning.

Table of Contents

List of Tables

# List of Figures

# Chapter 1: Introduction

## 1.1 Background

Manganese (Mn) is the third most abundant (9.5 x10$^2$ ppm or 0.1 %) redox-active transition metal in the earth's crust and a common contaminant in drinking water supplies (Cox, 1995; Kohl and Medlar, 2006; Kohl and Dixon, 2012). Mn is not regulated in drinking water due to potential health concerns, but for consumer complaints related to water fouling at concentrations above 0.05 mg·L$^{-1}$, the US Environmental Protection Agency's (USEPA) Secondary Maximum Contaminant Level (SMCL) (Kohl and Medlar, 2006). Mn can impair water quality with metallic taste as dissolved Mn(II) and can induce black discoloration and staining as oxidized Mn(IV) precipitates (Mn oxides). Mn concentrations above USEPA's SMCL are more common in anoxic water supplies, including groundwater, and below the thermocline in stratified lakes and reservoirs, where its kinetic stability is attributed to the pH and oxidation/reduction (E$_h$) conditions of these environments (Hem, 1985; Ehrlich and Newman, 2008; Gantzer et al., 2009). Dissolution of Mn-mineral assemblages in host sediments, soils, and rocks in contact with aquatic environments represent the primary pathways for Mn entry (Hem, 1985). Anthropogenic sources may account for some Mn in water supplies and include industrial and commercial releases, pesticides, and impurities in drinking water treatment chemicals (Kohl and Medlar, 2006; Gabelich et al., 2006).

Drinking water utilities commonly use either chemical oxidation followed by solid filtration or rely on Mn(II) adsorption to Mn-oxide coated filter material (induced oxide-coated media effect (IOCME)) for Mn removal (Kohl and Medlar, 2006). Both processes require the addition of a strong oxidizer such as chlorine. Water industry's concerns for chemical costs and the associated environmental impact are adding to the incentive to develop and implement green engineering treatment technologies (Ghernaout et al., 2011). Foremost are biological filtration or biofiltration water treatment, which is increasingly being considered to supplement or replace existing physicochemical water treatment processes, due in part to promulgation of stricter drinking water regulation on the use of chemical oxidants, such as USEPA's Stage I and II Disinfectants and Disinfection Byproduct Rules (USEPA, 1998; Kohl and Dixon, 2012).

Biological filtration has been successfully applied for a number of years, first by European, and more recently, North American water utilities, to provide finished drinking water quality Mn levels below the SMCL (Beger, 1937; Czekalla et al., 1985; Korth et al., 2002; Kohl and Dixon, 2012). The biological process consists of filtering aerated, untreated water over thin biofilms hosting Mn(II)-oxidizing microbes that are surface-attached to packed beds of granular filter material. Anthracite, gravel, sand or granular activated carbon (GAC) are common filter material and the beds can be constructed as gravity filters or, for smaller installations, pressurized filters. Biofiltration occurs as Mn(II) in the bulk water diffuses into

the biofilms and is converted to Mn oxides (e.g., $MnO_2$) by the mechanism of direct microbial enzymatic oxidation. The black-brown, solid Mn oxides accumulate on the biofilm surfaces and the biofilters are periodically backwashed to maintain biofilter performance. At pH conditions typical of water supplies, the bacteriogenic, dark colored oxides have a net negative surface charge and are considered to autocatalytically participate in Mn(II) cation removal through electrostatic adsorption processes.

Communities of diverse bacteria species having heterotrophic metabolism are considered to be the dominant microbes responsible for Mn(II) oxidation in biological filters. Heterotrophic bacteria, unlike plants and algae, generally are unable to utilize inorganic compounds for carbon or energy and require sources of biodegradable organic carbon (BDOC). A minimum threshold concentration, $S_{min}$, of BDOC flux from the bulk water to the biofilm is considered necessary for biofilm growth and maintenance requirements to sustain biofilter performance (Rittmann and McCarty, 2001).

The largest fractions of natural organic matter (NOM) in freshwater environments are humic substances (HS), which are heterogeneous macromolecules having an aromatic core structure (Moran and Hodson, 1990; Basu and Huck, 2004). HS - which can be separated into humic and fulvic acids - represent the chemical and biochemical decay products of plant and microbial material. HS are chemically reactive though oxygen containing functional groups attached to the aromatic core, but are largely biodegradation resistant due to their structural heterogeneity and are not considered a viable carbon and energy source for heterotrophic bacteria. Drinking water sources often represent oligotrophic environments that contain low concentrations of BDOC electron donor substrates such as amino acids and carbohydrates, challenging the sustainability of biological filtration in terms of $S_{min}$. It has been previously demonstrated that the solid oxidizing agent Mn-oxide can degrade refractory humic material to more polar, oxygenated, lower molecular weight products that may possibly serve as bacteria carbon substrate (Sunda and Kieber, 1994, Tebo et al., 1995).

Biofiltration offers several advantages over conventional physicochemical treatment methods, which include lower operating costs, reduced chlorine demand, reduction of disinfection by-products (DBPs) and DBP precursors, higher filtration rates and potential role as a pre-filter to reduce water biological instability in the water distribution system (Mouchet, 1992; Kohl and Dixon, 2012). Physicochemical methods, which remove manganese by chemical oxidation of soluble Mn(II) to insoluble Mn(IV), can fail to provide consistent effluent quality which meets the SMCL for manganese in the presence of NOM due to organic ligand complexation and chemical oxidant consumption. High oxidant doses or pre-oxidation with chemicals such as chlorine, ozone or permanganate are needed to remove humic substances for effective manganese control by conventional processes (Gregory and Carlson, 2000). These oxidants can react with NOM in the raw water to produce carcinogenic compounds such as DBPs, or other smaller molecular weight organics that can lead to heterotrophic and opportunistic bacteria regrowth problems downstream of the treatment processes (Chowdhury, 2012). In addition, biofiltration is actively being

investigated as a potential treatment technology for emerging drinking water contaminants, including pesticides, endocrine disrupters, personal care products, and pharmaceuticals (Zearley and Summers, 2012).

## 1.2 Problem Statement

Biofiltration has demonstrated great potential for water treatment, but to achieve its full potential for Mn removal requires improving our understanding of the fundamental processes involved and optimal conditions for sustainability (Kohl and Dixon, 2012). Sustainability requires the availability of growth substrate in the source waters and flux into the biofilms (fixed films). The fate of NOM fractions that are considered recalcitrant to biodegradation, specifically HS which comprise up to 50% of NOM in natural aquatic environments, as a potential growth substrate for Mn(II)-oxidizing bacteria has not been well-studied. Particularly interesting is the potential of HS as a growth substrate in the presence of Mn oxide, the product of biological Mn(II) oxidation. Mn oxide is one of the most potent, naturally occurring catalysts in nature and has been shown to oxidatively degrade HS. Furthermore, Mn biofiltration is hindered by lack of understanding of the fate of Mn in the biofilter, including unpredictable releases of Mn (Cerrato et al., 2010; Kohl and Dixon, 2012). Desorption of Mn from biofilters has been observed following the conversion from physicochemical (chlorine) treatment to pre-ozonation and biologically active filtration (Gabelich et al., 2006). The source of the Mn was concluded to be from buildup of Mn impurities originating from ferric chloride, a chemical coagulant. The observed releases of Mn raises the issue of whether Mn(IV)-reducing microbes are active in biofilters and represent a potential release mechanism/pathway for Mn via reduction of accumulated Mn(IV) oxide (Cerrato et al., 2010).

Finally, steady-state and transient biofiltration models for Mn(II) removal have not been developed for fully defined water media and Mn(II)-oxidizing microorganisms. Mn biofiltration involves complex reaction kinetics and mechanisms that govern electron transfer between dissolved and solid Mn speciation that are microbially mediated. Several studies have provided valuable insight into removal of Mn during biological filtration (Burger at al., 2008; Kohl and Dixon, 2012). However, many of these studies involved undefined conditions for bench, pilot- and full-scale water treatment biofilters. Important conditions that can affect biofilter performance include water chemistry, pH, oxygen concentration, temperature, oxidation-potential (ORP), filter bed material/construction and microorganism species. If these conditions are not controlled or defined, fundamental process information may be difficult to obtain.

## 1.3 Research Hypothesis

The research hypothesis formulates that the transition metal oxide, Mn Oxide, can increase the biodegradability of HS and sustainability of biological control for Mn removal. More formally, for controlled bioreactor systems containing appropriate amounts of Mn(II), $MnO_2$, HA, and Mn(II)-oxidizing bacteria, $MnO_2$ under certain conditions will oxidize HA to more biodegradable products that can serve as the primary electron donor and carbon source for bacteria growth. The Mn(II)-oxidizing bacteria, upon utilization of the oxidized organic substrate products, will regenerate (oxidize) Mn(II) to particulate $MnO_2$, thus controlling/removing Mn(II) from solution. Subsequent reduction and dissolution of $MnO_2$ will release Mn(II) into the bulk solution and undergo bacteria oxidation or autocatalytic adsorption by $MnO_2$ in the bioreactors. For this study, humic acids (HA) will be the surrogate for HS. Mn oxide, which is considered to occur more commonly as the mixed oxide $Mn(III,IV)O_x$ (where $1 < x < 2$) when biotically produced, will be represented as manganese dioxide or $MnO_2$ in the following discussion and equations. The reaction sequence in Eqns. (1-1)-(1-4), a conceptual representation of the hypothesis, may describe the biological and chemical oxidation of Mn(II) and HA, respectively, and reduction of $MnO_2$ in bioreactor systems:

HA from the bulk solution diffuse to $MnO_2$ surface reaction sites and initially form a HA–$MnO_2$ precursor complex:

$$MnO_2 + HA \quad \leftrightarrow \quad HA- MnO_2 \qquad (1-1)$$

Electron transfer from HA in the HA- $MnO_2$ complex to $MnO_2$ will form oxidation product $HA_{(ox)}$ and reduced Mn(II):
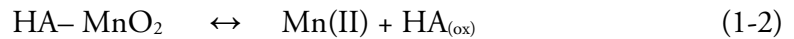
$$HA- MnO_2 \quad \leftrightarrow \quad Mn(II) + HA_{(ox)} \qquad (1-2)$$

Biological oxidation of Mn(II) formed from Mn oxide reduction and dissolution and Mn(II) originally present in source water, as $Mn(II)_{(in)}$, to form $MnO_2$, utilizing $HA_{(ox)}$ as the substrate (electron donor) for growth and $O_2$ as the final electron acceptor:

$$Mn(II) + Mn(II)_{(in)} + O_2 + HA_{(ox)} + \text{bacteria cells} \rightarrow MnO_2 + CO_2 + H_2O + \qquad (1-3)$$
$$\text{new bacteria cells}$$

      Overall reaction:

$$Mn(II)_{(in)} + MnO_2 + HA + O_2 + \text{bacteria cells} \rightarrow MnO_2 + CO_2 + H_2O + \qquad (1-4)$$
$$\text{new bacteria cells}$$
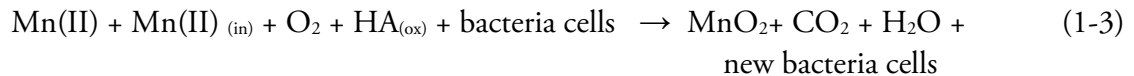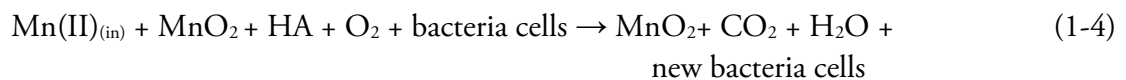
The term 'new bacteria cells' in Eqns. 1-3 and 1-4 represents the net growth of cells utilizing $HA_{(ox)}$ or $MnO_2$-oxidized HA as the sole carbon source. The net bacteria growth and quantity of $CO_2$ (in Eqns. 1-3 and 1-4) produced represent indicators of HA biodegradability. Carbon and energy demands for cell maintenance, motility and biofilm formation require separate considerations. Nutrients (N, P, S) and trace metals required for normal cell growth and function, except for compounds that may serve as energy or carbon sources, are assumed present in the bioreactors.

The specific reaction mechanism between HA and $MnO_2$ may involve weak and strong chemical bond formation which incorporate electrostatic, adsorptive, and surface complexation-ligand exchange reactions prior to electron transfer. HA oxidation rates, provided available metal reaction sites are not limiting, will likely be determined by HA adsorption and electron transfer rates to oxidizing Mn metal centers. Adsorption rates will likely be controlled by the dominant exchange mechanism and electrostatic HA and $MnO_2$ charge. Electron transfer rates will depend on the reduction and oxidation potential of HA and $MnO_2$. HA charge will be largely determined by oxygen functional groups attached to the aromatic core (carboxylic (COOH) and phenolic (OH)), which deprotonate and become negative at pH above their $pK_a$ values. Typical HA carboxylic and phenolic groups have a $pK_a$ < 5.0 and > 8.0, respectively. By definition, metal oxides have a net electrostatic surface charge of zero at the point of zero charge (PZC). Mn-oxides commonly have a PZC of 4 to 5. Therefore, for pH in the neutral range, both $MnO_2$ and HA will have a net negative charge which can minimize catalyst-substrate interaction. However, the presence of divalent cations $Ca^{+2}$ and $Mg^{+2}$ can bridge or shield negative repulsive charge effects and facilitate the HA and $MnO_2$ redox reaction.

## 1.4 Research Objectives

The overall research objective is to obtain a better understanding of suspended and fixed-film biological processes for Mn(II) control/removal in water supplies provided humic acids as the sole carbon source. At present there is no reported information available on this subject. The specific objectives for this research:

1. Isolate a Mn(II)-oxidizing bacteria and identify the species using 16s-rDNA gene sequencing. Determine optimal Mn(II)-oxidizing conditions (pH and temperature) and evaluate capacity of isolate to grow on selected substrates.

2. Test the hypothesis that Mn oxide (as $MnO_2$) can increase the biodegradability of humic acids.

3. Obtain the optimal ratio of humic acids / $MnO_2$ concentrations and reaction (contact) time to maximize humic acids' biodegradability.

4. Investigate Mn(II)-oxidation rates using the isolate in bench scale batch and continuous flow biological reactors (fixed-film) using $MnO_2$ treated humic acids as the sole carbon source.

5. Kinetically characterize biological Mn(II) oxidation and removal in the bioreactor systems.

6. Investigate Mn fate in bench scale fixed-film biological reactors.

## Chapter 2: Literature Review and Background

### 2.1 Overview

The goal of drinking water treatment utilities is to provide water that is safe to drink (void of harmful levels of pathogens and chemicals), aesthetically pleasing (free of odor, taste and color) and cost-effective (Edzwald, 2010). In this viewpoint, manganese (Mn), a naturally occurring metal, represents a common source of aesthetic water quality issues. Mn is particularly problematic for communities that rely on water supplies under suboxic conditions, including groundwaters, stratified lakes and reservoirs, where soluble Mn(II) is often coupled with reduced iron (Fe). The presence of Mn in drinking water can result in metallic taste, turbidity and discoloration as oxidized precipitates that stain water pipes, laundry and plumbing fixtures (Kohl and Medlar, 2006). Reduced divalent Mn(II) is a required micronutrient for living organisms, and serves as a cofactor in enzymes and enzyme complexes, and is not considered a health concern in the levels frequently encountered in drinking water (Kohl and Medlar, 2006). The United States Environmental Protection Agency (USEPA), World Health Organization (WHO), and the European Commission recognize a non-enforceable secondary maximum contaminant level (SMCL) for Mn in drinking water at 0.05 mg·L$^{-1}$ for most community water supplies, set to control taste and nuisance issues (USEPA, 1979; WHO, 1971; 98/83/1998).

The removal of manganese from raw water supplies relies on the mechanism of oxidation of soluble Mn(II) to oxidized Mn(IV) precipitates, which can be achieved with conventional physicochemical or biological treatment (Kohl and Dixon, 2012). Unlike conventional treatment, which involves the addition of chemical oxidants, biofiltration technology relies on microbial oxidation of Mn(II) in biofilms attached to granular filter media for removal. Bacteria are considered to be the primary microbes responsible for Mn(II) oxidation in the biofilters. Biofiltration offers several advantages over physicochemical treatment, including not requiring addition of a chemical oxidant to the raw water, reduction of disinfection by-products (DBPs) and DBP precursors, and it's role as a pre-filter to produce highly stable biological water in the distribution system (Mouchet, 1992; Carraro et al., 1999; Zhu et al., 2010; Dixon and Kohl, 2012).

With drinking water utilities traditionally striving to remove organisms during water treatment, the view of employing microbes (e.g., bacteria) for water treatment has been long discouraged in the US due to their potential as pathogens, despite widespread biological filtration application for water treatment in Europe. Their increasing use in water treatment in the US has come about because of their ability to produce highly stable biological water, and because of the establishment of more stringent regulation of disinfection by-products (DBPs) according to the Stage I and II Microbial/Disinfection By-Product rules (USEPA,

1998). Biofilters have the potential to remove Mn to levels below the SMCL for Mn. However, optimal use is limited by several factors, including: sufficient biodegradable dissolved organic carbon (BDOC) in the raw waters to support heterotrophic biofilm microbes, identification of the optimal conditions of Mn removal, and the fate of Mn in the biofilter, including understanding and management of unpredictable releases of Mn.

The largest portion of DOC in natural waters, humic substances, are present virtually in all surface waters and many groundwater environments in varying concentrations. Their presence is drinking water is undesirable due to their color and taste issues and reaction with chemical oxidants during conventional water treatment to produce trihalomethanes and other potential carcinogenic by-products. Humics represent a potential carbon source for microorganisms in biofilters, but their recalcitrant structures tend to make them largely unavailable to microbial carbon metabolism. Previous experimental work has shown that humic substances can be oxidized to more biodegradable products by Mn Oxides, possibly serving as a mechanism for Mn(II)-oxidizing bacteria to obtain bioavailable carbon. (Sunda and Kieber, 1994)

## 2.2 Manganese Chemistry

## 2.2.1 Oxidation States

Manganese (Mn) (atomic number 25 and standard atomic weight of 54.938) is the third most abundant ($9.5 \times 10^2$ ppm or 0.1% of earth's crust) transition metal in the lithosphere, from which it attributes many oxidation states and darkly colored catalytic oxides (Cox, 1995; Kohl and Medlar, 2006; Kohl and Dixon, 2012). The brown-black color of Mn-oxides and their impact on drinking water aesthetics is the primary motivation to control/remove Mn from water supplies.

Mn charge or oxidation state can exist as -3 to +7, with Mn(II), Mn(IV) and Mn(VII) of importance in drinking water treatment processes (Kohl and Medlar, 2006). In terms of Mn electronic configuration, $[Ar] 4s^2 3d^5$, the redox chemistry involves the 4s and 3d orbitals. Mn(II), complexed Mn(III) and Mn(VII) are soluble manganese forms, while Mn(IV) is the most common state and typically forms various oxide polymorphs as $MnO_2$ (Kohl and Dixon, 2012). Mn(II) is similar to Group 2 elements, such as $Ca^{2+}$ and $Mg^{2+}$, in terms of aquatic stability due to a half-filled $3d^5$ electronic shell. Mn(II) has the capacity to undergo ligand exchange reactions with natural organic compounds, including humic substances. Mn(III) and Mn(IV) prefer complexation with oxygen, forming compounds with higher oxidation potential. Mn Oxides promote the oxidation and degrdation of natural organic matter and xenobiotic pollutants while serving as sinks for trace metals. One of many manganese dioxide polymorphs, pyrolusite ($\beta$-$MnO_2$), is a naturally occurring manganese mineral formed in weathered, oxidizing environments and represents the most common

mining ore for manganese. Mixed oxyhydroxides containing $Mn(II,III)O_x$ and $Mn(III,IV)O_x$ are common as manganite (MnOOH) and hausmannite ($Mn_3O_4$). Mn oxides and oxyhydroxides, the most thermodynamically stable form of Mn at high pH and in the presence of $O_2$, are ubiquitous in soil and aqueous environments and microbial activity is considered to have a major role in their formation and cycling at low temperatures (Tebo et al., 2005; Saratovsky et al., 2006). Important properties of Mn-oxides that control their reactivity include surface area, Mn oxidation state and point of zero charge (PZC). High oxide specific surface areas are due to small particle sizes which relate to an unordered Mn – O structural arrangement. Biotic Mn oxides offer considerably different redox chemistries than synthetically or chemically generated forms, owing to their much higher surface areas, higher adsorption energies and an unorganized atomic structure (Saratovsky et al., 2006). Mn oxidation states, mineral forms, and specific surface areas of biogenic oxides have been characterized (Nelson et al., 2002).

## 2.2.2 Redox Considerations

Redox Mn chemistry is fundamental to the design and optimization of biological drinking water treatment processes for Mn. Biological Mn removal/control requires managing complex oxidation-reduction or electron exchange reactions between the II, III and IV oxidation states that are largely mediated by microorganisms, whose identity and characteristics are unknown outside of a few, well studied microorganisms (Tebo et al., 2005; Kohl and Dixon, 2012). Other than in relatively simple terms, the reaction pathways and kinetics of conversion between Mn oxidation states in complex systems such as biofilters are poorly understood (Kohl and Medlar, 2006).

Thermodynamic quantities such as the overall standard potential ($E^0$), or its related quantity, electron activity (pE), establish the tendency of a Mn redox reaction to proceed spontaneously. When in consideration with pH, the redox equilibrium and stability between Mn species in simplified aqueous systems can be accurately predicted only for simple systems (Figure 2.1). Rates of conversion between Mn oxidation states are dependent on the kinetics for the particular type of reaction, usually represented by experimental rate expressions, which are controlled by the thermodynamic constraints established by $E^0$ and $\Delta G^0$, the Gibbs Free energy (Stone and Morgan, 1984; Morgan, 2005).

The standard Gibbs Free Energy is related to the standard cell potential by Faraday's constant (F) and the number of electrons exchanged in the redox reaction (n):

$$\Delta G^0 = -nFE^0 \qquad\qquad (2\text{-}1)$$

Reactions with a positive $E^0$ or negative $\Delta G^0$ are reaction product favored and proceed as written.
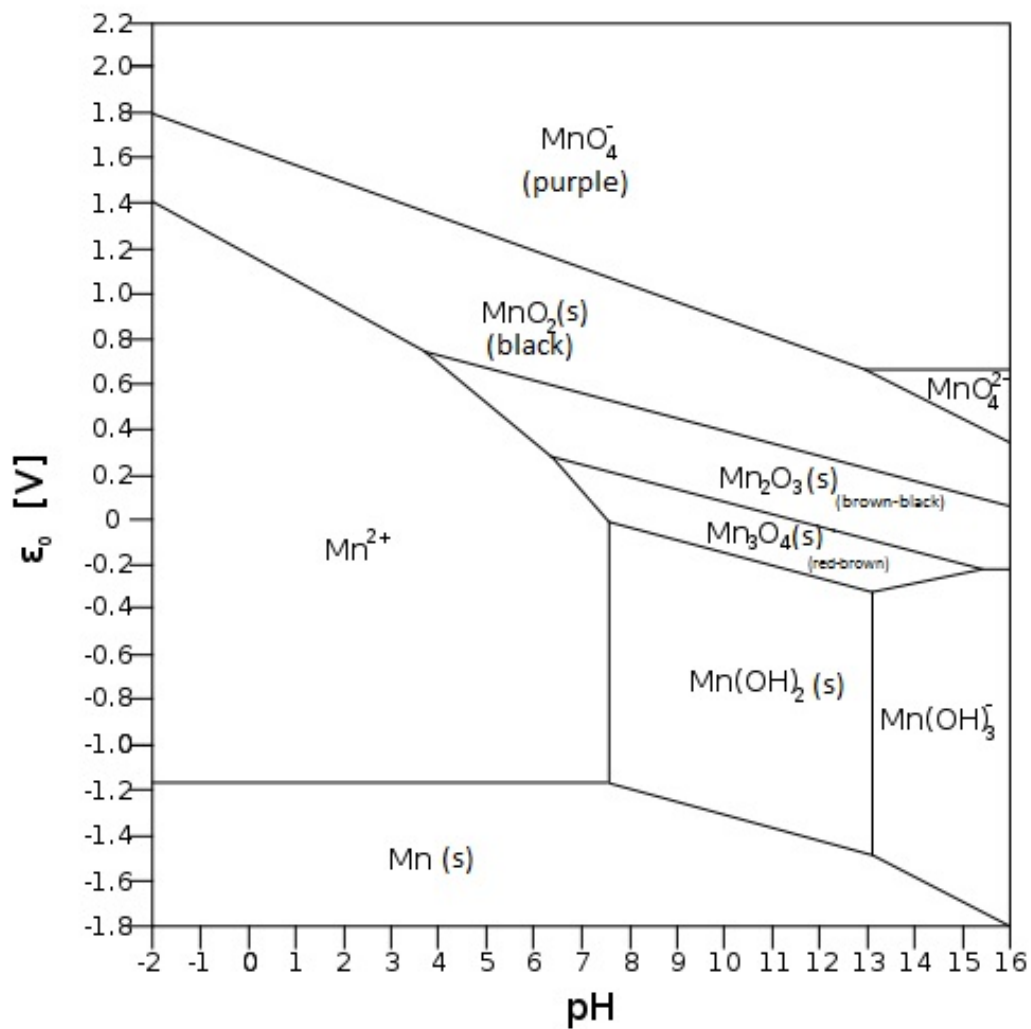
**Figure 2.1.** Mn Stability Diagram at 25°C and 1 atm. (Martin, 2005).

The overall standard potential is equal to the standard potentials of the half-cell reactions (Eqn. 2-2):

$$E^0 = E^0_{red} + E^0_{ox} \qquad (2\text{-}2)$$

For example, the stoichiometry of Mn(II) oxidation to insoluble $MnO_2$ may be represented as (Eqn. 2-2) followed by the corresponding reduction and oxidation half reactions (Eqns. 2-4 and 2-5) :

$$\tfrac{1}{2}\ Mn(II)\ +\tfrac{1}{2}\ H_2O + \tfrac{1}{4}\ O_2\ \rightarrow\ \ \tfrac{1}{2}\ MnO_2\ (s) + H^+ \qquad E^0 = 0.03,\ volts \qquad (2\text{-}3)$$

$$\tfrac{1}{4}\ O_2\ + H^+ + e^+ \rightarrow\ \ \tfrac{1}{2}\ H_2O \qquad E^0_{red} = 1.23,\ volts \qquad (2\text{-}4)$$

$$\tfrac{1}{2}\ Mn(II)\ +\ H_2O \rightarrow\ \ \tfrac{1}{2}\ MnO_2\ (s) + 2H^+ + e^+ \qquad E^0_{ox} = \text{-}1.21, volts \qquad (2\text{-}5)$$
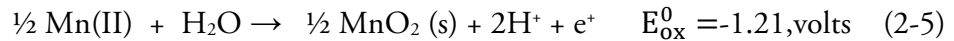
A relatively low $E^0$ potential indicates the reaction has a small tendency to proceed as written and favor Mn(II) reduction. Increasing the value of $E^0_{red}$ , the oxidizing agent, will more likely result in Mn(II) reduction. In water treatment practice, this is achieved by replacing molecular $O_2$ with an agent of higher oxidizing potential. The activation energy, or minimum input energy required for Mn(II) oxidation, is relatively high and the implications are that Mn(II) can persist in oxidizing aqueous environments (Stumm and Morgan, 1996). The half-life for homogenous Mn(II) oxidation with $O_2$ has been estimated to range from 1 to 350 days from pH 9.3 to pH 8.0 at 25°C and $P_{02}$ = 0.21 atm. (Morgan, 2005). Given the high half-life, the oxidation of Mn(II) can be catalyzed by increasing the pH or by microbial mediation.

The pathways describing redox Mn reactions include (1) homogenous oxidation, (2) heterogeneous oxidation (e.g. adsorption to mineral surface and autocatalysis), (3) reduction, and (4) microbial oxidation or reduction (Morgan, 2005).  Each of these pathways are represented in Table 2.1. Both homogenous and microbial oxidation can be represented by Eqn. 2-3. In this work, each of these pathways (2-4) are studied except for (1). Significant homogenous oxidation is not observed in the Mn control studies (Chapter 3).  The relative rates of homogenous, heterogeneous, and bacteria Mn(II) oxidation have been estimated to be 1:10:1000 (Morgan, 2005; Spiro et al., 2010).

## 2.3 Manganese in Water Supplies

The bivalent cation Mn(II) – the most common soluble form of Mn at low pH in suboxic or anoxic (absence of $O_2$) conditions – will persist in most natural waters as bicarbonate and hydroxyl (e.g., $MnOH^+$, $Mn(OH)_2$) complexes. Such reducing environments commonly exist in water supply sources including groundwaters, stratified lakes, and reservoirs, where Mn is a frequent contaminant in elevated concentrations. In oxygenated natural waters,

**Table 2.1.** Mn Oxidation and Reduction Pathways

Homogeneous Mn(II) Oxidation (Morgan, 2005):

$$Mn(OH)_2 + O_2 \rightarrow \quad Mn(OH)_2{}^+ + O_2{}^- \qquad \log k = 1.32$$
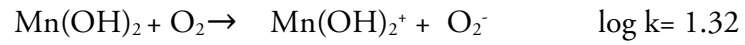
Heterogeneous Autocatalytic Mn(II) Oxidation (Martin, 2005):

$$\frac{-d[Mn^{2+}]}{dt} = k\,[MnO_x(s)]\,[Mn^{2+}]$$

Mn( III, IV) Oxide Reduction (Martin, 2005):

$$MnOOH + e^- + 3\,H^+ \rightarrow Mn(II)\,(aq) + 2\,H_2O$$

$$MnO_2 + 2\,e^- + 3\,H^+ \rightarrow Mn(II)\,(aq) + 2\,H_2O$$
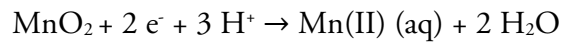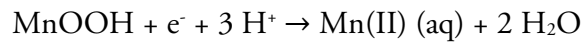
Examples:  $e^-$ = fulvic acids, humic acids, hydroquinone

particularly after a period time and subject to biological catalysis, manganese likely will transform to Mn(IV) or Mn(III), which may bond to organic materials or other ions. Mn stability diagrams predict Mn participation in a number pH-dependent speciation and redox reactions affecting its fate in water supplies. With increasing pH conditions, Mn(II) can complex and precipitate, causing objectionable water turbidity and color (Stumm and Morgan, 1996; Morgan, 2005).

In the presence of natural organic matter, higher pH deprotonate acidic functional groups of humic substances and facilitate manganese binding and precipitation (Brigante et al., 2007). Oxidation of Mn(II) forms brown-black precipitates as Mn(III,IV) or Mn(IV) oxides which results in darkening of the water and subsequent black deposits and clogging or narrowing of pipes in water distribution systems.

Mn(II) is the targeted species for removal in drinking water treatment operations. Oxidation of Mn(II) typically produces $3^+$ and $4^+$ species and can exist as black, brown and purple solid oxides, $MnO_x$, and oxyhroxides, and represent the primary source of discolored water and staining (Figure 2.1). Stoichiometric manganese dioxide, $MnO_2$, is used as a water treatment filter material, - commonly as pyrulosite or manganese greensand, for iron, manganese, and hydrogen sulfide removal. Mn(VII), or permanganate ($MnO_4^-$), can be produced by stronger oxidants of Mn(II), such as ozone, and is the common form of the highest Mn oxidation state and can persist in water distribution systems, having a long half-life. $MnO_4$ itself is a potent oxidizer used in water treatment.

The primary source of Mn in aquatic environments is considered to be due to the dissolution of manganese minerals in rocks, sediments and soils (Hem, 1985; Kohl and Medlar, 2006). Mn(II) will persist due to the kinetic stability of Mn at the pH and oxidation/reduction ($E_h$) conditions of these environments (Bowen, 1979; Ehrlich, 2002). Although manganese is primarily an issue for water utilities treating groundwater, detections are common in most Public Water Systems (PWSs). One study found that more than 3,660 groundwater PWSs have Mn exceeding three times the SMCL of 0.05 mg·L$^{-1}$ (USEPA, 2004). A survey of 242 U.S. water utilities that primarily treat groundwater revealed that almost 50% acknowledged a manganese problem and implement a specific unit treatment for manganese control and its attendant turbidity and discoloration issues (Kohl and Medlar, 2006).

Although largely considered to be an aesthetic issue, the USEPA released a health advisory for potential neurological effects (USEPA, 2004). It has been suggested that 0.02 mg·L$^{-1}$ is a more appropriate standard to minimize consumer concerns in drinking water (Kohl and Medlar, 2006).

## 2.4 Manganese Drinking Water Treatment

In the US, Mn drinking water treatment traditionally has relied on physicochemical technology, primarily chemical oxidation of soluble Mn to insoluble forms in the untreated water. Biological processes, more common in Europe, employ biological filters which consist of fixed films, primarily of bacteria attached to granular filter material. Biological filter design and operating conditions at full-scale water treatment plants are largely based on engineering and plant operator experience and not fundamental studies (Mouchet, 1992; Burger et al., 2008).

### 2.4.1 Conventional Mn Water Treatment

The presence of manganese in source water requires treatment by water treatment utilities because manganese is not oxidized by air to insoluble oxides at neutral pH during conventional water treatment processes unless a chemical oxidation step is included. In the U.S., Mn is removed from drinking water primarily by conventional physicochemical processes which convert soluble Mn(II) to insoluble Mn(IV) oxides through intense aeration or chemical oxidation followed by sand filtration of the oxidized, low-solubility products (Singer and Reckhow, 1999; Kohl and Medlar, 2006). In such treatment process, high pH and dissolved oxygen levels are needed to effectively convert Mn(II) to Mn(IV). At pH conditions below 9.0, aeration for Mn(II) removal is slow or may not occur at all (Singer and Reckhow, 1999). Thus lime or soda ash is often added to raise the pH to increase the rate of Mn(II) oxidation. The most common chemical agents used for Mn(II) oxidation are chlorine ($Cl_2$) and potassium permanganate ($KMnO_4$) (Kohl and Medlar, 2006). However, chlorine can react with natural organic matter to produce undesirable disinfection-by-products (DBPs) or smaller molecular weight organics that can lead to bacterial regrowth problems in distribution systems. The effectiveness of the chemical oxidant(s) to remove Mn is dependent on a variety of raw water conditions, including pH, alkalinity, temperature, Mn concentration and the presence of oxidizing compounds (e.g., iron, ammonia, natural organic matter (NOM) and sulfide) which can undergo competitive reactions with Mn, increasing the required oxidant dosage per mg of Mn(II) and overall treatment costs (Wilczak et al., 1993; Kohl and Medlar, 2006). For example, excessive dosages of ozone ($O_3$) in the presence of elevated levels of NOM in the raw water can react with Mn(II) to form permanganate, resulting in the pink discoloration of the effluent stream, eventually reducing to black deposits in the distribution system (Wilczak et al., 1993). Additionally, chemical oxidants can react with NOM and form potentially toxic disinfection by-products (DBPs), for which water utilities are facing increasingly stringent regulations.

Manganese greensand or GreensandPlus, which are particulate nodules coated with $MnO_2$, are widely used filter materials for Mn control in drinking water. The coated $MnO_2$ acts as a catalyst in the adsorption and oxidation of Mn(II) (Kohl and Dixon, 2012). However, $MnO_2$ must be regenerated, as its oxidizing power is depleted by the addition of a chemical oxidant such as $KMnO_4$ and/or chlorine upstream of the filter (Kohl and Medlar, 2006).

In the presence of naturally occurring humic substances, the physicochemical processes often fail to provide consistent effluent quality which meets the drinking water standard for manganese due to metal complexation, consumption of the oxidant by the organics, or membrane fouling (Mouchet, 1992; Routt, 2004; Basu and Huck, 2005). Thus, controlling Mn with the conventional processes can be cost prohibitive due to the requirement of preoxidation with chemicals or higher doses of permanganate in the presence of naturally occurring organic matter (e.g., humic substances) (Paillard et al., 1988).

## 2.4.2 Biological Water Treatment

Biological water and wastewater treatment methods are primarily aerobic processes that involve mechanisms including biodegradation, metal reduction (As, Cr, Se), adsorption, and suspended solid reduction (Rittmann and McCarty, 2001). Biological treatment is incorporated in technologies such as fluidized beds, biological towers, biologically active granular activated carbon, rotating biological contactors, trickling filters, and activated sludge (Rittmann and McCarty, 2001). Biological water treatment processes have been largely discouraged by the water industry, particularly in the U.S., because of the use of microorganisms to purify the water. However, their gain in acceptance is in part due to their effectiveness to achieving biological water stability, and in the US, is driven by more stringent regulations on disinfectants and disinfection by-products, which in some cases discourage the use of the addition of chemical oxidants for treatment. For example, the Stage 1 Disinfectants and Disinfection By-products Rules (USEPA, 1998) require the use of biological filtration for water utilities that use ozone. Furthermore, water utilities that use conventional filtration must remove specific percentages of the raw water organic matter (as TOC), favoring the consideration of biological filters.

## 2.5 Biofiltration

Biofiltration has primarily been a pre-filter unit of the treatment train of many water treatment facilities, primarily to remove biodegradable organic material (BOM), reducing organic precursors prior to disinfection and biological activity in the distribution system. Biological filtration has long been recognized by Europeans as an important unit operation for producing biologically stable water and prevent bacterial regrowth in distributions systems and thus reduce the amount of residual chlorine required. As previously stated, interest is increasing in alternatives to the physicochemical processes in the U.S. due to their potential for reducing organic carbon as required by the Stage 1 and 2 Disinfectant/Disinfection By-product Regulations set by the U.S.EPA (USEPA, 1998). The rule mandates utilities using disinfectants to remove predetermined levels of total organic carbon (TOC) as a means of reducing disinfection by products. In addition, biological filtration offers the advantages such as higher Mn(II) oxidation rates, reduction in

disinfection by-products, and elimination/reduction of chemicals (Mouchet, 1992; Kohl and Medlar, 2006).

Biological filtration has been successfully applied for a number of years, first by European and more recently, North American water utilities, to provide finished drinking water quality Mn levels below the SMCL (Beger, 1937; Czekalla et al., 1985; Korth et al., 2002; Kohl and Dixon, 2012). The biological process consists of filtering aerated, untreated water over thin biofilms a few millimeters thick that host Mn(II)-oxidizing microbes that are attached to packed beds of granular filter material. Anthracite, gravel, sand or granular activated carbon (GAC) are common filter material and the beds can be constructed as gravity filters or for smaller installations, pressurized filters. Biofiltration occurs as Mn(II) in the bulk water diffuses into the biofilms and is oxidized to $Mn(III,IV)O_x$ by microbial enzymatic oxidation. The black-brown, solid Mn oxides accumulate on the biofilm surfaces and the biofilters are periodically backwashed to maintain biofilter performance. At pH conditions typical of water supplies, the bacteriogenic, dark-colored-oxides have a net negative surface charge and are considered to autocatalytically participate in Mn(II) cation removal through electrostatic adsorption processes.

Biological filtration has been reported to successfully lower Mn concentrations from >0.50 mg/L to <0.02 mg/L (Hope and Bott, 2003). Manganese removal by biofilters has been studied using bench-scale reactors (Sly et al., 1993; Katsoyiannis and Zouboulis, 2004; Hope and Bott, 2004) and pilot as well as full-scale biological treatment plants (Pacini et al., 2005; Yang et al., 2004; Li et al., 2005). Biological removal of manganese has been modeled with pure cultures using a continuous fluidized bed reactor (Sly et al., 1993) and bench scale biofilters (Hope and Bott, 2004). The removal of biodegradable organic matter in a biological filter has been modeled using a steady-state-biofilm model (Saez and Rittman, 1992; Zhang and Huck, 1996) with results showing a linear relationship between substrate removal and influent concentration. However, no information regarding biological filtration performance and biofilm Mn(II) oxidation in the presence of humic substances is available.

Bioreactor performance is hindered by lack of understanding of the fate of Mn in the biofilter, including unpredictable releases of Mn (Cerrato et al., 2010; Kohl and Dixon, 2012). Desorption of Mn from biofilters has been observed following the conversion from physicochemical (chlorine) treatment to pre-ozonation and biologically active filtration (Gabelich et al., 2006). The source of the Mn was concluded to be from buildup of Mn impurities originating from ferric chloride, a chemical coagulation. This raises the issue of whether Mn(IV)-reducing microbes are active in biofilters and have the potential to release Mn via reduction of accumulated Mn(IV) oxide (Cerrato et al., 2010).

## 2.6 Biological Mn(II) oxidation

The formation of Mn (III/IV) oxides from soluble Mn(II) is believed to be a biologically controlled process in most natural waters since abiotic oxidation of Mn(II) proceeds only at a limited rate (Tebo et al., 2004). Numerous microorganisms, including bacteria and fungi, can oxidize Mn(II) to insoluble manganese oxides (Tebo et al., 2005). Either direct (enzymatic or specific binding) or indirect (modification of the pH and/or redox conditions) processes may be involved in bacterial oxidation of Mn(II) (Nealson, 2006).

The formation of Mn(IV), primarily as $MnO_2$, occurs as two one-electron transfer steps from Mn(II) through the transient intermediate Mn(III) (Tebo et al., 2005). For direct Mn(II) oxidation, the enzymes responsible for bacterial Mn(II) oxidation are of two types (1) calcium binding haem peroxides (MopA), and (2) multicopper oxidase (MCO). MCO enzymes catalyse the one-electron transfer from substrates that include Fe(II) and lignin to reduce $O_2$ to $H_2O$ (Geszvain et al., 2012). MCOs incorporate multiple copper ligands, including a copper-binding site and a trinuclear center. One electron is removed from the substrate at the copper site then transferred to the trinuclear centre where it is added to $O_2$.

Oxidation-reduction potential (ORP) is a water quality indicator and a measure of the tendency for electron exchange reactions to occur between 'donors' and 'acceptors' species. Measurement of ORP is considered important condition for biological Mn(II) oxidation during biological filtration. ORP conditions for biological filtration Mn(II) oxidation at treatment plants exhibit a wide $E_h(mV)$ variation (Kohl and Dixon, 2012). It is often assumed that optimal ORP conditions coincide with the thermodynamic stability fields for homogeneous oxidation/reduction of Mn(II) and Mn(III,IV) oxides (Mouchet, 1992; Burger et al., 2008). For example, the conditions (pH $\leq$ 8 and $E_h \geq$ +200 mV) of most natural freshwater environments are assumed to favor microbial oxidation of Mn(II) as shown by the thermodynamic stability fields in Figure 2.1 and 2.2 (Mouchet, 1992). In addition, optimal bacteria enzymatic Mn(II)-oxidation rates are pH dependent and can vary considerably between bacteria species. In natural aquatic environments, biological Mn(II) oxidation often occurs in the transition zone between oxygen-rich and suboxic water and sediments, with the oxidized manganese deposited as $Mn(III,IV)O_x$ coatings on filamentous sheaths or external cell membranes surfaces (Mouchet, 1992; Tebo and He, 1999).
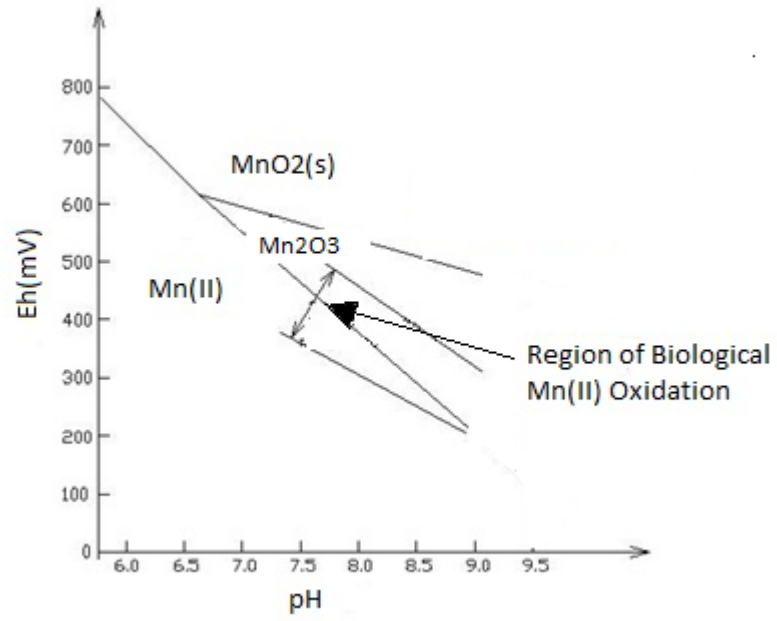
**Figure 2.2.** Field of biological Mn activity (Mouchet, 1992).

Mn(II) oxidation is an autocatalytic reaction whereby the Mn oxides catalyze the oxidation (Stumm and Morgan, 1996). In general, the rate of redox reactions between Mn oxide and Mn(II) increases as pH increases. Bacteria Mn(II) oxidation rates are dependent on the environmental conditions including pH, temperature, cell concentration and dissolved oxygen (Zhang et al., 2001).

Mn(II)-oxidizing bacteria constitute a broad lineage among the bacterial domain and include the *Firmicutes, Actinobacteria* and *Proteobacteria* (Tebo et al., 2005), however, only a few species are well investigated. Mn(II) oxidation has been studied with pure bacterial cultures of *Pedomicrobium* ACM 3067 (Larsen et al., 1999), *Pseudomonas Putida* MnB1 and GB-1 (Brouwers et al., 2000; Villalobos et al., 2003), and *Leptothrix discophora* strains SS-1 and SP-6 (Adams and Ghiorse, 1985; Boogerd and de Vrind, 1987; Brouwers et al., 1999). The Mn oxides formed extracellularly by *L. discophora* were shown to be mixed Mn(III, IV) oxides and oxyhydroxides with an average oxidation state of 3.6. The biogenic Mn oxide produced by *P. putida* has an average Mn oxidation number of 3.9 and a form most similar to birnessite $\delta$–$MnO_2$ (Villalobos et al., 2003). The decrease in the average oxidation number from 4 is due to the presence of Mn(II)/Mn(III) sorbed at Mn(IV) vacancy sites. Mn(II) oxidation has also been reported with chemolithoautotrophs including *Sphaerotilus discophorus* (Johnson and Stokes, 1966; Ali and Stokes, 1971), *Pseudomonas* S-36 (Kepkay and Nelson, 1987), and *Pseudomonas siderocapsa* sp. (Falamin and Pinevich, 2006). However, the correlation between Mn(II) oxidation and $CO_2$ fixation has yet to be established (Tebo et al., 2004).

Optimal bacteria enzymatic Mn(II)-oxidation rates are pH dependent and can vary considerably between bacteria species. This would imply that the pH optima for Mn removal by biofiltration may be primarily controlled by the Mn(II)-oxidizing bacteria species representing the largest populations in the biofilms. This simplification may be complicated if autocatalytic removal mechanism by Mn oxide has a significant role in Mn removal capacity. Mn oxide net surface charge, which controls the oxide electrostatic adsorption capacity, is strongly pH dependent.

## 2.7 Biofilms

Most biological water treatment processes are biofilm based reactors in which microorganisms are attached to granular filter media and form aggregates of microorganisms encapsulated in thin, slimy layers of extracellular polymeric substances (EPS) (Rittmann and McCarty, 2001). EPS is the 'glue' for the biofilm and provides biomass retention and serves as the host structure for microorganisms that provide removal mechanisms for inorganic and organic substrates in raw water (Donlan and Costerton, 2002). The EPS consists of polysaccharides, proteins, glycoproteins, glycolipids and extracellular DNA (Flemming et al., 2007). Biofilms are considered to create a protected environment for the microorganisms by providing a more controlled environment than the bulk liquid, protecting them from severe

changes in bulk water pH, toxic substances and predatory organisms (Watnick and Kolter, 2000; Rittmann and McCarty, 2001; Flemming and Wingender, 2002).

Single species bacteria biofilms form in multiple steps with the initial step typically considered to be colonization of a solid surface in response to food which eventually leads to the formation of a three-dimensional biofilm matrix (Watnick and Kolter, 2000; Rittmann and McCarty, 2001). Biofilm formation by *P. Putida* species has been shown to be uninhibited by temperature (5 to 30° C) or under nutrient rich or poor conditions (Morimatsu et al., 2012). However, in this same study, biofilm detachment occurred more readily in rich nutrient condition under high temperatures whereas detachment was prevalent under all temperature conditions at low nutrient conditions.

Diverse microbial communities have been identified in biofilters, but Mn-oxidizing bacteria are considered to predominant. They catalyze Mn(II) to Mn(III,IV) oxides as aerated, raw water passes over the biofilms attached to the filter bed, depositing the brown/black oxidized precipitates on their extracellular surfaces. The immobilized coatings of Mn(III,IV) oxides are considered to provide an autocatalytic Mn removal mechanism, acting as adsorption sites for Mn(II) in the bulk liquid, accelerating the removal of Mn at rates dependent on pH and the number of sites available.

With heterotrophic microbes being the dominant biofilter hosts, steady-state biofilm kinetic models predict that a minimum substrate concentration, $S_{min}$, is required to provide a constant, diffusive flux of supporting nutrients and BOM to the biofilm (Rittmann and McCarty, 2001). Maintaining steady-state biofilms in typical surface waters that contain 2-10 mg·L$^{-1}$ DOC is more achievable than in carbon-limited natural waters, such as oligotrophic lakes (2 mg·L$^{-1}$ DOC) and groundwater aquifers (<1 mg·L$^{-1}$ DOC), where Mn(II) concentrations are higher. Should the bulk liquid substrate concentration decrease below $S_{min}$, the threshold level that supports zero net growth, substrate flux from the surrounding bulk liquid into the biomass will diminish and impair biofilter maintenance, as cell death and biofilm-detachment and sloughing losses gradually erode the biofilm.

DOC in most natural environments, including freshwater lakes and organic rich groundwaters, consist of measurable amounts of biologically labile and higher concentrations of refractory organic constituents, primarily derived from the decomposing remains of terrestrial vegetable matter and microorganisms (Moran and Hodson, 1990; Alborzfar et al., 2001). The biologically labile fraction can include aldehydes, ketones, simple carbohydrates and amino acids, all substrates that are more susceptible to direct utilization by heterotrophic microbes, resulting in a shorter persistence in natural environments (Rittmann and McCarty, 2001). Gagnon and Huck (2001) showed that that easily biodegradable organic compounds suffer negligible mass transfer limitations and readily diffuse into drinking water biofilms, obeying first-order kinetic modeling under steady-state conditions, balancing substrate flux and utilization. However, the bulk of DOC in most freshwater environments is considered

to be comprised of largely refractory humic and fulvic acids. These are anionic polymers of varying molecular weight (1000 to 100,000 Daltons) with a substituted aromatic core and lacking specific chemical structure (Aiken and Cotsaris, 1995). Oxygen functional groups play key roles in their chemical reactivity. Humic acids are resistant to utilization as growth substrates due to their size and molecular heterogeneity, which elude the specificity of microbial metabolic enzyme systems (MacCarthy, 2001; Krull et al., 2003). To a lesser extent, complexation of humic functional groups with inorganic ions (e.g., ionized carboxylic groups binding divalent calcium) reduces intramolecular negative repulsion between anionic functional groups while altering the broad humate conformation to a tighter aggregated arrangement, with the effect of ultimately decreasing substrate availability (Tipping, 1981; Guggenberger and Kaiser, 2003).

Humic organics are reported to have lower molecular diffusion coefficients ($D$, $D_f$), in the bulk liquid and within biofilms and higher $S_{min}$ values, by factors of 10 or higher, in comparison to smaller, biodegradable substrates (Rittmann, 1990; Woolschlager and Rittmann, 1995). This unfavorable physical and kinetic characterization of humic material further exacerbates the utilization of refractory organic matter by biofilms, either directly or through biosorption mechanisms involving slow, catabolic biodegradation kinetics (Rittmann and McCarty, 2001).


## 2.8 Reaction of Mn oxides with Humic Substances

While biodegradable carbon in the source water is considered necessary for biofiltration sustainability, the fate of recalcitrant NOM and potential for utilization as a carbon and energy source by biofilm microbes is unknown. This is particularly true if the biofilter contains a buildup of Mn oxide produced by biological Mn(II) oxidation. Mn oxide is one of the most potent naturally occurring catalysts in nature and has been shown to oxidatively degrade HS (Suna and Kieber, 1994). Further, HS, via oxygenated substituents, is a potential binding agent for metal-ions, including Mn.

Mn oxides are among the strongest oxidizing agents in natural environments and are implicated in a variety of metal and natural organic matter (NOM) sorption and redox reactions (Tebo et al., 2005). Their catalytic power can be largely attributed to variations in their layered structures and cation vacancies within these structures (Saratovsky et al., 2006). Mn oxides are highly stable in oxygenated environments but can be reduced through the interaction with organic matter, with the release of Mn(II) and oxidized organic products. Estimates of biodegradability of humic substances range from 1 to 27% for individual species of bacteria and mixed cultures from various aquatic ecosystems (Volk et al., 1997). Increase of biodegradability of HS by various chemical oxidation techniques has been previously observed and has been quantified utilizing $BOD_5$, TOC, $UV_{280}$, $UV_{254}$ and $Color_{400}$ (Bekbolet, et al., 1996). However, no studies have been done to investigate the increase in

biodegradability of HS due to the reactions with Mn oxides. Generally, humic and fulvic acids are unreactive with molecular oxygen ($O_2$, $E^0$=1.23 V).

The interactions between Mn oxides and humic substances involve complex surface reactions and depend on the types of functional groups present. An earlier study suggests that rapid adsorption of the humic substances to the oxides is followed by slower electron transfer at the surface to produce Mn(II) and organic oxidation products (Sunda and Kieber, 1994).

$MnO_x$, which catalyzes reactions due to their high redox potential ($MnO_2$, $E^0$ = +1.29 V), are potent oxidizing and adsorptive agents for various metallic and anthropogenic organic pollutants, as well as recalcitrant NOM. In drinking water treatment, as previously stated $MnO_x$ is used as a coated filter material (e.g., manganese greensand or pyrolusite) in packed beds to adsorb Mn(II) from solution. For a solution pH above the oxide point of zero charge (pH), the net oxide surface charge is negative and Mn(II) removal occurs by electrostatic adsorption. Mn(II) oxide-adsorption capacity decreases with lower pH and as available adsorption sites are lost, free chlorine can be intermittently or continuously added to the filter to oxidize adsorbed Mn(II) to $MnO_x$, regenerating new adsorption sites.

Despite $MnO_x$ being the most thermodynamically stable Mn form in oxidizing environments, it has been demonstrated that natural organics, structurally related phenolics and organic acid compounds are reactive with $MnO_x$, releasing mobile Mn ions into solution (Stone and Morgan, 1984, Stone, 1987, Waite et al., 1988). Reductive dissolution rates have been shown to be dependent on pH, reactant concentration and class of the organic. Furthermore, the degree of humic adsorption increases with lower pH and higher $Ca^{+2}$ concentrations (Tipping and Heaton, 1983). Natural organic matter adsorption to metal oxides has been proposed to occur by ligand exchange and surface complexation, via acidic humate groups and $OH^-$ or $H_2O$ oxide groups (Sposito, 1984; Gu et al., 1994), while FTIR and NMR spectroscopy indicates that hydroxyl and carboxyl functional groups may be the dominant NOM reactive groups involved (Gu et al., 1995).

A wide variety of aromatic compounds containing functional groups, including humic and fulvic acids, have been shown to be oxidized by Mn oxides with rate laws for the dissolution of the oxides established (Stone and Morgan, 1984; Waite et al., 1988). Sunda and Kieber (1994) have shown that synthetically prepared Mn(III,IV)-oxides can oxidize humic substances to lower-molecular-weight products including pyruvate, acetone, acetaldehyde and formalydehyde, products that can serve as growth substrate for microorganisms. In their study it was proposed that Mn(II)-oxidizing bacteria may use the biotic Mn-oxides as an oxidative agent to access the refractory organic carbon in natural environments, such as humic substances. Humic reaction with Mn(III,IV)-oxides under illumination has been shown to produce pyruvate and could provide a mechanism for a more rapid-breakdown of refractory NOM (Waite et al., 1988; Kieber et al., 1989).

# Chapter 3: Batch Reactor Studies

## 3.1 Abstract

A new bacterium, *Pseudomonas Putida* strain EC112, was isolated from a soil sample and found capable of oxidizing dissolved Mn(II) in the stationary growth phase as a carbon-stressed, enzymatic constitutive feature, not requiring added Mn for induction. Optimal Mn(II)-oxidation conditions for cultures of strain EC112, under aerobic conditions, were determined to be at pH 6.5 and 30°C. Strain EC112 can utilize a variety of growth substrates as a carbon and energy source, a trait common for the metabolically diverse *P. Putida* species. Among the trial substrates, robust growth appeared for D-glucose and benzoate.

In order to assess the effect of catalyst $MnO_2$ on humic acid biodegradability, reactors with solutions of Aldrich Humic Acids (HA) (a model humic acid) and $MnO_2$ were continuously stirred prior to inoculation with strain EC112. HA biodegradability was evaluated for the oxidized HA solutions utilizing viable cell counts (preliminary experiments only) and a modified 48-hr. Biochemical Oxygen Demand (BOD). The effect of HA-$MnO_2$ contact (stirring) time, solution pH, $MnO_2$ concentration and $Ca^{2+}$ addition on HA biodegradability were studied. Preliminary results indicated that $MnO_2$ increased HA biodegradability and is dependent on $MnO_2$ concentration and HA-$MnO_2$ contact time. Subsequent experiments using 48-hr. BOD ($mg \cdot L^{-1}$) for 50 $mg \cdot L^{-1}$ HA solutions determined optimal HA-$MnO_2$ contact time and $MnO_2$ concentration to be 45 minutes and 4.6 $g \cdot L^{-1}$, respectively. The role of solution pH and addition of $Ca^{2+}$ were significant. For reactions at pH 3.0, 7.0 and 9.0, 48-hr. BOD increased ca. 3, 5, and 0.5-fold, respectively, compared to controls. At pH 7.0, 30 $mg \cdot L^{-1}$ of added $Ca^{2+}$ significantly increased the 48-hr. BOD compared to no addition.


Stationary phase batch Mn(II)-oxidation kinetics were studied for strain EC112. Experimental Mn(II) data sets were fitted to the no-growth Monod Model using nonlinear least-squares regression and the Marquardt-Levenberg algorithm (MLA). Kinetic parameter model calibration and validation was performed using separate carbon sources for growth of strain EC112, D-glucose and the HA-$MnO_2$ products, respectively. Best fit model parameters for half-saturation coefficient, $K_s$, was 1.086 ± 0.029 $mg \cdot L^{-1}$, and for maximum specific substrate utilization rate, $k_{mc}$, 0.180 ± 0.003 Mn(II)/mg dry cell mass/hour. Autocatalytic Mn(II) removal from bulk solution by sorption to $MnO_2$ was negligible in control studies and Mn(II) kinetic data sets were modeled without such consideration.

To identify changes in HA structure induced by $MnO_2$ oxidation, Fourier transform infrared (FT-IR) and proton nuclear magnetic spectroscopy ($^1$H-NMR) of HA and HA-$MnO_2$ were obtained and interpreted.

## 3.2 Introduction

Mn(II)-oxidation has been studied with and without biocatalysts in laboratory batch reactors (Morgan and Stumm, 1964; Jung and Schweisfurth, 1976; Adams and Ghiorse, 1984; Boogerd and Vrind, 1987; Zhang et al., 2002; Jiang et al., 2010). The general observations, supplemented with other reactor and in-situ studies in aquatic natural environments, have supported the hypothesis that biological catalysts accelerate Mn oxidation rates several orders higher than homogeneous abiotic rates (e.g., direct reaction by $O_2$) (Spiro et al., 2010). Homogenous Mn oxidation at pH < 9 becomes increasingly kinetically inhibited in the absence of catalysis, implicating microorganisms as the dominant Mn(II)-oxidizers in freshwater and marine environments (Emerson et al., 1982; Hastings and Emerson, 1986; Stumm and Morgan, 1996; Tebo et al., 2005; Geszvain et al., 2012). Given the higher rates of Mn(II) oxidation mediated by bacteria, it is recognized that biological drinking water treatment processes are viable alternatives to conventional treatment for Mn in water supplies. However, even though the potential for biological Mn(II) oxidation control has been realized, little information regarding kinetics of such oxidation for pure cultures is available.

This chapter reports the isolation, growth, and Mn(II)-oxidation of a new isolate, *Pseudomonas Putida* strain EC112, in batch reactors. The specific research objectives are:

1. Isolate a Mn(II)-oxidizing bacterium and identify the species using 16s-rDNA gene sequencing.

2. Determine optimal conditions (pH and temperature) for biological oxidation of Mn(II) for isolate.

3. Evaluate isolate growth on selected carbon substrates.

4. Determine model kinetic parameters for Mn(II) oxidation utilizing a single carbon source.

5. Test the hypothesis that $MnO_2$ can enhance the biodegradability of a model humic acid and thus promote the growth of Mn(II)-oxidizing organisms.

6. Obtain the optimal concentration ratio of humic acid/$MnO_2$ and contact time for enhancing humic acid biodegradability.

7. Investigate isolate Mn(II)-oxidation kinetics in batch reactors with $MnO_2$ oxidized humic acid as the sole carbon source.

8. Identify changes in humic acid structure introduced by oxidation with $MnO_2$ using FT-IR and $^1$H-NMR spectroscopy.

## 3.3 Materials and Methods

All experiments described below were prepared using Millipore Super-Q Plus (SQ) water (18-M$\Omega$ cm$^{-1}$). Spectrophotometric sample readings were made with a GENESYS 5 Spectrophotometer (Thermo Electron Corporation, Madison, Wisconsin). Constant stiring conditions were maintained by rotary shaking using an Innova 2100 table (New Brunswick Scientific, Edison, New Jersey). Batch experiments, when cited as conducted at 30°C, were placed in an incubator room controlled at 30.2±0.2 °C. For experiments conducted below 25°C, a G-24 Environmental Incubator was employed (New Brunswick Scientific, Edison, New Jersey). When required pH adjustment was performed using 0.1 N NaOH and 0.1 N H$_2$SO$_4$ in most instances.

### 3.3.1 Bacteria Strain Isolation and Identification

Organisms that can oxidize reduced Mn(II) to insoluble, dark colored Mn(III,IV)-oxide deposits comprise a broad, phylogenetic collection, and include algae, fungi, bacteria, and protozoa  (Tebo et al., 2005; Geszvain et al., 2012) Among these, bacteria, and more recently recognizing  fungi, are considered to possess the most robust Mn(II)-oxidation rates (Greene and Madgwick, 1991; Tebo et al., 2005).  Clear explanation for a physiological function for the  widespread ability among organisms to oxidize Mn is lacking, however, with bacteria considered to be the first organisms to evolve on earth, they may have been the first Mn(II)-oxidizing organisms, preceding the eukaryotes (Spiro et al., 2010; Geszvain et al., 2012).

Mn(II)-oxidizing bacteria, which normally reside in pH environments in the range 6 – 8, can be readily isolated from virtually any aquatic or terrestrial habitat, and favor aerobic environments containing several micromoles of Mn (Depalma, 1994; Tebo et al., 2005; Nealson, 2006). A diverse array of Mn(II)-oxidizing bacteria and fungi have been isolated from man-made biofilters, rapid sand filters, water distribution systems, and passive water treatment systems (Czekalla et al., 1985; Murdoch and Smith, 2000; Santelli et al., 2010; Cerrato et al., 2010).  Three model manganese oxidizing bacteria and their cultivation have been described in detail: *Bacillus* sp. Strain SG-1, a marine, spore-forming organism isolated from a near-shore sediment (Nealson et al., 1980); the freshwater, sheath-forming *Leptothrix discophora* strain SS-1, isolated from a metallic surface film collected from a swamp-pond (Ghiorse and Hirsch, 1979); and *Pseudomonas Putida* MnB1, which represents one of the first well-studied Mn(II)-oxidizing bacteria in batch reactors. Strain MnB1 oxidizes Mn(II) during the stationary growth phase and was cultivated from a Mn-oxide deposit sample collected from a drinking water pipeline (Schweisfurth, 1973).

Generally, Mn(II)-oxidizing bacteria are not discriminating with respect to carbon source and pure cultures have been isolated in liquid or solid media using simple organic sources (e.g., acetate, glucose, glycerol) or undefined  media, containing yeast extract and peptone (Nealson, 2006).  Enrichment culture techniques, though frequently used, have shown

minimal advantages and elevated levels of Mn(II) can be inhibitory to successful cultivation (Nealson, 2006).

Using the following procedures, a Mn(II)-oxidizing bacterium *Pseudomonas Putida* strain EC112 was isolated from a surface soil sample, collected near the main sidewalk bisecting University of Kentucky's Main Field in June 2007 (also known as the Great Lawn) in Lexington, KY. Using an iPhone 4S, the A-GPS coordinates were measured to be 38.03926°N and 85.50555°W in March 2013. During collection, the sample was field tested for oxidized Mn with addition of a few drops of the redox colorimetric reagent LeucoBerbelin Blue I (LBB, Sigma-Aldrich), prepared as described below. Formation of a deep blue color confirmed the presence of oxidized Mn.

Laboratory isolation procedures for strain EC112 began by adding 1 to 2 grams of soil particle sample to 400-ml Kimax glass beakers, each containing 200-ml of isolation media. The isolation media consisted of SQ water supplemented with (mg·L⁻¹): α-D-glucose, 10 (Sigma-Aldrich); Bacto™ Yeast Extract, 5 (BD™ Difco); and Mn(II), 2 from stock solution (MnSO$_4$·H$_2$O, Fischer Scientific). Following 3 days of incubation at 30°C, a brown, metallic film developed on the water's surface in one of the glass beakers. Addition of LBB to a sample of the brown film confirmed the presence of oxidized Mn. A loopful of the crusty, surface film was transferred to a 500-ml Erlenmeyer flask containing 300-ml of autocalved isolation media. The flask was capped with a sterile cotton plug and wrapped with aluminum foil prior to incubation at 30°C on a rotary shaker set at 130 rpm. Within 24 hours, suspended brown particles were observed in the liquid media and Mn(II) oxidation was again confirmed using LBB. This was followed by collection and transfer of 1-ml sample of the liquid media to a 500-ml Erlenmeyer flask containing 300-ml of the isolation media. After 3 transfers, 5 to 10 mg·L⁻¹ of Aldrich Humic Acid (HA) (unpurified as sodium salt) was added to the culture media. Enrichment of the isolation media was added to favor isolation of a Mn(II)-oxidizing bacteria strain(s) capable of utilizing humic acids as a carbon source. Mn(II)-oxidation was observed within 24 hours, and a loopful of the brown, suspended precipitates were streaked on PYG agar plates containing 5 mg·L⁻¹ of Mn(II). Flat, brown colonies were observed growing on the surface of the agar within 24 hours. Spot tests with LBB directly on several brown colonies confirmed the presence of Mn oxide.

A pair of agar plates containing the brown colonies was shipped to Laragen, Inc. (Los Angeles, CA) for organism identification. Using the 16S rDNA partial sequencing technique, universal primers amplified a ~1200 bp 16S rDNA fragment (Appendix A). The consensus sequence had a 100% match with *Pseudomonas Putida* using GenBank, referenced in this study as *P. Putida* strain EC112.

### 3.3.2 Bacteria Strain Maintenance

For short term preservation, strain EC112 was maintained on agar plates stored in a 4°C (4°C±1°C) walk-in incubator. In 2 to 3 week intervals, fresh cultures were grown and a loopful of fresh culture was used for agar plate streaking. A sterile inoculation loop was used to transfer isolate culture (i.e., a colony) from a PYG agar plate to a sterile 1-L Erlenmeyer flask containing 250 to 500-ml of autoclaved PYG media. Following overnight growth at 30°C on a rotary shaker (set at 130 rpm), cells grew to the middle stationary growth phase based, according to optical (cell) density (OD) measurements using a spectrophotometer at 600 nm (OD$_{600}$=0.350 to 0.600). A loopful of growing culture was streaked on a PYG agar plate under a germ-free hood and kept at 30°C incubation for 24 to 48 hours. Strain EC112 typically forms flat, brown colonies within 24 hours on the surface of the agar plates and were transferred for storage at 4°C. Streak plates were sealed using Parafilm® M.

The agar medium was prepared by adding 15 g·L$^{-1}$ Difco™ Nutrient Agar (Becton, Dickinson and Company) to the PYG media. Solutions were autoclaved for 15 minutes at 121°C prior to addition of 1-2 mg·L$^{-1}$ of Mn(II) (stock solution) to the hot solution. Approximately 15 to 20-ml aliquots of the hot solution were poured into 100 mm x 15 mm petri dishes (Fischer Scientific) under the germ-free hood. Plates were allowed to cool at room temperature prior to storage at 4°C.

For long term (6 months – 2 years) preservation, strain EC112 cells were stored in a -80°C freezer (Thermo Scientific Revco Upright Freezer, Model ULT 1386-3-A36). For storage preparation, cells were grown in PYG media or NB media to middle exponential growth phase at 30°C on a rotary shaker (set at 130 rpm). A 1-ml of culture was pipetted to a 2.0-ml microcentrifuge tube (with snap caps) and 1-ml of 20%(v/v) glycerol (C$_3$H$_8$O$_3$, 92.09 g·mol$^{-1}$) was added. Tubes were capped and hand agitated a few seconds prior to placement in the freezer.

### 3.3.3 Bacteria Strain Harvesting

Isolate cultures for all experiments were grown for harvesting using either PYG Media or NB. Cultures for experiments utilizing glucose as the primary carbon substrate were harvested from PYG Media, while all others (primarily those utilizing HA) were harvested in NB Media, with pH adjusted to 6.5 to 7.0. A colony of strain EC112 from a PYG agar plate stored at 4°C were added to autoclaved, 500-ml of harvest media in a 1-L Erlenmeyer Flask and placed on a rotary shaker (set at 130 rpm) in the 30°C temperature controlled walk-in incubator. Cells were harvested following 10-12 hours when the middle to late exponential phase of growth was reached.

Harvested cells were washed three times with 20-ml of 7.5% NaCl solution followed by centrifugation at 4000g for 10 minutes. The cell pellet was resuspended in 20-ml of trace metal solution prior to use.

### 3.3.4 Media and Stock Solution

Harvested isolate cultures for all experiments were grown using either the PYG Media or NB Media. Mn(II) stock solutions were prepared as described in section 3.3.4.6 below. All experiments were conducted in low-light conditions.

### 3.3.4.1 Peptone-Yeast-Glucose (PYG) Media

PYG media consisted of ATCC Medium 1503 *Leptothrix* 2X PYG with minor modifications. The media was prepared by adding 2 mg·L$^{-1}$ MnSO$_4$· H$_2$0, 0.5 g of α-D-glucose (Aldrich Chemical Company), 0.5 g Bacto$^{TM}$ Peptone (BD$^{TM}$ Difco), 0.5 g Bacto$^{TM}$ Peptone Yeast Extract (BD$^{TM}$ Difco), 2.57 g of HEPES acid (Sigma-Aldrich), 0.6 g of MgSO$_4$ ·7 H$_2$0 and 0.07 g of CaCl$_2$·2 H$_2$0 to 1-L of SQ water in a screw cap Pyrex bottle. MnSO$_4$·H$_2$0 was added first to minimize chemical precipitation of Mn(II) ions. PYG media solutions were filter sterilized using 0.22μm Stericup® GV Filters.

### 3.3.4.2 Nutrient Broth (NB) Media

NB media was prepared in sterile 1-L Erlenmeyer flasks by adding 2 g·l$^{-1}$ Difco Nutrient Broth medium supplemented with 0.6 MgSO$_4$ ·7 H$_2$0 and 0.07 g CaCl$_2$·2H$_2$O to 500-ml of SQ water. The NB media was autoclaved for 15 minutes at 121°C prior to the addition of 1 mg·L$^{-1}$ of Mn(II) from stock solution.

### 3.3.4.3 Substrate Screening Media

The basal media for the substrate screening experiments was prepared by adding 50 mg·L$^{-1}$ (or equivalent in μM) of each carbon substrate to the following basal media (mg·L$^{-1}$): (NH$_4$)SO$_4$, 5; H$_2$KPO$_4$, 10; K$_2$HPO$_4$, 10; CaCl$_2$·2H2O, 10; MgSO$_4$·7 H$_2$O, 20; Mn(II), 1; trace metal solution, 1-ml.

The trace element solution was prepared by adding 6.5 mL of HCl (25%), 1.5 g of FeCl$_2$·4 H$_2$O, 60 mg of H$_3$BO$_3$, 120 mg of CoCl$_2$·6 H$_2$O, 70 mg of ZnCl$_2$, 25 mg of NiCl$_2$·6 H$_2$O, 15 mg of CuCl$_2$·2H$_2$O and 25 mg of Na$_2$MoO$_4$·2 H$_2$O to 1-L of SQ water.

### 3.3.4.4 Glucose Media

Glucose media was prepared by aseptically adding 0.5 g of α-D-glucose (Aldrich Chemical Company), 0.05 g of $MgSO_4 \cdot 7 H_2O$, 0.05 g $(NH_4)SO_4$, 0.05 g $H_2KPO_4$, 0. 07 g of $CaCl_2 \cdot 2 H_2O$ to 1-L of SQ water in a screw cap Pyrex bottle. The concentration of Mn(II) added from stock solution, depended on the experiment, and was added first to minimize chemical precipitation of Mn(II) ions. Final solutions were filter sterilized using 0.22μm Stericup® GV Filters.

### 3.3.4.5 Humic Acid Stock Solution

Aldrich Humic Acid (HA)

Humic acid was purchased from Sigma-Aldrich (technical grade, Germany) as sodium salt (Batch #: 07726DD). For purification of stock solution, 1 g of HA was added to 1-L SQ water containing 0.5% (v/v) concentrated HF/HCL solution. The solution was stirred for 12 hrs. with a magnetic stirrer prior to a 30 min. centrifugation at 4500 rpm for insoluble residue removal. The residue was then washed with SQ water prior to being added to a NaOH solution at pH 9 and placed on a rotary shaker table overnight. The solution was then filtered using a 0.22μm Stericup® GV Filters.

HA characterization was not performed in this study but obtained from literature. Published elemental analysis of purified Aldrich Humic Acid (PAHA) consists of (wt %) C, 60.0 %; O, 34.5%; H, 4.5%; and N, 1.0%, and is comparable to other commercial humic acids. The degree of ionization for AHA is reported to be >90% at pH above 7, determined by direct titration (using $NaClO_4$ at 20°C) (Kim et al., (1990)). AHA molecules have a broad molecular weight range (1000 kDa to > 300kDa) and an average molecular weight ($M_w$) of 4,500 - 23,000 (Beckett et al., 1987; Chin and Gschwend, 1991; Vermeer et al., 1998).

### 3.3.4.6 Mn(II) Stock Solution

Mn(II) stock solution was prepared by adding 3.076 g of $MnSO_4 \cdot H_2O$ to 1-L of SQ water to make a 1000 mg$\cdot$L$^{-1}$ solution of Mn(II). The solution was standardized according to Standard Methods 3500-Mn B (APHA, 1998) and stored at 4°C in subdued light conditions.

### 3.3.4.7 *Pseudomonas Putida* MnB1

*Pseudomonas Putida* MnB1 (ATCC 23483) was purchased from American Type Culture Collection (ATCC). Growth and Mn(II)-oxidation was investigated for strain MnB1 and strain EC112 in parallel experiments. Upon receipt of the culture from ATCC, strain MnB1 was immediately revived following ATCC procedures for bacteria. This involved aseptically

adding 0.5-ml of PYG liquid medium to the freeze-dried culture and mixing. A small aliquot of this solution was then pipetted to a sterile 500-ml Erlenmeyer flask containing 200-ml of autoclaved PYG media. The flask containing the MnB1 culture was placed on a rotary shaker (set at 130 rpm) at 30°C for overnight growth.  Streak plates were made from this growing liquid culture and stored at 4°C.

### 3.3.4.8 MnO$_2$

Manganese dioxide (MnO$_2$) was obtained from Inversand Co. (Clayton, H.J.) as GreensandPlus (GSP), a product replacement for manganese greensand. GSP, a catalytic filter media widely used in drinking water treatment primarily for Mn and Fe sorption/oxidation, consists of 0.30 to 0.35 mm sized silica (SiO$_2$) sand nodules (≥96% of the bulk mass), with a thermally fused exterior coating of MnO$_2$. GSP was pre-treated prior to use, as recommended by the manufacturer by soaking in 4.0 g·L$^{-1}$ KMnO$_4$ solutions then rinsed thoroughly in flowing SQ water.

Powder X-ray diffraction patterns of GSP  were recorded on a Bruker-AXS D8 Discover diffractometer using Cu K$\alpha_1$ radiation ($\lambda$ = 1.5406 Å) with a step size of 0.02° and 2$\Theta$ range of 20-70°.  The sand nodules were ground to a fine powder prior to analysis using a mortar and pestle. Sharp, narrow diffraction XRD patterns indicated the powder consisted of crystalline matter, primarily $\delta$-MnO$_2$ (birnessite) mixed with smaller amounts of $\alpha$-Mn$_3$O$_4$ (hausmannite) and Mn$_2$O$_3$ (bixbyite). The strongest peak identified was the quartz (SiO$_2$ sand nodules) core.

The Mn oxidation state was determined by iodometric titration using duplicate flasks (Murray et al, 1984).

The average pore width and Barrett–Emmett–Teller (BET) surface area of the GSP nodules were determined using a Micromeritics TriStar 3000 analyzer and the N$_2$ adsorption and desorption isotherms. The Barrett–Joyner–Halanda (BJH) method was used to derive the average pore width from the isotherm adsorption branches The pH at the point of zero charge (PZC), pH$_{pzc}$, of GSP was determined by potentiometric titration (Raij and Peech, 1972).

### 3.3.5 Analytical Methods

### 3.3.5.1 Mn(II)

Mn(II) was determined using the persulfate method (3500-Mn B in  Standard Methods (APHA, 1998)).  In this method, persulfate (S$_2$O$_8^{-2}$) is added to the sample, oxidizing soluble Mn(II) to permanganate (Mn(VII)). The violet color is subsequently measured colorimetrically using a spectrophotometer at 525 nm. Prior to the addition of persulfate, samples were centrifuged for 10 minutes and/or filtered using a 0.22 $\mu$m filter to remove particulate Mn.

### 3.3.5.2 Mn(IV)

Mn(IV) concentration was measured colorimetrically with the LeucoBerbelin blue assay (LBB) (Krumbein and Almann, 1973; Boogerd and de Vrind, 1987). LBB is a reduced triphenyl compound dye that reacts with oxidized $Mn(III,IV)O_x$. The deep blue color froms in seconds and is measured at 620 nm using a spectrophotometer. Raw samples (0.1 ml) containing Mn were added to 0.5 ml of 0.04% LeucoBerbelin I blue in 45 mM acetic acid. The calibration curve for Mn(IV) measurement were prepared with $KMnO_4$.

### 3.3.5.3 Dissolved Organic Carbon (DOC)

Humic acid concentration was characterized as Dissolved Organic Carbon (DOC) using a Total Organic Carbon (TOC) analyzer (Shimadzu, TOC-VCSH).  Samples were centrifuged for 10 minutes at 10,000 rpm (Eppendorf 5415C centrifuge) and/or filtered with 0.22 μm membrane filters (PVDF, Millipore) then preserved with 2 drops of 2 N HCL. Samples were stored at 4°C prior to analysis.

### 3.3.5.4 UV$_{254}$

In addition to DOC, UV absorbance at 254 nm (UV$_{254}$) was measured to characterize HA concentration. Samples were centrifuged at 10,000 rpm for 10 minutes and/or filtered using a 0.22 μm membrane filter (PVDF, Millipore) prior to the spectrophotometer reading.

### 3.3.5.5 Glucose Assay

Glucose was determined using the Nelson's colorimetric modification of Somogyi's procedure (Hodge and Hofreiter, 1962). Briefly, 2 ml of arsenomolybdate solution was added to an equal mixture of boiling copper reagent and sample. Development of a green-orange color was read using a spectrophotometer at 500 nm (Chirwa, 2000).

### 3.3.5.6 Strain EC112 Growth

The following methods were used to enumerate batch bacteria growth:  (1) spectrophotometric, (2) standard plate count, (3) volatile suspended solids (VSS), and (4) a modified Biochemical Oxygen Demand (BOD).

### 3.3.5.7 Spectrophotometric

Cell density was measured by optical density at 600 nm using a spectrophotometer (Spectronic Genesys 5) as an indirect measure of cell growth.

### 3.3.5.8 Standard Plate Count

The suspended cell count was determined following the spread plate method in Section 9215-C of Standard Methods (1998, APHA). The agar medium for the spread plate method was prepared as described in section 3.3.2 without the addition of stock Mn(II).

### 3.3.5.9 Volatile Suspended Solids (VSS)

Total biomass dry weight was measured as volatile suspended solids (VSS) following Section 2540-E of the Standard Method (APHA, 1998).

### 3.3.5.10 Biochemical Oxygen Demand (BOD)

Biochemical oxygen demand (BOD) was used as a measure of HA biodegradability. Standard Methods 5210-B 5-Day BOD Test was followed (1998, APHA) with two minor modifications: (1) strain EC112 served as the seed and the incubation temperature was 30°C instead of 20°C, and (2) the incubation period was 48-hrs., shortened from the standard 5-day. Samples were filled in standard 300-ml capacity glass bottles and capped with ground-glass stoppers. Samples were analyzed promptly on conclusion of the 48-hr. incubation period.

### 3.3.6 Substrate Screening Evaluation

Substrate screening tests were performed to evaluate strain EC112 growth on single carbon sources under aerobic conditions at 30°C and pH 7.0±0.25. Approximaely 50 mg·L$^{-1}$ of carbon source at 50 mg·L$^{-1}$ was added to 50-ml of basal media then inoculated with 0.5-ml aliquot of harvested culture in 200-ml flasks. The flasks (duplicates) were placed on a rotary shaker (set at 130 rpm) for 5 days and observed for changes in optical density.

### 3.3.7 Optimal pH and Temperature for Mn(II)-Oxidation

The effect of pH (5.5, 6.0, 6.5, 7.0, 7.5, 8.0) and temperature (5-35°C) on Mn(II)-oxidation by strain EC211 were evaluated separately for glucose, HA, and without added carbon. The carbon source was added to basal media as prepared as in section 3.3.4.3 with 50 mg·L$^{-1}$ of carbon substrate. Three of the Good's buffer's were selected for pH control: 5.0 – 6.0 [MES (2-(*N*-morpholino)ethanesulfonic acid), pK$_a$=6.10 at 25°C]; 6.5-7.0 [PIPES (piperazine-N,N′-bis(2-ethanesulfonic acid), pK$_a$=6.76 at 25°C], and 7.5-8.0 [HEPES (4-(2-hydroxyethyl)-1-piperazineethanesulfonic acid), pK$_a$=7.48 at 25°C] (Larsen et al., 1999).

Experiments were initiated by adding 5 % (v/v) of harvested culture obtained according to Section 3.3.3 to 250 ml of media in sterile 500-ml Erlenmeyer flasks adjusted to the appropriate pH. Samples were collected for Mn(II) analysis at appropriate intervals.

## 3.3.8 Chemical and Biological Controls

Experimental controls were conducted to differentiate between biologically catalyzed Mn(II)-oxidation (direct oxidation by strain EC112) and other potential oxidation/removal processes, including passive biosorption (e.g., sorption by the negative surface charges on bacterial surfaces, exopolysaccharides (EPS) or biogenic Mn(III,IV) oxides) and chemical oxidation or precipitation by components of the experimental media. The general approach involves adding known amounts of Mn(II) to flasks containing inactivated cells (for biological controls) and the various chemical media (for chemical controls) and monitoring Mn(II) over time. For biological controls, the use of poisons or metallo-enzyme inhibitors, e.g., redox enzyme inhibition by sodium azide ($NaN_3$) or cyanide ($CN^{-1}$), is a common technique to inactivate redox enzymes in laboratory cultures, but was avoided in this study due to the robust metabolism characteristic of strains of *P. Putida*. As an alternative, strain EC211 was autoclaved at 121°C for 15 minutes to 'kill' or inactivate biologic Mn(II)-oxidizing ability (Dastidar and Wang, 2010).

Chemical controls were prepared in 100-ml solutions of 250 mg·L$^{-1}$ PYG media in 500-ml Erlenmeyer flasks spiked with 11 mg·L$^{-1}$ Mn(II). Biological controls were prepared by adding 20 mg of inactivated cells to 100-ml of SQ water in 500-ml flasks. The cells were first grown separately in 500-ml of PYG media containing 5 mg·L$^{-1}$ Mn(II) and harvested following Mn(II) oxidation in stationary phase by centrifugation.

To evaluate the effect of cell sorption as a Mn(II) removal mechanism from solution, both Mn(II) and Mn(IV) were monitored in an additional Mn(II)-oxidation experiment.

## 3.3.9 FT-IR-Spectroscopy of Aldrich Humic Acids

Samples for FT-IR-Spectroscopy analysis were prepared by freeze-drying solutions of $MnO_2$ oxidized HA and HA prepared as described in Section 3.3.11. The freeze dried samples were ground and mixed with infrared grade KBr pellets at a concentration of approximately 2%. Spectra were recorded in absorbance mode on a Nicolet FT-IR 6700 Spectrometer. Spectral resolution was 4 cm$^{-1}$ and 16 scans were run. Spectra were normalized to a maximum of 1.0 for comparison (He et al., 2009).

## 3.3.10 $^1$H-NMR of Aldrich Humic Acids

Samples for $^1$H-NMR -Spectroscopy analysis were prepared by freeze-drying solutions of Ha-$MnO_2$ and HA.

$^1$H-NMR spectra of the freeze dried samples in 5 mm diameter probes were acquired with a Varian INOVA 400 Mhz. Approximately 25 mg of HA was dissolved in 0.5 ml of $D_2O$. Methanol was the internal reference standard (3.3 ppm). Spectra were obtained using 1024 scans, 8400 Hz spectrum width, acquisition time of 1s and a 1.5s pulse delay (Weng et al., 2006).

## 3.4 Mn(II) Oxidation Kinetic Analysis

The kinetics of Mn(II) oxidation in batch cultures of strain EC112 was analyzed using the Monod kinetic expressions which are frequently used to model the relationship between microbial growth and substrate depletion. Various modifications to these equations have been applied, including zero-, first-order and no growth kinetics (Simkins and Alexander, 1984). These nonlinear, ordinary differential equations can be integrated and estimation of the model kinetic parameters can be obtained by fitting the single substrate (S) consumption data to t (time) using the integrated forms and nonlinear regression. The consumption rate of the substrate is represented by the kinetic parameters $k_{mc}$ and $K_s$ (Eqns. 3-1 and 3-2).

$$\frac{dX}{dt} = [\frac{k_{mc}S}{K_S + S}]YX \qquad (3\text{-}1)$$

$$\frac{dS}{dt} = -[\frac{k_{mc}S}{K_s + S})]X \qquad (3\text{-}2)$$

Where X=bacteria biomass (mg), S=Mn(II) concentration (mg/L), $k_{mc}$=maximum specific Mn(II) oxidation rate, $K_s$=half-velocity saturation rate, Y= yield coefficient. The Lenvenberg-Marquardt nonlinear least-squared algorithm is used to optimize the Monod model parameters using SigmaPlot 11.0 (Systat Software Inc.). The optimized model parameters will be obtained by minimizing the residual sum of squares (SSE) between experimental data and model calculated values as given by Eqn. 3-3:

$$\text{SSE} = \sum_{n=1}^{n} \left( S_i^{obs} - S_i^{pred} \right)^2 \qquad (3\text{-}3)$$

where $S_i^{obs}$ is the measured Mn (II) concentration in the $i^{th}$ experimental sample, and $S_i^{pred}$ is the corresponding model prediction of Mn (II) for the same sample point.

## 3.5 Sensitivity Analysis

Evaluation of whether the kinetic model parameters representing Mn(II) oxidation may be optimally estimated using nonlinear regression relies on the use of sensitivity coefficients. Sensitivity coefficients measure the sensitivity of the dependent variable, S, to changes in

each model parameter and are used to predict the uniqueness and relative precision of the estimated parameters (Robinson and Tiedje, 1983). Derivation of the sensitivity equations are obtained by determining first derivatives $\dfrac{dS}{dK_S}$ and $\dfrac{dS}{dk_{mc}}$ of the model with respect to each model parameter. The sensitivity equations for the batch kinetic model parameters, $K_s$ and $k_{mc,}$ are obtained by taking the first derivative of the integrated no growth Monod model with respect to each parameter, using implicit differentiation (Simkins and Alexander, 1984) (Eqns. 3-4 and 3-5).

$$\frac{dS}{dk_{mc}} = -\frac{t}{\frac{K_S}{S}+1} \tag{3-4}$$

$$\frac{dS}{dK_S} = -\frac{\frac{\ln S_0}{S}}{\frac{K_S}{S}+1} \tag{3-5}$$

The sensitivity equations are plotted against the independent variable, t, allowing a curve comparison and evaluate where the model is most sensitive to changes in parameters (Robinson and Tiedje, 1983).

## 3.6 Results and Discussion

### 3.6.1 MnO$_2$ Characterization

The Mn oxidation state of the surface coating of Mn oxide on the GSP nodules was determinedto be 3.95±0.03, by iodometric titration (Murray et al., 1984). For comparision, the Mn oxidation state of δ-MnO$_2$ has been measured at 4.02 (Villalabos, 2003).

The average pore width and Barrett–Emmett–Teller (BET) surface area of the GSP nodules were 6.28 nm and 2.637 m$^2 \cdot$g$^{-1}$, respectively. Lie et al., (2001) report a specific surface area of 2.53 m$^2 \cdot$g$^{-1}$ for birnessite (δ-MnO$_2$), which is comparable to the result obtained for GSP. In addition, the mineral pyrolusite (β-MnO$_2$), a filter material also used in water treatment for Mn/Fe removal, has reported IEP and specific surface areas of 4.3 to 4.4 and 2.2 m$^2 \cdot$g$^{-1}$, respectively  (O'Reilley and Hochella, 2003; Cristiano et al., 2011).

The pH at the point of zero charge (PZC), pH$_{pzc}$, of GSP is 4.5, determined by potentiometric titration, and shown on Figure 3.1 where the MnO$_2$ surface begins to have a net negative surface charge (Raij and Peech, 1972).  The net surface charge increases sharply above pH 8.

The Mn oxide surface coating for GSP may be best compared to birnessite, δ-MnO$_2$, in terms of oxidation state and dominant XRD diffraction patterns, but will be referenced as MnO$_2$. Discrepancies in oxidation state between the mixed phases determined by XRD (+3 and +4) and the oxidation state from titration may be that transition metal oxides, such as MnO$_2$, are characteristically non-stoichiometric.
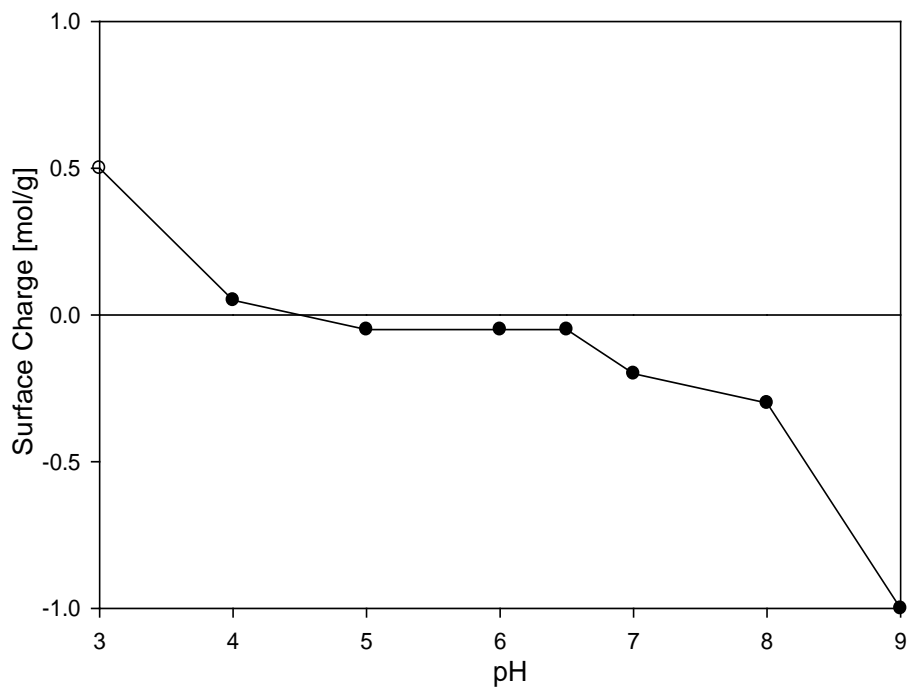
**Figure 3.1:** Surface charge ($H^+$) of $MnO_2$ (GreensandPlus) determined from potentiometric titration (duplicate averages).

### 3.6.2 Substrate Screening Experiment

As shown in Table 1, strain EC112 demonstrated the ability to grow on six-carbon sugars, organic acids, and recalcitrant organic substrates, representative of the diverse metabolism similar to other *Pseudomonads* and *P. Putida* strains. *P. Putida* strains have been demonstrated to have the most versatile number of enzymes capable of cleaving aromatic and aliphatic hydrocarbon bonds. For example, *P. Putida* CSV86 utilizes aromatics such as benzaldehyde, benzyl alcohol, naphthalene, and benzoate prior to glucose (Basu et al., 2009).

Growth was particularly strong for glucose and sodium benzoate, a monoaromatic, bacteriostatic acid. Without the addition of organic carbon, or with the addition of inorganic carbon (as sodium bicarbonate), no growth is observed, indicating the isolate is an aerobic heterotrophic.

The apparent utilization by strain EC112 of acetone, acetaldehyde, formaldehyde, and pyruvate as substrate is particularly of interest. These aldehydes and keto acids have been all have been identified as products of the reaction between humic substances and Mn Oxide (Sunda and Kieber, 1994). This result suggests that strain EC112 may have the ability to grow on humic substance oxidation products as microbial growth substrates.

### 3.6.3 Biological and Chemical Controls for Mn(II)-Oxidation

The time-course Mn(II) data shown in Figure 3.2 for chemical and biological controls indicate negligible Mn(II) removal from solution. This observation is supported by computation of the relative standard deviation (RSD) and test for slope significance (determined by the P-value) of a regression line for each data (n=4) set. The RSD computed for the chemical and biological control data set are 6.29% and 6.67% respectively, within the analytical error of 26.3% for a synthetic sample containing Mn and analyzed by several laboratories, according to Standard Methods for the Mn assay using the persulfate method (3500-Mn B). P-values for the slope significance of the regression line fitted to each data sets are p=0.115 and p=0.853, which exceed the 0.05 significance level, supporting that the slope is equal to zero (i.e., no significant change in Mn(II) concentration with time). It can be concluded that neither the PYG chemical media nor inactivated strain EC112 cells encrusted with Mn(III,IV) act as oxidizing/removal mechanism for Mn(II).
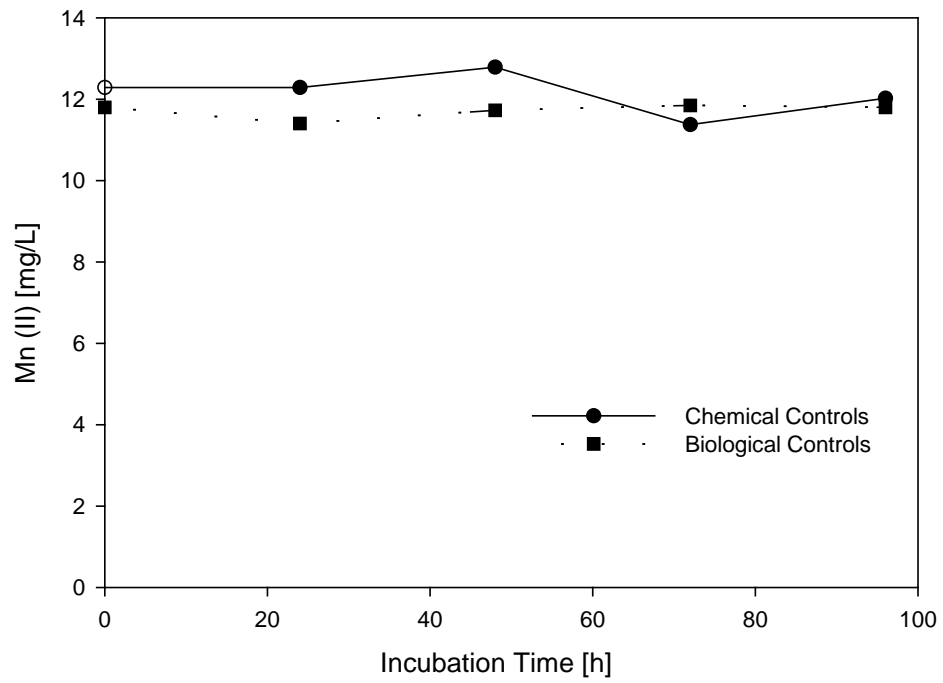
**Figure 3.2:** Mn(II) concentration in chemical and biological controls.

To investigate the oxidation of Mn(II) and the concurrent production of Mn(IV) by strain EC112, both Mn(II) and Mn(IV) were monitored in batch experiments (Figure 3.3). The initial and final Mn(II) concentration were 0.72 mg·L$^{-1}$ and 0.70 mg·L$^{-1}$, exceeding 95% recovery,  indicating cell sorption is not a significant Mn(II) removal mechanism.
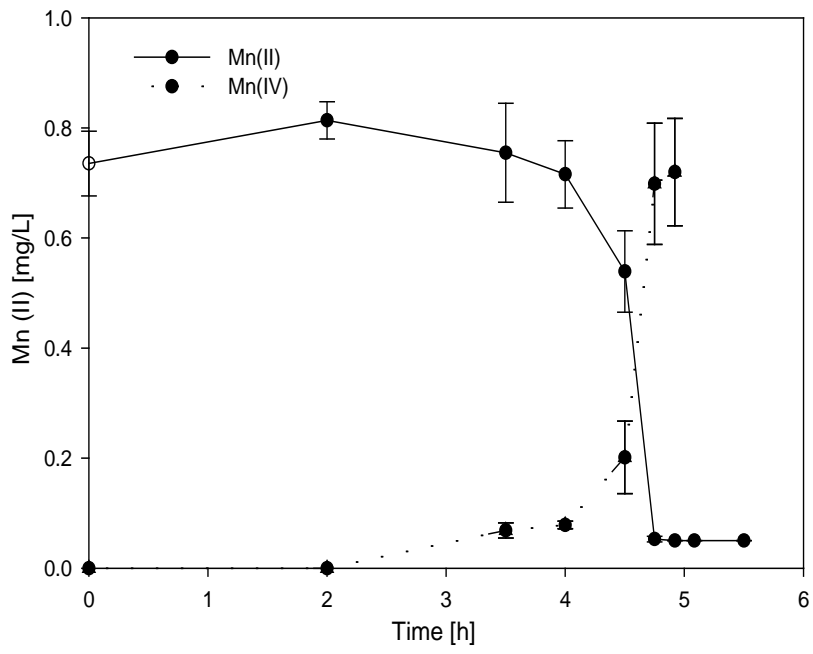
**Figure 3.3:** Mass Balance of Mn(II) and Mn(IV) for Mn(II) oxidation by strain EC112.

### 3.6.4 Strain EC112 Comparison to *Pseudomonas Putida* MnB1

Mn(II) oxidation and growth of strain EC112 and MnB1 (ATCC 23483), a model Mn(II)-oxidizer, were investigated in parallel experiments, provided glucose as the sole carbon source. Growth, Mn(II)-oxidation (shown as Mn(IV) production), and glucose consumption for each strain under identical conditions are   shown in Figure 3.4. The results show comparable growth and Mn(II) oxidation rates for both strains. Stationary growth phase is reached 3 to 4 hrs. after cell innoculation onset of Mn(II) oxidation and concomitant production of Mn-oxides.
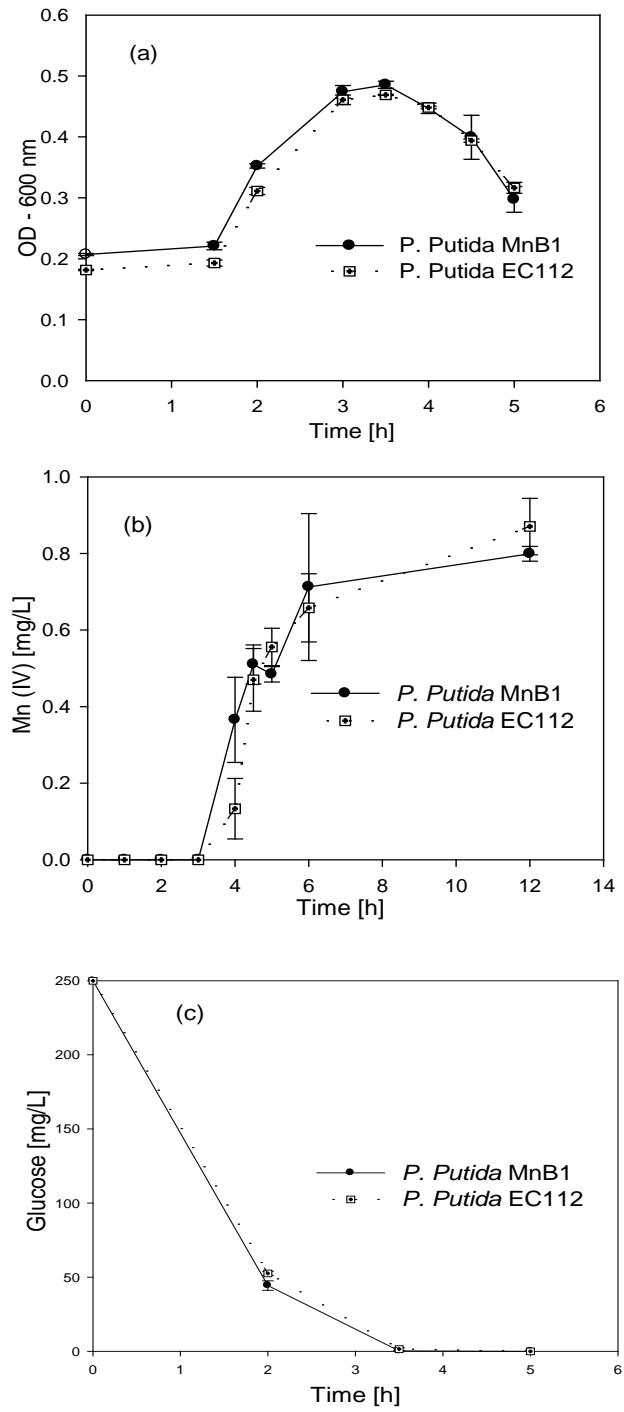
**Figure 3.4:** *P. Putida* strain EC112 and MnB1 comparison, (a) growth, (b) Mn(II) oxidation (measured as Mn(IV)), and (c) substrate (glucose) consumption.

### 3.6.5 Effect of Mn(II) and Glucose Spikes on strain EC112 Mn(II)-oxidation

Drinking water utilities report that treatment of Mn in raw source waters with variable amounts of Mn presents more significant challenges to conventional treatment than those with constant, high levels of manganese. Specifically, untreated waters with maximum Mn to average concentration ratios greater than 10:1 have been frequently observed to be the most problematic (Kohl and Medlar, 2006). To evaluate the effects of sudden variations in Mn(II) concentration on recoverability and sustainability of Mn(II)-oxidation, Strain EC112 cultures were repeatedly spiked with Mn(II) or glucose, respectively.

The results of Mn(II) spikes are shown in Figure 3.5, where the liquid medium initially contains 250 $mg\cdot L^{-1}$ glucose and 1 $mg\cdot L^{-1}$ Mn(II). The time course shows glucose consumption is complete by 3 hours, shown in Figure 3.5a, and no further amounts are added, followed by oxidation of the initial 1 $mg\cdot L^{-1}$ of Mn(II) within 4 hours. Subsequent Mn(II) spikes of 21, 30 and 14 $mg\cdot L^{-1}$ at 7, 12, and 23 hours respectively, shown in Figure 3.5b, were all subsequently oxidized below 0.05 $mg\cdot L^{-1}$. These results demonstrate the robustness of strain EC112 to oxidize relatively high concentrations of Mn under repeated Mn(II) spikes without the growth substrate glucose.

The results of Mn(II) and glucose spikes are shown in Figure 3.6, where the liquid medium initially contains 175 $mg\cdot L^{-1}$ glucose and 6.3 $mg\cdot L^{-1}$ Mn(II). Glucose consumption is near complete by 2 hours (Figure 3.6a), followed by oxidation of the initial 6.3 $mg\cdot L^{-1}$ of Mn(II) within 6.5 hours (Figure 3.6b). At 11.5 hours, spikes of Mn(II) (6.5 $mg\cdot L^{-1}$) and glucose (170 $mg\cdot L^{-1}$) were added to the batch cultures. Subsequent oxidation of both substrates demonstrate that strain EC112 can oxidize Mn(II) in the presence of significant glucose concentration.
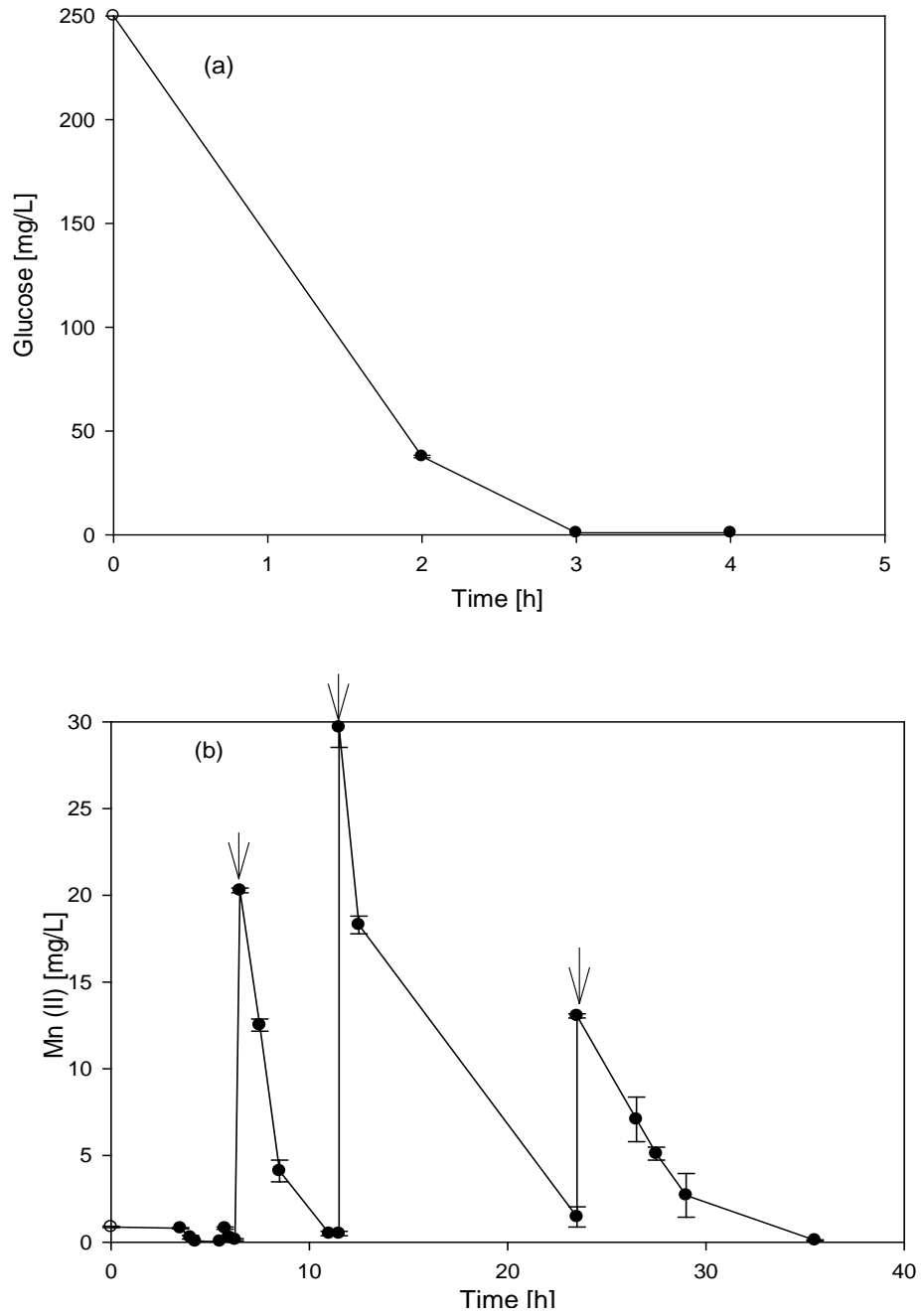
**Figure 3.5:** Mn(II) spikes and subsequent Mn(II) oxidation, (a) glucose consumption for strain EC112, (b) Mn(II) spikes (indicated with arrow).
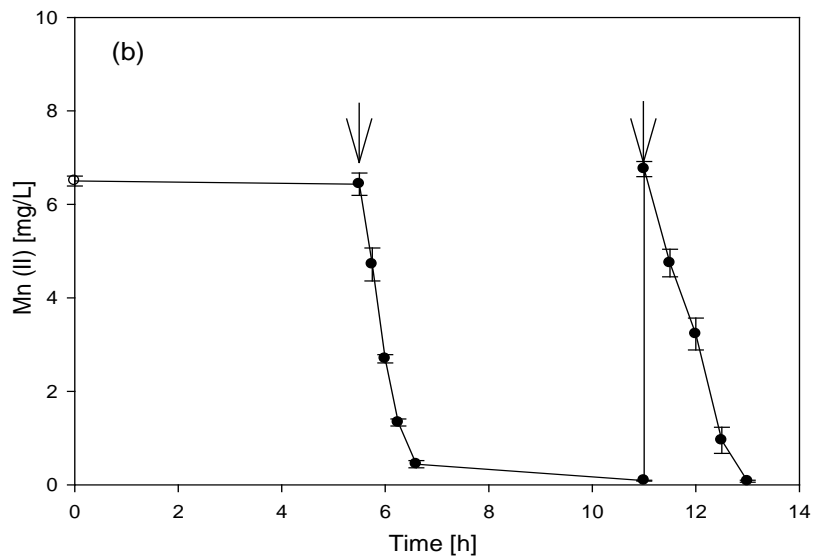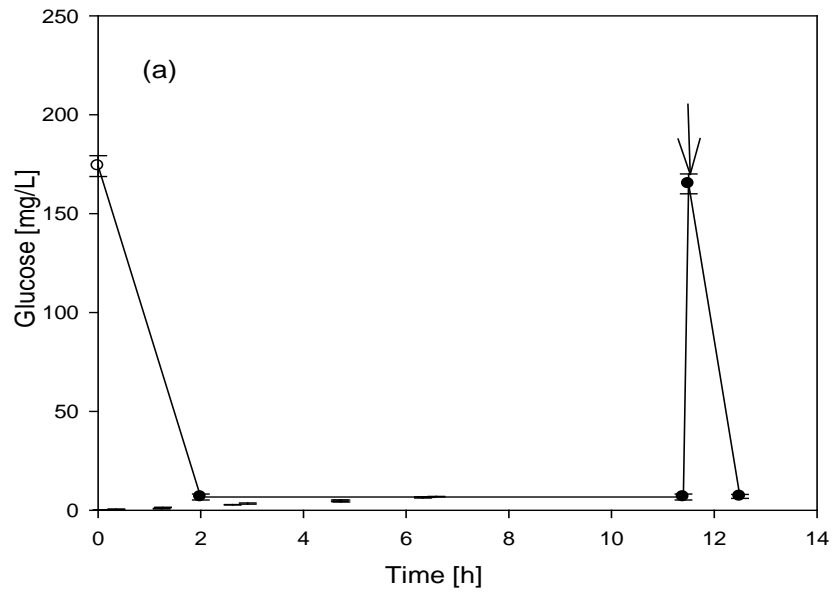
**Figure 3.6:** Mn(II) (a) and glucose (b) spikes following initial Mn(II) oxidation and glucose consumption for strain EC112.

### 3.6.6 Effect of Mn(II) concentration on Strain EC112 Growth

The effect of Mn(II) concentration on strain EC112 growth was studied. Glucose was provided as the sole carbon source. Batch reactors were spiked with Mn(II) concentration of 1.0, 4.0 10.0, 16.0, and 26.0 mg·L$^{-1}$. The results, shown in Figure 3.7, reveal that early stationary growth phase is reached 3 to 3.5 hrs. following cell inoculation, as measured by optical density at 600 nm ($OD_{600}$). Growth was enhanced for experiments spiked with Mn(II) concentrations of 1.0 to 26.0 mg·L$^{-1}$, compared to the experiment without added Mn(II). This is indicated by the higher optical density measurements, taken at 0.5 hr. intervals, for the experiments containing added Mn(II). The decrease in $OD_{600}$ observed after 3.5 hrs. is coupled with the onset of Mn(II)-oxidation (Section 3.6.7).

Reports for the effect of Mn(II) on growth on Mn-oxidizing bacteria generally show growth inhibition for both in-situ and laboratory studies at high enrichment levels (10 to 55 µM Mn(II)) (Adams and Ghiorse, 1985; Chapnick et al., 1982). Here, Mn(II) concentrations at 26 mg·L$^{-1}$ (468 µM) did not show growth inhibition. Lack of cell inhibition may be that strain EC112 has a preference for enriched levels of Mn(II) or the apparent effect observed for other strains is masked by Mn(II) chelation or complexation with components of the test media, lowering Mn(II) stress on the cells (Nealson, 2006).
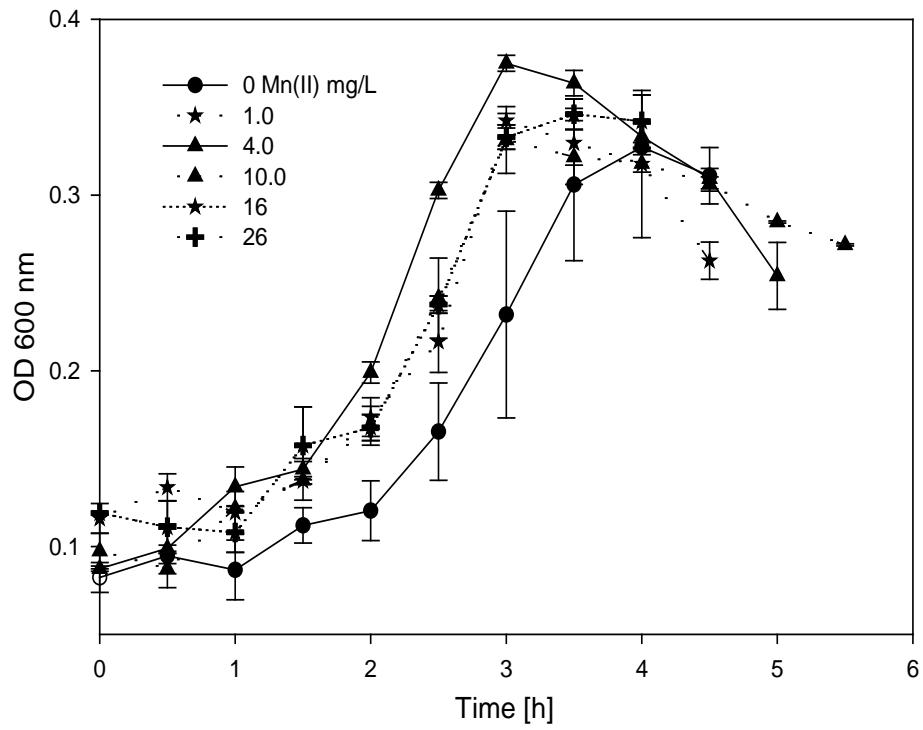
**Figure 3.7:** Effect of Mn(II) concentration on strain EC112 growth.

### 3.6.7 Effect of Mn(II) Concentration on Strain EC112 Mn(II)-Oxidation

The corresponding Mn(II) depletion curves for the experiments first reported in Section 3.6.6 are described here. The results are shown in Figure 3.8 (the corresponding growth curves are in Figure 3.7). For strain EC112, Mn(II)-oxidation begins 1 to 1.5 hrs. after the onset of stationary growth phase for Mn(II) concentrations to 5 mg·L$^{-1}$. For Mn(II) concentrations of 6 and 9 mg·L$^{-1}$, Mn(II)-oxidation begins at approx. 6 and 9 hrs. into the stationary growth phase. Mn(II) oxidation was inhibited and no significant Mn(II) removal was observed for 26 mg·L$^{-1}$ .

Increased lag phases for higher Mn(II) concentrations is a characteristic shared with other metal-oxidizing bacteria, including arsenite oxidizing species (Sehlin and Lindstrom, 1992; Suttigarn and Wang, 2005), and may indicate toxic metal concentration levels. These results are comparable to Jung and Schweisfurth (1979) and Depalma (1992), studying cell-free extracts of *P. Putida* strain MnB1 (formerly *Pseudomonas manganoxidans*), where Mn(II) oxidation occurred during stationary phase or under nutrient or carbon starvation. Particularly, Mn(II) oxidation was observed after approx. 2 hrs. of starvation.

A mechanism of growth inhibition has been proposed describing that biologic Mn(II)-oxidation may serve as a detoxification mechanism, reducing dissolved, ambient environmental Mn(II) concentrations from toxic levels. Mn toxicity may be due to various factors, including adverse effects on DNA replication, whereby the presence of excess Mn(II) may cause it to substitute for Mg(II), a critical cofactor for normal function of DNA polymerase (Goodman et al., 1983).

For *P. Putida*, and several other Mn(II)-oxidizing bacteria (Bromfield, 1956; Zhdanov, 1976), Mn(II)-oxidation is a starvation induced response. However, the physiological function of Mn(II)-oxidation has not been unequivocally defined (Geszvain et al., 2012).
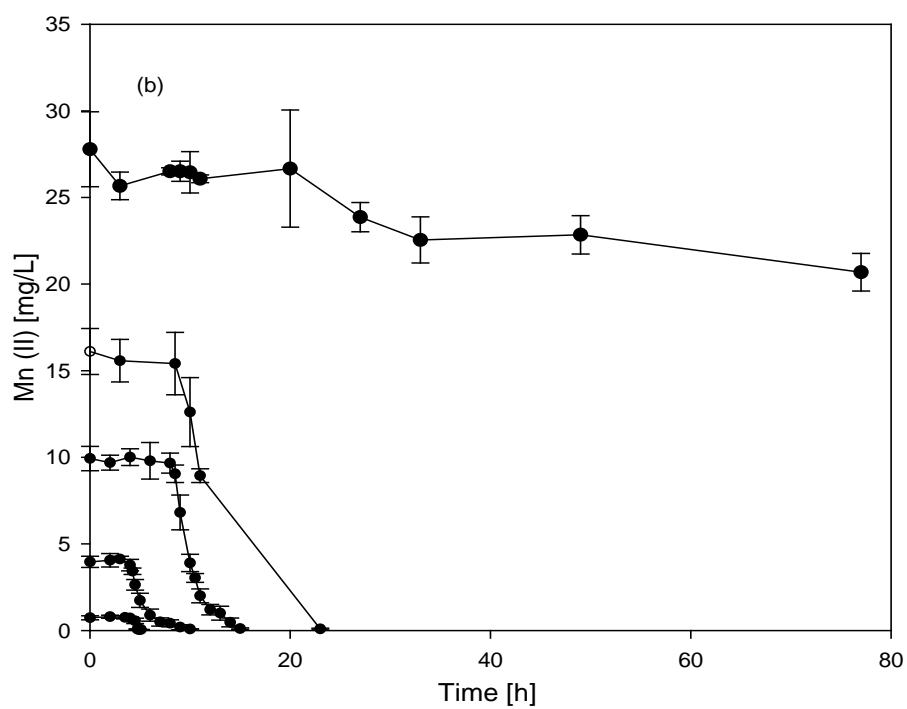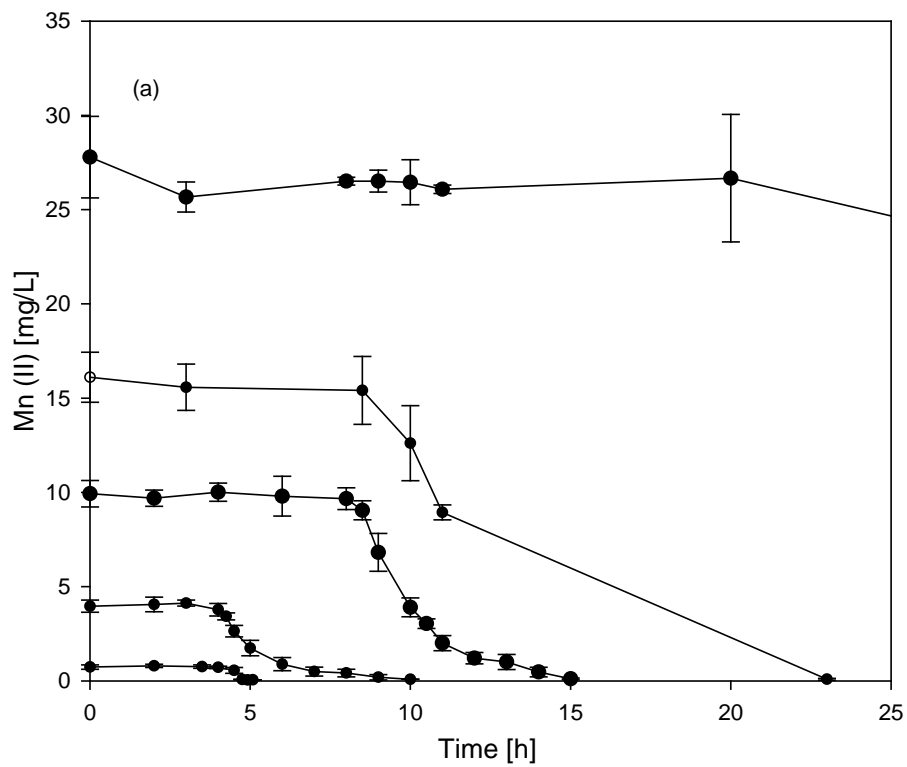
**Figure 3.8:** Effect of Mn(II) concentration on Mn(II) oxidation, (a) first 25-hrs., (b) entire incubation shown.

Bacteria induced responses to low nutrient environments are designed to increase cell survivability. Cell response mechanisms include formation of protective endospores and cell dwarfism, accompanied with decreased endogenous metabolism (Kjelleberg et al., 1983). Dwarfisms, whereby bacteria rapidly morph to smaller volumes, often by fragmentation mechanisms, allow cells to increase their surface/volume ratio, effectively increasing the apparent nutrient flux across their cell membranes (Kjelleberg et al., 1983). As an example, Mn(II)-oxidizing *P. fluorescens* strain GB-1, which initially oxidizes Mn(II) in the early stationary phase, first undergoes a size reduction, from 4 to 7 um and 1 to 2 um in length with comparable width reduction, and produce polar flagella (Okazaki et al., 1997). In addition, encrustation with coatings of negatively surface charged Mn(III,IV) oxide, coupled with reduced size and improved motility, may increase cell mobility in competitive oligotrophic environments to locate nutrients, particularly surface-attached nutrients, which may lead to biofilm formation (Kjelleberg et al., 1983; Parikh and Chorover, 2005).

### 3.6.8 pH and Temperature Effect on Mn(II) Oxidation

The effect of pH (5.5 to 8.0) and temperature (5 to 40°C) on Mn(II)-oxidation for whole cells of strain EC211 was investigated in the presence of glucose, AHA, and without added carbon, in separate batch experiments. At pH > 8.5, Mn(II) is susceptible to oxidation with $O_2$, and can oxidize and precipitate, therefore isolate Mn(II) oxidation at pH > 8.0 were not investigated.

### 3.6.8.1 Effect of pH

The experimental results, shown in Figure 3.9, are typical 'bell-shaped' profiles characteristic of enzymatic activity. Mn(II)-oxidation occurred over a pH range from 5.5 to 7.5, with an apparent pH optimum of 6.5, and sharp decreases in activities outside the optimum. The ordinate data represents the percentage of 5 mg·L$^{-1}$ oxidized in the first 10 hours for each respective pH. The experiments were monitored for 24 hours and no Mn(II) oxidation was observed at pH 5.0 and 8.0. For the experiment with no added carbon, Mn(II) is 100% oxidized, compared to 90% and 85% for Aldrich Humic Acid and glucose respectively. Without a carbon source, strain EC112 begins Mn(II) oxidation shortly after inoculation. In the presence of a carbon source, Mn(II) oxidation by EC112 was delayed to stationary phase. This pH profile is comparable to Mn(II)-oxidizers *Pedomicrobium* sp. ACM 3067 (Larsen et al., 1999) and *Arthrobacter* sp. (Broomfield and David, 1976), two species with favorable comparisons to *Pseudomonas Putida* strains. Optimal Mn(II)-oxidation rates by *Arthrobacter* sp., obligate, gram-positive aerobes common in soil and can grow on a variety of aromatic compounds, occur in cell suspension at pH 6.5 with rates rapidly decreased below pH 5.7 and above 7.5. *Pedomicrobium* sp. ACM 3067, a budding-hyphal bacterium; and *Pseudomonas Putida* MnB1, two heterotrophic Mn(II)-oxidizing bacteria common in soil, and are frequent hosts in biofilms in engineered aquatic bioreactors and water distribution systems. Each have a pH optimum of 7.0 to 7.5 and a higher alkaline range up to pH 8.0. Similarly, *Leptothrix discophora* SS1, a sheath-forming, freshwater
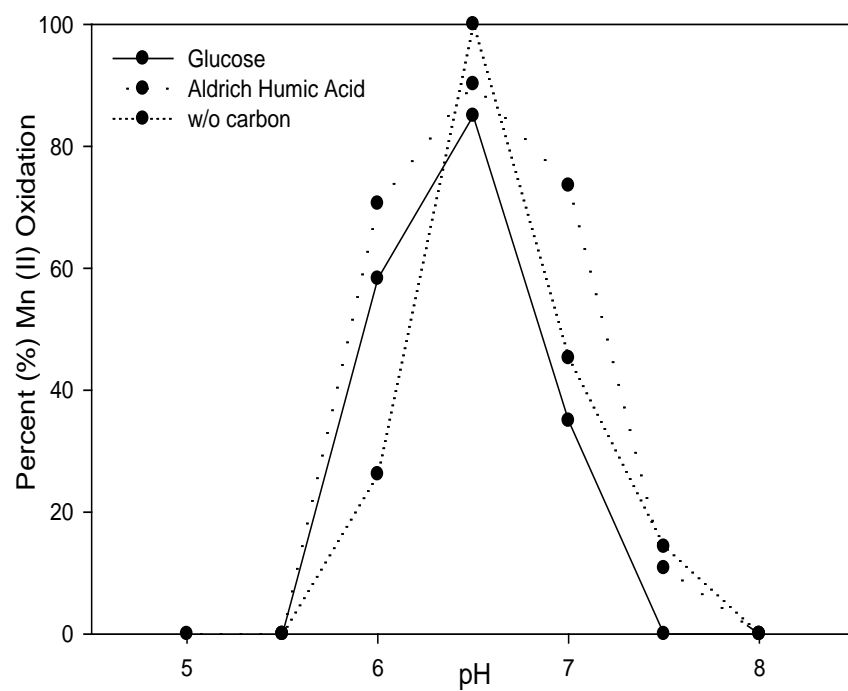
**Figure 3.9:** Effect of pH on strain EC112 Mn(II)-oxidation with initial Mn(II) of 5 mg·L$^{-1}$ at 10 hr. incubation (duplicate averages).

Mn(II)-oxidizing bacterium, oxidizes Mn(II) in the pH range of 6.0 to 8.5 with a pH optimal of approximately 7.5.

Hydrogen ion concentration has a marked effect on enzyme activity, on the secondary and tertiary conformation of enzymes, and the degree of ionization of the enzyme's active site(s). This effect is manifested as pH variation alters the degree of ionization of the amino group's side chains, hence altering the shape of the enzyme and the active site.

Bacteria with varying pH-optimum for Mn(II) oxidation may gain an advantage under different environmental conditions. A possible advantage could be offered in terms of energy: at a higher pH-optimum may gain an energetic advantage compared to bacteria with lower pH-optimum. Thermodynamic calculations utilizing the standard Gibbs free energy of formation can readily support this assertion. The Gibbs free energy ($\Delta G$) released during Mn(II) oxidation, using oxygen as the terminal electron acceptor, is an exergonic reaction and increases with pH. In addition, at higher pH values, activation energy requirements diminish, due to the increased levels of $OH^-$ which aid in the transfer of electrons. (Luther, 2005). For example, -6.15 kcal·mol$^{-1}$ and -8.85 kcal·mol$^{-1}$ of free energy are released at pH 6.5 and 7.5 respectively for 1 μM of reactant and 225 μM of $O_2$ (Nealson et al., 1988). Various Mn(II) oxidation reactions can occur and produce Mn(III), mixed (III,IV) or Mn(IV) oxidation states. The precipitation oxidation of Mn(II) to yield stoichiometric manganese (IV) dioxide can be represented as:

$$Mn(II) + 0.5O_2 + H_2O \rightarrow MnO_2 + 2H^+ \tag{3-9}$$
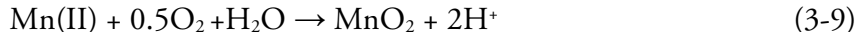
The larger free energy release (-8.85 kcal·mol$^{-1}$) at pH 7.5 would be advantageous to bacteria with a higher pH optimum. At pH values higher than 8-9, and redox conditions, $E_h$, >200 mV, homogenous Mn(II) oxidation with $O_2$ is expected in days to weeks, in the absence of biological catalyst (Morgan, 2005). In addition, below pH 6.0, the energetics of Mn(II) oxidation is unfavorable, which may explain why bacteria grow and oxidize Mn(II) in the range from pH 6.0 to 8.5 (Nealson et al., 1988).

Mn(II)-oxidizing bacteria that prefer to operate in oxidizing conditions in near neutral pH range may be advantaged to tap recalcitrant natural organic compounds (e.g., humic acids) for growth or energy requirements. Hydrogen ion concentration is expected to have a significant effect on the redox reaction involving manganese oxides and humic acids producing lower-molecular-weight bioavailable products. This may be due to modifications in the molecular humate structure from expanded, linear colloids at alkaline pH to compact, aggregated configurations at lower pH values, effectively promoting adsorption to the hydrophilic metal oxide surfaces and increased rates of humate oxidation. Various research results involving humic and fulvic acids have clearly demonstrated the relationship between pH and apparent humate radius and adsorption to metal oxides.

### 3.6.8.2 Effect of temperature

The experimental results to investigate the effect of temperature on Mn(II)-oxidation at the optimum pH 6.5 is shown in Figure 3.10. All three experimental conditions, without added carbon, Aldrich Humic Acids, and glucose, observed an apparent temperature optima for Mn(II)-oxidation at 30°C. The ordinate data represents the percentage of 5 mg·L$^{-1}$ oxidized in the first 10 hrs. for each temperature, while the experiments were monitored for 5 days. Temperature activation was most rapid for the experiment without added carbon, beginning at 20°C. Without carbon, strain EC112 begins Mn(II) oxidation shortly after inoculation, compared to after consumption of the carbon source, in the stationary phase, for the experiments with added carbon. All of the experiments reveal abrupt temperature inactivation above 30°C and Mn(II)-oxidation was not observed at 35°C or higher. Results are consistent with enzymatic activity observed in other Mn(II)-oxidizing bacteria in which Mn(II)-oxidation is characterized by a temperature optimum. Members of the genus *Pseudomonas* typically share similar growth and Mn(II)-oxidation conditions, which are mesophilic and have optimal growth at 25° to 30°C. Mn(II)-oxidation was observed at 5°C following one week of incubation. The temperature profiles are similar to *Pedomicrobium sp.* ACM 3067, for which an apparent optimum was 20° to 30°C and Mn(II)-oxidation was not observed above 37°C.

Jung and Schweisfurth (1979), using cell extracts from *P. Putida* MnB1, observed a temperature optima of 40°C followed by rapid temperature inactivation above 45°C for Mn(II)-oxidation. Tipping (1984) provided strong evidence for biologic temperature optimum of 15° to 30°C for water samples from freshwater lakes. *L. discophora SS1* was studied over a range of 10° to 40°C and had temperature optima of 30°C, with sharp deactivation at 40°C (Zhang et al., 2001).

### 3.6.9 Kinetics of Mn(II) Oxidation with Glucose as Sole Substrate

The kinetics of Mn(II) oxidation mediated by whole cells of strain EC112 was analyzed using the Mn(II) progress curves in Figure 3.8. Strain EC112 was spiked with five different Mn(II) concentrations in separate experiments in batch reactors amended with glucose as the sole carbon source. Three of progress curves more representative of the Mn range found in raw waters (1.0, 4.0, and 10.0 mg·L$^{-1}$) were selected for kinetic model calibration, with each set beginning with the onset of observable Mn(II) oxidation. For model calibration, the S-t data sets were globally fit using nonlinear regression to the no growth, integrated Monod equation (Eqn. 3-10) and optimized with the Lenvenberg-Marquardt nonlinear least-squared algorithm using Sigmaplot 11.0 (Table 2). The S-t data set for Mn(II) was used for model calibration to obtain estimated kinetic parameters $k_{mc}$ and $K_s$. The dry cell biomass concentration in stationary phase, $X_0$, was determined in separate experiments under identical conditions as VSS was 25 ± 0.8 mg·L$^{-1}$.
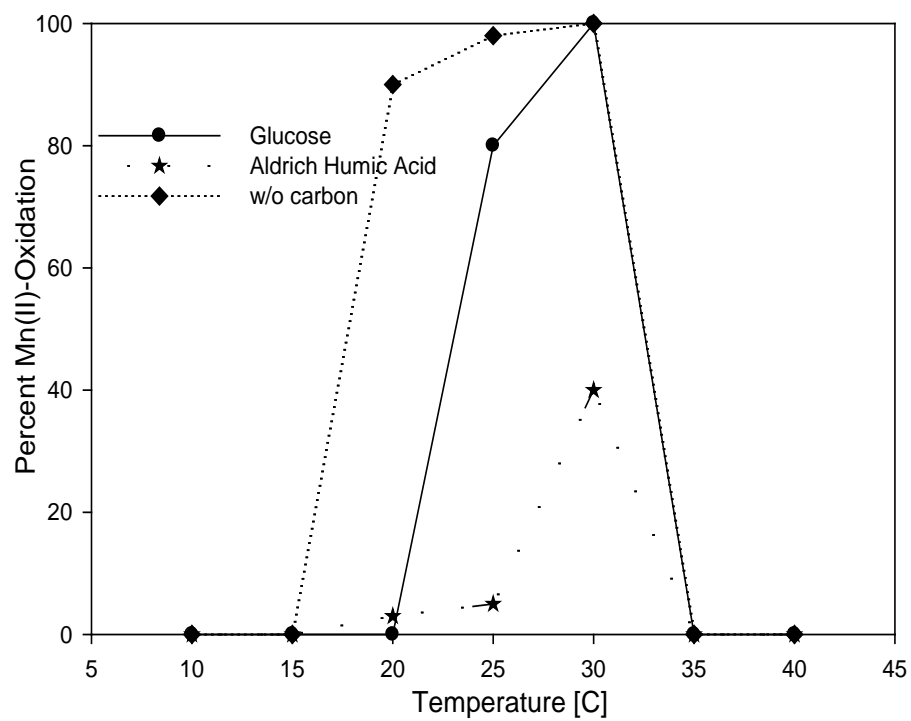
**Figure 3.10:** Effect of temperature on strain EC112 Mn(II)-oxidation with initial Mn(II) of 5 mg·L⁻¹ at 10 hr. incubation.

The derivative forms of the Monod Kinetic equations (Eqns. 3-1 and 3-2), which relate microbial growth to uninhibited substrate consumption are given and have been used to estimate the model kinetic parameters in batch studies. These are nonlinear, ordinary differential equations which can be integrated and estimation of the model kinetic parameters can be obtained by fitting the single substrate (S) consumption data vs. time (t) using the integrated forms with nonlinear regression. The consumption rate of the substrate is represented by the kinetic parameters $k_{mc}$ and $K_s$. Since Mn(II) oxidation by strain EC112 was observed in the stationary phase, cell growth can be ignored.

The integrated Monod Eqn., with no growth ($X=X_0$) (Simkins and Alexander, 1984) (Eqn. 3-10):

$$t = -\frac{1}{X_0}[\frac{1}{k_{mc}+S}]*(K_S*(\ln(\frac{S}{S_0}))+(S-S_0))$$ (3-10)

The fitting process of each experimental data set (S vs. t) is often not straightforward, and is hindered by the requirement of the existence of initial first estimates of the model parameters and verification of the nonexistence of model parameter linear correlation.

For strain EC112, Mn(II)-oxidation occurs in the stationary phase and is assumed to proceed under constant biomass conditions. To support this assumption, biomass was measured in separate experiments. Therefore, Mn(II) oxidation occurs under no growth conditions not directly related to EC112 growth. Within the time-frame of Mn(II) oxidation observed in the experiments, loss of biological activity or endogenous metabolism are assumed negligible. While these detrimental effects are likely inevitable and occurring to some degree, model verification utilizing the estimated model verification provide support for appropriateness for these underlying model assumptions.

Mn(II) removal from solution in the batch experiments, for purposes of modeling kinetics, is assumed to be solely due to direct biological Mn(II)-oxidizing activity by stationary phase strain EC122 cells. Removal of dissolved Mn by cell uptake mechanisms or adsorption to charged cell membranes or solid phase Mn(III,IV) oxides precipitates in suspension or encrusting cell surfaces are assumed negligible. These model considerations are supported by the results of the biological control study involving active and inactivated strain EC112 cells shown in Figures 3.2 and 3.3.

Mn(II) removal from solution by strain EC112 follows exhibits rates that are independent of concentration, according to the substrate progress curves in Figure 3.11. The best fit ($R^2=0.997$) model kinetic parameter estimates are (Table 3.2) $K_s=1.086\pm0.029$ mg·L$^{-1}$ (~19.55±0.522 µmol) and $k_{mc}$ = 0.180±0.003 mg Mn(II)/(mg cell· hr)(~3.24±0.054 µmol
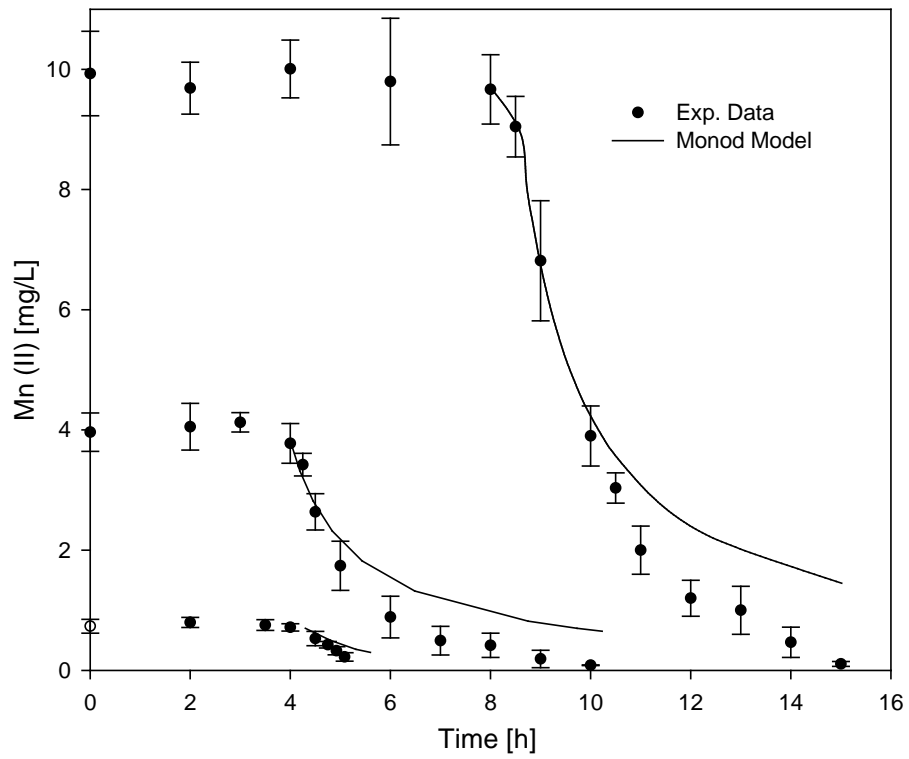
**Figure 3.11:** Mn(II)-oxidation modeling for strain EC112. Biomass for Monod Model measured in stationary growth phase.

Mn(II)/mg·cell·hr) indicate the no growth, integral form of the Monod kinetic model is a good fit to the experimental data. For comparison to *P. Putida* MnB1, kinetic parameter values for $K_s$ and $k_{mc}$ have been estimated at 8.81 mg Mn(II)·L$^{-1}$ and $1.33 \times 10^{-3}$ Mn(II)/(mg cell· hr (Jiang et al., 2010). The relatively large estimated value for $K_s$ has implications, such that the initial Mn(II) concentration is equal to the half-saturation constant ($S_0 = K_s$) and kinetics cannot be approximated with zero or first order. If $K_s << S_0$, substitution of $K_s$ into the Monod Eq., effectively reduces the expression to zero-order kinetics for the range of substrate concentration utilized. Zero-order kinetics would imply saturation substrate conditions and the Mn(II) oxidation proceeds at the fastest rates ($k_{mc}$) capable by strain EC112. In addition, at the Mn(II) concentration levels studied, it would suggest diffusion controlled mechanisms are controlling oxidation rates (Stone and Morgan, 1984). In this simplified case, the kinetics have been simplified by the zero-order integral model (Simkins and Alexander, 1984).

Several reports involving Mn(II)-oxidation kinetics incorporate the Michaelis-Menton model (Zhang et al., 2001; Clement et al., 2009). The biologic and kinetic disparity between the Michaelis-Menton enzymatic and the Monod growth model kinetic parameters, $K_s$ and $k_{mc}$, have been previously discussed and reviewed (Monod, 1949; Kovarova-Kovar and Egli, 1998). Albeit the differences, comparisons between $K_s$ and $k_{mc}$ can be made purely in terms of the rate kinetics of Mn(II)-oxidation, without the necessity to consider the original mechanistic significance of the models, considering the mathematical forms of Monod and Michaelis-Menton Eqs. are equivalent in the no growth case (Liu and Zachara, 2001) and these parameters determine the shape of the Mn(II) depletion curve. Therefore, in this context, increasing $K_s$ and $k_{mc}$ values effectively represents a shift toward mixed and first-order kinetics, away from zero-order kinetics (Simkins and Alexander, 1984).

Morgan (2000) summarized that $K_s$ for microbial Mn(II)-oxidation activity in natural aquatic environments has been reported to range from $10^{-3}$ to 5 µM. For pure cultures, Zhang et al., (2001) reported a Michaelis-Menton half-saturation constant ($K_m$) of 5.7 µmol and maximum oxidation rate $V_{max}$ of 0.35 µmol Mn(II)/mg·cell·hr for *L. discophora* cells for Mn(II) oxidation grown in a chemically defined media. Larsen et al (1999) reported 26 µmol and 0.75 µmol Mn(II)/mg·cell·hr for $K_m$ and $V_{max}$, respectively, for cells of *Pedomicrobium* sp. ACM 3067 grown in an undefined chemical media. These $V_{max}$ rate constants compare remarkably well with the $k_{mc}$ estimate for strain EC112, indicating a one-order of magnitude equivalency between the maximum Mn(II) oxidation rates.

The onset of Mn(II) oxidation and structural architecture disparities may have a role in the apparent, faster Mn(II)-oxidizing activity of strain EC112, as indicated by the lower $K_m$. Two key differences between strain EC112 (and other *P. Putida* strains) may have a role in the faster Mn(II)-oxidizing activity. First, for strain EC112 and several other *P. Putida* strains, Mn(II) oxidation has been demonstrated to be a carbon starved stress-induced phenomenon, with the onset initially occurring in the stationary phase of growth subsequent to the depletion of the carbon source (Depalma, 1993). Therefore, during stationary phase

Mn(II)-oxidation, Mn(II), and possibly dead cell material, comprise the electron donors for suspended cells of strain EC112. This contrasts with *L. discophora* SS1 and *Pedomicrobium* sp. ACM 3067, for which initial Mn(II)-oxidation occurs concurrently with growth in the early or middle exponential phase of growth.

Second, *L. discophora* and *Pedomicrobium* sp. have the ability to assemble proteinaceous, extracellular structures including filamentous sheaths and stalked prosthecates, respectively. These extracellular structures may serve as diffusive barriers to Mn(II) ions in the bulk liquid, reducing the flux towards oxidation sites either within the structures themselves or on the outer cell wall or membranes. For *P. Putida* strains similar to EC112, Mn-oxides are formed and directly deposited on the cell surface. This architecture may be more of a factor for *Pedomicrobium* sp., in light of the fact that *L. discophora* SS-1, is a sheathless strain, having strain lost the ability to form well-defined fibrillar networks of sheaths after several months of cultivation on laboratory media (Adams and Ghiorse, 1985). SS-1 excretes Mn-oxidizing proteins into the bulk solution that are responsible for the activity (Adams and Ghiorse, 1985).

Furthermore, Mn(II)-oxidation by *Pedomicrobium* sp. has been shown to be a two-step process involving adsorption of Mn(II) to extracellular polysaccharides followed by subsequent oxidation to Mn oxide (Ghiorse and Hirsch, 1979). The rate limiting step is likely the catalysis of electron transfer kinetics. For *Pedomicrobium* sp. ACM 3067, the assignments of Mn(II)-oxidizing activity is complicated by its dimorphic budding life cycle, producing swarmer and parent cells, with the Mn(II)-oxidizing activity of each phase likely unequal.

### 3.6.10 Sensitivity Analysis

Sensitivity equations, derived by taking the partial derivatives of the no-growth integrated Monod model (Eqn. 3-10) with respect to $K_s$ and $k_{mc}$, were used to evaluate the uniqueness of the best fit kinetic model parameter estimates obtained by nonlinear regression. Sensitivity coefficients calculated from these equations, using initial Mn(II) levels of $S_0=1$, 4, and 10 mg·$L^{-1}$ and the model parameter best estimates (Table 2), are shown in Figure 3.12. Sensitivity coefficients are plotted against the independent variable, t, allowing a curve comparison and evaluate where the model is most sensitive to changes in parameters (Robinson and Tiedje, 1983). The utility of a sensitivity analysis is to identify favorable initial experimental conditions (e.g., $S_0$ and $X_0$) enabling the design of experiments that enable the collection of substrate depletion data that provide accurate and unique parameter estimates. For a qualitative comparison, visual superimposition of each pair of curves relative to each other, generated at each initial substrate level, $S_0$, reveals parameter sensitivities are not proportional and have relatively good separation, suggesting that the model parameters represent unique estimates. The model separation in sensitivity coefficients and sensitivity to $k_{mc}$ increases with Mn(II) concentration ($S \gg K_s$), representative of a shift towards a single-parameter, saturation kinetic growth model (Knightes and Peters, 2000).
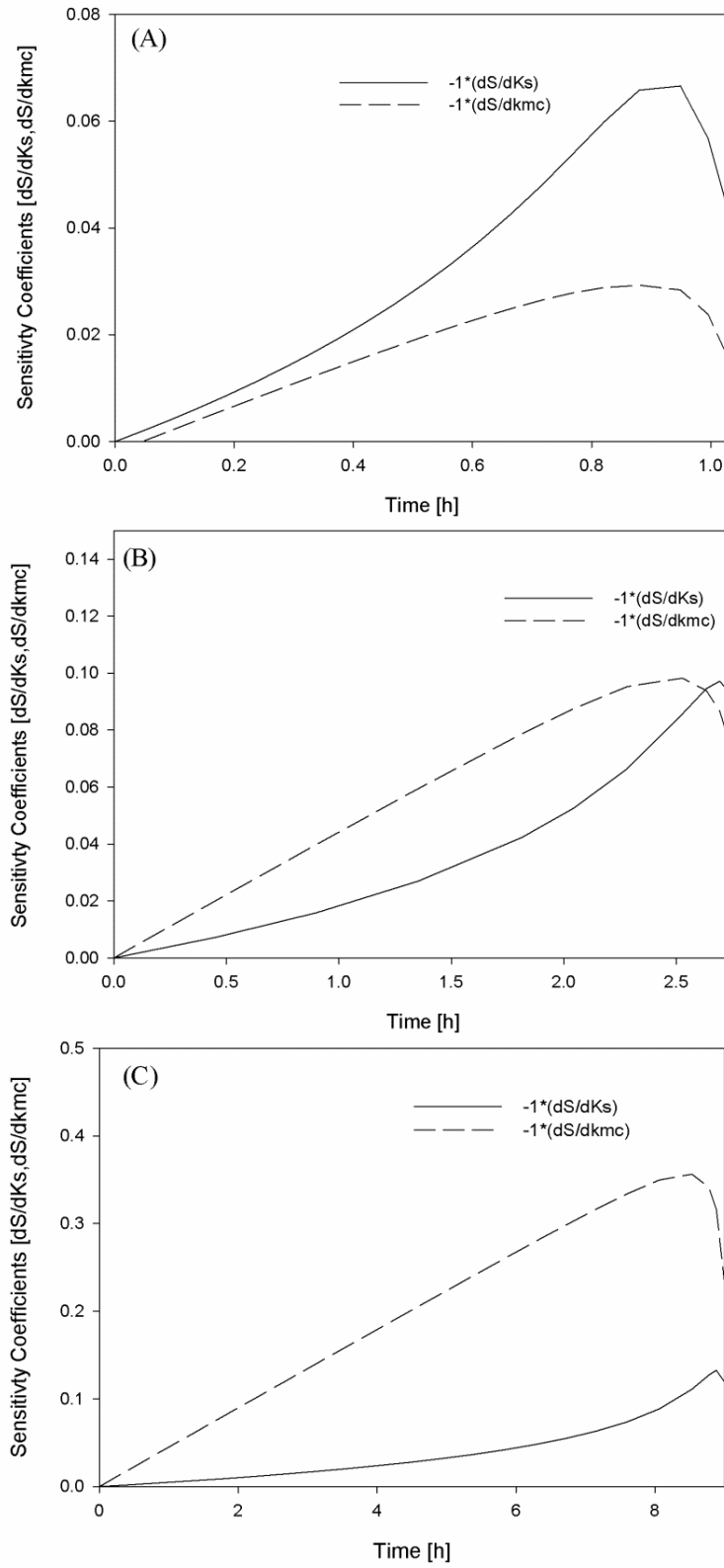
**Figure 3.12:** Sensitivity plots for $S_0$=1, 4, 10 mg·L$^{-1}$, and $S_0/K_s$=25, 75, 250.

Previous sensitivity analyses by various authors using this approach for the integrated Monod model have shown that $S_0/K_s$ and $S_0/X_0$ ratios are important factors in determining parameter identifiability. Robinson and Tiedje (1984) determined that unique estimates of the Monod parameters $\mu_{max}$, $K_s$ and Y were attainable at $S_0/K_s$ of 4, for $S_0$ in the mixed-order region, but not for the first-order (0.02) or zero-order (50) kinetic regions. Ellis et al., (1996) performed a sensitivity analysis to evaluate model parameters for batch respiratory experiments involving constant cell concentrations of activated sludge biodegradation kinetics of single organic compounds at low concentrations. They examined sensitivity coefficients at different $S_0/K_s$ ratios, and for a 0.1 ratio concluded high correlation between $q_{max}$ and $K_s$, but not for 1.0 ratios or higher. Liu and Zachara (2001), utilizing a statistical dimensionless analysis approach to evaluate parameter uncertainty and correlation for both the integrated growth and no-growth Monod equations, determined optimal experimental conditions for $S_0/K_s$ to be equal or greater than 5. Liu and Zachara (2001) argue that their statistics approach, involving calculation of parameter correlation coefficients, standard deviations, and confidence regions, offers the advantages of providing quantitative relationships that are more robust in determining parameter correlation and identification of optimal experimental conditions.

For the sensitivity coefficients simulations in this study, which match the batch experimental conditions for $S_0$, the $S_0/K_s$ ratios of 25, 75, and 250 have corresponding $S_0/X_0$ ratios of 0.04, 0.12, and 0.40 under stationary phase constant biomass conditions of 25 mg·L$^{-1}$. For comparison, Figure 3.12 shows the sensitivity coefficients for $S_0/K_s$ ratios of 0.02, 5 and 50 using $S_0$=1.0 and $K_s$=52.5. For $S_0/K_s$ = 0.02, the sensitivity coefficients, dominated by $K_s$, are proportional and could not provide unique parameter estimates. For $S_0/K_s$ = 5 and 50, the sensitivity coefficients have good separation. In general, the degree of separation improved for higher $S_0/K_s$ ratios, agreeing with the sensitivity results by Ellis et al., (1996) and Liu and Zachara (2001). Owing to the no-growth conditions, Ellis et al., (1996) and Liu and Zachara (2001) results are more directly comparable to this study than those of Robinson and Tiedje, (1984).

Considerable literature attention has been given to the influence of initial substrate ($S_0$) to the initial biomass ($X_0$) on kinetic parameter identifiability (Grady et al., 1996). For this reason, kinetics at low and high $S_0/X_0$ values have been termed extant and intrinsic kinetics, respectively, and specific numerical values to define either condition have been proposed. Expressed as chemical oxygen demand (COD) mg/L, parameter kinetics determined with greater than 20/1 mg·L$^{-1}$ or below 1/40 (0.025) $S_0/X_0$ thresholds levels describe intrinsic and extant kinetics respectively (Dang et al., 1989; Barbeau. 1992; Grady et al., 1996). Intermediate threshold conditions should be described as undefined or defined, as proposed by Grady et al., (1996), with defined referring to conditions with a specific purpose.

Intrinsic kinetics parameters occur with growing biomass and unrestricted growth with physiological changes in culture, while extant kinetics occurs with minimal growth or changes in culture. Chudoba et al., (1985), in their studies involving activated sludge bulking kinetics, preferred low $S_0/X_0$ values for batch design studies. The applicability and

significance of $S_0/X_0$ values to this study as a useful check on parameter identifiability is tentative, considering strain EC112 Mn(II) oxidation as suspended cells in batch mode are modeled as unlinked to cell growth, rather Mn(II) oxidation is observed to occur as carbon-stressed cultures with constant biomass. Nevertheless, expressed as COD, the batch kinetic parameter estimates made here, would be intermediate or defined conditions, with $S_0/X_0 >$ 0.025, though very close to the extant kinetic threshold at 0.04 to 0.12. However, clearly the description as extant kinetic parameters is more appropriate for this study, considering the pure cultures of strain EC112 were representative of the conditions during growth for harvesting. No growth is assumed to occur during Mn(II)-oxidation in the stationary phase.

## 3.6.11 Strain EC112 Growth and Mn(II)-Oxidation in the presence of Humic Acid and MnO₂

Although biofiltration has great potential for manganese control, its efficiency may also depend upon the availability of organic growth substrate in source waters. Mn(II)-oxidizing bacteria, which are heterotrophic require biodegradable organic for growth and energy needs. In drinking water sources in which Mn is frequently elevated, such as groundwater and oligotrophic environments where Mn can be often found in elevated levels, low total organic carbon concentrations may limit the application of biofiltration. Humic substances comprise 30-50% of the dissolved natural organic matter found in groundwater, streams and lakes (Moran and Hodson, 1990; Basu and Huck, 2004). Humic substances are generally considered to be recalcitrant to biodegradation due to their structural heterogeneity. However, it has been previously demonstrated that Mn oxides can degrade humic substances to low-molecular-weight, biodegradable compounds (Stone and Morgan, 1984; Waite et al., 1988; Sunda and Kieber, 1994; Saratovsky, 2006). The objective of the following experiments is to evaluate strain EC112 growth on humic acids in the presence of $MnO_2$.

Batch experiments were conducted to investigate cell growth and Mn(II)-oxidation in the presence of HA and $MnO_2$. The effect of pH and $MnO_2$ concentration on the HA-$MnO_2$ reaction were investigated at 30°C, the optimal growth temperature for strain EC112. Three separate experiments were completed to: (1) evaluate the effect of $MnO_2$ concentration and HA-$MnO_2$ contact time on HA biodegradability, (2) evaluate the effect of pH and $MnO_2$ concentration on HA biodegradability, (3) measure the isolate growth and Mn(II)-oxidation rates on HA-$MnO_2$ oxidation products. In addition, to identify changes in HA by $MnO_2$ oxidation, Fourier transform infrared (FT-IR) and proton nuclear magnetic spectroscopy (^{1}H-NMR) of HA and HA-$MnO_2$ are first presented and interpreted.

### 3.6.11.1 Spectroscopy of Aldrich Humic Acids

The noninvasive spectroscopic methods of FT-IR and ^{1}H-NMR, which involve the interaction of electromagnetic energy with the study sample, have been used to investigate humic substance chemical structure. Both methods can identify humic functional groups and distinguish chemical and microbial humic degradation (Shin and Lim, 1996). In particular,

among the most reactive humic functional groups are carboxylic and phenolics, which have been previously studied using FT-IR, $^1$H-NMR, and $^{13}$C-NMR (Ruggiero and Interesse, 1980; Gu et al., 1994). In this study, FT-IR and $^1$H-NMR spectra are obtained and utilized to identify changes introduced in HA by $MnO_2$ oxidation. From an interpretation of the spectra, presented below, supported with UV-254, DOC, can be used to develop a mechanistic understanding of the $MnO_2$ oxidation of humic acids. In addition, identification of the reactive functional groups of humic substances with $MnO_2$. The FT-IR and $^1$H-NMR spectra for the following discussion are shown in Figure 3.13a and 3.12b.

### 3.6.11.1.1 FT-IR-Spectroscopy

The FT-IR spectra of HA before and following oxidation with $MnO_2$, at pH 7.0 with added 30 mg·L$^{-1}$ $Ca^{2+}$ (as $CaCl_2$), are shown in Figure 3.13a. Major adsorption bands assignments, largely based on FTIR conventions for Aldrich Humic Acids in the literature, are provided in Table 3.2. The main absorption bands for Spectra a exhibit the broad bands typical for humic acids and are qualitatively comparable with those in literature for HA, with the exception of stronger and more pronounced bands at 1110 cm$^{-1}$ and 1020 cm$^{-1}$, respectively, attributed to alcoholic hydroxyl groups and/or C-O stretching of polysaccharides. The weak shoulder bands at 2918 cm$^{-1}$ and 2967 cm$^{-1}$ (stretching of $CH_3$ and $CH_2$) are attributed to large, molecular weight aliphatic chains (H.S Shin et al., 1999). FT-IR spectra of HA have previously shown that, according to molecular weight size fractions, larger molecular size components (>100,000 Daltons) are more aliphatic C in content and smaller size components (<10,000 Daltons) are higher in aromatic and carboxylate groups (H.S Shin et al, 1999). These chemical and functional characteristics have been observed in other humic acid studies (Huang et al., 2003).

The oxidized HA (spectra b) shows the same broad bands as Spectra a, the only differences involve changes in absorption intensity that are attributed to $MnO_2$ oxidation. A very broad weak band increase occurs from 1710-2800 cm$^{-1}$ and a sharp peak at 1380 cm$^{-1}$.

Spectra b band increases include a broad, weak band from 1800 cm$^{-1}$ to 2400 cm$^{-1}$ and a sharp, narrow band at 1380 cm$^{-1}$. The broad band is difficult to interpret and several tentative explanations are possible. The band could represent an overlap of carboxylate, carbonyl and fatty acid oxidation fragments. Spectra a reveals insignificant change in the aromatic content of the humic acids during the oxidation process. The sharp peak at 1380 cm$^{-1}$ is assigned to C-H symmetrical deformation in β-$CH_3$ groups.

Spectra b band intensity was attenuated from 1020-1150 cm$^{-1}$, 1400-1500 cm$^{-1}$, and 2900-2970 cm$^{-1}$. For 1020-1150 cm$^{-1}$ , the substantial attenuation in band intensity is attributed to loss of alcohol C-O functional groups, the shoulder at 1710 cm$^{-1}$ is interpreted as C=O of carbon acids, esters, aldehydes, or ketones (Kim et al., 1990). The principal molecular reactions likely involve primary and secondary alcohol $MnO_2$-oxidation.
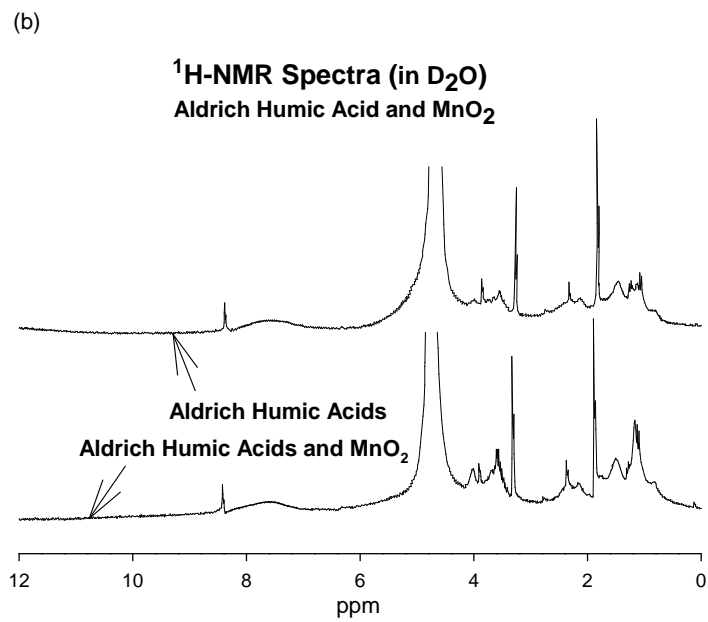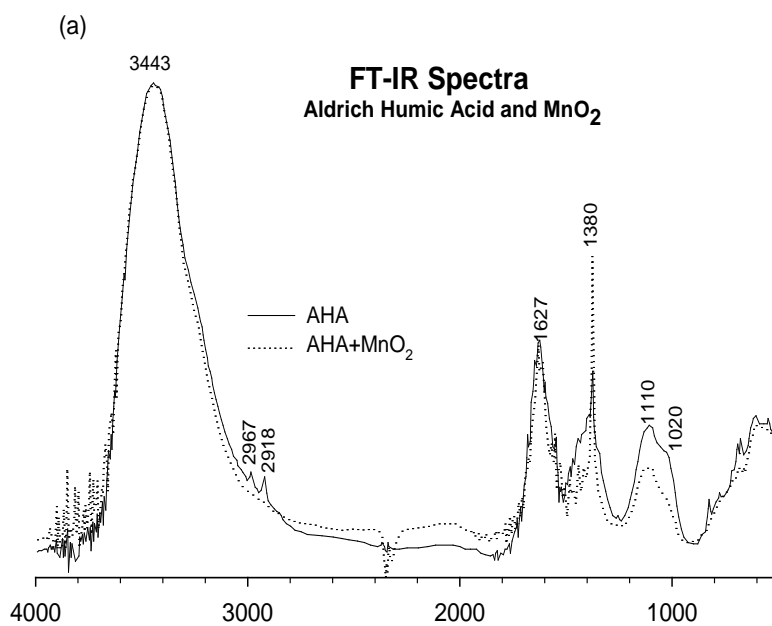
**Figure 3.13:** FT-IR (a) and ^{1}H-NMR (b) spectra for HA and HA-MnO[2] .

Various adsorption mechanisms of NOM on solid metal-oxide surfaces have been proposed, but numerous studies supported with direct measurements, indicate that ligand exchange reactions between humic carboxyl and hydroxyl functional groups and surface coordinated $H_2O$ or OH groups. In addition, NOM adsorption increases with ionic strength and concentration of divalent cations, and decreasing pH. Gu et al., (1994) provide evidence by using FT-IR spectroscopy that the dominant bond formation is between C-O and phenolic $OH^-$ functional groups of NOM and iron oxide surfaces. NOM adsorbed on iron oxide showed strong FT-IR adsorption bands at 1100 cm$^{-1}$, bands representative of carbohydrates or polysaccharide substances. The FT-IR and $^1$H-NMR results do not allow a clear mechanistic interpretation of the oxidation reactions. However, the results are consistent with previous results involving humic acid adsorption on metal oxide surfaces.

### 3.6.11.1.2 $^1$H-NMR -Spectroscopy of Aldrich Humic Acids

The $^1$H-NMR spectra of HA before and following reaction with $MnO_2$ at pH 7.0 (with added $Ca^{2+}$) are also shown in Figure 3.13b. Chemical shift assignments, largely based on literature for HA, are divided into the following spectral regions: (1) 0.5-1.1 ppm (resonances from protons on terminal methyl groups of methylene chains). (2) 1.3-2.0 ppm (resonances from protons from methine and methylene groups); (3) 2.0-3.2 ppm (resonances from protons on carbons with carbonyls or carboxylic functional groups or aromatic rings; (4) 3.5-4.9 ppm (resonances from protons on carbon directly bonded to electronegative functional groups, primarily containing oxygen); (5) 7.0-8.4 ppm (resonances from unhindered aromatic protons including phenols and quinones).

The strong peak at 4.8 ppm is due to exchangeable protons from HA and $D_2O$. The reference compound, methanol, represents the sharp peak at 3.3 ppm. The peak at 8.4 ppm is identified as formate, a naturally occurring compound in HA previously described as deriving from lignin hydrolysis (Wilson, et al., 1988).

By comparison, the oxidized HA (spectra b) has more intense signals than spectra a within several of the assigned regions, including the 1.1-1.3 ppm, 2.2-2.3 ppm, 3.5-3.8 ppm, and 4.0-4.2 ppm regions.

The intense upfield signal shift at 1.1-1.3 ppm corresponds to the sharp peak at 1380 cm$^{-1}$ in the oxidized FTIR spectra. This signal originates from terminating methyl protons on chain β or γ attached to aromatic rings (Grasso et al., 1990). Ruggiero and Interesse (1980), reported FTIR spectra for the peracetic oxidation of a soil humic and fulvic acid, describing a sharp peak at 1390 cm$^{-1}$ as originating from protons on acetyl groups. They assigned the corresponding $^1$H-NMR signal to be at 1.9 ppm and deriving from ester $CH_3$–CO– groups. Peracetic acid, is more oxidizing than δ-$MnO_2$, with a standard potential of 1.81 eV, compared to 1.29 for δ-$MnO_2$. They found possible partial cleavage of the fulvic aromatic rings, and little humic aromatic ring cleavage.

Degradation studies of humics designed to elucidate core structure show that despite a variety of oxidative methods (alkaline CuO, $H_2O_2$, $ClO_2$, $KMnO_4$, $CH_3CO_3H$) and humic substances, produce qualitative similar products are consistently produced (Maximov et al., 1977; Schnitzer, 1978; Liao et al., 1982; Sonnenberg et al., 1989). Benzenecarboxylic acid methyl esters, methyl esters of aliphatic mono- and dicarboxylic acids, and methoxy benzenecarboxylic acid methyl esters are representative of the major water structural groups identified as soluble oxidation products, with regards to the aromatics , tri-, tetra-, penta-, and hexacarboxylic acids are the major ring substitution patterns. and some of them are probably derived from oxidative cleavage of carbon side chains of alkyl substituted aromatic rings. The intense upfield signal shift at 1.1-1.3 ppm corresponds to the sharp peak at 1380 $cm^{-1}$ in the oxidized FTIR spectra. These peaks originates from terminating methyl protons on chain β or γ attached to aromatic rings (Grasso et al., 1990) and likely correspond to methyl groups in benzenecarboxylic acid methyl esters fragments.

### 3.6.11.2 Strain EC112 Growth on HA-MnO$_2$ Oxidation Products: Effect of MnO$_2$ and Contact Time

Screening experiments were conducted to evaluate strain EC112 growth by providing HA-$MnO_2$ oxidation products as the sole carbon source under a range of $MnO_2$ concentrations and HA-$MnO_2$ contact times. Viable plate counts were used to enumerate cell growth. Temperatures and pH of the reaction solutions were maintained at 30°C and 7.0±0.30. Controls evaluated isolate growth provided only HA as the sole carbon source and without added $MnO_2$ and treated to same conditions as tests.

HA solutions for the growth experiments were prepared by adding HA powder (25 mg·$L^{-1}$) to SQ water in 2-L bottles. The pH was adjusted to 9.0 using 1 N NaOH and solutions were stirred for an hour to solubilize the HA. Solutions were supplemented with 30 mg·$L^{-1}$ $Ca^{2+}$ (as $CaCl_2$) prior to pH adjustment to approximately 7.20 to 7.30.

Figure 3.14 shows the growth of strain EC112 at 30°C and pH 6.5 on the HA-$MnO_2$ oxidation products in 200-ml duplicate batch cultures at contact times of 0, 10, 30, and 60 mins. Suspended cells of strain EC112 were incubated in 200-ml batch solutions of HA-$MnO_2$ oxidation products and growth was enumerated as viable cell counts.

The results indicate relatively rapid cell growth, as measured by colony forming units (CFU·$ml^{-1}$) (duplicate mean) within 16 hrs., compared to little or no growth for the control (Figure 3.14a). Bacterial utilization of dissolved organic matter (DOC) containing humic substances from freshwater environments, including lakes,
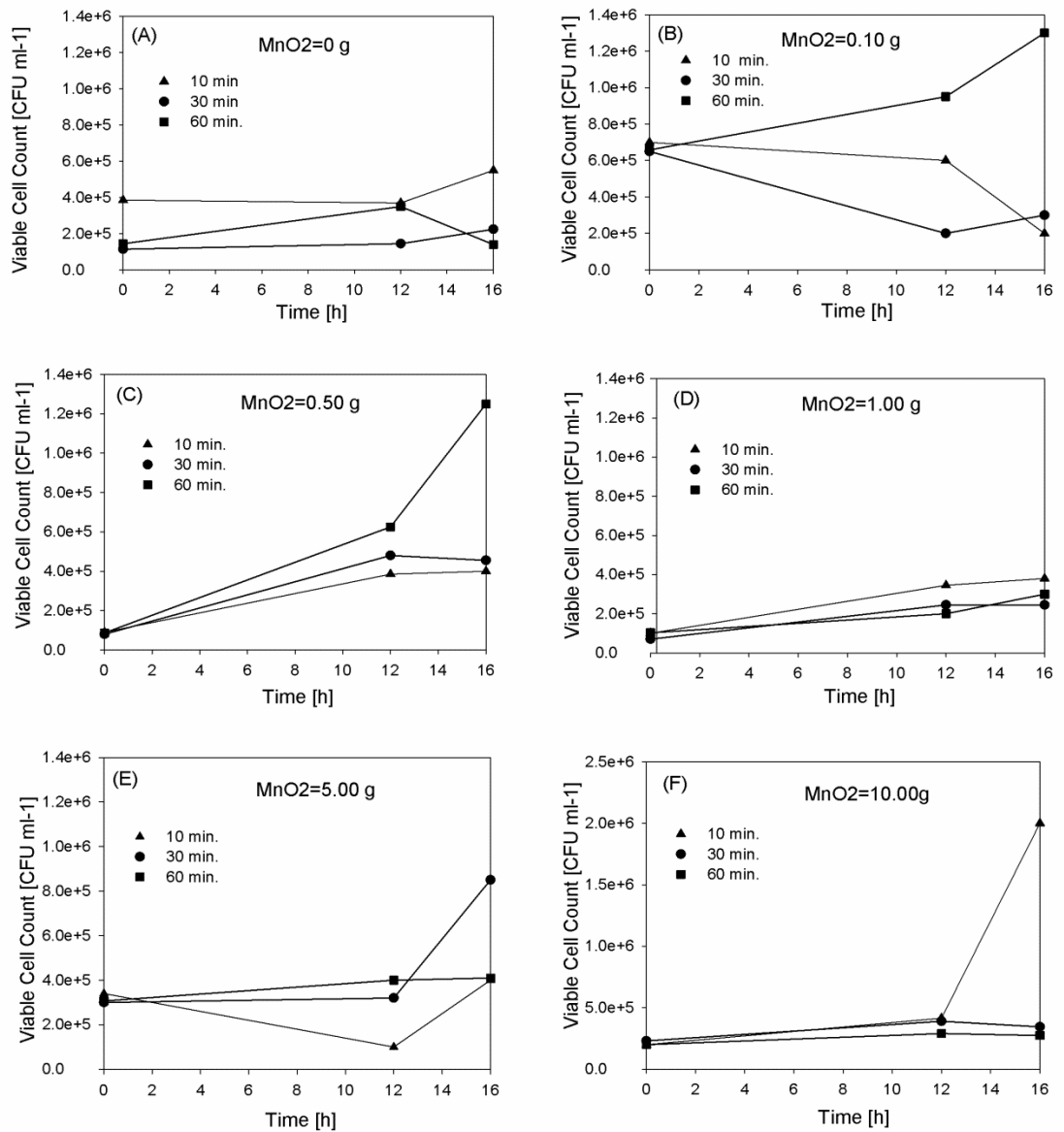
**Figure 3.14:** Strain EC112 growth on HA reacted with $MnO_2$ concentrations of (a) 0 (b) 0.10 g (c) 0.50 g (d) 1.00 g (e) 5.00 g and (f) 10.00 g for HA 25 mg·L$^{-1}$ and pH 6.5 and 30°C. Reactant contact times shown in figures.

streams and marshes, was observed before and reports of bacteria production on a time scale of days, much longer than the observed times in this study (Moran and Hodson, 1990; Volk et al., 1997).

As shown in Figures 3.14b-f, both $MnO_2$ concentration and $HA-MnO_2$ contact time have significant effects on humic biodegradability as indicated by the cell growth.

The most significant growth was observed with 10.00 g-$MnO_2$ and a contact time of 10 min., where a ten-fold increase in viable cell count, from $2 \times 10^5$ to $2 \times 10^6$ CFU·ml$^{-1}$ was observed (Figure 3.14f). The corresponding 30 and 60 min. contact times did not produce significant growth. For 5 g-$MnO_2$ and 30 min. contact time, growth almost tripled, from $3.0 \times 10^5$ to $8.5 \times 10^6$ CFU·ml$^{-1}$ (Figure 3.14e).

For 0.10 g and 0.50 g-$MnO_2$ both had the highest growth yield for the 60 min. contact time (Figure 3.14b and 3.14c). For the control, with no added $MnO_2$ (0 g), the 10 min. contact time had an increase of $2.0 \times 10^5$ to $3.9 \times 10^5$ CFU·ml$^{-1}$. For 1.00 g-$MnO_2$, marginal growth was observed for the 10 min. contact time, from $1.0 \times 10^5$ to $3.9 \times 10^5$ CFU·ml$^{-1}$.

For the cultures with 10-g $MnO_2$ and 50 mg·L$^{-1}$ HA, lack of growth were observed for the 30 and 60 min. contact times, implying the lack of bioavailable growth $HA-MnO_2$ oxidation substrates. Oxidation products produced during the first 10 minutes of contact time were apparently no longer available as growth substrates for the 30 and 60 min. contact times.

During late exponential and early stationary phase of growth cells initiate clustering prior to the onset of Mn(II) oxidation, reducing apparent cell density and rendering cell counts unreliable.

Pyruvate and acetone, two of the largest yielding oxidation products identified in Sunda and Kieber's (1994) study of the reaction products from humic substances and Mn-oxides, showed a maximum production prior to decreasing at higher metal oxide concentrations. This was interpreted as subsequent oxidation of these products following their initial production. In this study, oxidized HA moities produced during the initial 10 minutes of contact time may have been readsorbed onto the $MnO_2$ surface without further reaction or oxidized to products less biodegradable prior to subsequent to release back into the bulk solution.

Stone and Morgan's (1984) study of the dissolution of Mn(III,IV) oxide suspensions by model organics under near neutral conditions, showed that several aromatic organics – containing functional groups representative of core structure of freshwater humics (e.g., catechol, methoxyphenol) - displayed appreciable reduction rates of the metal oxides within minutes. The results here suggest $HA-MnO_2$ reaction rates of the same order, as evidenced by significant growth of strain EC112 on the $HA-MnO_2$ oxidation products for 10 minutes of contact time.

These experiments show that $MnO_2$ concentration and $HA$-$MnO_2$ contact time have a critical role in the biodegradability of HA. Low experimental $MnO_2$ concentrations (0.10 and 0.50 g) require longer contact time (60 min.) while the larger $MnO_2$ concentrations require a shorter reaction time to produce the growth patterns. This inverse relationship observed between contact time and $MnO_2$ concentration effects on biodegradability suggests competition between HA molecules for the available reaction sites, implicating the negatively charged $MnO_2$ surface as a limiting factor. These observations are consistent with adsorption isotherms from the Langmuir or Freundlich Model, which predict initial rapid adsorption when the availability of surface reaction sites are unrestrictive (Stone and Morgan, 1984). Furthermore, the observed effects of reaction time and $MnO_2$ concentration on HA biodegradability imply optimal conditions exist to maximize biodegradability.

Two exchange mechanisms that have been proposed in the literature for humic substance adsorption on metal oxides include anion exchange and ligand-exchange surface complexation (Sposito, 1984; Gu et al., 1994). Ligand-exchange mechanisms, involving humic $COO^-$ and $OH^-$, have been favored for adsorption below the metal oxides pH of PZC, accounting for considerable adsorption of the bulk humics (Gu et al., 1994). Gu et al., (1994) provide evidence by using FT-IR spectroscopy that the dominant bond formation is between C-O and phenolic $OH^-$ functional groups of NOM and iron oxide surfaces. NOM adsorbed on iron oxide showed strong FT-IR adsorption bands at 1030 to 1100 $cm^{-1}$, bands interpreted as representing of aliphatic or carbohydrate OH functional groups (Gu et al., 1995).

### 3.6.11.3 Biodegradability of HA-$MnO_2$. Oxidation Products: Effect of $MnO_2$ Concentration and pH

Additional experiments were conducted to evaluate the biodegradability of HA-$MnO_2$ oxidation products as the sole carbon source. $MnO_2$ concentration and solution pH of the HA-$MnO_2$ reaction on strain EC112 cell growth were evaluated. Biochemical oxygen demand (BOD) was used as the measure of isolate growth on HA-$MnO_2$ oxidized products. The incubation period was 48 hours at 30°C. The experimental range of $MnO_2$ concentrations were selected based upon the results in Section 3.11.10.1. Control experiments evaluated growth provided only HA as the sole carbon source and else wise experimental conditions were same as the test conditions.

Earlier experiments using viable cell counts to determine cell growth demonstrated $MnO_2$ as an effective oxidant to increase HA biodegradability, while HA-$MnO_2$ contact time and $MnO_2$ concentration are important experimental variables. Here, experiments were completed using 48-hr. BOD as the measure of biodegradability of HA-$MnO_2$ oxidation products, replacing the viable cell count as a more reliable growth measure. During late exponential and early stationary phase of growth cells initiate clustering prior to the onset of Mn(II) oxidation, reducing apparent cell density and rendering cell counts unreliable.

Preparation of the HA solutions followed the same procedures as experiments in Section 3.3.11.1. For these experiments, the effect of pH (3.0, 7.0, and 9.0) and bivalent calcium ($Ca^{2+}$) (at pH 7.0±0.25 only) on the HA-$MnO_2$ reaction was investigated.

$MnO_2$ (0.5, 1.0, 1.5, 2.0, 2.5, 3.0 g) was added to 325-ml of 50 mg·L$^{-1}$ HA in 1-L Erlenmeyer flasks. The 1-L flasks were placed on a rotary shaker at 160 rpm and room temperature (approx. 25°C) for 45 minutes. Samples were collected before and after shaking for dissolved organic carbon (DOC) and uv-254 nm analysis. Both DOC and uv-254 are commonly used surrogate parameters for HA concentration. Uv-254 more specifically measures the aromatic HA fraction while DOC measures the total dissolved carbon concentration of the organic compounds. These parameters reflect changes in the aromatic structure of the HA and concentration of the HA due to adsorption to $MnO_2$ or conversion to $CO_2$.

Following shaking, 1-mL of trace metal solution (stock trace metal solution), $KH_2PO_4$, 10 mg/L; $(NH_4)_2SO_4$, 1 mg·L$^{-1}$; were added to the $MnO_2$ oxidized HA solutions. The oxidized AHA solutions were adjusted to the desired experimental pH using 0.1 N NaOH and 0.1 N $H_2SO_4$. The solutions were then each poured into standard BOD bottles (300-ml volume) following addition of 0.5 ml of isolate culture prior to capping with tapered ground glass stoppers. A residual volume of oxidized solution remained in the shaking flasks containing the solid $MnO_2$ (GreensandPlus) sand particles. A blank experiment in duplicates was performed that did not involve addition of isolate culture or $MnO_2$.

The stoppered BOD bottles were placed on a rotary shaker at 100 rpm and 30°C for 48-hrs. Dissolved oxygen concentration was determined immediately upon completion of the 48-hr incubation using the Winkler Titration Method with undiluted samples (Standard Methods, 4500-O B). Winkler Titration results for the blanks were averaged and subtracted from both the control and test experiments.

The biodegradability of the HA-$MnO_2$ oxidation products, as a function of reaction $MnO_2$ concentration, pH, and for added $Ca^{2+}$ at pH 7, is shown in Figure 3.15. The highest BOD was observed at pH 7 with added $Ca^{2+}$, and exhibits an apparent optimum of 2.4 mg·L$^{-1}$ at 1.5 g-$MnO_2$. For pH 7 (without added $Ca^{2+}$), the 48-hr. BOD is significantly less compared to added $Ca^{2+}$, demonstrating the effect of the bivalent cation, with an increase up to 1.5 g-$MnO_2$ followed by a plateau for higher $MnO_2$ levels.
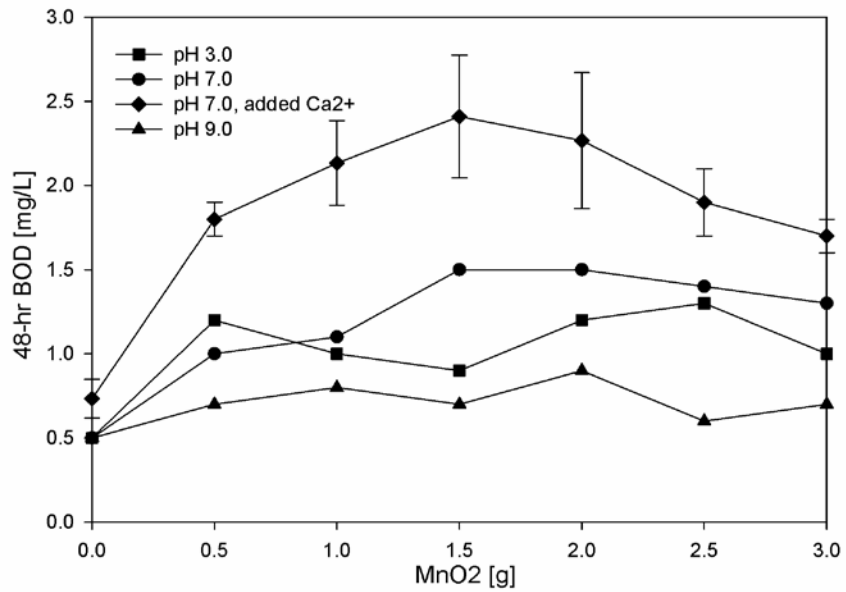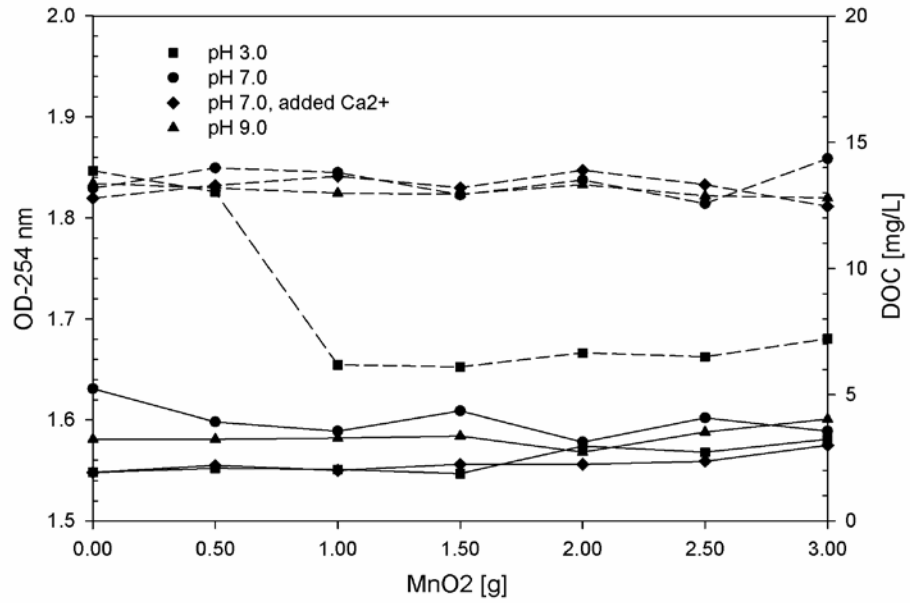
**Figure 3.15:** 48-hr. BOD results for strain EC112, (a) HA concentration (measured as UV-254) and DOC, (b) 48-hr. BOD. For pH 7.0, values represent triplicates, remaining experimental values are singlets and no error bars.

BOD at pH 9.0 is small or insignificant, with 48-hr.BOD increases < 0.4 mg·L$^{-1}$ compared to controls. At pH 3.0, $MnO_2$ had a more significant effect on the 48-hr. BOD, although no trend in BOD relative to $MnO_2$ concentration is observed. The BOD of the controls at pH 7.0 with added $Ca^{2+}$ range from 0.5 mg·L$^{-1}$ to 0.7 mg·L$^{-1}$.

Except for a significant decrease in DOC at pH 3.0 for $MnO_2$ levels 1.0 g and higher, no significant changes in DOC are observed at pH 7.0 or 9.0, indicating HA moieties are not irreversibly adsorbed or mineralized by $MnO_2$ (e.g., to CO or $CO_2$) during the HA-$MnO_2$ reaction. Additionally, no significant changes in UV-254 are observed at any pH, suggesting that aromatic HA rings are not directly altered (e.g., cleavage of aromatic C-C bonds) or adsorbed to $MnO_2$ in the HA-$MnO_2$ reaction.

These results are in agreement with the general trend of increasing adsorption of HA with decreasing pH, which has been previously observed for humic substance adsoprtion on Mn-oxides and other metal oxides (Davis, 1982; Tipping, 1981; Walte et al., 1988; Avena and Koopal, 1999). For comparison, freshwater aquatic humic substances adsorb >60% on mixed Mn-oxides ($Mn_3O_4$ and $\beta$-MnOOH) at pH 4.0 and <10% at pH 10.0 in 0.01 mol dm$^{-3}$ NaCl (Tipping and Heaton, 1983). $CaCl_2$, at 10$^{-3}$ mol·dm$^{-3}$, exhibits  no observable effect on adsorption at pH 4.0 for either mixed Mn-oxide, but has an increasing effect for higher pH, particularly above each oxides point of zero charge (PZC) (pH 5.4 and 2.8, respectively).

Oxidation of organic substrates by metal oxides is considered to be a surface reaction and can be generalized by the following steps: (1) diffusion/flux of organic substrates from bulk solution to the charged oxide boundary surface; (2) complex formation between the organic substrate and the oxide; (3) electron transfer from the substrate to the oxide; and (4) release of the oxidized organic and reduced metal into bulk solution (Stone and Morgan, 1984; Walte et al., 1988). The production of oxidized biodegradable organic substrates from HA is shown here to be dependent on $MnO_2$ concentration, pH and $Ca^{+2}$. Electrostatic charge has been previously attributed as a major mechanism for adsorption of humic substances on metal oxides and can provide a conceptual understanding (Tipping and Heaton, 1983; Gu et al., 1994). At high pH, both HA and $MnO_2$ have a net negative electrostatic charge and will repel each other. Assuming the $MnO_2$ surface reactive groups are primarily hydroxyl groups, many of which will be deprotonated, producing a strong net negative charge. The dominant humate reactive functional groups are carboxylic groups and phenolic groups whose charge density is pH dependent. HA carboxylics are >90% deprotonated above pH 7.0, (Shin et al., 1999). In addition, phenolics, which generally begin to ionize above pH 8, will add to the negative net humate charge and repulsion at high pH from the negatively charged surface. Though contributing a smaller effect, ionized phenolic groups lose the ability to hydrogen bond with the highly negative oxide surface, further reducing adsorption (Stone, 1987). These strong electrostatic forces increase the intramolecular repulsion between carboxys prevent diffusion/flux of HA to the metal oxide surface and explain the apparent lack of production of biodegradable oxidized products at pH 9.

At pH 3, HA and $MnO_2$ surface are electrostatically attracted, with the HA weakly negative most carboxylic groups protonated, and the $MnO_2$ surface having a net positive charge since pH < $pH_{pzc}$. Ligand exchange reactions between humic $COO^-$ and $OH^-$ and surface hydroxyl or water groups have been favored as the dominant adsorption mechanism, particularly at low pH (Tipping and Heaton, 1984; Gu et al., 1994).

At pH 7, the oxide surface charge is weakly negative and HA has a net negative charge, comparable to conditions at pH 9. The addition of $Ca^{2+}$ significantly increased the biodegradable oxidized products. Bivalent cations has been previously shown to enhance adsorption of humic substances to oxide surfaces by serving as a bridge between humic anionic groups and surface $O^-$, as an effective screening of the negative charge of the surface, and reduce humate charge density and overall size of HA molecules (Tipping and Heaton, 1983). Clearly, the high HA adsorption coupled with relatively low 48-hr. BOD observed at pH 3, the adsorption mechanisms at pH 7 must differ, particularly with added $CaCl_2$. Adsorption-desorption experiments for HA (protonated) on iron oxide ($Fe_2O_3$) using stagnation point flow have shown that adsorbed molecules at low pH can be desorbed by increasing the pH (Avena and Koopal, 1998). HA adsorbed at pH 3.25 can be rapidly desorbed by increasing the pH to 7.8, which effectively increases the molecule-surface repulsion (Avena and Koopal, 1998). The increase of 48-hr. BOD up to 1.5 g-$MnO_2$ for both pH 7 experiments suggest the availability of surface reaction sites is limiting at lower $MnO_2$ concentrations.

The decrease in 48-hr. BOD observed for >1.5 g-$MnO_2$ for at pH 7 suggests oxidized, biodegradable HA molecules may have been readsorbed onto the $MnO_2$ surface without further reaction or oxidized to products less biodegradable prior to subsequent to release back into the bulk solution. In a keynote laboratory study investigating the oxidation of humic substances by synthetic Mn-oxides, it was demonstrated that low molecular weight bioavailable carbonyls, including pyruvate, acetone, formaldehyde and acetaldehyde were among the oxidation products (Sundra and Kieber, 1994). Oxidative production rates within the first hours after oxide addition were linear for formaldehyde and acetaldehyde and nonlinear for pyruvate and acetone, results which were argued to be consistent with subsequent reaction of the ketone pair with Mn oxide following their production. The estimated total carbonyl yield, as a percentage of natural organic carbon, was 0.46%, with pyruvate (0.32%) being the major LMW product. Pyruvate and acetone, the two of the largest yielding oxidation products identified, showed a maximum production prior to decreasing at higher metal oxide concentrations. This was interpreted as subsequent oxidation of these products following their initial production.

### 3.6.11.4 Relative Cell Yield and Mn(II)-oxidation Rates on HA and HA-MnO$_2$ Oxidation Products

In order to evaluate the potential of Mn(II) oxidation in the HA-MnO2 system, strain EC211 growth and Mn(II)-oxidation rates were studied in batch reactors provided with HA-MnO$_2$ oxidation products as the sole carbon source. MnO$_2$ oxidized HA solutions were obtained following the procedures in section 3.11.10.2 except the HA concentration was increased to 50 mg·L$^{-1}$. In addition, 30 mg·L$^{-1}$ of Ca$^{2+}$ (as CaCl$_2$) was added to the HA solution, since Ca$^{2+}$ was observed to enhance HA oxidation and the 48-hr. BOD values (Fig. 3.15). The MnO$_2$ concentration and HA-MnO$_2$ contact time were fixed at the observed optimal amount of 45 min. and 2 g, respectively for 300 ml solutions of HA obtained in section 3.11.10.2. Two 4-L volume reactors, one containing HA-MnO$_2$ oxidized products and the second containing HA only, were used for the study. Each reactor was maintained at pH 6.5±0.25 and an incubation temperature of 30°C.

Growth was measured using volatile suspended solids (VSS) according to the Standard Methods 2540 E. The large reactor volume was necessary in order to permit sufficient amounts of biomass to be sampled for VSS analysis.

To measure strain EC112 growth and Mn(II) oxidation, cells were inoculated in 4-L reactors containing 3.5-L of 200 mg·L$^{-1}$ HA and HA-MnO$_2$ solutions. The relatively large HA concentration, compared to HA present in natural environments, was utilized to facilitate observance of significant difference in the measured parameters. DOC, VSS, and Mn(II) were measured and results are shown in Figures 3.16, 3.17, and 3.18.

Growth, as measured by VSS, increased from approx. 6.2 mg·L$^{-1}$ to 10.5 and 13.6 mg·L$^{-1}$ for HA and HA-MnO$_2$, respectively. Approximate biomass growth yields are 1.9% and 3.9% respectively for 200 mg·L$^{-1}$ each of HA and HA-MnO$_2$ solutions. These yields are obtained from the quotient of VSS and HA multiplied by 100%. Mn(II)-oxidation rates were 0.083 mg/l/hr and 0.14 mg/L/hr, measured in the late exponential to stationary growth phase (5 to 24 hours following isolate
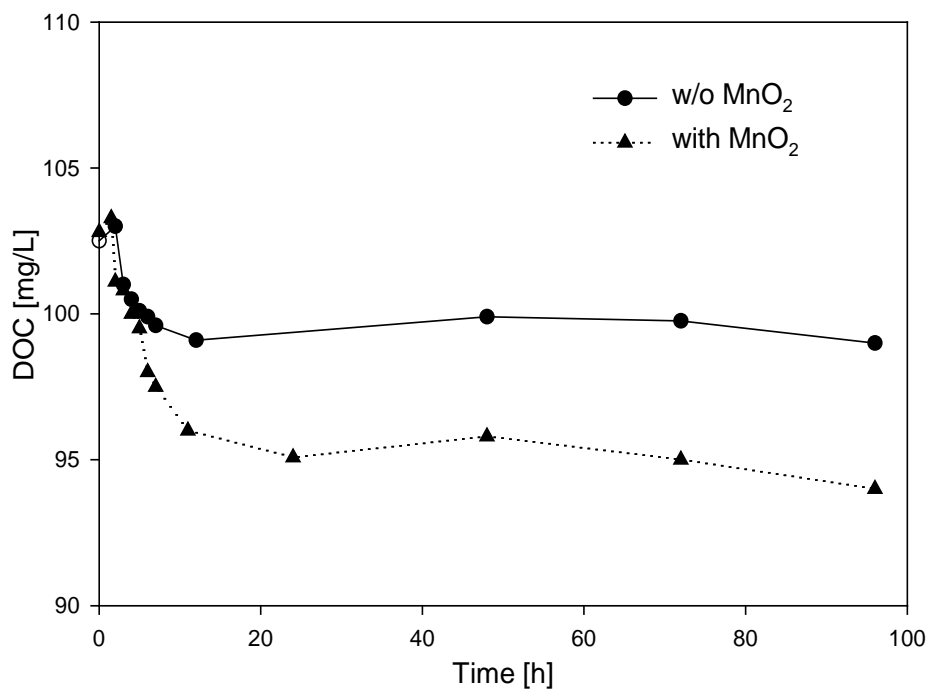
**Figure 3.16:** HA (as DOC) utilization by strain EC112 in separate 4-L reactors.
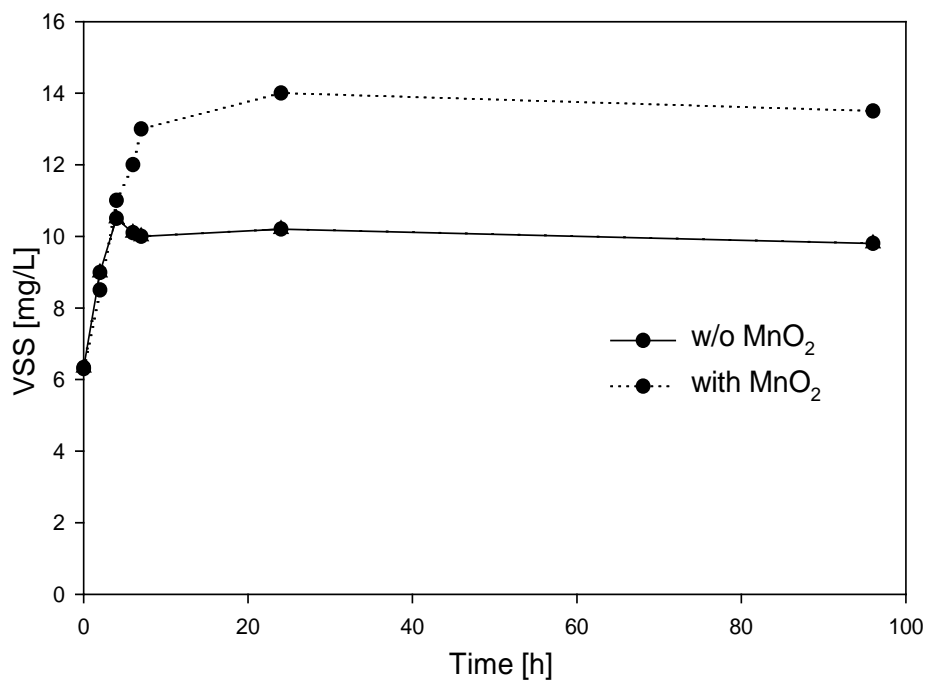


**Figure 3.17:** Strain EC112 Growth (as VSS) in separate 4-L reactors.
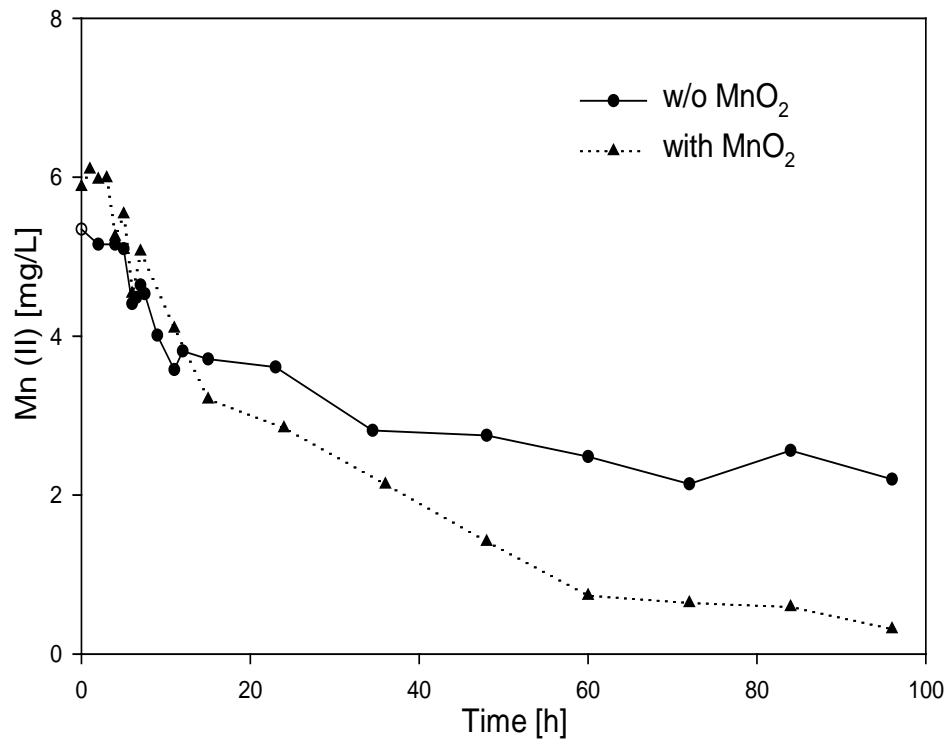
**Figure 3.18:** Biological Mn(II)-oxidation by strain EC112 in separate 4-L reactors.

inoculation). The 1.9% growth yield, which serves as the control yield, may largely represent utilization of labile compounds bound to the humic matrix in HA, such as simple carbohydrates and amino acids.

From the 4-L reactor results, strain EC112 growth on HA and HA-$MnO_2$ both show single phase growth. This suggests that energy favorable, easily assimiable carbon-energy sources were available in the oxidized products and constantly utilized. Diauxic growth (diauxic lag) or multiple growth phases with the easily metabolized products utilized first, is not observed, implying the bacterial cells did not expend energy to create a new pathway and/or enzymes for utilization of less favorable carbon-energy electron donors. A single growth phase is consistent with those under growth-limited conditions, whereas simultaneous utilization of the various HA-$MnO_2$ oxidation products is observed. If substrates were present in high (not growth-limiting) concentrations, sequential utilization and diauxic growth is an often observed characteristic and the substrate that supports the highest growth rate is utilized preferentially from the mixture.

Growth rates represented in the 4-L reactor experiments most likely underestimate the actual available pool of oxidized organic carbon produced from HA oxidation with $MnO_2$. No additional inorganic carbon sources (e.g., $HCO_3^-$) were added to the 4-L reactor growth experiments, a requirement for several essential anabolic reactions. For example, heterotrophic bacteria growth on low molecular weight compounds, such as pyruvate, require $CO_2$ (as $HCO_3^-$) fixation to regenerate carbon in the citric acid cycle. Pyruvate carboxylase, which is found in *Pseudomonas*, catalyzes the production of oxolaacetate from pyruvate and requires $HCO_3^-$ (Jitrapakdee et al., 2008). In addition, following oxidation, small highly polar molecules produced such as dicarboxylic acid methyl esters may sorb onto the HA, including the cross-linked regions of the remaining HA and participate in H-bonding networks and may not be available as a growth substrate (Niederer, 2007). Terrestrial humic acids such as Aldrich Humic Acids commonly have higher sorption capacities compared to aquatic HA. Furthermore, loss of volatile, low-molecular-weight oxidized components during experimentation likely underestimated growth on the oxidized humic acids (Maximov et al., 1977). In addition, high HA concentrations of 200 mg·$L^{-1}$, significantly greater than those used in the 48-hr. BOD growth experiments, likely resulted in humic aggregation, shielding available nucleophiles (e.g., alcohols) with reduced adsorption and oxidation with $MnO_2$. Finally, the reaction conditions for HA-$MnO_2$ represent the apparent but not true optimum for production of biodegradable oxidation products.

Mn-oxides are widely used in oxidation of alcohols to carbonyls, hydroxyl substituents of heterocyclic. However, most saturated alcohols, aldehydes and ketones, and carboxylic acids are unreactive with Mn-oxides, with pyruvic acid being an exception.

The improved biodegradability of HA may be largely attributed to oxidation of primary and secondary short-chained, aliphatic, branched alcohols. This implicates HA alcohols as being recalcitrant to strain EC112. *Pseudomonas* sp., particularly, *P. Putida* strains, are well-known

for their ability to induce nonspecific enzymes and degrade generally recalcitrant compounds, including aromatic hydrocarbon compounds, such as benzene, toluene, and phenol (Reardon et al., 2000). However, several studies show recalcitrance to oxidizing certain primary, secondary, heterocyclic, and aromatic alcohols and that carbon chain length affects activity with alcohols. The presence of multiple alcohol hydroxyl groups is considered to improve substrate solubility and susceptibility to biodegradation of C-C bonds. Experiments with *Pseudomonas* O-3 show enzyme activity on secondary alcohols increases with longer alkyl chains, in particular with alcohols with carbon number greater than 5 (Suzuki, 1976).

Alcohols dehydrogenases (ADHs) are common in bacteria and have been classified in three groups, ADH I, II, and III, with each type having specific alcohol affinities. Type I ADH can be produced by *pseudomonads*, including *P. Putida*, and are produced while growing on smaller, short-chained alcohols (Gorisch and Rupp, 1989). Some Type II ADHs can oxidize heterocyclic and longer chain primary and secondary alcohols.

Most ADH bacteria produce just one of the three types of ADHs, however, *P. Putida* HK5 is the first isolate identified to produce three types of ADHs and can utilize a variety of alcohols, including primary, secondary and diols (Toyama, 1995). The apparent low affinity by strain EC112 for primary and secondary alcohols may be due to the lack of producing ADHs with the specificity for HA coupled with steric hindrance posed by the humic macromolecular structure.

Phenolic compounds with electron-donating substituents such as alky or alkoxy ring groups degrade more rapidly compared to phenols with electron-withdrawing such as aceto, chloro, nitro, or carboxyl groups (Stone, 1987). Manganese oxides have been used as a selective reagent for the production of aldehydes and ketones from aliphatic primary and secondary alcohols. Sunda and Kieber's (1994) study of the Mn-oxide products of Mn-oxide and humic substances identified ketones and aldehydes as the major oxidation products – including pyruvate, ketone, formaldehyde, and acetaldehyde. For longer reaction times, aldehydes may be further oxidized to carboxylic acids.

Mn(II) oxidation rates will depend on the rate of Mn(II) adsorption to $MnO_2$ oxide and Mn(II)-bacteria concentration. Rates of Mn(II) adsorption will depend on available metal center reaction sites. Rates of Mn(II)-bacteria oxidation will be dependent on bacteria cell concentration, bacteria species, pH, temperature, ionic strength and Mn(II) concentration.


### 3.6.11.5 Mn(II)-oxidation Rates by strain EC112 utilizing HA-$MnO_2$ Oxidation Products

Experiments to study the kinetics of strain EC112 Mn(II)-oxidation were conducted in batch reactors provided HA-$MnO_2$ oxidation products as the sole carbon source. $MnO_2$ oxidized HA solutions were obtained following the procedures outlined in section 3.11.10.3

except the HA concentration was increased to 50 mg·L$^{-1}$ and with 30 mg·L$^{-1}$ Ca$^{2+}$. The MnO$_2$ concentration and HA-MnO$_2$ contact time were fixed at the optimal conditions, 2 g of MnO$_2$ and 45 minutes, as determined in section 3.13.2.

Experiments were initiated by adding 0.5-ml of fresh, harvested cells of strain EC112 to 200 ml of oxidized HA solution in 500-ml Erlenmeyer flasks, in triplicate. Mn(II) was added as 1, 2, 3 and 4 mg·L$^{-1}$, respectively in each of flasks. VSS was used as the measure of growth and which consisted of an initial VSS (VSS$_i$) and final VSS (VSS$_f$). For VSS$_i$, aliquots of 0.5 ml culture were pipetted in then immediately poured through glass fiber filters then held for drying prior to VSS analysis. Final VSS$_f$ measurements were obtained after completion of the time course experiment measuring Mn(II) oxidation, by filtering the entire 200-ml culture volumes through the glass filters and oven dried for at least 1-hr. at 103°C to 105°C prior to VSS analysis. The flasks were placed on a rotary shaker at 140 rpm and each reactor were maintained at pH 6.5±0.25 and incubated at a temperature of 30°C. The results, shown in Figure 3.19, reveal Mn(II) oxidation begins at approximately 3-4 hours after cell inoculation. The initial VSS$_i$ 2.0±0.3 mg·L$^{-1}$ and the final VSS$_f$ was 3.8±1.0 mg·L$^{-1}$. The measured difference, VSS$_f$ - VSS$_i$, represents a growth or increase on biomass of 0.5 to 3.1 mg·L$^{-1}$ of cells through utilization of MnO$_2$ oxidized HA as the sole carbon source.

The kinetic parameters for Mn(II) oxidation obtained in Section 3.11.9 for the Monod no-growth model were validated using the Mn(II) progress curves for 2, 3, and 4 mg·L$^{-1}$ in Figure 3.19. Biomass values for model validation were obtained by simulation using values from the range 0.5 to 3.1 mg·L$^{-1}$ of cells to determine a good-fit validation curve. For the initial Mn(II) concentrations of 2, 3, and 4 mg·L$^{-1}$ and 1.50, 1.25, and 0.75 mg·L$^{-1}$ of biomass respectively, show good fit model curves.

Mn(II) removal from solution by strain EC112 follows an initial more rapid trend prior to slower Monod type kinetics according to the substrate progress curves in Figure 3.19, similar to the progress curves for Mn(II) oxidation obtained for cells grown on glucose, indicating the Monod kinetic model is a good fit to the experimental data. The Mn(II) oxidation kinetics may be influenced by the harvesting conditions or culture history of the cells prior to inoculation into the flasks, which involved glucose as the sole carbon source, and the relative size of the increase in cell biomass of 2.0±0.3 increases to 3.8±1.0 mg L$^{-1}$ by the stationary phase. This low yields of biodegradable oxidized products from the HA-MnO$_2$ reaction hinder Mn(II) oxidation study involving oxidized humic substances as the sole carbon source is hindered by the low yield of oxidized products to produce large biomass.
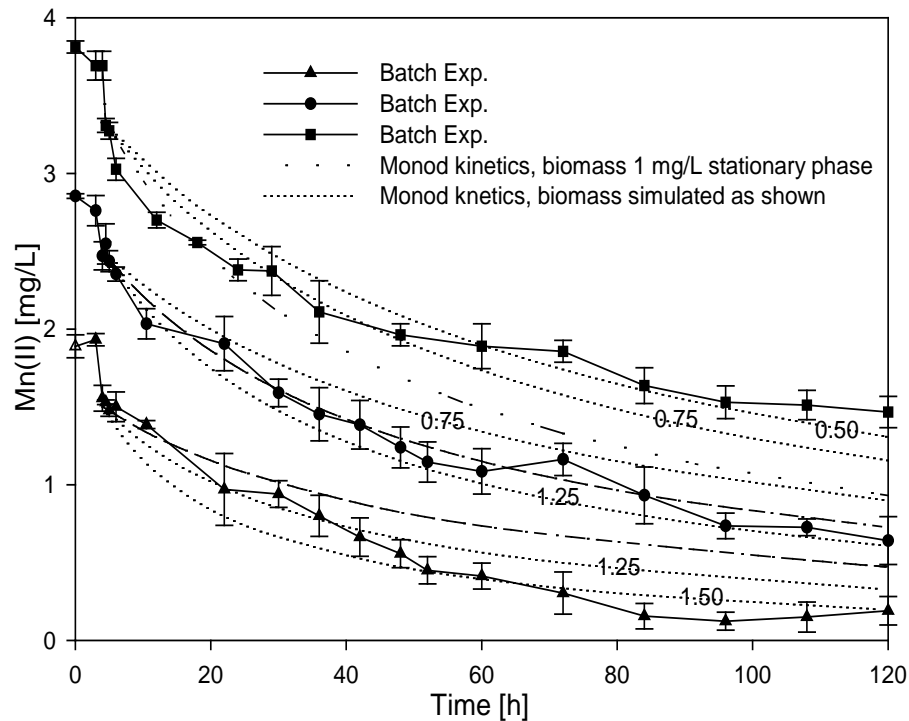
**Figure 3.19:** Mn(II)-oxidation by strain EC112 provided HA-MnO₂ oxidation products (prepared separately) as sole carbon source. Monod kinetic model and experimental Mn(II) depletion curves shown for initial Mn(II) concentrations of 2, 3, 4 mg·L⁻¹ at pH 6.5 and 30°C. Model biomass values were measured during the exponential growth phase and ranged from 0.5 to 1.50 mg·L⁻¹.

**Table 3.1:** Growth of strain EC211 on carbon sources.

| Carbon Source | Growth[a] |
|---|---|
| Acetaldehyde | + |
| Acetate | + |
| Acetic Acid | + |
| Acetone | + |
| Sodium Benzoate | + |
| Catechol | + |
| Citrate | + |
| Formaldehyde | + |
| Fructose | + |
| Glucose | + |
| 3-Nitrophenol | + |
| Phenol | + |
| Pyruvate | + |
| Sodium Citrate | + |
| Succinate | + |
| Trichloroethylene | + |
| Trichloroacetic Acid | - |
| Sodium Bicarbonate | - |

[a]Growth measured by changes in visual optical density after
5 days following culture inoculation.

**Table 3-2:** No-growth Monod kinetic parameters for Mn(II) oxidation and their standard error.

| Substrate | Parameter | Best Estimate | Standard Error |
|-----------|-----------|---------------|----------------|
| glucose | $k_{mc}$ | 0.180 | 0.003 |
| | $K_S$ | 1.086 | 0.029 |

**Table 3.3:** FT-IR band peak assignments for Aldrich Humic Acid.

| Wavelength ($cm^{-1}$) | Spectral Assignments |
|------------------------|----------------------|
| 3400-3450 | O-H stretching of hydroxyl groups carboxyl, hydroxyl, and phenolic groups. |
| 2900-3000 | Stretching in CH of $CH_2$ and $CH_3$ of aliphatic chains. |
| 2400-2700 | O-H stretching of COOH (very broad intensity). |
| 1710-1725 | C=O stretching of COO-, aldehydes, esters, and ketones. |
| 1600-1630 | Stretching of COO- and aromatic C=C. |
| 1510-1540 | Aromatic ring stretching C=C. |
| 1380-1435 | COO- stretching, -$OCH_3$ groups, O-H alcoholic and aliphatic $CH_2$ or $CH_3$ |
| 1150-1050 | C-O stretching of polysaccharides, primary and secondary alcohols. |

## 3.7 Summary and Conclusion

A Mn(II)-oxidizing bacterium, *P. Putida* strain EC112, was isolated from a soil sample and found capable of oxidizing Mn(II) in the stationary growth phase as a carbon-stressed, enzymatic constitutive feature. The optimal incubation pH and temperature for Mn(II) oxidation for liquid cultures of strain EC112 were determined to be pH 6.5 and 30°C.

When compared to the untreated HA control, enhanced strain EC112 growth and Mn(II)-oxidation rates were observed in the presence of HA-$MnO_2$ oxidation products as sole carbon source. The oxidative degradation of HA to more biodegradable and smaller substrates is attributed to the higher rates. HA-$MnO_2$ contact (stirring) time, solution pH, $MnO_2$ concentration and $Ca^{2+}$ addition were found to have an effect on HA biodegradability. Negligible amounts of HA were adsorbed to $MnO_2$ or mineralized to $CO_2$ during the HA-$MnO_2$ reaction.

Biological Mn(II)-oxidation kinetics for strain EC112 were adequately described using the no-growth Monod equation. Autocatalytic Mn(II) removal from bulk solution by sorption to $MnO_2$ was negligible in control studies and Mn(II) kinetic data sets were modeled without such consideration.

FT-IR and $^1$H-NMR spectra of HA-$MnO_2$ degradation products reveal distinctive changes in humic structure. The FT-IR spectra revealed the most significant HA degradation in the range 1000-1150 $cm^{-1}$, which are assigned to alcohol OH- and C-O functional groups. These are interpreted to be evidence of exchange reactions between humic hydroxyl and C-O functional groups and $MnO_2$ surface reaction sites. Sharp peaks on the $^1$H-NMR (at 1.05 ppm) and FT-IR (at 1380 $cm^{-1}$) are correlated and interpreted as representing oxidized HA fragments of the same source.

The HA-$MnO_2$ reaction is consistent with a mechanism of rapid humic adsorption and release of oxidation products from the oxide surface into the bulk solution.

# Chapter 4: Fixed-film Bioreactor Studies

## 4.1 Abstract

Mn(II)-oxidation by *Pseudomonas Putida* EC112 was investigated in fixed-film continuous flow bioreactors. Preliminary bioreactor experiments revealed D-glucose as a sole carbon source could not sustain bioreactor Mn(II) removal capacity (<0.05 mg·L$^{-1}$). Bioreactor failure initiated after 14 days of operation for an influent Mn(II) concentration of 0.45±0.03 mg·L$^{-1}$ using a 12-hr. HRT and an effluent recycle ratio of 150. Periodic (each 4 to 5 days) addition of nutrient/carbon spikes (nutrient broth/yeast extract) to the recycle line was required to sustain biological Mn(II) oxidation and Mn(II) effluent levels below <0.05 mg·L$^{-1}$.

Steady-state Mn(II) oxidation kinetics were studied and modeled using Monod Kinetics. A fixed-film kinetic parameter for Mn(II) oxidation was obtained, which was calibrated and validated in separate bioreactors without the addition of a feed carbon source. For model calibration, 6 steady-states (1.1 to 25 hrs. HRT) and a reactor Mn(II) influent concentration of 690±45µg were used. Model validation was obtained for 3 steady-states (12.6, 6.3, 1.3 hrs. HRT) and a reactor influent Mn(II) concentration of 750±45µg. Experimental Mn(II) data sets were fitted to the Monod Model using nonlinear least-square regression and the Marquardt-Levenberg algorithm (MLA). Autocatalytic Mn(II) removal from bulk solution by sorption to MnO$_2$ was not observed in control studies and Mn(II) kinetic data sets were modeled without such consideration.

A continuous flow bioreactor, packed with MnO$_2$-coated filter media (GreensandPlus), using Sewannee River Humic Acid (a model humic acid) as the sole carbon source, showed enhanced Mn(II) removal capacity compared to controls.

Biofilter Mn(II) releases were observed during the continuous flow bioreactor studies. Bioreactor conditions for release were identified and releases were modeled using pseudo first-order kinetics. The releases of Mn(II) into the bulk solution are interpreted to represent biotic Mn oxide reduction by strain EC112 and occur under Mn(II) saturating biofilter conditions.

A 3 to 5-day cell attachment time was sufficient for filter media biofilm development using strain EC112 culture seed in the continuous flow studies.

## 4.2 Introduction

Engineered biological treatment reactor systems to remove pollutants from wastewater and water are of one of two design types which use either aggregates of suspended cells or biofilms. In Chapter 3, Mn(II) oxidation was studied by the first type, suspended cells of strain EC112, also known as suspended floc, in the stationary phase of growth. The cells served as active biomass, catalyzing the oxidation of Mn(II) using enzymes as the Mn removal mechanism. Mn(II) served as the electron donor and the active biomass served as the electron acceptor. In Chapter 4, the second reactor design, which incorporate biofilms or fixed films, will be studied and represent the most common type of biological reactor for Mn(II) control/removal for water treatment.

The specific objectives of the fixed-film reactor studies are:

(1) To evaluate the potential of Mn(II) oxidation in the fixed-film reactor using a single carbon source (e.g., glucose).

(2) To estimate the intrinsic kinetic model parameters for biological Mn(II) oxidation. Parameters were obtained using the steady-state effluent Mn(II) conditions and the predictive flux equation derived from the pseudo-analytical solution of the biofilm model given by Atkinson and Davies (1974).

(3) To investigate the fate of Mn(II) in the biofilter.

(4) Assess humic acids as a sole carbon and energy source to sustain bioreactor capacity to remove Mn(II).

## 4.3 Materials and Methods

Some of the report format and kinetic parameter discussion in the following sections is in accordance with Dastidar (2010).

### 4.3.1 Fixed-Film Bioreactor

Biological oxidation of Mn(II) was investigated in laboratory-scale fixed-film bioreactors. For objectives (1), (2), and (3), pure cultures of strain EC112 were immobilized by attachment to spherical 3-mm diameter glass beads using a 3-day (static conditions) period prior to reactor start-up. For objectives (4), pure cultures of strain EC112 were immobilized by attachment to GreensandPlus (GSP), using a 3 to 5-day (static conditions) period prior to reactor start-up. Bioreactors were operated with effluent recycle to maintain completely mixed conditions inside the bioreactor.

### 4.3.2 Reactor Configuration and Operating Conditions

The biofilm reactor used for all continuous flow, fixed-film studies was constructed from an acrylic column (internal diameter: 2.3 ± 0.02 cm, height: 20.1 ± 0.03 cm). The filter material consisted of 3 mm diameter spherical pyrex glass beads (Fisher Scientific) or GSP as the filter material (Figure 4.1). The empty bed volume of the reactor measuring at 83.6 mL. Total reactor surface area cell attachment in the packed bed reactor was constant for each reactor, depending on the number of beads.

### 4.3.3 Bacterial Strain and Feed Composition

The culture and feed composition and preparation procedures used in the biofilm reactor studies are described in Sections 3.3.3 and 3.3.4. For objective (1), glucose and an undefined carbon source (yeast extract/nutrient broth) were feed separately into reactors. For objective (2) and (3) the reactor influent feed composition consisted of the carbon-free medium described in section 3.3.4.3 supplemented with trace metal solution. For objective (4) humic acids (Sewannee River Humic Acid) was the sole carbon source supplemented with basal medium and trace metal solution.
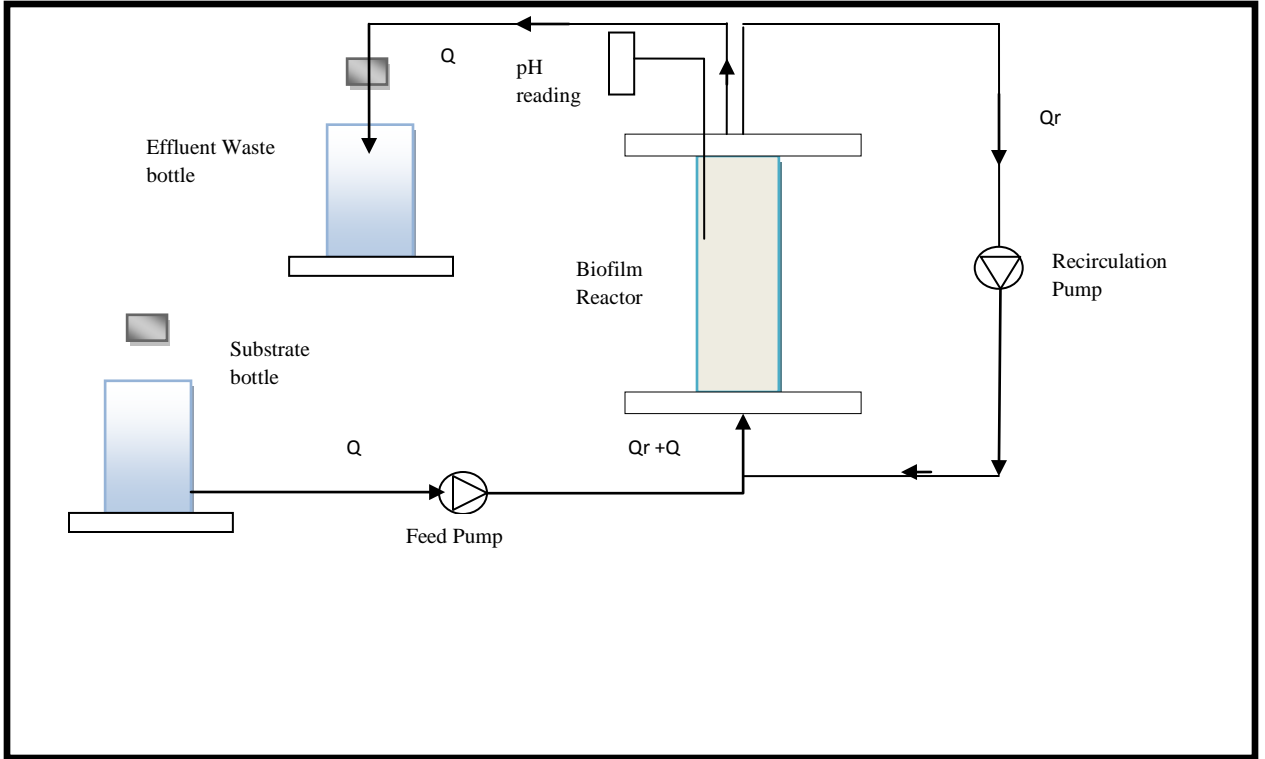
**Figure 4.1:** Schematic of the fixed film reactor system used for all continuous flow experiments (Dastidar, 2010).

and the connecting tubings were autoclaved at 121°C for 15 mins. The interior of the reactor was rinsed in 90% ethanol and dried before assembling the components under a germ free hood (Steril Gard Class II Model, The Baker Company, Stanford, ME).

Biological growth in the feeding tubes was minimized by frequent replacement of parts and tubings. Bolted flanges and rubber gaskets were used on the top and bottom of the reactor to prevent leakage of the effluent from the reactor. Peristaltic pumps (Masterflex, Cole-Parmer) were calibrated and used for the influent and recycle flows and the reactor was operated in an up-flow mode to provide near completely submerged conditions in the reactor.

### 4.3.4 Tracer Study

A tracer study was conducted to determine the flow characteristics in the reactor. Mn(II) was used as the tracer with influent concentration of 5 mg·L$^{-1}$ and an influent feed flow rate of 4.0 mL·hr$^{-1}$ (HRT = 0.48 days). The measured effluent Mn(II) concentrations were compared to the tracer response curve for an ideal completely mixed reactor using:

$$\frac{C}{C_O} = (1\text{-}e^{-t/\tau})$$

(4-1)

where C and $C_0$ are influent and effluent Mn(II) concentration, t is the time of sample measurement and tau is the HRT based on the feed flow rate Q. Mn(II) was determined using the pesulfate method (Section 3.3.3.2).

### 4.3.5 Control Study

A control study was performed to investigate whether dissolved Mn(II) in the reactor influent could be oxidized or sorbed to the glass beads, tubing or the walls of the acrylic column reactor. The reactor was packed with 3 mm diameter glass beads that were autoclaved and oven dried and operated at 12-hr. HRT for 10 days. The feed solution consisted of 5 mg·L$^{-1}$ stock Mn(II) added to SQ water and pH adjusted to 7.0. Samples were collected daily from the reactor and analyzed for influent Mn(II) and effluent Mn(II).

## 4.3.6 Reactor Startup

The bioreactors and its components were assembled under a laminar flow hood (Steril Gard, class II type A/B3, Baker Company, Sanford, ME), and packed with autoclaved oven dried solid glass beads (Fisher Scientific). The reactor was then inoculated with (15 to 30 mL) harvested cultures of strain EC112 of volume that filled the reactor about 1 inch above the top of filter material column.  Generally, 3 days was sufficient for visible biofilm development on glass bead filter material. For sand filter material (GreensandPlus), up to 5 days was required. Optimum operating conditions were maintained in the reactor by frequent monitoring of pH which was maintained at ~ 6.5. The reactors for Objective 1 were operated under an influent Mn(II) concentration of 200 µg·L$^{-1}$ and HRT of 12 to 24 hrs.

## 4.3.7 Steady-State Determination in the Biofilm Reactor

For the steady-state biofilm reactors in Objective 2, the bioreactor was continuously operated under completely mixed-flow conditions at least four times the HRT following reactor start-up to create steady-state conditions before changing the Mn(II) loading rate. Foggler (1999) and Jensen (2001) showed that in terms of pure hydraulics, a completely mixed reactor reaches a 95% steady-state concentration following four times the HRT.  Two separate reactors were studied for purposes of kinetic parameter modeling, a calibration and validation reactor. Samples were also collected for determining the viable suspended cells in the effluent from the reactor. For attached biomass analysis, samples were collected at reactor start-up and at the end of the reactor study. Intermittent samples were not collected due to the potential to disturb immobilized cells and release of accumulated Mn from the biolfilter.

## 4.3.8 Analytical Methods

### 4.3.8.1 Sample Handling and Quality Control

Samples from the bioreactor were collected using 1 mL sterile disposable pipets (Fisher Scientific CO) at appropriate time intervals. The collected samples were immediately centrifuged at 10,000 rpm for 10 mins.. For Mn analysis using ICP, samples were acidified with 1 N HNO$_3$ (pH < 2) and preserved at 4°C. Microbial biomass analysis involved determination of the total protein content of bacterial cells, and attached/suspended viable cell concentrations at the beginning and end of reactor operation. The biological samples were analyzed immediately to prevent any changes that may occur after collection.

For protein analysis, the microreaction vessels (Supelco, Inc., Bellefonte, PA) were washed, rinsed, and oven dried prior to use. The 2.0 mL centrifuge tubes (Fisher Scientific CO., Pittsburg, PA) used for protein analysis and were first autoclaved at 121°C for 15 mins, and

then stored under the germ free hood (Steril Gard Class II Model, The Baker Company, Stanford, ME) before each use.

## 4.3.8.2 Mn(II), Mn(IV)

For the steady-state Mn oxidation reactor studies Mn was analyzed using ICP as described in section 3.3.3.2 in Chapter 3. The persulfate method was used for Mn for the remaining reactor studies.

## 4.3.8.3 pH and Dissolved Oxygen Determination

pH was measured using a pH meter (Denver Instrument, Denver, CO) equipped with an ATC Combo, Silver/Silver chloride electrode. The pH meter was calibrated with standard buffers of 4, 7 and 10 disinfected by 95% ethanol before use. DO was determined *in situ* using a DO meter (YSI 550A, Yellow Springs, Ohio), also calibrated and disinfected with 95% ethanol before use.

## 4.3.9 Biomass Analysis

Biomass analysis for the continuous flow bioreactor studies was performed for Objectives (2) and (4) using the following procedures.

## 4.3.9.1 Attached Cell Count

For the steady-state reactor for kinetic modeling five glass beads each from top and bottom of the reactor were removed under the laminar flow hood (Steril Gard Class II Model, The Baker Company, Stanford, ME). Each of the removed glass bead was placed inside a 10 mL microreaction vessel containing 1 mL MCSM (without yeast extract) solution. Six glass beads (three from top and bottom) were used for the determination of viable attached cell count, whereas, the rest were used for protein analysis of the attached cells.

## 4.3.9.2 Viable Attached Cell Count

The glass beads in the capped 10-mL vessels were shaken vigorously in a vortex mixer (Fisher Vortex Genie 2, Fisher Scientific Co, PA) for 10 mins. to achieve cell detachment. Samples (1.0 mL) from each microreaction vessel were serially diluted in 30-mL test tubes containing 9.0 mL of MCSM (without yeast extract) solution. The diluted samples of 1.0-mL were then transferred to the solidified agar medium on the agar plates for colony counting.

### 4.3.9.3 Protein Measurement

The vessels containing glass beads for protein analysis were also shaken in a similar manner for the occurrence of cell detachment. Samples (1.0-mL) from each vessel were transferred to 2.0 mL centrifuge tubes (Fisher Scientific Co., Pittsburg, PA). The cell pellet obtained by centrifuging the samples at 10,000g for 15 mins. was then analyzed for protein concentration.

Bradford reagent (Bradford 1976) sample (0.5-mL) was added to the cell pellet in the centrifuge tube and the contents were mixed for 15s, followed by incubation at room temperature for at least 5 mins. SQ water (0.5-mL) was then added to the tube and the contents mixed for 10 s and incubated for 25 to 30 mins. The absorbance reading of the samples was measured at 594 nm in a spectrophotometer. The true absorbance value of the collected samples was estimated by measuring the difference between the measured and the control (1:1 ratio of Bradford reagent and SQ water) values. The protein concentration in $mg \cdot L^{-1}$ was then computed using a standard calibration curve obtained by treating different dilutions of bovine serum with Bradford reagent.

### 4.4 Basic Biofilm Model For Steady-State Analysis

A kinetic parameter was obtained using steady-state effluent Mn(II) conditions and the predictive flux equation derived from the pseudo-analytical solution of the biofilm model given by Atkinson and Davies (1974).

### 4.4.1 Properties

The physical properties and characteristic concentration profiles of an idealized homogenous biofilm (Figure 4.2) are listed as follows (Rittmann, 2001):

1. The biofilm has a uniform biomass density $X_f (M_x \cdot L^{-3})$.

2. The biofilm is homogenous in nature with a uniform biofilm thickness ($L_f$) through out the reactor.

3. The external mass transport resistance is represented by the effective diffusion layer of thickness (L), whereas, the internal mass transport resistance is due to molecular diffusion.

4. The consequence of the mass transport resistance leads to the lowering of the actual bulk Mn (II) concentration (S) to a value ($S_f$) inside the biofilm.

5. A deep biofilm is characterized by the substrate concentration approaching zero at a certain point in the biofilm, whereas, in a shallow biofilm, the concentration ($S_f$) remains above zero at all points in the biofilm matrix.

6. A fully penetrated biofilm is characterized by identical substrate concentrations at the outer ($S_s$) and attachment ($S_w$) surfaces.

7. The increase in the biofilm thickness is due to growth of the biofilm itself with attachment from suspended cells negligible.
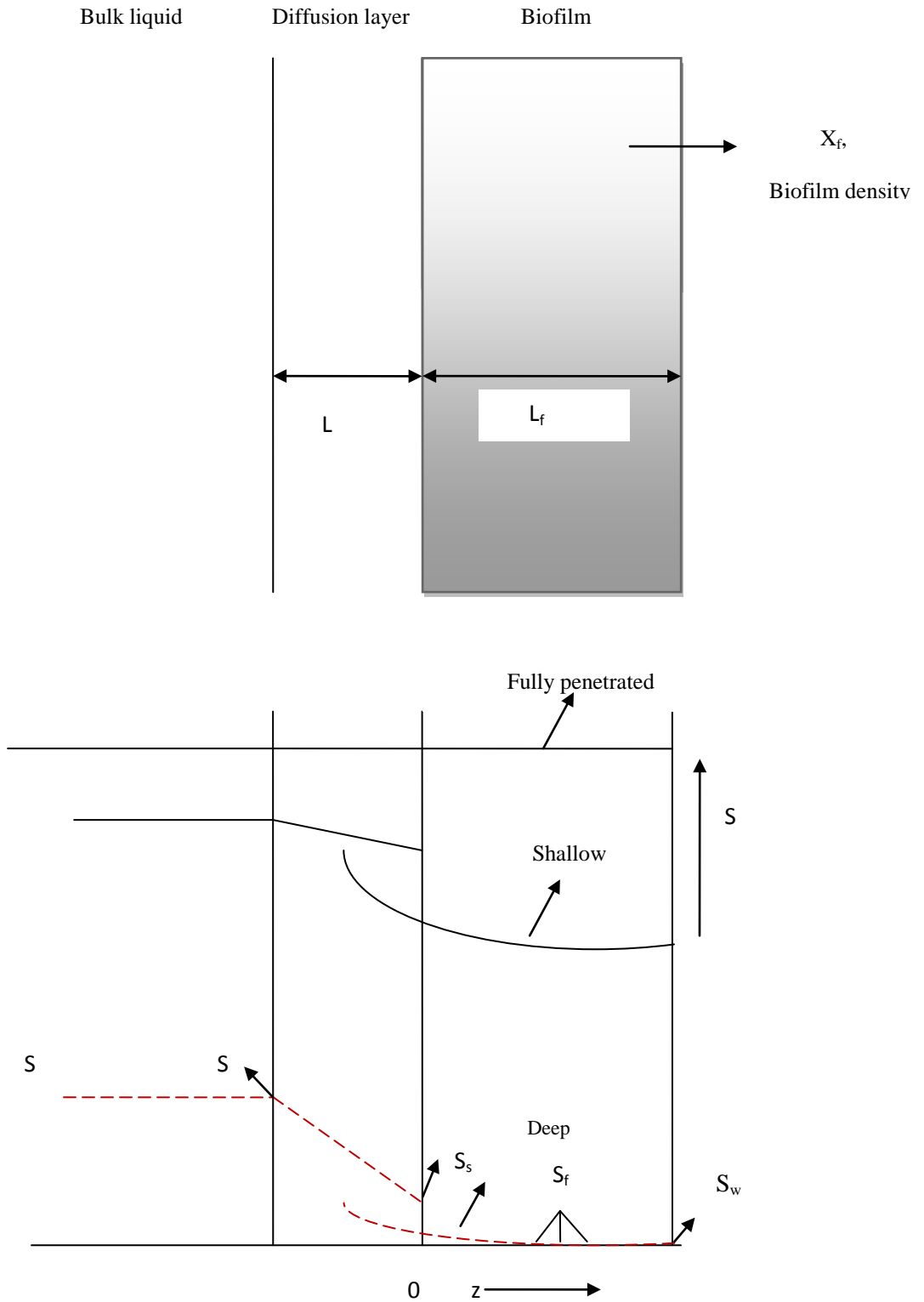
**Figure 4.2:** Idealized biofilm schematic with physical properties and characteristic concentration profiles (Rittmann, 2001).

## 4.5 Liquid–Phase Parameters
### 4.5.1 Effective Diffusivity

The diffusivity of Mn(II) in water was estimated using the Nernst-Haskell equation (Longsworth, 1972):

$$D_{Mn(II)} = \frac{RT\,\lambda}{F^2\,|z|}$$

(4-2)

where $D_{Mn(II)}$= diffusion coefficient of Mn(II) in water (cm$^2$s$^{-1}$), T = absolute temperature (K), R= universal gas constant (J·mo1$^{-1}$·K$^{-1}$), F = Faraday's constant (C·g·mol), $\lambda$ = Electrolytic conductance (cm$^2$·ohm·c), and z is the charge on the ion. The value of electrolytic conductance ($\lambda$) was obtained from the table of ionic conductivity and diffusion at infinite dilution (CRC Handbook, 2009). According to the CRC handbook guidelines (CRC Handbook, 2009), the listed electrolytic conductance ($\lambda$) value at 25°C should be increased 15% for every 5°C temperature rise in the medium.

### 4.5.2 Porosity of the Medium Bed

The porosity of the packed bed was estimated using the direct volumetric method:

$$\varepsilon = \frac{V_v}{V_T}$$

(4-3)

where $V_v$ is the volume of the void-space in the medium bed, and $V_T$ is the total or bulk volume of the medium bed. The porosity of the medium bed was assumed constant for the purpose of model calculations under different operating conditions.

### 4.5.3 Absolute Viscosity of Water

The absolute viscosity of water ($\mu$) used for model calculation was obtained at 30°C from the CRC handbook (2009).

### 4.5.4 Modified Reynolds Number and Schmidt Number

The modified Reynolds number $Re_m$ was calculated using the following equation (Jennings 1975):

$$Re_m = \frac{2\rho d_p u}{(1-\varepsilon)\mu} \qquad (4\text{-}4)$$

where $Re_m$ = the modified Reynolds number, $\rho$ = density of water (g·cm$^{-3}$), $d_p$= diameter of the solid medium bed, u= superficial velocity (cm·d$^{-1}$), $\varepsilon$= porosity of the medium bed, and $\mu$= absolute viscosity (g·cm$^{-1}$·d$^{-1}$).

The superficial velocity (u) was estimated according to the following relationship between the feed flow rate and the cross sectional area of the flow stream:

$$u = \frac{Q}{A_c} \qquad (4\text{-}5)$$

where Q is the feed flow rate to the reactor (cm$^3$·d), and $A_c$ is the cross sectional area of the flow stream (cm$^2$). The calculated modified Reynolds number of 1.66 was within the limits typical for water ($1 \leq Re_m \leq 30$) (Rittmann, 2001).

The Schmidt number was calculated using the following equation:

$$S_c = \frac{\mu}{\rho D_{Mn(II)}} \qquad (4\text{-}6)$$

### 4.5.5 Effective Diffusion layer

The thickness of the effective diffusion layer (L) or the external mass transfer layer was estimated using the empirical formula reported by Jennings (1975) for porous media:

$$L = \frac{D_{Mn(II)}(Re_m)^{0.75}Sc^{0.67}}{5.7u} \qquad (4\text{-}7)$$

The thickness value of the effective diffusion layer (L) used for steady-state data analysis was estimated by substituting the other liquid phase parameter coefficients into the Eqn. (4-7).

### 4.5.6 Molecular Diffusivity of Mn(II) in the biofilm

The molecular diffusivity ($D_f$) of Mn(II) in the biofilm was estimated according to Williamson and McCarty (1976) by using the ratio:

$$\frac{D_f}{D_{Mn(II)}} = 0.8 \tag{4-8}$$

### 4.5.7 Biofilm Specific Surface Area

The biofilm specific surface area was estimated using the following relationship:

$$a = \frac{nA}{V} \tag{4-9}$$

where a is the biofilm specific surface area ($L^{-1}$), n is the number of glass beads in the reactor, A is the surface area of glass beads ($L^2$), and V is the empty bed volume of the reactor ($L^3$).

### 4.5.8 Biofilm Thickness and Biofilm Density

The biofilm thickness and the biofilm density were computed from the following equations (Rittman et al.1986) assuming biofilm mass to be 99% water by weight:

$$L_f = \frac{W_w}{\rho nA(0.99)} \tag{4-10}$$

$$X_f = \frac{W_d}{AL_f} \tag{4-11}$$

where $W_w$ is the wet weight of the biofilm (M), $\rho$ is the density of water ($M{\cdot}L^{-3}$), n is the number of glass beads in the packed bed reactor, $X_f$ is the biofilm density ($M{\cdot}L^{-3}$), and $W_d$ is the biofilm dry weight (M).

### 4.5.9 Model Inputs for Steady-State Analysis

The parameters listed in Table 4.1 were used as inputs of the predictive flux model for analyzing the steady-state flux data obtained under steady-state conditions (Objective 2). The parameter values in Table 4.2 were used for validation of the steady-state biofilm model kinetic parameter.

### 4.6 Steady-State Analysis

### 4.6.1 Steady-State Mass Balance on Mn(II)

The steady-state mass balance on Mn(II) in the completely mixed packed bed reactor is described by

$$QS_o - QS_e - J_{exp}aV = 0 \qquad (4\text{-}12)$$

where Q is the steady-state flow rate ($L^3 \cdot T^{-1}$), $S_0$ is the influent Mn(II) concentration ($M \cdot L^{-3}$), $S_e$ is the effluent Mn(II) concentration ($M \cdot L^{-3}$), $J_{exp}$ is the observed steady-state Mn(II) flux ($M \cdot L^{-2} \cdot T$) into the biofilm, a is the biofilm specific surface area ($L^{-1}$), and V is the reactor volume ($L^3$).

The steady-state Mn (II) flux expression calculated from Eqn. (4-12) for the various steady-state conditions in the packed bed reactor is given by:

$$J_{exp} = \frac{S_o - S_e}{\tau a} \qquad (4\text{-}13)$$

where T is the empty bed detention time (T) = $\dfrac{V}{Q}$

Table 4.1: Model Inputs for the Steady-State Calibration Data Analysis

| Parameters | Description | Units | Values |
|---|---|---|---|
| $D_{Mn(II)}$ | Diffusivity Coefficient of Mn(II) | $cm^2 \cdot hr^{-1}$ | $5.0 \times 10^{-4}$ |
| $\varepsilon$ | Porosity of the medium bed | ------ | 0.46 |
| $\mu$ | Absolute viscosity of water | g/cm.day | 689.47 |
| $Re_m$ | Modified Reynolds number | ------ | 1.62 - 17.06 |
| Sc | Schmidt number | ------- | 962.28 |
| L | Effective diffusion layer thickness | cm | 0.137 - 0.255 |
| $D_f$ | Molecular diffusivity | $cm^2 \cdot day^{-1}$ | 0.702 |
| a | Biofilm specific surface area | $cm^{-1}$ | 600.31 |
| $L_f$ | Biofilm thickness | cm | 0.005 |
| Xf | Biofilm density | $\mu g \cdot cm^{-3}$ | 12,000 |

Table 4.2: Model Inputs for the Steady-State Valibration Data Analysis

| Parameters | Description | Units | Values |
|---|---|---|---|
| L | Effective diffusion layer thickness | cm | 0.147 - 0.255 |
| $L_f$ | Biofilm thickness | cm | 0.005 |
| Xf | Biofilm density | $\mu g \cdot cm^{-3}$ | 13,000 |

## 4.6.2 Mn (II) Volumetric Loading Rate

The Mn (II) volumetric loading rate was calculated based on Eqn. (4-14):

$$VL = \frac{QS_o}{V} \tag{4-14}$$

where V·L is the volumetric Mn(II) loading rate ($M \cdot T^{-1} L^{-3}$), Q is the influent Mn(II) flow rate to the reactor ($L^3 T^{-1}$), $S_0$ is the influent Mn(II) concentration ($M \cdot L^{-3}$), and V is the volume of the reactor ($L^3$).

## 4.6.3 Mn (II) Applied Surface Loading Rate

The Mn (II) applied surface loading rate was estimated using Eqn. (4-15) shown below:

$$J_{Mn(II)} = \frac{QS_0}{M_S(\frac{a}{M})} \tag{4-15}$$

where $J_{Mn(II)}$ is the mass of Mn (II) applied per unit of biofilm surface area per unit of time ($M \cdot L^{-2} \cdot T^{-1}$), $M_s$ is the total mass of glass beads in the reactor (M), and a/M is the surface area per unit mass of the glass beads ($L^2 \cdot M^{-1}$).

## 4.6.4 Mn(II) Oxidation Rate

The Mn(II) oxidation rate was evaluated using the following Eqn. (4-16):

$$v = \frac{S_o - S_e}{\tau} \tag{4-16}$$

where $v$ is the Mn(II) oxidation rate ($M \cdot L^{-3} \cdot T^{-1}$), $\tau$ is the HRT (T), and $S_e$ is the effluent Mn(II) concentration ($M \cdot L^{-3}$).

## 4.6.5 Components of the steady-state biofilm model

A recycle ratio of 150 was used to maintain completely mixed conditions in the bioreactors. The influent Mn(II) concentration $S_0$ at the inlet of the reactor was estimated using the following mass balance equation:

$$S_o = \frac{QS_o + Q_rS_e}{Q + Q_r} \qquad (4\text{-}17)$$

where $Q_r$ is the recycle flow rate ($L^3 \cdot T^{-1}$).

The Mn (II) concentration at the biofilm/liquid interface ($S_s$) ($M \cdot L^{-3}$) was determined from the Fick's first law:

$$S_s = S_e - \frac{LJ_{exp}}{D} \qquad (4\text{-}18)$$

where L the thickness of the external mass transfer diffusion layer, $S_e$ is the effluent Mn(II) concentration ($M \cdot L^{-1}$), and D is the diffusion coefficient of Mn(II) in water ($L^2 \cdot T^{-1}$).

## 4.6.6 Predicted Flux Model and the Optimization Algorithm

The Mn(II) mass balance for a steady-state concentration profile in the biofilm can be described as:

$$0 = D_f \frac{d^2 S_{Mn(II)}}{dz^2} - \frac{kX_f S_{Mn(II)}}{K_s + S_{Mn(II)}} \qquad (4\text{-}19)$$

A pseudo-analytical solution of the above equation can be expressed according to Atkinson and Davies (1974):

$$J_{pr\ Mn(II)} = \frac{\eta L_f S_s k X_f}{K_s + S_s} \qquad (4\text{-}20)$$

$S_{Mn(II)}$ flux in the biofilm. The biomass density ($X_f$) used in Eqn. (4-23) was calculated from the biomass dry weight (mg VSS). The kinetic parameters k and $K_s$ in Eqn. 4-23 were estimated using a nonlinear regression analysis with SigmaPlot 11 application software (Systat Software Inc.). The software uses Marquardt-Levenberg algorithm (Marquardt, 1963) to estimate the optimized value of the parameters by minimizing the residual sum of squares between the observed flux (Eqn. 4-13) and the predicted flux (Eqn. 4-23) and is given by the equation:

$$\min \sum_{i-1}^{n}(J_{exp,i} - J_{prMn(II),i}(k, K_s))^2 \qquad (4-21)$$

where n= number of d The effectiveness factor (η), which represents the ratio of the actual flux to the flux that would occur in a fully penetrated biofilm (Rittmann, 2001), can be estimated using Atkinson's numerical solution to the biofilm model (Atkinson and Davies, 1974):

$$\eta = 1 - (L_f (\frac{kX_f}{K_s D_f})^{-0.5}) \tanh(L_f (\frac{kX_f}{K_s D_f})^{0.5})(\frac{\varphi}{\tanh\varphi} - 1) \quad \text{If} \quad \varphi < 1 \qquad (4-22)$$

$$\eta = \frac{1}{\varphi} - (L_f (\frac{kX_f}{K_s D_f})^{-0.5}) \tanh(L_f (\frac{kX_f}{K_s D_f})^{0.5})(\frac{\varphi}{\tanh\varphi} - 1) \quad \text{If} \quad \varphi \geq 1 \qquad (4-23)$$

The Thiele modulus (φ) can calculated using the following expression (Atkinson and Davies 1974):

$$\varphi = L_f (\frac{kX_f}{K_s D_f})^{0.5} (1 + \frac{2S_s}{K_s})^{-0.5} \qquad (4-24)$$

where k is the maximum specific Mn (II) oxidation rate ($Ms \cdot Mx^{-1} \cdot T^{-1}$), $K_s$ is the saturation constant ($M \cdot L^{-3}$), and $D_f$ is the diffusion coefficient of Mn (III) in the biofilm ($L^2 \cdot T^{-1}$). The biofilm was considered fully penetrated if η was estimated to be ≈ 1.

When $S_s$ << $K_s$, Monod Kinetics (Eqn. 4-20) can be approximated by the first order expression:

$$J_{pr\,Mn(II)} = \eta S_s k_0 L_f k X_f \qquad (4-25)$$

$$\text{with } k_o = \frac{k}{K_S}.$$

While the effectiveness factor ($\eta$) can be approximated from (Levenspiel, 1998):

$$\eta = \frac{\tanh(\varphi)}{\varphi} \tag{4-26}$$

and $\varphi$ can be obtained:

$$\varphi = L_f \left[\frac{k_0}{D_f}\right]^{1/2} \tag{4-27}$$

## 4.7 Model evaluation and reliability of the parameter estimates

A steady-state model kinetic parameter k was obtained by data calibration using phases III - VII of operation of the steady-state continuous bioreactor effluent Mn(II) data (Table 4.3 and Figure 4.7) and the non-linear estimation routine. The model kinetic parameter k was validated using the steady-state Mn(II) data for Phases I to III of a second bioreactor (Table 4.4 and Figure 4.8).

Kinetic parameter reliability estimates were assessed using a 95% prediction interval. The coefficient of variation between the predicted $J_{prMn(II)}$ and the observed $J_{exp}$ was obtained using a linear regression analysis plot.

## 4.8 Results and Discussion

### 4.8.1 Reactor Tracer study

The flow data in Figure 4.3 show that tracer response curves generated at a $Q_R/Q_F=150$ using Mn(II) matched well with the ideal completely mixed flow curve. The difference between the observed data and the ideal tracer response curve was statistically insignificant at the 95% confidence level ($\alpha$ =0.05) for Mn(II) ($p = 0.32$).

The completely mixed regime in the reactor was also investigated at a recycle ratio of 50 and 125. The comparison between the observed data and the tracer response curve was not very good with the difference statistically significant ($p = 0.01$) at the 95% confidence level.

The results of the study indicate that operation of the biofilm reactor at a recycle ratio of 150 would ensure completely mixed conditions under the different Mn(II) loading rates.
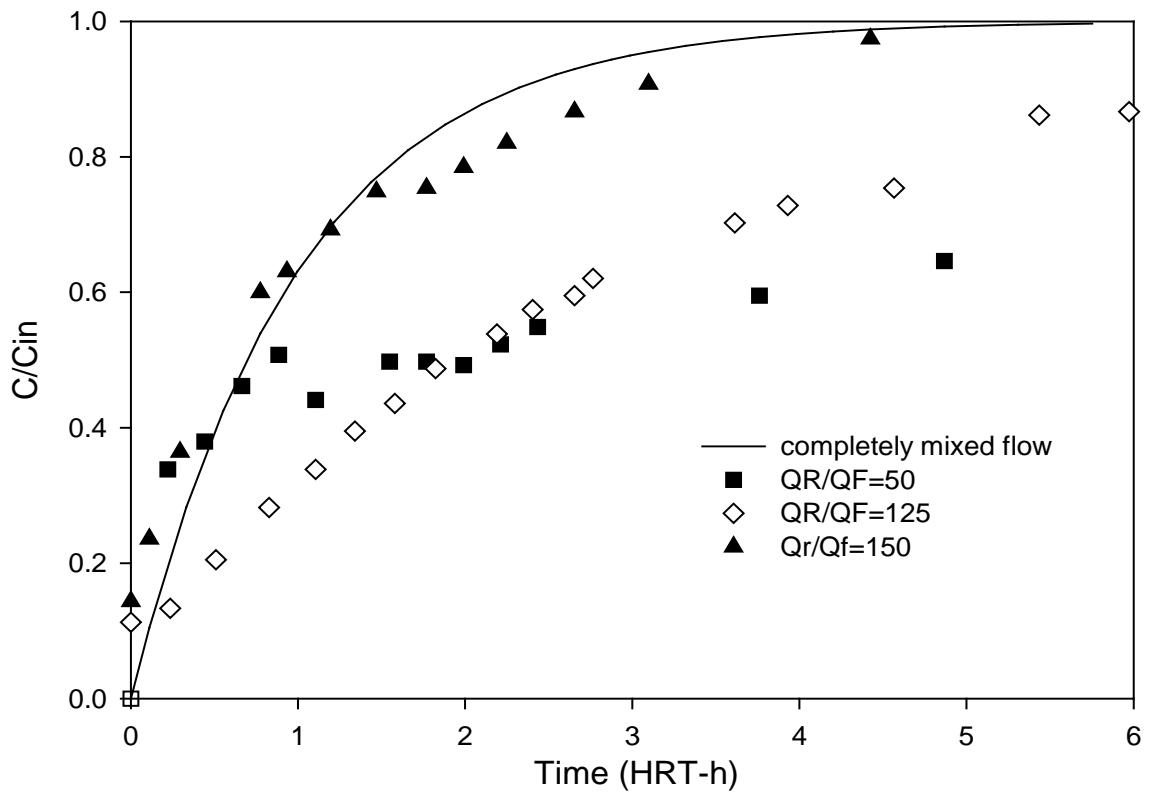
**Figure 4.3:** Tracer study results to determine the optimum recycle rate.

## 4.8.2 Chemical Control Experiment

The reactor was operated under an influent Mn(II) concentration of 5 mg·L$^{-1}$ and a HRT of 5 hrs. to investigate whether abiotic mechanisms such as adsorption and chemical oxidation are significant in the bioreactor. Figure 4.4 shows that the measured influent and effluent Mn(II) levels in the reactor were statistically insignificant ($p$ = 0.119). The results of the control experiment demonstrate that abiotic Mn(II) oxidation or removal by adsorption in the bioreactor is negligible.
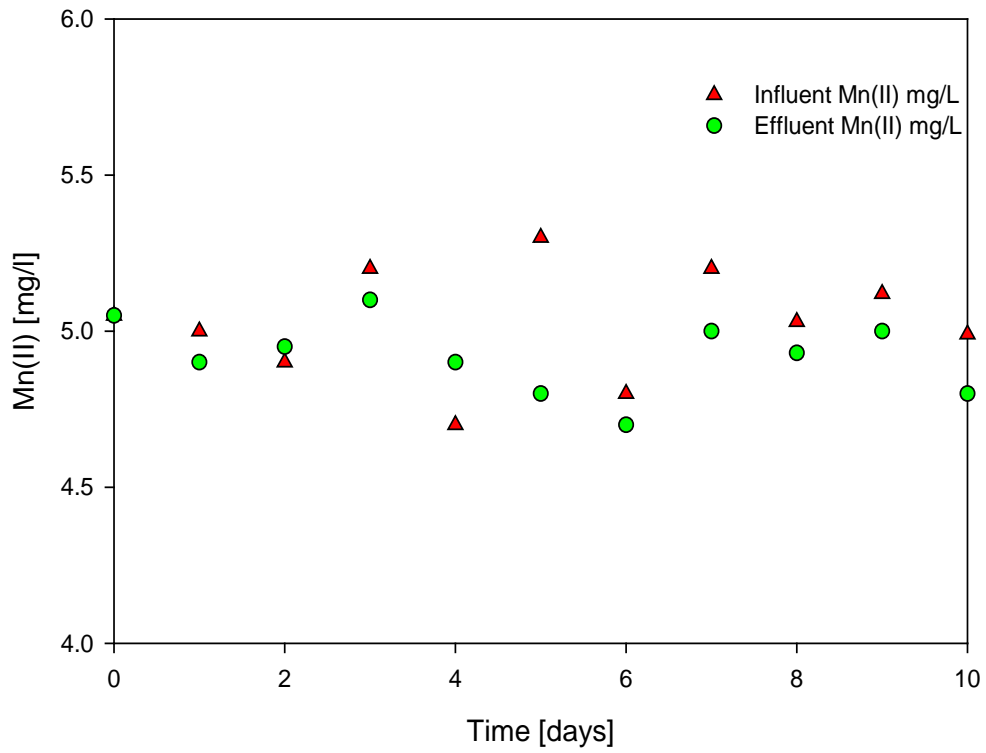
**Figure 4.4:** Results of control study for Mn(II) oxidation and sorption in the bioreactor.

### 4.8.3 Performance Analysis of the Glucose-feed Biofilm Reactors

**Reactor I**: Figure 4.5 shows the influent and effluent concentrations of Mn(II) for 26 days for a continuous flow biofilm reactor feed 150 mg·$L^{-1}$ glucose as the sole carbon source. Reactor start-up commenced following 3 days allowed for cell immobilization to the glass beads under static flow conditions on the glass beads. The biofilm reactor was operated under a feed Mn(II) concentration of 0.45 mg·$L^{-1}$ and a HRT of 12-hrs. and conditions maintained at pH of 6.5 ± 0.3 and DO of 7.2 ± 0.5 mg·$L^{-1}$.

After 1 day of operation, development of a light brown color was observed on the surface of the reactor bead coatings which darkened on each successive day. The effluent Mn(II) was maintained at <0.05 mg·$L^{-1}$ from start-up to 6 days. After 14 days the effluent Mn(II) began an increasing trend (above 0.05 mg·$L^{-1}$) until complete reactor failure at 23 days when the feed and effluent concentrations were equal. During the 26 days four episodes of Mn(II) release were observed, at 7, 10, 21, and 22 days, increasing the effluent concentration above the influent concentration.
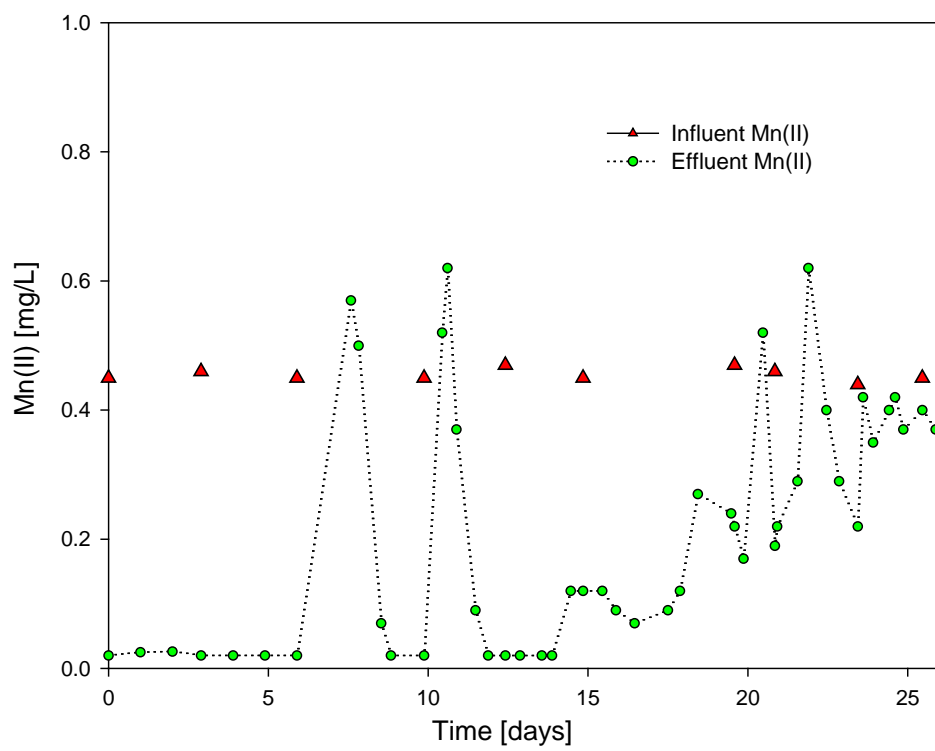
**Figure 4.5:** Mn(II) levels for a continuous flow bioreactor. HRT=12-hrs., 150 mg·L$^{-1}$ glucose sole carbon source.

**Reactor II:** Figure 4.6 shows the influent and effluent concentrations of Mn(II) for 150 days for a continuous flow biofilm reactor initially feed 15 mg·L$^{-1}$ glucose as the sole carbon source. The feed phosphate concentration was reduced to 5 mg·L$^{-1}$, compared to 50 mg·L$^{-1}$ in Reactor I. Similar to Rector I, start-up commenced following 3 days allowed for cell attachment to the glass beads under static flow conditions on the glass beads. The biofilm reactor was operated under a feed Mn(II) concentration of 0.45 mg·L$^{-1}$ and a HRT of 12-hrs. and conditions maintained at pH of 6.5 ± 0.2 and DO of 7.9 ± 0.3 mg·L$^{-1}$.

Similar to Reactor I, development of a light brown color was observed on the surface of the reactor bead coatings within 1 day of reactor operation and darkening with each successive day. The effluent Mn(II) was maintained at <0.05 mg·L$^{-1}$ from start-up for 16 days. After 16 days the effluent Mn(II) began an increasing trend (above 0.05 mg·L$^{-1}$). At 23 days, the feed glucose concentration was increased to 150 mg·L$^{-1}$ with the assumption the intitial glucose feed concentration was insufficient to support the attached biomass. Subsequent improvement in the reactor performance was observed with the effluent Mn(II) concentration decreasing below <0.05 mg·L$^{-1}$ within 24 hrs. Reactor performance was maintained with the Mn(II) concentration <0.05 mg·L$^{-1}$ until 43 days, when the effluent begin increasing until complete reactor failure by 48 days. The reactor was operated for 32 days under failed conditions then the decision was made to add nutrient broth (5 mg/10 ml SQ water) to the recycle line. Within 24 hours the effluent Mn(II) had decreased <0.05 mg·L$^{-1}$.
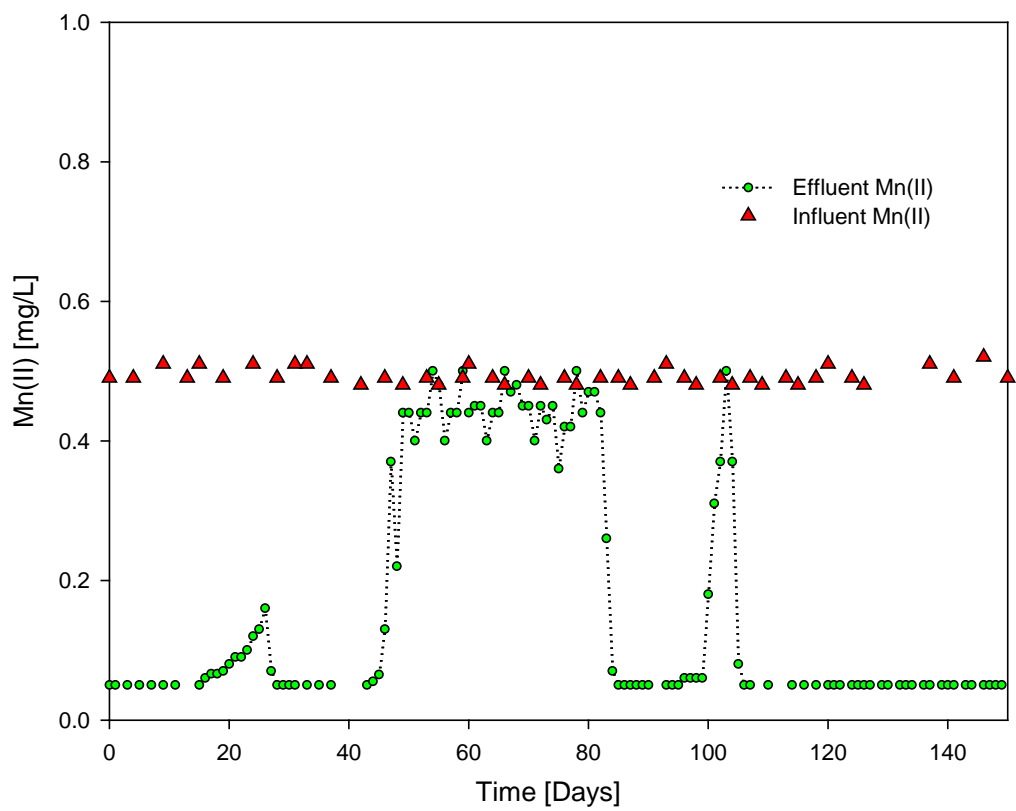
**Figure 4.6:** Mn(II) levels for a continuous flow reactor study for Objective 1, HRT=12-hrs., initial 15 mg·L$^{-1}$ glucose as carbon source.

Reactor performance <0.05 mg·L$^{-1}$ continued until 100 days, when effluent levels sharply increased and complete reactor failed by 103 days. Again, nutrient broth (5 mg/10 ml SQ water) was added to the recycle line and subsequent improvement in reactor performance (<0.05 mg·L$^{-1}$) was observed. For the remaining duration of the reactor operation, nutrient broth (5 mg/10 ml SQ water) was added to the recycle line every 4-5 days.

### 4.8.4 Performance Analysis of the Steady-State Biofilm Reactor

For Objective 2, two separate continuous flow reactor experiments were performed to study steady-state Mn(II)-oxidation by pure cultures of strain EC112. The first reactor was for model calibration of the observed effluent Mn(II) data sets. The second reactor was for model validation.

The operating conditions and the performance data for the steady-state biofilm reactor for Phases I to VIII are in Table 4.3 and Figure 4.7. Biomass data for the steady-state reactor is shown in Table 4.4. Bioreactor (validation) steady-state performance data is shown in Table 4.5

Figure 4.9 is a plot of Mn(II) oxidation efficiency of the biofilm reactor versus Mn(II) loading rates. Figure 4-10 shows the Mn(II) oxidation rates versus Mn(II) loading rates for Phase I to VIII.

The Mn(II) oxidation efficiency of the biofilm reactor is characterized by decreasing efficiency with higher Mn loading rates. Mn(II) oxidation efficiency was 93.5 to 95.0 % for the last two phases (VII and VIII) of the reactor operation. The efficiency of the reactor dropped to 85.3% under a higher Mn (II) loading rate of 2.67 mg·L$^{-1}$·day$^{-1}$ in phase III. The efficiency dropped to 59.1% with a quadrupling of the Mn(II) loading rate to 12.0 mg·L$^{-1}$·day$^{-1}$ in phase IV.

The reactor Mn(II) effluent data in Figure 4.10 show the decrease in the Mn(II) oxidation rate with increase in the Mn(II) loading rates for each phase of reactor operation.

**Table 4.3:** Reactor (calibration) steady-state operating and performance data.

| Phase | Duration (hrs.) | HRT (hrs.) | Influent Mn(II) ($\mu g \cdot L^{-1}$) | Effluent Mn(II) ($\mu g \cdot L^{-1}$) | Mn(II) SLR[1] | Effluent Mn(IV) ($\mu g \cdot L^{-1}$) | DO ($mg \cdot L^{-1}$) |
|---|---|---|---|---|---|---|---|
| I | 0-49 | 25 | 690±45 | 30±5 | ±29.3 | <50 | 8.5±0.2 |
| II | 49-54 | 0.4 | 690±45 | 50-500 | 465±25 | * | * |
| III | 54-70 | 1.1 | 690±45 | 333±3 | 1005±22 | * | * |
| IV | 70-98 | 1.4 | 690±45 | 286±4 | 2535±121 | * | * |
| V | 98-117 | 3.2 | 690±45 | 171±3 | 998±35 | * | 8.2±0.3 |
| VI | 117-140 | 6.3 | 690±45 | 103±2 | 998±35 | <50 | * |
| VII | 140-190 | 12.6 | 690±45 | 35±3 | 2205±79 | <50 | * |
| VIII | 190-286 | 25 | 690±45 | 45±3 | 4140±98 | <50 | 8.3±0.5 |
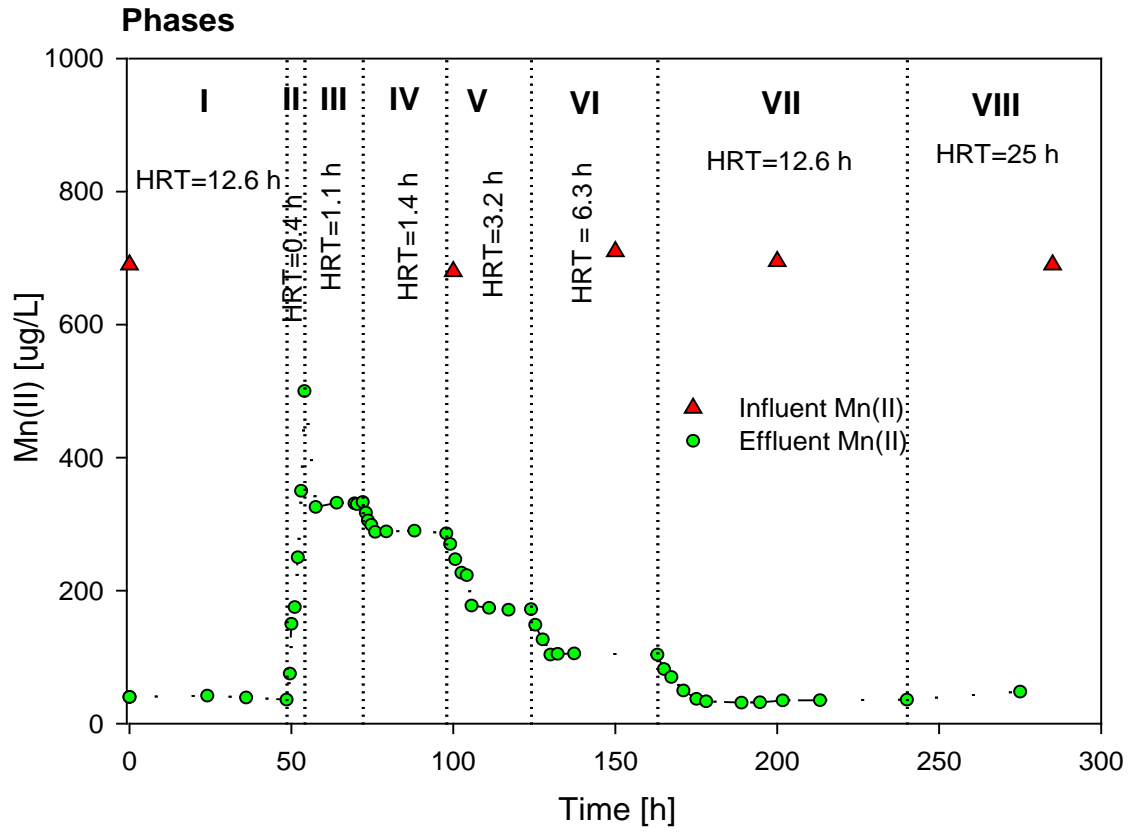
**Figure 4.7:** Steady-state performance data showing effluent Mn(II) for bioreactor study for Objective 2.

Table 4.4: Biomass Data for Steady-State bioreactor (calibration).

| Phase | Mn(II) LR $(mg \cdot L^{-1} \cdot day^{-1})$ | Viable Suspended Cell Count | Viable Attached Cell Count | Total Attached Cell in Reactor (mg) |
|---|---|---|---|---|
| I | 1.33 | $5.8 \times 10^4$ | $7.6 \times 10^{11}$ | 71.3 |
| II | 42.00 | a | a | a |
| III | 15.27 | $2.6 \times 10^4$ | a | |
| IV | 12.00 | $7.8 \times 10^3$ | a | a |
| V | 5.25 | $2.2 \times 10^3$ | a | a |
| VI | 2.67 | $4.7 \times 10^2$ | a | a |
| VII | 1.33 | $6.7 \times 10^2$ | $6.3 \times 10^{11}$ | 69.1 |
| VIII | 0.67 | a | a | a |

a: measurement not available

Table 4.5: Bioreactor (validation) steady-state performance data.

| Phase | Duration (hrs.) | HRT (hrs.) | Influent Mn(II) $(\mu g \cdot L^{-1})$ | Effluent Mn(II) $(\mu g \cdot L^{-1})$ | Mn(II) SLR[1] | Effluent Mn(IV) $(\mu g \cdot L^{-1})$ | DO $(mg \cdot L^{-1})$ |
|---|---|---|---|---|---|---|---|
| I | 0-49 | 12.6 | 750±13 | 33±3 | ±29.3 | <50 | 8.0±0.2 |
| II | 49-105 | 6.3 | 750±13 | 124±14 | 465±25 | <50 | * |
| III | 105-184 | 1.3 | 750±13 | 350±26 | 1005±22 | <50 | 7.9±0.5 |
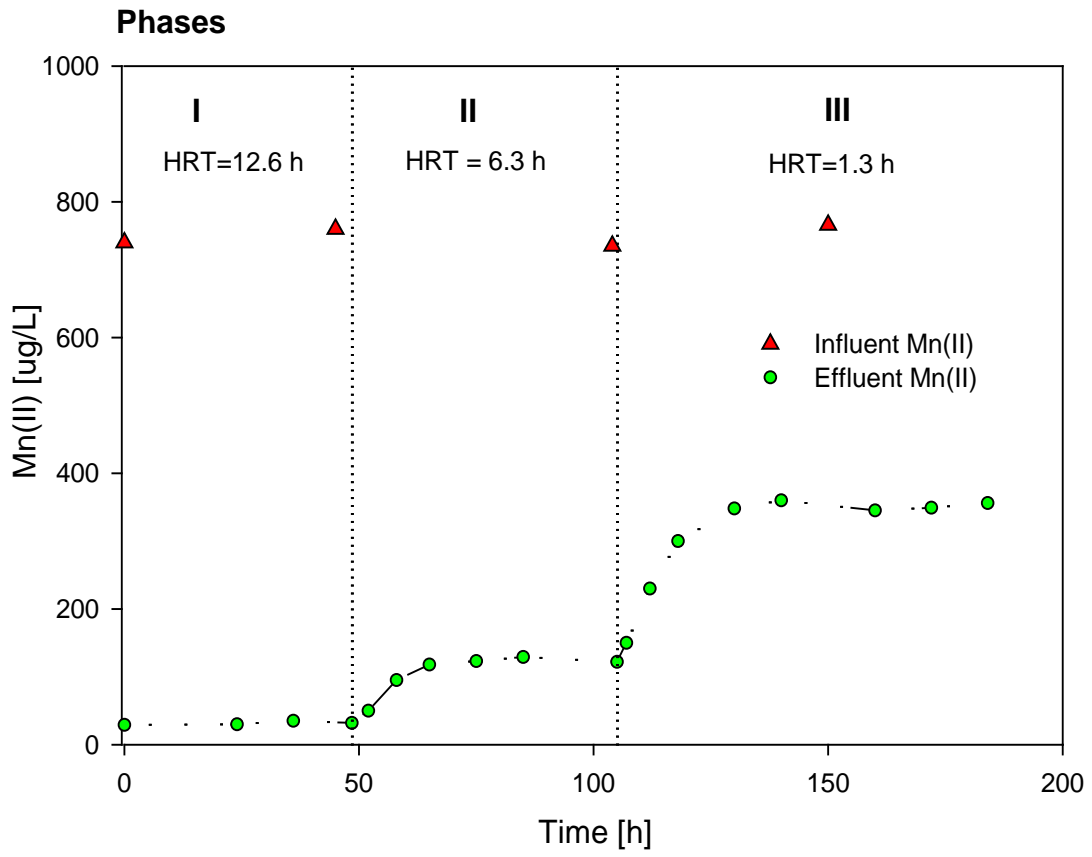
**Figure 4.8:** Steady-state performance data showing effluent Mn(II) for validation bioreactor study for Objective 2.
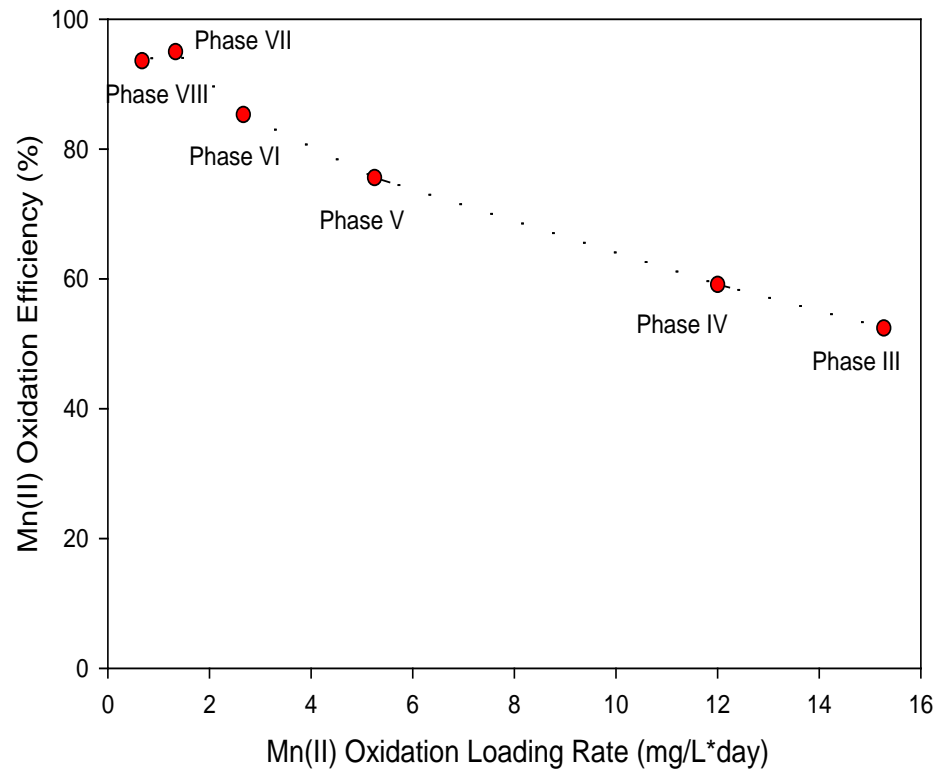
**Figure 4.9:** Plot of Mn(II) oxidation efficiency of the bioreactor versus Mn(II) loading rates.
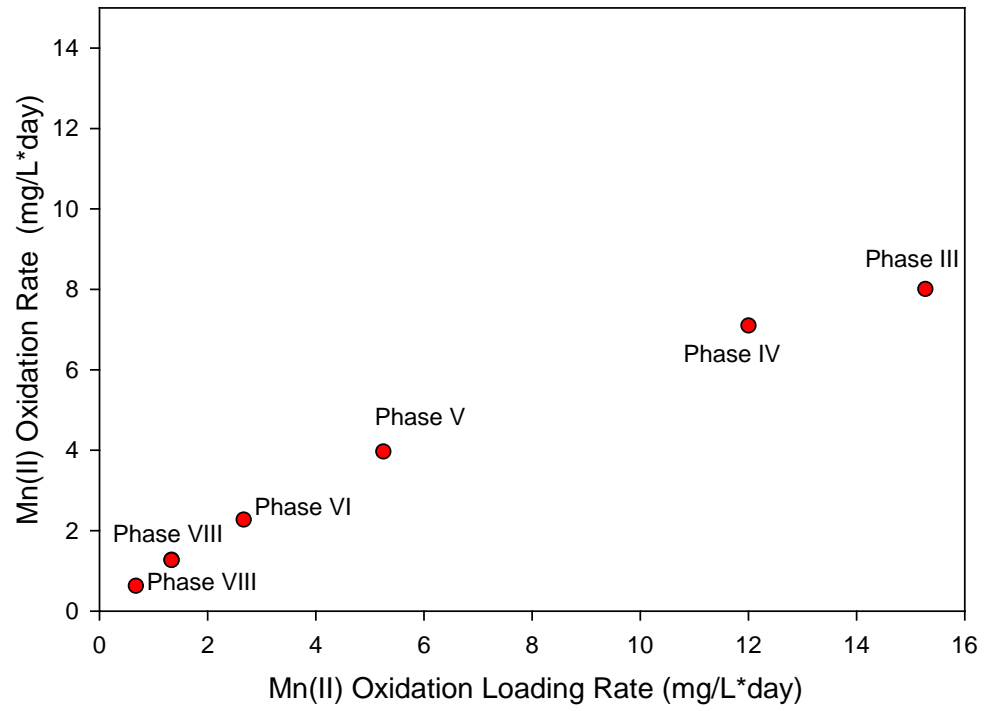
**Figure 4.10:** Plot of Mn(II) oxidation rates versus Mn(II) loading rates Phase I to VIII.

### 4.8.8 Kinetic Parameter Estimation

Several estimation techniques exist for steady-state biofilm kinetic parameters estimation for steady-state conditions. Estimation methods include influent and effluent substrate concentration curve comparison for (Rittmann et al., 1986), use of fluidized reactors (Nguyen and Shieh (1995); linearization models (Eisenthal and Cornish-Bowden, 1974; Robinson, 1985); batch estimation using suspended cells of biofilm parameters (Van Loosdrecht et al., 1990; Grady et al., 1996); and use of dissolved oxygen concentration profiles (Riefler et al., 1998).

In this study, a kinetic parameter (k) describing biological Mn(II) oxidation was obtained using an approach similar to Smets et al., (1999). The method involved using numerical solution derived for a biofilm model developed by Atkinson and Davies (1974). Measured Mn(II) flux into the biofilm under various HRT were fitted to a first order approximation of a predictive flux expression, which is a function of the Mn (II) concentration at the biofilm-liquid interface ($S_s$). The parameters were characterized by their corresponding 95% confidence levels.

### 4.8.8.1 Parameter Estimation Technique

The average steady-state effluent Mn(II) concentrations measured from Phases III thru VIII of the reactor operation were used to compute the ($J_{exp}$,$S_s$) data pair for kinetic parameter estimation. Sigma Plot 11.0 (Systat Software Inc.), which employs the Marquardt-Levenberg algorithm (Marquardt, 1963) was used to estimate the parameters by minimizing the residual sum of squares between the observed flux (Eqn. 4-13) and the model simulation (Eqn. 4-24), respectively.

The optimized parameter obtained from the non-linear estimation routine and steady-state data is shown in Table 4.6. The covariance % (asymptotic standard error) of 3.85 indicates 95% prediction intervals are bounding. Sigma Plot 11.0 was run for the ($J_{exp}$,$S_s$) data using different initial starting values of the parameters to ensure repeatability of the optimized estimate.

### 4.8.9 Evaluation of the Model Fit

The model fit (Figure 4.11) was evaluated by means of a linear regression analysis of the plot between observed and model predicted Mn(II) flux values. A correlation coefficient of $R^2$= 0.98 suggested a good fit between the model and the experimental data (Figure 4.12). Two statistical tests (two-tailed paired $t$-test, and chi-square goodness of-fit-test) were also performed to evaluate any significant difference between the observed and predicted Mn(II) flux values. The two-tailed $p$-value (0.54 > 0.05) and the chi-square goodness of-fit test result ($p$ =1) showed that the difference between model predicted and obtained Mn(II) flux values were statistically insignificant at the 95% confidence level. The good fit of first-order flux model with the experimental data indicates the robust character of strain EC112 for Mn(II) oxidation in biofilms. This is in addition to ignoring biofilm losses during reactor operation and without an added carbon source in the effluent.

**Table 4.6:** Optimized steady-state biofilm parameter k.

| Parameter | Value | CV%[a] |
|---|---|---|
| k , mg Mn(II)/cells.hr | 0.0229 | 3.85 |

[a] CV%: relative asymptotic standard error of the parameter
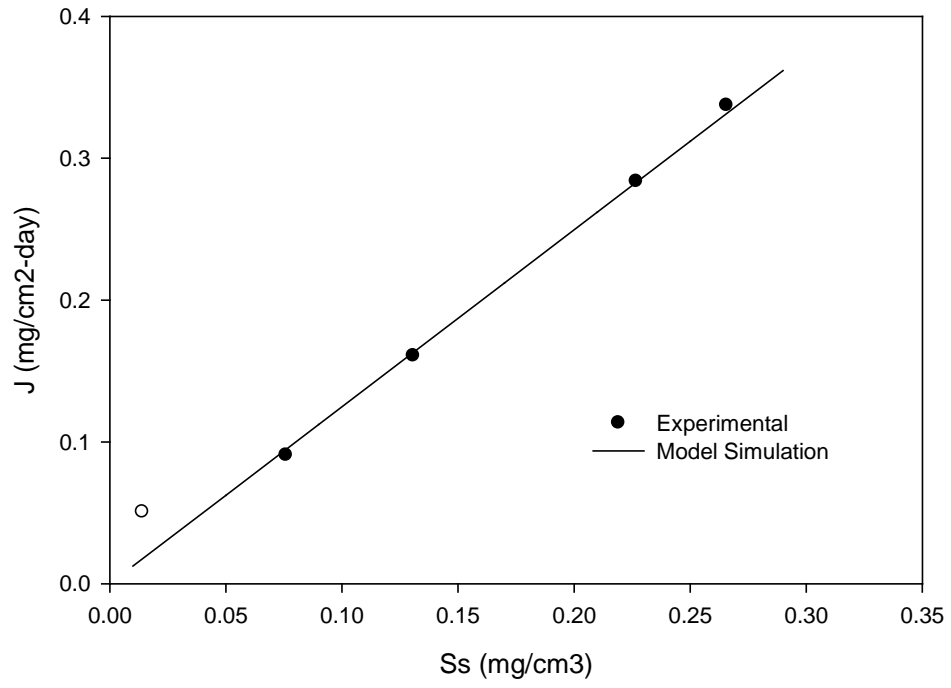
**Figure 4.11:** $J_{exp}$ versus $S_s$ and model best fit for parameter estimation.
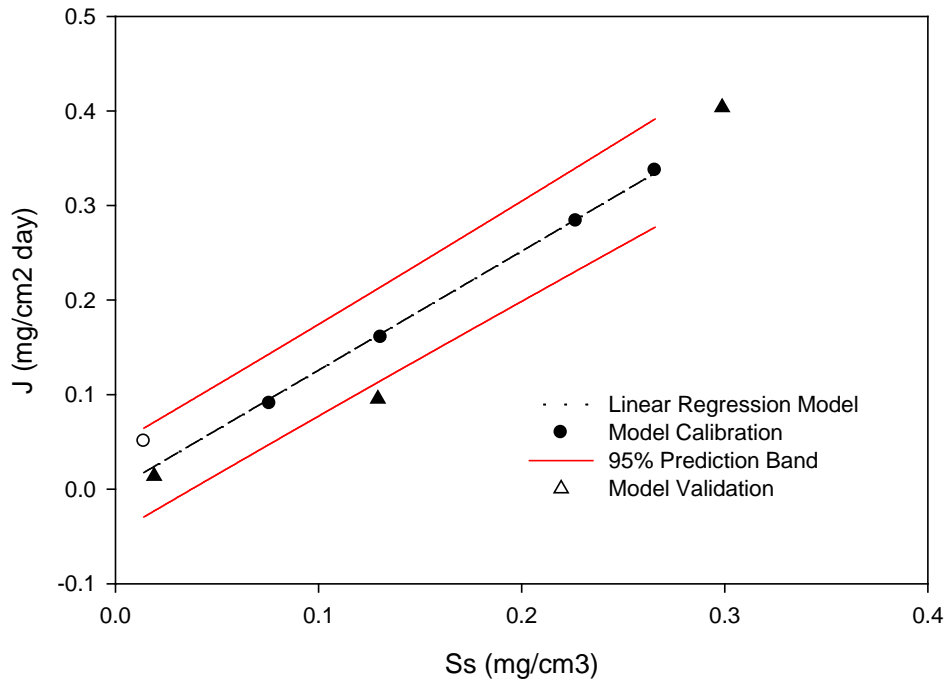
**Figure 4.12:** Linear regression analysis between the observed and predicted flux values.

## 4.8.10 Validation of the Steady-State Model

The flux model (Eqn. 4-19) and the obtained best-fitted kinetic parameter (k) along with reactor specific parameters in Table 4.3 were used to predict the steady-state Mn(II) flux values for the three phases (I-III) of operation for a separate continuous flow bioreactor. The biofilm thickness ($L_f$) was estimated using Eqn. 4-10, whereas, the biofilm density ($X_f$) was calculated using Eqn. 4-11 respectively. Results in Table 4.7 show that the model predicted Mn(II) flux values were within an order of magnitude of the observed values. Phase I had the largest discrepancy, with a $J_{obs.}/J_{pred.}$ value of 2.84 compared to 0.744 and 0.621 for Phase I and II. For Phase I the Mn(II) effluent levels were below 50 $\mu g \cdot L^{-1}$ and loss of analytical accuracy for the Mn assay (ICP) at these low levels could have contributed the higher J for this phase.

**Table 4.7:** Validation of the steady-state model.

| Phase | $L_f$ (cm) | $X_f$ (mg·cm$^{-3}$) | P | $S_s$ | $J_{obs}$ | $J_{pred.}$ | $J_{obs.}/J_{pred.}$ |
|-------|------------|---------------------|------|-------|-----------|-------------|----------------------|
| I | 0.005 | 13 | 0.065 | 0.014 | 0.054 | 0.019 | 2.84 |
| II | --- | --- | --- | 0.096 | 0.096 | 0.129 | 0.744 |
| III | 0.005 | 13 | 0.065 | 0.299 | 0.251 | 0.404 | 0.621 |

## 4.8.11 Biofilter Mn Releases

During preliminary continuous flow biofilm reactor experiments, described in Section 4.8.3, releases of Mn were observed from the biofilter involving pure cultures of strain EC112 (i.e., fixed films of pure cultures of strain EC112 attached to glass beads). These releases appeared as Mn 'spikes' in the reactor effluent and were identified when effluent Mn(II) concentrations exceeded the reactor feed influent Mn(II) concentrations (Figure 4.5). The Mn(II) releases could be attributed to be a consequence of high concentrations of chemical reducing agents in the feed solution, particularly phosphate ions. A plausible mechanism describing the observed biofilter Mn releases would involve diffusion of the chemical reducing agents (e.g., $PO_4^{-3}$) to $Mn(III,IV)O_x$ reaction sites either coating the surface or intermixed within the attached biofilms and subsequent reductive dissolution of the bacteriogenic Mn oxide and release of Mn(II) back into the bulk solution.

In the preliminary continuous flow reactor studies, biofilter Mn releases were successfully abated by reducing the concentration or eliminating the suspected redox agent from the feed influent solution. For example, reduction of the phosphate concentration from 50 mg·L$^{-1}$ to 5 mg·L$^{-1}$ resulted in the abatement of Mn releases from the preliminary glucose feed continuous flow biofilm reactor experiments. Batch control studies involving $PO_4^{-3}$ (as $K_2HPO_4^{-3}$ and $KH_2PO_4^{-3}$) and solid $Mn(III,IV)O_x$ harvested from strain EC112 showed that phosphate concentrations at 20 mg·L$^{-1}$ or higher reduced measurable amounts of the biotic Mn-oxide to soluble Mn(II).

### 4.8.11.1 Biofilter Mn-Release Reactor Experiments

During a subsequent, continuous flow biofilm reactor experiment designed to investigate the steady-state kinetics of Mn(II) oxidation by biofilm cultures of strain EC112, biofilter Mn releases were observed following an increase in the influent flow rate (increase in Mn(II) loading on the biofilter). The observation of Mn(II) releases was unexpected, and not considered to be a reactive product of chemical reducing agents in the feed solution, considering the previous discussion, i.e., that the reactor feed solution was absent of sufficient concentrations of chemical reducing agents capable of reducing accumulated $Mn(III,IV)O_x$ in the biofilter.

For this reactor, the feed media consisted of (mg·L$^{-1}$): α-D-glucose, 20; Difco Yeast Extract, 2; Difco Nutrient Broth, 2; Mn(II), 0.75; $CaCl_2$·2 $H_2O$, 1; $MgSO_4$·7 $H_2O$, 1; $(NH_4)_2SO_4$·7 $H_2O$, 1; and 0.5 ml of trace metal solution (Section 3.3.1). The reactor conditions were maintained at 29±2 °C and pH 6.6±0.3, within the optimal conditions for Mn(II)-oxidation by strain EC112.

The reactor was operated at an initial HRT of 12.6-hrs., corresponding to an influent flow rate of 1.9 ml·hr$^{-1}$, and an influent Mn(II) concentration of 0.75 mg·L$^{-1}$. After 72 hours of operation reactor start-up, the influent flow was increased to 6.0 ml·hr$^{-1}$, decreasing the HRT

to 4.0-hrs., while increasing the Mn(II) loading from 0.0024 to 0.0076 $\mu g \cdot cm^{-2} \cdot hr^{-1}$, following the original experimental objective (Section 4.10.4) to establish a steady-state Mn(II) reactor conditions. The effluent Mn concentration and mass balance profiles for this reactor are shown in Figure 4.13a and Figure 4.13b. As shown in Figure 4.13a, the effluent Mn(II) concentration steadily increased until complete breakthrough at 75.5 hrs., and a Mn(II) steady-state was unobtainable at this flow rate, similar to the reactor experiment previously described. Shortly thereafter, the influent flow was decreased back to 1.9 ml·hr.$^{-1}$, with the expectation that the reactor would recover and effluent Mn(II) concentrations would decrease to levels prior to the increase in Mn(II) loading (i.e., <0.05 mg·L$^{-1}$). Subsequent monitoring of the reactor Mn(II) effluent revealed that at 80 hrs. the effluent concentration had increased to 1.93 mg·L$^{-1}$ and a maximum of 2.06 mg·L$^{-1}$ at 95 hrs. prior to returning to the feed influent level at 131 hrs.

Prior to the initiation of Mn(II) release from the biofilter at 75.5 hrs., a mass balance of the inflow (126 µg), and outflow (29.16 µg) indicates 96.84 µg of Mn(II) from bulk solution had accumulated in the biofilter. Calculation of the curve area assumed to represent biofilter Mn(II) releases, between 75.5 to 224 hrs., yields a total release of 94.30 µg to bulk solution. The biofilter, which had visibly began acquiring the dark-brown color of $Mn(III,IV)O_x$ within a few hours following reactor start-up, clearly lightened in color as the Mn(II) release progressed from 75.5 to 224 hours. In addition, the release of Mn(II) from the biofilter had an effect on the Mn(II)-oxidizing activity by strain EC112, which apparently ceased subsequent to the release or at least occurred at rates significantly less than the Mn(II) release rates.

Thus, Mn(II) releases from the biofilter may be predictable and subject to control. To further investigate biofilter Mn(II) releases, several reactors were prepared and studied subject to various Mn(II) load increases until complete effluent breakthrough.
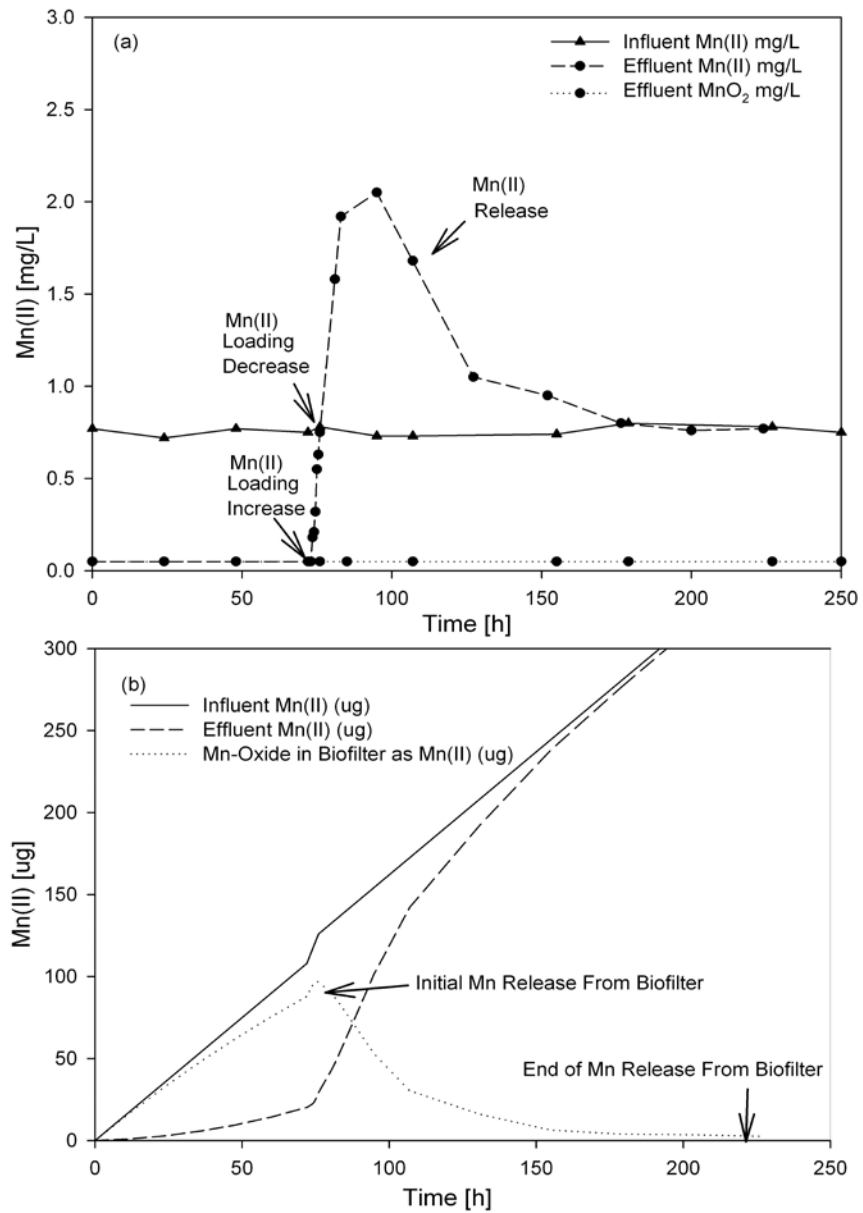
**Figure 4.13:** Preliminary biofilter Mn(II) release reactor experiment results. Effluent Mn concentration profiles (a) and cumulative Mn mass balances (b).

## 4.8.11.2 Biofilter Mn(II) Release Studies

To provide further insight into the conditions and mechanisms for the Mn(II) releases observed during the steady-state kinetic experiment, reactor experiments were repeated for a fresh reactor prepared (with glass bead filter material) with strain EC112 cultures following the same procedures.

Reactor experiments were conducted with the operation strategy of increasing the Mn(II) biofilter load until complete effluent Mn(II) breakthrough, followed by influent flow rate reduction back to the initial (start-up) HRT. The experimental hypothesis, that Mn(II) release from the biofilter would occur, as observed for the glucose feed reactor in Figure 4.13, when complete Mn(II) breakthrough was reached in the effluent. This strategy required real-time monitoring of Mn(II) ($mg \cdot L^{-1}$) and was achieved using the persulfate method (Standard Method's 3500-B), as in the previous experiment.

The reactor feed media consisted of ($mg \cdot L^{-1}$): $Na_2SO_4$, 25; Mn(II), 0.75; $CaCl_2 \cdot 2\ H_2O$, 1; $MgSO_4 \cdot 7\ H_2O$, 1; $(NH_4)_2SO_4 \cdot 7\ H_2O$, 1; and 0.5 ml trace metal solution (Section 3.3.1). No carbon source was included in the reactor feed solution. Reactor operating conditions were maintained at $29 \pm 1$ °C and pH $6.5 \pm 0.2$, within the optimal conditions determined for Mn(II)-oxidation for strain EC112 in batch studies. No buffer was included in the feed solution for pH control. Influent reactor feed solutions were adjusted to pH 6.7. During reactor operation the pH measured in the recycle line was generally 0.1 to 0.2 pH units lower than the feed solution. Dissolved oxygen (DO) measurements in the recycle line remained above 8.0 $mg \cdot L^{-1}$. Steady-state Mn(II) kinetic rector experiments in Section 4.10.4 using fixed film cultures of strain EC112 indicate oxygen cell consumption did not deplete oxygen significantly below DO saturation levels.

For reactor biofilm development, 25-ml solutions of harvested cultures of strain EC112 were incubated for 3-days with the reactor filter material (glass beads) prior to reactor start-up. Five reactors (1 through 5) were operated under an initial HRT of 12.6-hrs. (inflow rate of 1.9 $ml \cdot hr^{-1}$) and subject to the strategy of increasing the inflow feed rate, then awaiting complete Mn(II) effluent breakthrough, whereby increasing biofilter Mn(II) loading (Table 4.8). Reactor 6 was prepared and operated under similar conditions, except for the loading conditions, and served as a control for Reactors 1 to 5. A summary of the influent and effluent reactor Mn(II) concentration profiles for Reactors 1 to 3 and Reactors 4 and 5 are shown in Figures 4.14(a) and 4.14(b), respectively.

For this preliminary reactor experiment and the biofilter Mn(II) release experiments in the next section, Tables 4.8 and 4.9 summarize the operating conditions and the Mn mass balances, respectively. Table 4.8 summarizes reactor influent Mn(II) concentrations, influent flow rates per time period, hydraulic retention times (HRT), and Mn(II) loading ($\mu g \cdot cm^{-2} \cdot hr^{-1}$) rates. Mn(II) mass balances were obtained at the (1) beginning of Mn(II) release from the biofilter and (2) end of reactor operation.
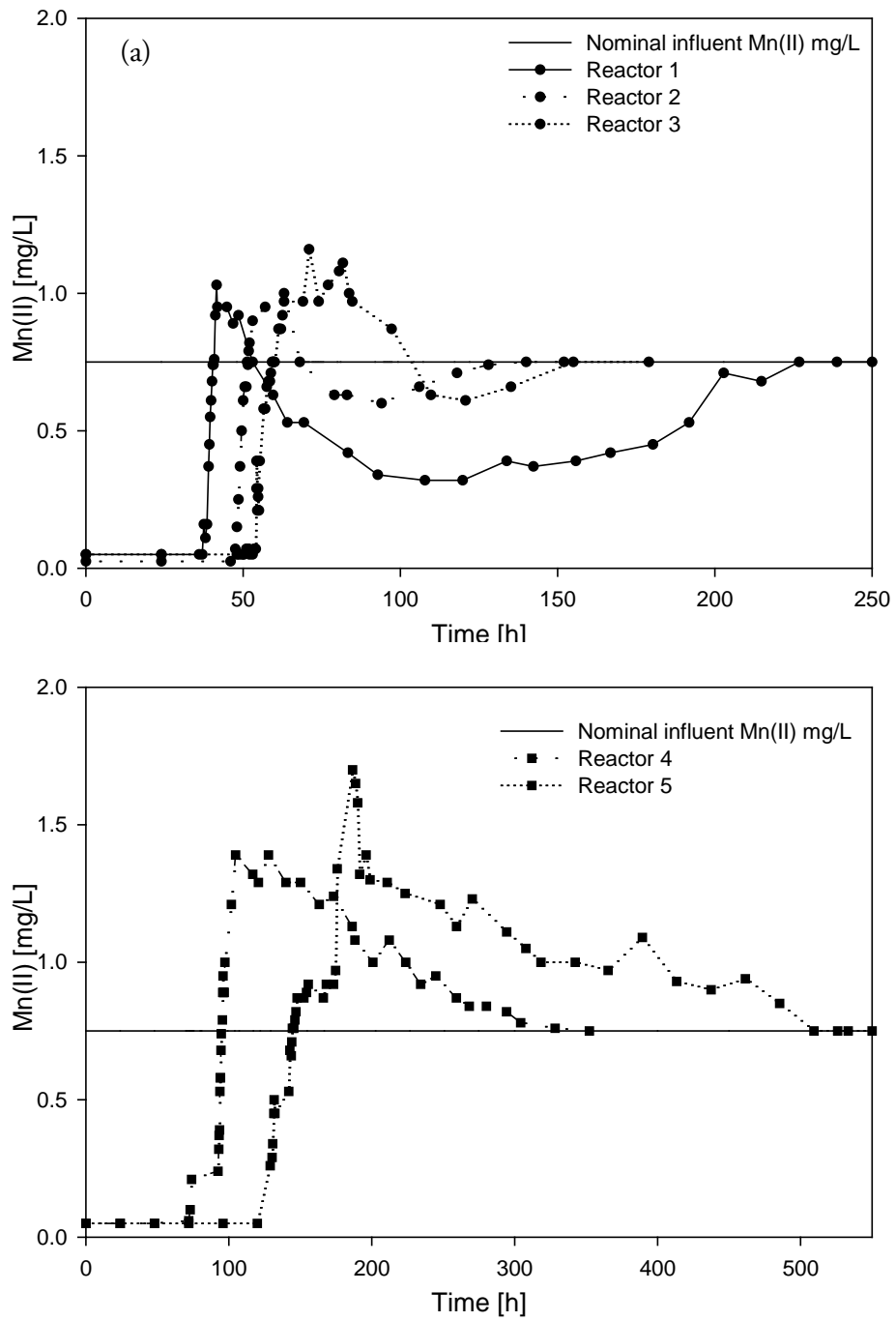
**Figure 4.14:** Biofilter Mn(II) release summary for Reactor 1-3 (a) and 4-5 (b) showing the nominal influent Mn(II) concentration and measured effluent Mn(II) concentration.

**Table 4-8:** Reactor influent Mn(II) concentrations, flow time period/rates, hydraulic retention times (HRT), and Mn(II) loading rates for Mn biofilter release experiments.

| Reactor ID | Mn(II) mg·L$^{-1}$ | Time (hrs.) | Influent Flow Rate (ml·hr$^{-1}$) | HRT (hrs.) | Load Rate (µg·cm$^{-1}$·hr$^{-1}$) |
|---|---|---|---|---|---|
| Prelim. | 0.75±0.03 | 0-72.0 | 1.9 | 12.6 | 0.0024 |
| | | 72.0-75.5 | 6.0 | 4.0 | 0.0076 |
| | | 75.5-224 (rp$^*$) | 1.9 | 12.6 | 0.0024 |
| 1 | 0.76±0.02 | 0-36.4 | 1.9 | 12.6 | 0.0024 |
| | | 36.4-39.0 | 24.0-72.0 | 1.0-0.3 | 0.0304-0.0912 |
| | | 39.0-53.0 (rp) | 1.9 | 12.6 | 0.0024 |
| | | 53.0-250 | 1.9 | 12.6 | 0.0024 |
| 2 | 0.84±0.03 | 0-48.0 | 1.9 | 12.6 | 0.0024 |
| | | 48.0-52.0 | 22.8 | 1.1 | 0.0289 |
| | | 52.0-67.0 (rp) | 1.9 | 12.6 | 0.0024 |
| | | 67.0-152 | 1.9 | 12.6 | 0.0024 |
| 3 | 0.79±0.03 | 0-45.8 | 1.9 | 12.6 | 0.0024 |
| | | 45.8-58.9 | 11.4-23.0 | 2.1-1.0 | 0.0144-0.0291 |
| | | 58.9-103.7(rp) | 1.9 | 12.6 | 0.0024 |
| | | 103.7-179 | 1.9 | 12.6 | 0.0024 |
| 4 | 0.79±0.03 | 0-68.5 | 1.9 | 12.6 | 0.0024 |
| | | 68.5-95.5 | 11.4-23.0 | 2.1-1.0 | 0.0144-0.0291 |
| | | 95.5-353(rp) | 1.9 | 12.6 | 0.0024 |
| 5 | 0.74±0.03 | 0-130.5 | 1.9 | 12.6 | 0.0024 |
| | | 131.0-144.7 | 11.4-23.0 | 2.1-1.0 | 0.0144-0.0291 |
| | | 144.7-509(rp) | 1.9 | 12.6 | 0.0024 |
| 6 | 0.76±0.02 | 0-93.0 | 1.9 | 12.6 | 0.0024 |
| | | 93.0-98.3 | 23.0 | 1.0 | 0.0291 |
| | | 98.3-153.0 | 1.9 | 12.6 | 0.0024 |
| | | 153.0-155.5 | 23.0 | 1.0 | 0.0291 |
| | | 155.5-165.0 (rp) | 1.9 | 12.6 | 0.0024 |
| | | 165.0-220 | 1.9 | 12.6 | 0.0024 |

*Mn(II) biofilter release period.

**Table 4-9:** Summary of biofilter Mn(II) release amounts.

| Reactor ID | Mn(II)(µg) [In – Out = Accum.] |
| --- | --- |
| Prelim. | (1)126.00 – 29.16 = 96.84<br>(2) 352.50 –350.00 = 2.54<br>Total Mn(II) release = 94.30 |
| 1 | (1) 158.35 – 59.45 = 98.90<br>(2) 428.89 –243.98 = 184.90<br>Total Mn(II) release = 2.49 |
| 2 | (1)142.04 – 33.33 = 108.72<br>(2)302.44 –171.59 = 130.85<br>Total Mn(II) release = 2.79 |
| 3 | (1)163.23 – 46.95 = 116.28<br>(2)358.36 –239.41 = 118.95<br>Total Mn(II) release = 12.15 |
| 4 | (1)189.04 – 50.25 = 138.78<br>(2)614.94 –614.27 = 0.67<br>Total Mn(II) release = 138.11 |
| 5 | (1)270.14 – 62.99 = 207.16<br>(2)580.42 –536.00 = 0.64<br>Total Mn(II) release = 206.52 |
| 6 | (1)354.75 – 156.10 = 198.65<br>(2)576.40 –213.74 = 362.66<br>Total Mn(II) release = 1.21 |

For Reactor 1, the influent feed flow rate was 1.9 ml·hr$^{-1}$ (HRT 12.6-hrs.) for 36.4 hrs. prior to an increase in flow from 24.0 to 72.0 ml·hr$^{-1}$ for 2.6 hrs., ending at 39.0 hrs. with reduction of the inflow rate back to 1.9 ml·hr$^{-1}$ (Figure 4.15a). Within 1-hr of complete Mn(II) effluent breakthrough (40.8 hrs.), a Mn(II) release was observed at 41.2 hrs., marked by an effluent concentration of 0.92 mg·L$^{-1}$, higher than the influent concentration of 0.76 mg·L$^{-1}$. The maximum Mn(II) release concentration measured, 1.03 mg·L$^{-1}$, at 41.6 hrs. prior to apparent cessation in releases at 53.0 hrs. Subsequently, Mn(II) oxidation activity by strain EC112 apparently reduces the inflow Mn(II) concentration to approx. 0.30 mg·L$^{-1}$ between 95 hrs. and 102 hrs. until gradual loss of activity followed by complete Mn(II) breakthrough at 226 hrs.

Prior to the initiation of Mn(II) release from the biofilter at 39.0 hrs., a mass balance of the inflow (158.35 μg), and outflow (59.45 μg) indicates a biofilter accumulation of 98.90 μg of Mn(II) from bulk solution, as shown in Table 4.9 and Figure 4.15b. Computation of the curve area assumed to represent biofilter Mn(II) releases, from 36.4 to 39.0 hrs., yields of total release of 2.49 μg.

For Reactor 2, the time period for the initial influent feed flow rate at 1.9 ml·hr$^{-1}$ is extended to 48 hrs., an additional 11.6 hrs. in comparison to Reactor 1 (Figure 4.16a). The time period of increased loading is similar but the loading rate average is lower, resulting in an almost equal amount of biofilter Mn(II) accumulation at 153.22 μg. At 52.0 hrs. complete Mn(II) breakthrough was observed, and a Mn(II) release was detected at 53.0 hrs., marked by an effluent concentration of 0.90 mg·L$^{-1}$, higher than the influent concentration of 0.84 mg·L$^{-1}$. The peak Mn(II) release concentration measured, 1.00 mg·L$^{-1}$, was at 63.0 hrs. prior to apparent cessation in releases at 67.0 hrs. Subsequent to the cessation in release, Mn(II)-oxidation activity by strain EC112 appears to resume or become dominant, lowering the inflow Mn(II) concentration to approx. 0.60 mg·L$^{-1}$ between 82 hrs. and 94 hrs. until a slow loss of activity and observance of complete Mn(II) breakthrough at 140 hrs.

Prior to the initiation of Mn(II) release from the biofilter, a mass balance of the reactor inflow (142.04 μg), and outflow (33.33 μg) indicates a biofilter accumulation of 108.72 μg as Mn(II), as shown in Table 4.9 and Figure 4.16b. Computation of the curve area assumed to represent biofilter Mn(II) releases, from 52.0 to 67.0 hrs., yields a total release of 2.79 μg.

For Reactor 3, the initial influent feed flow period is 45.8 hrs., 2.2 hrs. lower than Reactor 2. The time period interval for increased Mn(II) loading was significantly longer, from 45.8 to 58.9 hrs., for 13.1 hrs., increasing the amount of Mn(II) accumulated in the biofilter. Within 1.0 hr. of obtaining complete Mn(II) breakthrough (58.9 hrs.), a Mn(II) release was observed at 61.3 hrs., marked by an effluent concentration of 0.87 mg·L$^{-1}$, higher than the influent concentration of 0.79 mg·L$^{-1}$ (Figure 4.17a). The peak Mn(II) release concentration measured 1.16 mg·L$^{-1}$ at 71.0 hrs. Mn(II) releases appear to cease by 104.0 hrs., when Mn(II)-oxidation activity by strain EC112 appears to resume, but more weakly compared to the recoveries observed for Reactors 1 and 2, lowering the inflow Mn(II) concentration to
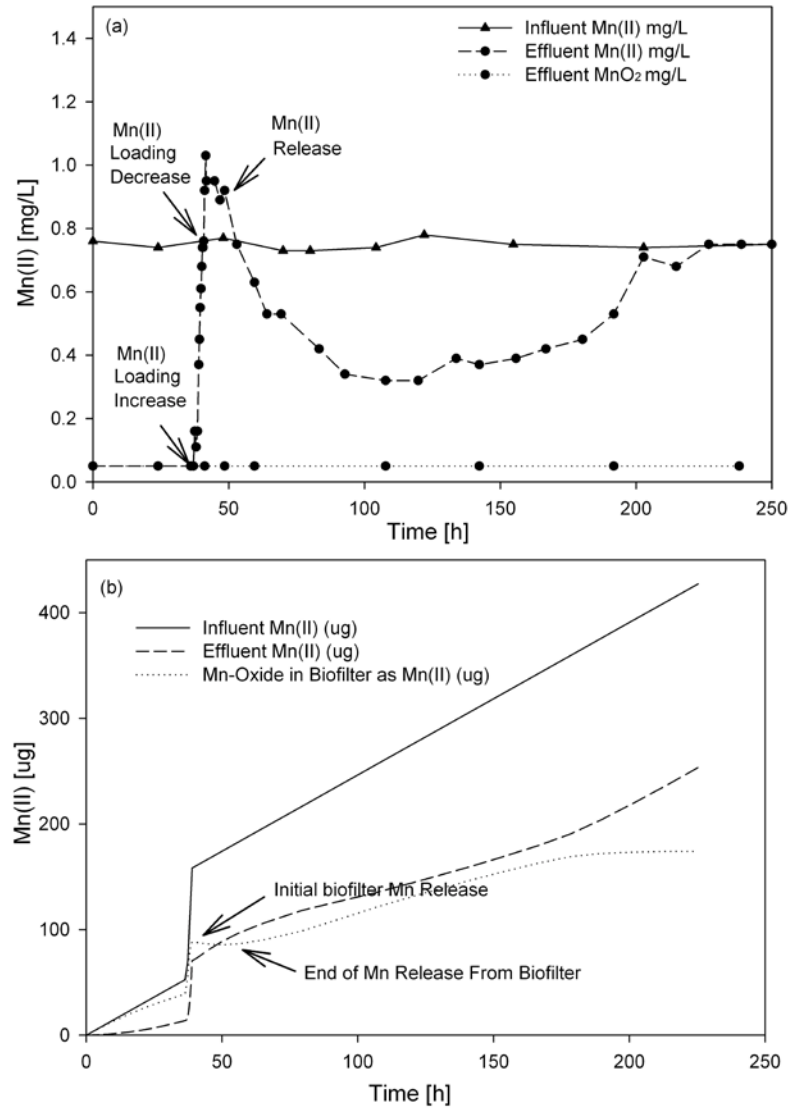
**Figure 4.15:** Biofilter Mn(II) release results for Reactor 1. Effluent Mn concentration profiles (a) and cumulative Mn mass balances (b).
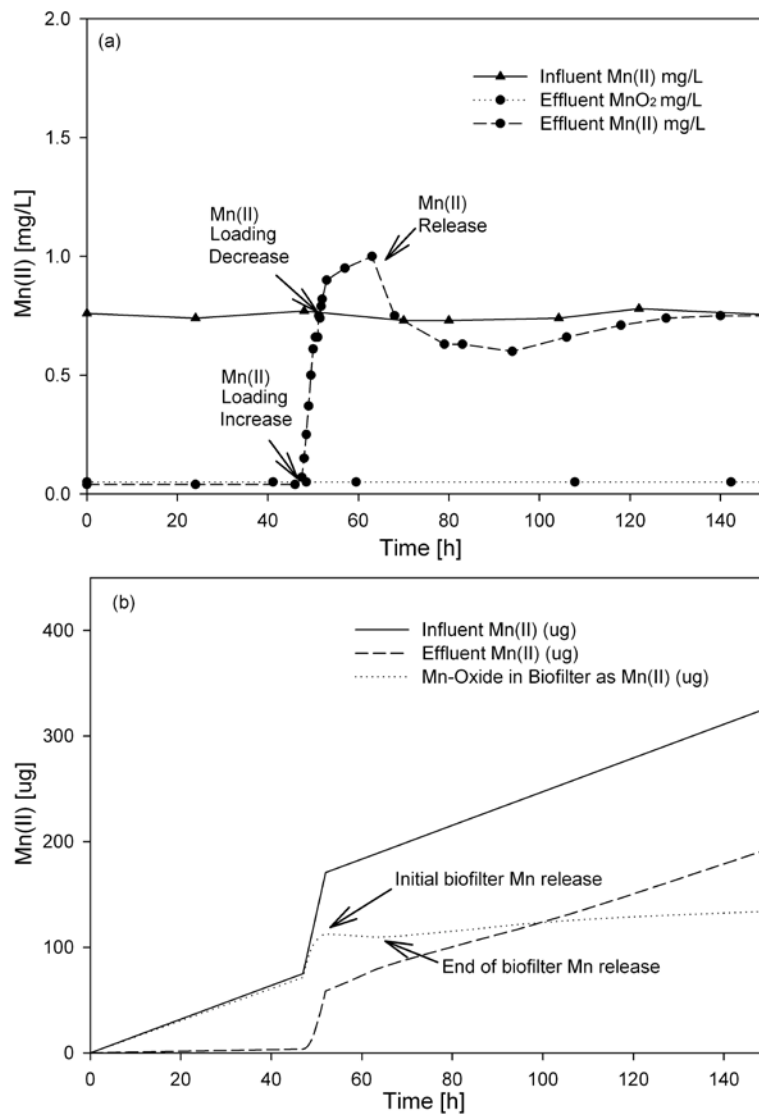
**Figure 4.16:** Biofilter Mn(II) release results for Reactor 2. Effluent Mn concentration profiles (a) and cumulative Mn mass balances (b).
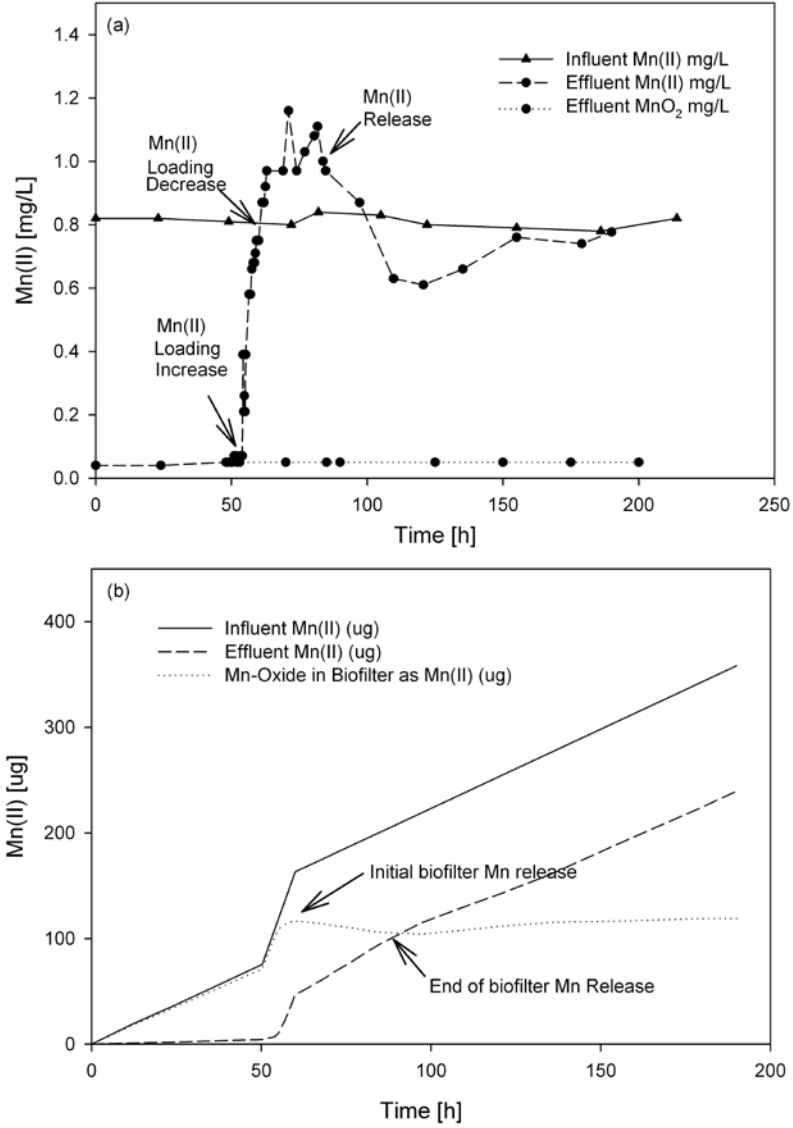
**Figure 4.17:** Biofilter Mn(II) release results for Reactor 3. Effluent Mn concentration profiles (a) and cumulative Mn mass balances (b).

approx. 0.60 mg·L$^{-1}$ by 82 hrs. Loss of activity and complete Mn(II) breakthrough occurs at 155 hrs.

A Mn(II) mass balance of the reactor inflow (163.23 µg), and outflow (46.95 µg) before the initiation of Mn(II) release indicates a biofilter accumulation of 116.28 µg as Mn(II), as shown in Table 4.9 and Figure 4.17b. Computation of the biofilter Mn(II) releases, between 58.9 to 103.7 hrs., yields of total release of 12.15 µg, a larger release compared to Reactor 1 and Reactor 2.

For Reactor 4, the time period for the initial influent feed flow rate of 1.9 ml·hr$^{-1}$ was increased to 68.5 hrs. and the loading time interval was significantly longer, from 68.5 to 95.5 hrs., for 27.0 hrs., increasing the amount of Mn(II) accumulated in the biofilter. Within 1.0 hr. of obtaining complete Mn(II) breakthrough at 94.8 hrs., a Mn(II) release was measured at 95.0 hrs., marked by an effluent concentration of 0.89 mg·L$^{-1}$, higher than the influent concentration of 0.79 mg·L$^{-1}$ (Figure 4.18a). The peak Mn(II) release concentration measured 1.39 mg·L$^{-1}$ at 127.75 hrs. Mn(II) releases continued significantly longer than the previous reactors, until approx. 305 hrs. Further Mn(II)-oxidation activity by strain EC112, if any, did not contribute to recovery of the reactor below the influent Mn(II) level of 0.79 mg·L$^{-1}$.

A Mn(II) mass balance of the reactor inflow (189.04 µg), and outflow (50.25 µg) before the initiation of Mn(II) release indicates a biofilter accumulation of 138.78 µg as Mn(II), as shown in Table 4.9 and Figure 4.18b. Computation of the biofilter Mn(II) releases, between 95.5 to 352 hrs. yields of total release of 138.11 µg, which represents essentially all of the accumulated Mn(II) from bulk solution.

For Reactor 5, the initial influent feed flow rate interval at 1.9 ml·hr$^{-1}$ was increased to 130.5 hrs., and the loading time interval was from 131.0 to 144.7 hrs., for 13.7 hrs. Within 1.5 hr. of obtaining complete Mn(II) breakthrough at 144.5 hrs., a Mn(II) release was measured at 146.3 hrs., marked by an effluent concentration of 0.79 mg·L$^{-1}$, higher than the influent concentration of 0.74 mg·L$^{-1}$ (Figure 4.19a). The peak Mn(II) release concentration measured 1.70 mg·L$^{-1}$ at 186.7 hrs. Apparent Mn(II) releases continued significantly longer than for Reactors 1 to 4, until approx. 510 hrs. Further Mn(II)-oxidation activity by strain EC112 was not apparent, as suggested by the failure of the reactor to recover below the influent Mn(II) level of 0.79 mg·L$^{-1}$.

**Figure 4.18:** Biofilter Mn(II) release results for Reactor 4. Effluent Mn concentration profiles (a) and cumulative Mn mass balances (b).
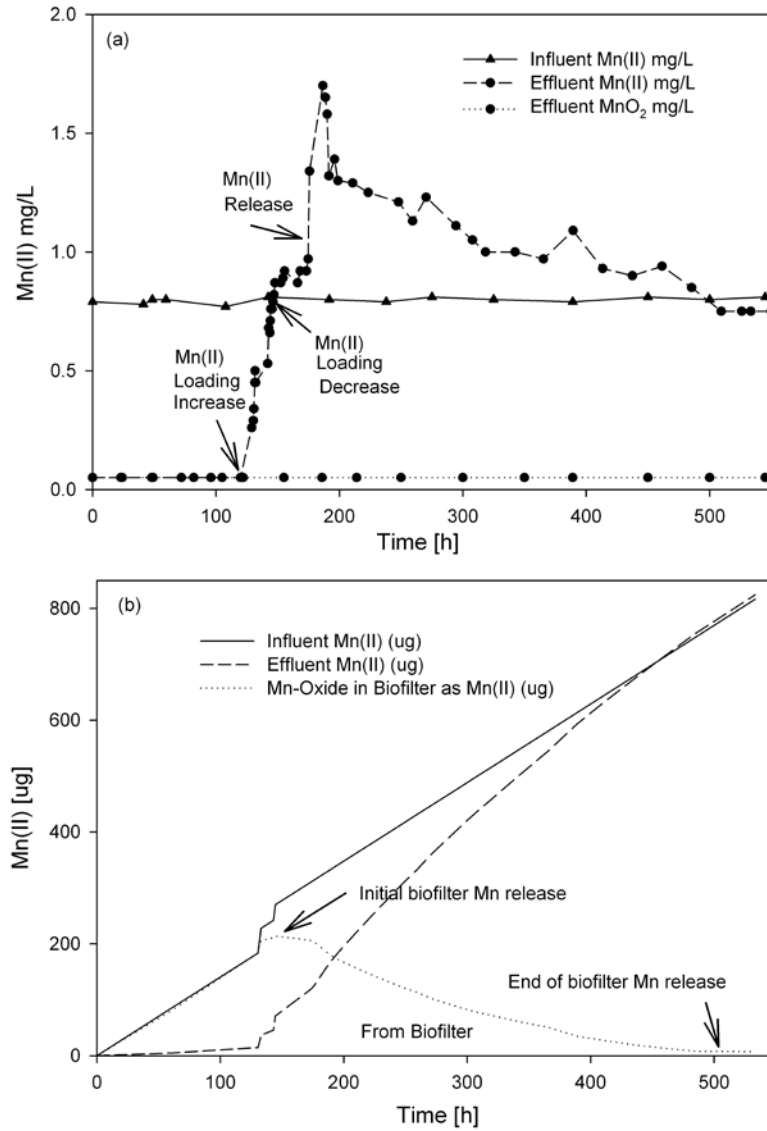
**Figure 4.19:** Biofilter Mn(II) release results for Reactor 5. Effluent Mn concentration profiles (a) and cumulative Mn mass balances (b).

Within 1.5 hr. of obtaining complete Mn(II) breakthrough at 144.5 hrs., a Mn(II) release was measured at 146.3 hrs., marked by an effluent concentration of 0.79 mg·L$^{-1}$, higher than the influent concentration of 0.74   mg·L$^{-1}$ (Figure 4.19a).   The peak Mn(II) release concentration measured 1.70 mg·L$^{-1}$   at 186.7 hrs. Apparent Mn(II) releases continued significantly longer than for Reactors 1 to 4,   until approx. 510 hrs. Further Mn(II)-oxidation activity by strain EC112 was not apparent, as suggested by the failure of the reactor to recover below the influent Mn(II) level of 0.79 mg·L$^{-1}$.

A Mn(II) mass balance of the reactor inflow (270.14 µg), and outflow (62.99 µg) before the initiation of Mn(II) release indicates a biofilter accumulation of 207.16 µg as Mn(II), as shown in Table 4.9 and Figure 4.19b. Computation of the biofilter Mn(II) releases, between 144.7 to 509 hrs., yields of total release of 206.52 µg, which represents release of all of the accumulated Mn(II).

For Reactor 6, followed the same operating conditions for Reactors 1 to 5 except the operation strategy was to increase the Mn(II) loading on the biofilter until the effluent Mn(II) concentration approached breakthrough prior to easing the loading, testing the hypothesis that Mn(II) release occurs at complete breakthrough and should not occur at loading levels just below breakthrough. The time period for initial influent feed flow rate interval at 1.9 ml·hr$^{-1}$ was 93.0 hrs. and 93.0 to 97.5 hrs.  at 24.0 ml·hr$^{-1}$ for the increased loading time and flow rate (Table 4.8).   As shown in Figure 4.20a, the effluent Mn(II) concentration was 0.68 mg·L$^{-1}$ at 97.5 hrs., 4.5 hrs. following the increased loading. At 103.0 hrs., 5.5 hrs. subsequent to the reduction in loading back to the initial (start-up) flow rate of 1.9 ml·hr$^{-1}$,    Mn(II) was 0.71 mg·L$^{-1}$, below the influent feed concentration of 0.76±0.02 mg·L$^{-1}$. The effluent level began a decreasing trend and at 152.5 hrs. the Mn(II) measured 0.45 mg·L$^{-1}$.   The influent flow rate was then increased to 24 ml·hr$^{-1}$ at 153 hrs. and complete Mn(II) breakthrough occurred at 155.5 hrs. with a measured concentration of 0.79 mg·L$^{-1}$.  Within 30 minutes, a Mn(II) release was measured at 156.0 hrs., marked by an effluent concentration of 0.81 mg·L$^{-1}$, higher than the influent concentration of 0.76±0.02 mg·L$^{-1}$.  The peak Mn(II) release concentration was 0.92 mg·L$^{-1}$ at 158.8 hrs. The biofilter demonstrated complete recovery by 230 hrs., with the effluent Mn(II) < 0.05 mg·L$^{-1}$, which Reactors 1 to 5 did not show.

A Mn(II) mass balance of the reactor inflow (354.75 µg), and outflow (156.10 µg) before the initiation of Mn(II) release indicates a biofilter accumulation of 198.65 µg as Mn(II), as shown in Table 4.9 and Figure 4.20b. Computation of the biofilter Mn(II) releases, between 155.5 to 165.0 hrs., yields a total release of 1.21 µg, the smallest release for all of the reactors.

**Figure 4.20:** Biofilter Mn(II) release results for Reactor 6. Effluent Mn concentration profiles (a) and cumulative Mn mass balances (b).
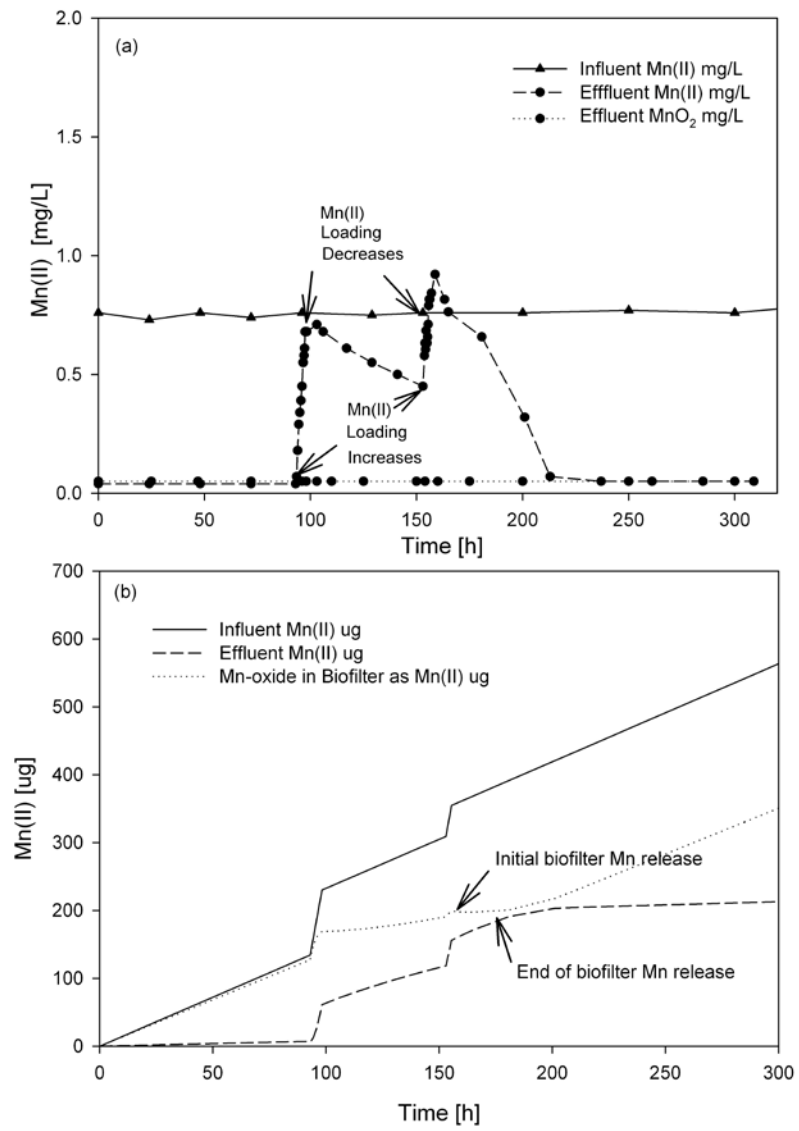
### 4.8.11.3 Kinetics of Biofilter Mn(II) Release

Biofilter Mn releases were modeled using pseudo first-order rate kinetics, as given in Eqn. 4-28 and Eqn. 4-29. The releases, for purposes of rate analysis, are interpreted to represent Mn(IV) reduction to Mn(II) in the biofilter and release of the soluble Mn into bulk solution.

$$d[Mn(IV)]/dt = k_1[Mn(IV)] \qquad\qquad (4\text{-}28)$$

$$\ln[Mn(IV)] = k_1 t \qquad\qquad (4\text{-}29)$$

Data sets used for the kinetic analysis for each reactor, consisted of 3 to 13 points, included the first release of Mn(II) (i.e., first effluent concentration exceeding the feed influent level) through the maximum Mn(II) release measured. The results for the rate constants range from 0.015 to 0.092 hrs.$^{-1}$ and the regression $R^2$ values range from 0.675 to 0.993, as shown in Figure 4.21 and Figure 4.22. The rate constants represent the maximum apparent release rate.

This approach of pseudo first-order kinetics has been previously used for Mn(IV) reduction rates by pure cultures of Mn-reducing bacteria (Dollhopf et al., 2000; Cerrato et al., 2010). Dollhopf et al., (2000) studied the release of Mn(II) from $MnO_2$ during reduction by a Black Sea strain *Shewanella putrefaciens* MR-4. MR-4 is a gram-negative facultative anaerobe capable of metabolic Mn(IV) reduction. Cerrato et al., (2010), isolated various bacteria strains from biofilms in chlorinated water distribution systems each have the ability to both oxidize and reduce Mn (Cerrato et al., 2010). One of these, MB-4, a *Bacillus pumilus* gram positive strain isolated from an anthracite filter media, was capable of Mn-oxidizing and reducing both aerobically and anaerobically. Pseudo-first-order obtained for rate constant aerobic Mn(IV) reduction in batch studies for MB-4 was 0.117 days$^{-1}$, or 0.005 hrs.$^{-1}$, reduction rates that are about 3 times slower than the lower biofilter release estimates obtained for strain EC112.   The kinetic rate constants obtained for strain EC112 represent the apparent maximum release rates. Lower kinetic release rates for Reactor 4 and 5 might be obtained if the complete release curve is taken into account.
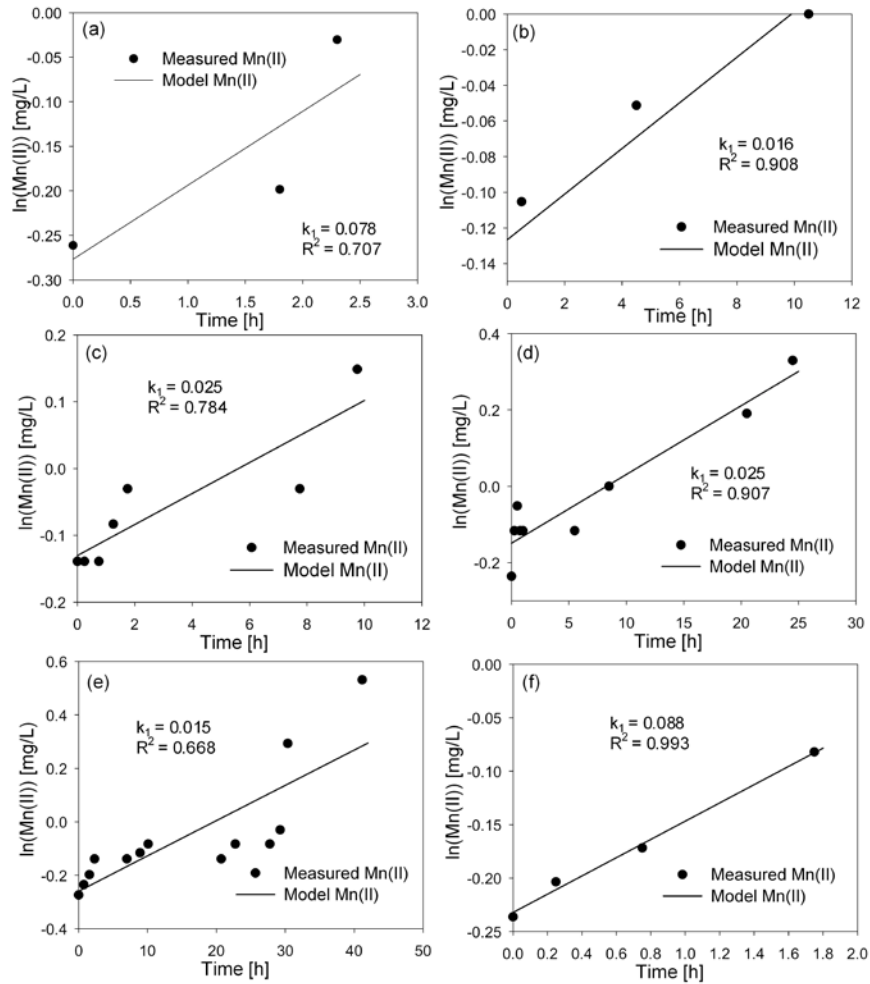
**Figure 4.21:** Kinetics of Mn(II) biofilter release for Reactor 1-6 (a-f). Pseudo-first order rate constant ($k_1$) and $R^2$ regression coefficient for each reactor shown.
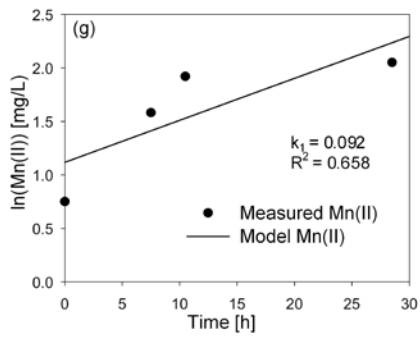
**Figure 4.22:** Kinetics of Mn(II) biofilter release for preliminary reactor (g). Pseudo-first order rate constant ($k_1$) and $R^2$ regression coefficient shown.

### 4.8.11.4 Discussion and Summary

The hypothesis that Mn(II) release occurs at complete effluent Mn(II) breakthrough is supported by Mn release data at various operating conditions for the continuous flow biofilm reactors, implicating direct or indirect activity by strain EC112 as being responsible for the release. The following conclusions can be made with regards to the experimental results:

(1) Biofilter Mn releases are observed for each reactor and occur within 0.5 to 1.5 hrs. of complete Mn(II) effluent breakthrough.

(2) Mn releases appear to be independent of Mn(II) loading rates and occur with and without the presence of an added carbon source in the feed media solution.

(3) The amount of released Mn(II) relative to the accumulated amount of $Mn(III,IV)O_x$ is dependent on the timing of complete Mn(II) breakthrough. For breakthroughs that occur < 60 hrs. following reactor startup, only a minor fraction (roughly <10%) of the accumulated Mn is released. For breakthroughs that occur >75 hrs. following reactor startup, the bulk (> 99%) of the accumulated $Mn(III,IV)O_x$ is released. This paradigm was not observed for Reactor 6, which released < 1% of the accumulated biofilter Mn following breakthough at 155.5 hrs.

(4) Mn releases are consistent with the mechanism of reduction of the oxidized $Mn(III,IV)O_x$ in the biofilter and subsequent release of reduced Mn(II) into bulk solution.

The increased loading intensity or loading duration has no apparent effect on the quantity of Mn release from the biofilter. A general observation from the reactor release studies shows that the quantity of Mn(II) release from the biofilter increases for longer durations of the initial time interval following reactor start-up prior to the sudden load increase. In addition, increasing the time duration of the load increases the amount of Mn(II) released from the biofilter.

The results for Reactor 6, a control reactor, support the hypothesis and that the Mn releases observed in Reactor 1-5 and the preliminary reactor cannot be attributed to cell detachment, cell lysis, or a similar mechanism. The lack of observance of a Mn release after the first increase in Mn load (at 93.0 to 98.3 hrs.) supports this hypothesis Conversely, the occurrence of a Mn release following the second increase in load until complete Mn breakthrough is observed in the effluent is consistent with the results of the other reactors. However, a larger release, perhaps release of all the accumulated biofilter Mn would have been expected. Apparently the first increase in Mn loading had a damping effect on the release mechanism.

The results of these biofilter Mn release experiments have many implications which are dependent on underlying assumptions concerning the mechanism of Mn(II) oxidation and

sorption. First, it is reasonable to assume that the accumulated Mn in the biofilter exists as biotic $Mn(III,IV)O_x$, produced by strain EC112 oxidizing the influent Mn(II). In addition, sorption of Mn(II) from bulk solution by $Mn(III,IV)O_x$ in the biofilter is assumed negligible. Analysis of the biofilter biofilm samples shows the bulk of the Mn to be either Mn(III) and/or Mn(IV), as indicated by the reaction with the Leucoberbelin Blue reagent, indicating at most that no measurable amounts of Mn(II) have been adsorbed. Control batch studies involving solutions of $Mn(III,IV)O_x$ produced by strain EC112 and Mn(II) did not reveal significant removal of the Mn cation from bulk solution, implicating biological Mn(II) oxidation as the removal mechanism, consistent with other studies involving Mn(II)-oxidizing bacteria.

For each reactor, Mn(II) releases from the biofilter occur within 0.5 to 1.5 hrs. following complete Mn(II) breakthrough in the effluent. At breakthrough, assuming the Mn(II) from bulk solution is due to the enzymatic Mn(II)-oxidizing activity of strain EC112 in biofilms attached to the reactor filter material, the enzymes are approaching substrate saturation. The Mn is in the Mn(III,IV) oxidation state in the filter biofilms. As saturation is obtained, Mn is released as Mn(II), as evidenced by the effluent Mn(II) concentration exceeding the influent feed concentration, suggesting the Mn in the biofilm is being reduced, implicating strain EC112 as having the dual capacity to both oxidize and reduce Mn. *P. Putida* strains have not been reported in the literature as $Mn(III,IV)O_x$ reducing, however few reports exist for the study of pure cultures of Mn(IV) reducing bacteria. For Reactor 4 and Reactor 5, complete release of the accumulated Mn in the biofilter occurred subsequent to the increased loading event or enzyme saturation. The release is consistent with Mn-reducing activity by strain EC112. These results indicate that sudden increases in Mn levels apparently saturate the biofilter would be capable of inducing Mn releases.

### 4.8.12 GreensandPlus Filter Reactor Studies

### 4.8.12.1 GreensandPlus Filter Reactor Studies Without Carbon Source

Figure 4.23 shows the results of separate continuous-flow GP filter reactor experiments under 0.4 and 1.0 hydraulic retention times (HRT) with and without biofilm pure cultures of *P. Putida* EC112. To the feed solution 1.0 mg·L$^{-1}$ Mn(II) was added and no added carbon source. For two of the reactors, prior to reactor start-up, cultures were incubated at room temperature (approx. 25°C) and pH 6.5 with the GP for 3 days to allow for cell attachment and biofilm development on the surface of the Mn-oxide coated filter nodules, identical to the conditions used for the steady-state continuous flow reactor modeling experiments using glass beads as the filter material. For the 0.4 and 1.0-hr. HRT reactors packed with GP filter and without added culture, the effluent Mn(II) concentrations steadily increased and breakthrough at 5.2 and 6.8 days, respectively. The poor, unexpected, Mn(II) removal
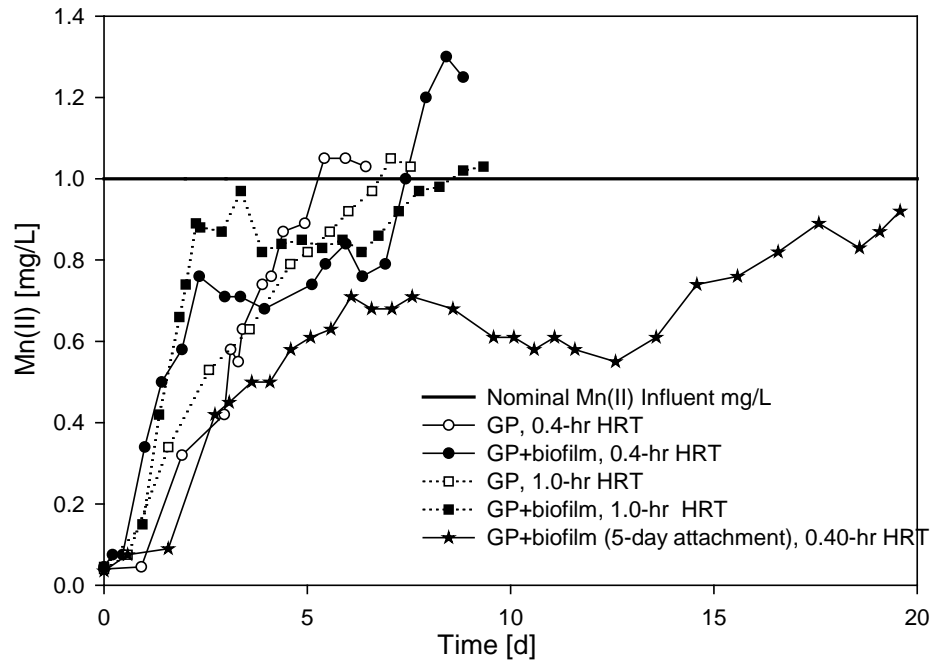
**Figure 4.23:** Continuous flow reactor experiments using GreensandPlus (GP) filter material. No added carbon source.

performance for the GP filter may be attributed to the experimental filter conditions, which differ considerably from the filter operating conditions recommended by the manufacturer, Inversand Company (Clayton, New Jersey). Specifically, a minimum filter bed thickness of 30 inches of GSP (for single media filters) and service flow rate of 5 to 12 gpm $\cdot$ft$^{-2}$ is suggested, compared to 2 inch bed thickness and flow rate of approx. 0.001 gpm $\cdot$ft$^{-2}$ (determined using a reactor inflow feed rate of 1 ml$\cdot$hr$^{-1}$ and inner diameter of 0.075 ft. and 1.0-hr HRT). Therefore, for the experimental reactor conditions, filter bed thickness is implicated as the limiting condition for Mn(II) removal capacity compared to service flow rate for the reactors.

For the 0.4 and 1.0-hr. HRT reactors incubated with strain EC112 cells for 3 days prior to reactor start-up, reactor effluent Mn(II) concentrations increased more sharply before plateauing at 2.2 and 2.3 days for 4 days. The plateau is followed by a second sharp increase until Mn(II) complete breakthrough at 7.4 and 8.6 days. The initial increase from t=2.2 to 2.3 days, the physical presence of strain EC112 or its biofilm products, presumably attached to the filter material, may have inhibited the Mn(II) ion flux from the bulk solution to abiotic Mn(II) surface sorption sites on the filter. The Mn(II) breakthrough time increase may be attributed to activity of enzymatic Mn(II) oxidation by strain EC112 in biofilms. The overall poor removal capacity of the reactors may have been due to lack of significant activity from the biotic Mn(II) oxidizing of the biofilms. The 3-day incubation time for cell-attachment prior to reactor start-up, although sufficient for attachment and biofilm development to glass beads as demonstrated in Section 4.2.1, was reconsidered. Repulsive negatively charged electrostatic surface forces (at pH 6.5) of the GP and the Gram negative cells of strain EC112 at pH 6.5 could have inhibited biofilm formation.

To investigate the effect of a longer incubation time on Mn(II) removal performance, a GP packed reactor was prepared and the incubation time for strain EC112 was increased to 5-days prior to reactor start-up. The results shown in Figure 4.23 for the reactor using a 0.4-hr. HRT show considerable improvement in reactor Mn(II) removal capacity. A more gradual increase in effluent Mn(II) concentration is shown prior to plateauing from 6 days to 12 days. After 12 days the Mn(II) effluent begins to increase and approaches complete breakthrough at 19 days. The plateau may attributed to the Mn(II) oxidizing activity of strain EC112 in a pseudo steady-state until loss or reduction in enzymatic activity at 12 days. Addiitonally, the plateau may be attributed to autocatalytic Mn(II) oxidation by new adsorption sites formed on the GSP surface. Bulk Mn(II) ions presumably sorbed to the original oxide adsorption sites in the first 6 days may have been slowly oxidized to MnO$_2$ to create new reaction sites. The oxidation of sorbed Mn(II) by oxide surfaces has been described as involving slow kinetics (Morgan, 1964; Coffey, 1994) These results indicate that increasing the incubation from 3 to 5-days the strain EC112 with the GP for biofilm development had a significant improvement on reactor performance compared to 3-days.

## 4.8.12.2 GreensandPlus Filter Studies with Humic Acid as sole carbon source

Reactor performance and sustainability in the presence of humic acids was evaluated. Prior to reactor start-up, a solution containing harvested culture of strain EC112 was incubated for 5-days at room temperature (approx. 25°C) and pH 6.5 with the GSP filter material to allow for cell attachment and biofilm development. A second reactor with GSP filter material without strain EC211 culture was studied under identical conditions. The Mn(II) concentration in the influent feed solution was lowered to 0.5 mg·L$^{-1}$ Mn(II) and 10 mg·L$^{-1}$ of Sewannee River Humic Acid was added as the sole carbon source. Previous reactor experience indicated that agitation of the reactor during a sampling event risked inducing releases of Mn from the filter, making sampling biofilm biomass precarious and discouraging their collection. Therefore, biofilm biomass (as viable cell counts) was measured by sampling the effluent side GP filter material, which was more easily accessible, at t=0 and t=25 days as viable cell counts. The reactor conditions were 29°C±2°C and reactor pH 6.5±0.2 with an 1.0-hr HRT. The results of both reactors are shown in Figure 4.24. For the GP filter reactor without culture the effluent Mn(II) concentration steadily increase for 6 days followed by a 6 day decreasing. The 6-day trend of decreasing Mn(II) concentrations parallels the performance for the reactor with GP filter and 5-day biofilm in Figure 4.23, suggesting the removal mechanism is similar and does not involve a biotic mechanism, either enzymatic or autocatalytic. After 12 days the effluent concentrations stabilize between 0.28 to 0.36 mg·L$^{-1}$ before increasing and complete breakthrough by day 30. For the reactor with strain EC112 biofilm the Mn(II) effluent was <0.05 mg ·L$^{-1}$ for 36 days until a rapid increasing trend and complete breakthrough on day 40. Addition of 10 mg/10 ml solution of nutrient broth/yeast extract to the recycle line restored reactor performance < 0.05 mg ·L$^{-1}$ Mn(II) in the effluent within 1 day. Bacteria counts from the biofilter were $3.5 \times 10^8 \pm 1.7 \times 10^8$ and $3.6 \times 10^8 \pm 3.3 \times 10^8$ at t=0 and t=25 days respectively.
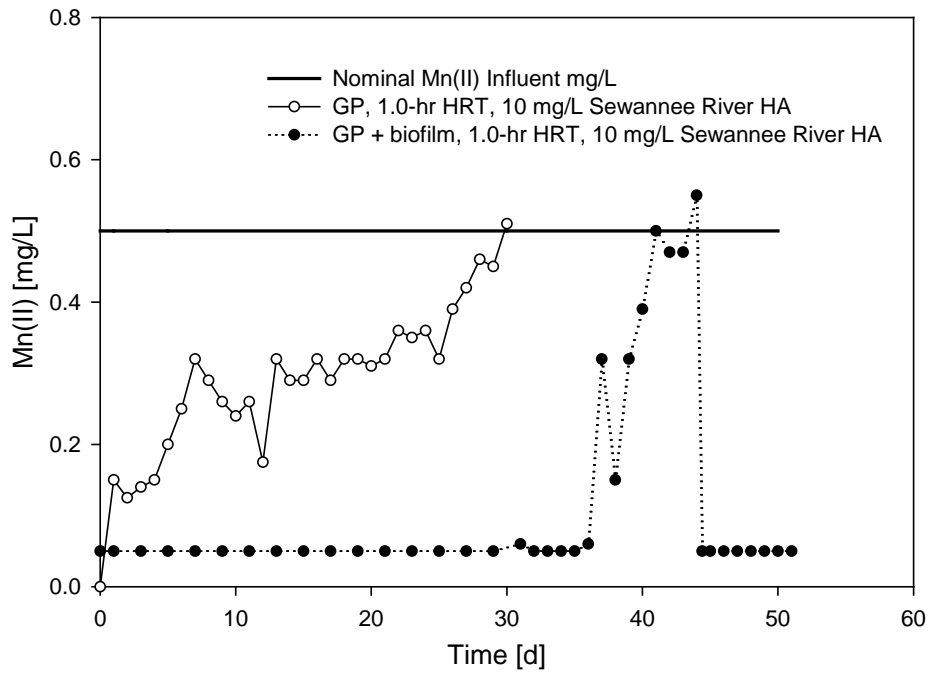
**Figure 4.24:** Continuous Flow Reactor experiments using GreensandPlus (GP) filter material and Sewannee River Humic Acid as sole carbon source

## 4.9 Summary and Conclusions

The potential of Mn(II) oxidation in fixed film continuous flow bioreactors was investigated using cells of *P. Putida* strain EC112. Four research objectives were undertaken to determine: (1) operating conditions for sustainable bioreactor performance for Mn(II) removal, (2) kinetic parameter(s) for Mn(II) oxidation, (3) potential for humic acids (HA) as a sole carbon and energy source to sustain bioreactor and capacity for Mn(II) removal, and (4) fate of Mn in the biofilter. Experiments were conducted at the optimal conditions (pH 6.5 and temperature 30°C) for strain EC112 Mn(II) oxidation.

Preliminary bioreactor experiments revealed D-glucose as a sole carbon source could not sustain bioreactor Mn(II) removal capacity (< 0.05 mg·L$^{-1}$). Reactor performance began to fail after 14 days of operation for an influent Mn(II) concentration of 0.45±0.03 mg·L$^{-1}$. A periodic (4-5 days) addition of a nutrient/carbon source (nutrient broth/yeast extract) to the recycle line was required to sustain the bioreactor.

A steady-state flux model incorporating Monod Kinetics was used to estimate a fixed-film kinetic parameter for Mn(II) oxidation, which was calibrated and validated in separate bioreactors without the addition of a feed carbon source. For model calibration, 6 steady-states (1.1 to 25 hrs. HRT) and a reactor Mn(II) influent concentration of 690±45µg were used. Model validation was obtained for 3 steady-states (12.6, 6.3, 1.3 hrs. HRT) and a reactor influent Mn(II) concentration of 750±45µg.

Experimental Mn(II) data sets were fitted to the Monod Model. Autocatalytic effects, described as Mn(II) removal from bulk solution by sorption to $MnO_2$, were shown to be negligible in control studies, and Mn(II) data sets were modeled while ignoring such effects.

A continuous flow bioreactor packed with $MnO_2$ coated media with immobilized cells of strain EC112 using HA as the sole carbon source showed enhanced Mn(II) removal capacity compared to a control bioreactor.

Biofilter Mn(II) releases were observed during the continuous flow reactors studies for reactors with and without an added carbon source. Bioreactor conditions for release were identified and releases were modeled using pseudo first-order kinetics. The mean kinetic constant ($k_1$) and regression $R^2$ were 0.048±0.036 and 0.824±0.128, respectively. The releases are interpreted to represent either direct or indirect reduction of Mn oxide by strain EC112 and release of Mn(II) into the bulk solution, occurring under Mn(II) saturating biofilter conditions.

# Chapter 5: Engineering Significance and Future Research

Biological treatment processes for drinking water have been largely discouraged by water utilities, particularly in the U.S., due to the presence of microorganisms in the water. However, their gain in acceptance is in part due to their effectiveness to achieve biological water stability, and in the US, driven by more stringent regulations on disinfectants and disinfection byproducts (DBS) which in some cases discourage the use of chemical oxidants for treatment.

In this study, it was shown that the substrate products from the reaction between a model humic acid (Aldrich Humic Acid) and Mn Oxide ($MnO_2$) potentially represent viable carbon and energy sources for biological water treatment processes. In Chapter 3 the optimal conditions for the HA-Mn oxide reaction in batch bioreactors were identified. Batch (Chapter 3) and continuous flow bioreactor (Chapter 4) experiments conducted showed enhanced Mn(II) oxidation and growth by a new Mn(II)-oxidizing bacteria isolate, *Pseudomonas Putida* strain EC112.

Water discoloration has been attributed to releases of Mn from water treatment filtration units and pipe walls of drinking water distribution systems. Biofilter Mn releases were observed in this study for continuous flow bioreactor experiments and release conditions were identified and release kinetics modeled in Chapter 4.

GreensandPlus (GSP), a common filter material used for Mn removal for drinking water treatment, requires frequent backwashing and use of chemical oxidants (e.g., chlorine) to regenerate the catalytic Mn oxide coating. In Chapter 4, biofilms of strain EC112 immobilized on GSP feed humic acids had higher Mn removal capacity compared to both biofilm/GSP without HA and GSP only, in separate continuous flow reactor experiments. Use of biofilms with GSP or other filter materials could also eliminate the frequent need to replace or regenerate adsorbents such as granular activated carbon (GAC) or use of chemical oxidants (e.g., chorine) to regenerate GSP. Such a strategy can also reduce the disinfection byproduct (DBP) potential by reducing the raw water natural organic matter (TOC is the surrogate parameter for NOM). This strategy can also reduce the quantity of for water utilities that practice enhanced coagulation. while additionally reducing the quantity of coagulants (e.g., ferric chloride) used further reducing the

The results from this study can potentially serve as an innovative water treatment technology and source of information for optimization of existing biological filters that treat Mn as part of drinking water treatment processes.

Based on the findings of this dissertation further research is warranted and includes:

1. Investigate potential for fulvic acids and other humic acids (from other sources) as a substrate for biological filtration. This study involved two model humic acids, Aldrich Humic Acid and Sewannee River Humic Acids. Other Humic acids and Fulvic acids will different percentages of the core elements, particularly O and C, and functional groups, would be expected to have different reactivities towards Mn-Oxide, and therefore potentially varying yields of biodegradable substrates as products. Such a study should allow the further identification of the specific characteristics of recalcitrant organic matter that are amendable to product favored biological substrates by Mn oxide. This should be useful for water utilities to identify or assess the potential of water supply sources for biological water treatment for Mn.

2. Investigate HA and biotic Mn Oxide reactivity. The Mn Oxide used in this study was a synthetic $MnO_2$ (GreensandPlus). Biotic Mn Oxide is structurally distinct, has larger surface area, and would be expected to have different reactivity with HA. Information gained from such a study could be used to assess the role of Mn Oxide in humic material cycling in the carbon cycle. Sunda and Kieber (1994) proposed that Mn Oxidizing bacteria may use the Mn Oxides as a mechanism to tap the recalcitrant carbon in humic materials.

3. Mn Oxide – HA reaction was investigated in this study using FT-IR and $^1$H-NMR. Analyze the raction using $^{13}$C-isotope based spectroscopy such as solid state $^{13}$C CP-MAS to provide further inside into oxidative changes induced by Mn Oxide in the humic structure is desirable.

4. Further research the mechanism(s) for Mn(II) release observed during continuous flow bioreactors. Mn(II) releases observed during complete Mn(II) effluent breakthrough and were apparently a condition of biofilter saturation and the enzymes responsible for Mn(II) oxidation for strain EC112. It is speculated, due to the systematic timing and controlled nature of the releases, that the release of Mn(II) into bulk solution represent Mn reduction activity by strain EC112. Further elucidation of the conditions for the release may allow exploitation of this observance in biological filters. For example, biological filters are regularly backwashed to remove biofilm material and for filters that treat Mn, oxidized Mn. This may be a mechanism that could be used by water treatment operators to remove the oxidized Mn periodically.

5. Repeat Mn release experiments observed for continuous flow bioreactors using different filter materials (e.g., $MnO_2$ coated material such as GSP).

6. Repeat Mn release experiments for other Mn-oxidizing bacteria species in continuous flow bioreactors. Test the hypothesis that the Mn release observed in this study is a common trait among Mn(II) oxidizing bacteria. If so, does this characteristic have a cell physiological function?

7. The release studies implicate strain EC112 as a Mn reducer. Further study strain EC112 for the ability to reduce Mn(IV). No *Pseudomonas Putida* strains have been identified as Mn reducers.

# Chapter 6: Summary and Principal Findings

The overall dissertation hypothesis, that in controlled bioreactor systems containing appropriate amounts of Mn(II), Mn oxide, humic acids and Mn-oxidizing bacteria, Mn oxide under certain conditions will oxidize humic acids to more biodegradable products that can serve as the primary electron donor and carbon source for microbial energy and growth. The Mn(II)-oxidizing bacteria, upon utilization of the oxidized substrate products, will regenerate (oxidize) Mn(II) to insoluble, biotic Mn oxide, thus controlling/removing Mn(II) from solution. Subsequent reduction and dissolution of Mn oxide will release Mn(II) into the bulk solution which can be oxidized by the bacteria and autocatalytically by $MnO_2$ in the reactors. The overall HA-$MnO_2$-Mn(II) oxidizing bacteria reaction described in Chapter 1 (Eqns. 1-1 to 1-4) can now be modified for this study (Eqns. 6-1 to 6-4):

Bulk solution humic acids (HA) diffuse to Mn oxide surface reaction sites and initially form a HA–$MnO_2$ precursor complex:

$$MnO_2 + HA \quad \leftrightarrow \quad HA-\ MnO_2 \tag{6-1}$$
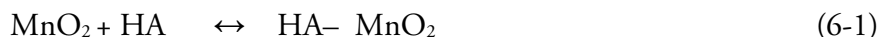
Electron transfer from HA in the HA-$MnO_2$ complex to Mn oxide to form oxidation product $HA_{(ox)}$ and reduced Mn(II):
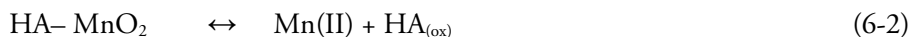
$$HA-\ MnO_2 \quad \leftrightarrow \quad Mn(II) + HA_{(ox)} \tag{6-2}$$

Biological oxidation of Mn(II) formed from Mn oxide reduction and dissolution and Mn(II) originally present in source water, as $Mn(II)_{(in)}$, to form $MnO_2$ utilizing $HA_{(ox)}$ as the substrate (electron donor) for growth and $O_2$ as the final electron acceptor:

$$Mn(II) + Mn(II)\ _{(in)} + O_2 + HA_{(ox)} + \text{strain EC112 cells} \rightarrow MnO_2 + H_2O \tag{6-3}$$
$$+ \text{new strain EC112 cells}$$

Overall reaction:

$$Mn(II)_{(in)} + MnO_2 + HA + O_2 + \text{strain EC112 cells} \rightarrow MnO_2 + H_2O + \tag{6-4}$$
$$\text{new strain EC112 cells}$$
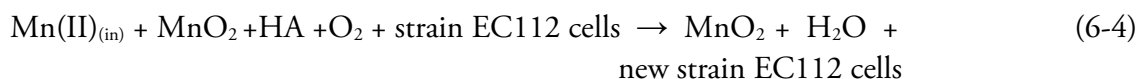
This reaction should proceed in bioreactor systems as shown in Eqn. 6-4 which contain Mn(II) oxidizing bacteria, humic material, and $MnO_2$ and at appropriate conditions. At HA concentrations typical of natural waters, HA reaction with Mn Oxide to produce bioavailable organic substrates and growth of new bacteria cells within 1 – 2 hrs. Optimal pH and temperature conditions for reaction will be pH 6.5 to 7.0 and 25 to 30°C respectively. Biological treatment of Mn in waters below 15°C and above 30°C will be negligible. At pH >7.5 and pH < 6.0, Mn(II)-oxidation activity by strain EC112 will be severely inhibited. Mn Oxide reaction with HA can proceed as low as pH 3.0, for higher pH that approach 9.0 reaction will not occur. Freshly formed biological Mn Oxide as a product of removal of $Mn(II)_{in}$ from bulk solution may not contribute significantly as an autocatalytic Mn(II) removal mechanism, particularly for biological treatment of waters that are moderate to hard water where other divalent cations (e.g., $Ca^{2+}$) are present to compete for sorption sites, at least in comparison to enzymatic Mn(II) oxidation rates by strain EC112. Mineralization of HA by Mn Oxide to $CO_2$ will be negligible or absent and is not included as a product in Eqn. 6-3. For continuous flow bioreactors, sudden increases in $Mn(II)_{in}$ that saturate the biofilter, or localized biofilm regions, for periods lasting for several minutes may induce Mn(II) releases of Mn(II).

The principal findings of this dissertation are:

(1) A Mn(II)-oxidizing bacterium, *Pseudomonas Putida* strain EC112, was isolated and found to oxidize Mn(II) in the stationary growth phase as a carbon-stressed, enzymatic constitutive feature, not requiring added Mn for induction. Optimal Mn(II)-oxidation conditions for cultures of strain EC112 were determined to be pH 6.5 and 30°C. Strain EC112 can utilize a variety of growth substrates as a carbon and energy source, showing robust growth for glucose and benzoate.

(2) The potential of AHA as a substrate for Mn(II) oxidation was evaluated in a batch bioreactor containing $MnO_2$ and strain EC112. The effect of $MnO_2$ oxide on AHA biodegradability was evaluated utilizing viable cell counts and a modified 48-h BOD. The results indicate that the biodegradability of AHA is dependent on both $MnO_2$ concentration and $AHA$-$MnO_2$ contact time. Lower amounts of $MnO_2$ oxide required longer reaction times and shorter reaction required higher amounts of $MnO_2$ to yield comparable results. The optimal contact time and $MnO_2$ concentration were found to be 45 min. and 6.6 g $L^{-1}$ for 50 mg/L AHA. The pH of the AHA-$MnO_2$ reaction and added $Ca^{2+}$ had a significant effect on biodegradability. For reactions at pH 3, 7 and 9, 48-h BOD increased ca. 3, 5, and 0.5-fold respectively compared to controls for the optimal AHA/ $MnO_2$ oxide ratio. For reactions at pH 7, 40 mg $L^{-1}$ added $Ca^{2+}$ had a significant effect on 48-h BOD for $MnO_2$ oxide levels up to 1.5 g.

(3) The growth and Mn(II)-oxidation rates of strain EC112 utilizing the oxidation products from the reaction of AHA and $MnO_2$ (GreensandPlus) were higher compared to control experiments involving AHA only, validating the research hypothesis. Kinetic parameters were obtained by fitting experimental Mn(II) data sets to the Monod Model using nonlinear least-square regression and the Marquardt-Levenberg algorithm (LMA). Experiments were conducted at the optimal condition for Mn(II) oxidation for strain EC112, pH 6.5 and temperature 30°C. Batch kinetic parameter model calibration and validation was performed using separate carbon sources for growth of strain EC112, D-glucose and the substrate products from $HA-MnO_2$, respectively. The best fit model parameters were determined for half-saturation coefficient, $K_s$ = 1.086 ± 0.029 and, and maximum specific substrate utilization rate, $k_{mc}$ = 0.180 ± 0.003 and Mn(II)/ mg dry cell mass/hour. Autocatalytic effects, described as Mn(II) removal from bulk solution by sorption to $MnO_2$, were shown to be negligible in control studies, and Mn(II) data sets were modeled by ignoring such effects.

(4) Changes in AHA by $MnO_2$ oxidation are studied using Fourier transform infrared (FT-IR) and proton nuclear magnetic spectroscopy ($^1$H-NMR). Comparison of the FT-IR and $^1$H-NMR spectra of AHA and the $MnO_2$ degradation products of AHA reveal striking changes in AHA structure. The most prominent change is interpreted to be evidence of exchange reactions between humic hydroxyl and C-O functional groups and $MnO_2$ surface reaction sites.

(5) Biological Mn(II)-oxidation kinetics of strain EC112 cultures was investigated in continuous flow (fixed film) bioreactors and kinetic parameters were obtained by fitting experimental Mn(II) data sets to the Monod Model using nonlinear least-square regression and the Marquardt-Levenberg algorithm (LMA). Experiments were conducted at the optimal condition for Mn(II) oxidation for strain EC112, pH 6.5 and temperature 30°C. A steady-state flux model was used to estimate a first-order kinetic parameter, which was calibrated and validated in separate bioreactors without the addition of a feed carbon source. For model calibration, data obtained from 6 steady-states (1.1 to 25 hrs. HRT) under a reactor Mn(II) influent concentration of 690±45µg were used. Model validation was performed with for 3 steady-states (12.6, 6.3, 1.3 hrs. HRT) and a reactor influent concentration of 750±45µg. Autocatalytic effects, described as Mn(II) removal from bulk solution by sorption to $MnO_2$, were shown to be negligible in control studies, and Mn(II) data sets were modeled by ignoring such effects.

(6) A continuous flow bioreactor packed with $MnO_2$ coated media with immobilized cells of strain EC112 using HA as the sole carbon source showed enhanced Mn(II) removal capacity compared to control bioreactors.

(7) Mn(II) releases in water treatment filters and distribution systems, which contribute to dirty water events, were observed during the continuous flow reactors studies. Reactor conditions for release were identified and releases were modeled using pseudo first-order kinetics. The releases are interpreted as Mn oxide reduction by direct or indirect activity by strain EC112 in the biofilter and release of Mn(II) into the bulk solution, occurring under Mn(II) saturating biofilter conditions.

APPENDICES

**Appendix I:** *P. Putida* strain EC112 Sequence

NNNNNNTNCCGCGGCAGCTGATCCGCGATTACTAGCGATTCCGACTTCACGCACTC
GAGTTGCAGACTGCGATCCGGACTGCGACGGGTTTTGTGGATTTGGCTCCCCCCCC
CGTCTTGCCGCCCCTCGGTACCACCATTGGTATGACGTGTGTAGCCCTACCCATAAG
GGCCATGAGAACCTGACGTCATCCCCACCTTCCTCCGGTTTATCACCGGCAGTCTCC
TTAGAGTGCCCTTTCGTATGCTGTAATGACAAGGGTAGGGCTGCGCTCGTTGCTTAA
CTTAACCTCTCATCTCACGAGCTGACGACAGCCATGCCATGCCTGTGTCTAGGTGCT
CTTTCGAGAACTGACAGATCTCTGCTCGAGTCCTAGCAAGCCAAAGGTAAGTAACGG
TTTTCGCGTTGCGTCTAATTTCAAATTATCATCCATGCTCCACCGCTTGCCCCGGCC
CTTCCTTTGAGTTTTGACCTTTAATCTTGCCTCCCCACTCCCCAGGCTTAATGTTTAA
TGCTACGTTACTGACACCAAACCTCCCACTGCCCAATTGACATCATTCAGGGCGTGG
ACTACCAAGGTATCTAATATCTGTTTGCTGTTTGCTCTTTCGCTTTGACACGTCAGTA
CAGGTCCATGGACCTGCCTTCCGCCTTCGCCACTGGCGTTCCATCTACTATCTTCAA
TGCTACCTCTACAATTCCAAATTCCTCTACCCTCTTCTATACTATAAGATAACCAATAT
CAAACGCAGGTTGAGAGTTGAGCTCTGGCATCTCACCCCTGACATCGATATGCGCAC
GCTATGCGCTTTACAATTCCTATTAACGAATGCGCTAACCCCCTACCGATTACTGCTG
GCTGCTGGTTAGACGGTGCTTAGTCCTCCTGCTCCGACTACC

# REFERENCES

American Public Health Association, American Water Works Association, and Water Environment Federation, 1998. Standard Methods for the Examination of Water and Wastewater, 20th edition. American Public Health Association, Washington, D.C.

Adams, L.F., Ghiorse, W.C., 1985. Influence of Manganese on Growth of a Sheathless Strain of *Leptothrix discophora*. Applied and Environmental Microbiology, 49 (3), 556-562.

Aiken, G. R., Brown, P. A., Noyes, T. I., Pinckney, D. J., 1994.  In Humic Substances in the Suwannee River, Georgia: Interactions, Properties, and Proposed Structures; Averett, R. C., Leenheer, J. A., McKnight, D. M., Thorn, K. A., Eds. U. S. Geol. Survey. Water-Supply Paper, No. 2373, 89-98.

Alborzfar, M., Villumsen, A., Gron, C., 2001. Artificial recharge of humic ground water. Journal of Environmental Quality, 30 (1), 200-209.

Ali, S.H., Stokes, J.L., 1971. Stimulation of Heterotrophic and Autotrophic Growth of *Sphaerotilus discophorus* by Manganous Ions. Antonie van Leeuwenhoek Journal of Microbiology, 37 (4), 519-528.

Atkinson, B., Davies, I.J. 1974. The overall rate of substrate uptake (reaction) by microbial films. Part I. Biological rate equation. Transactions of the Institution of Chemical Engineers, 52 (3), 248-259.

Avena, M.J., Koopal, L.K., 1998. Desorption of Humic Acids from an Iron Oxide Surface. Environmental Science and Technology, 32 (17), 2572-2577.

Barbeau, D.S., 1992. Determination of extant biodegradation kinetics from a single oxygen consumption curve, Master Science Thesis, Clemson University, South Carolina.

Basu, A., Das, D., Bapat, P., Wangikar, P.P., Phale, P.S., 2009. Sequential utilization of substrates by *Pseudomonas putida* CSV86: Signatures of intermediate metabolites and online measurements. Microbiological Research, 164 (4), 429-437.

Basu, O.D., Huck, P.M., 2005.  Impact of Support Media in an Integrated Biofilter – Submerged Membrane System.  Water Research, 39 (17), 4220-4228.

Beckett, R., Jue, Z., Giddings, J.C., 1987. Determination of Molecular-Weight Distributions of Fulvic and Humic Acids Using Flow Field-Flow Fractionation. Environmental Science & Technology, 21 (3), 289-295.

Bekbolet, M., Cecen, F., Ozkosemen, G., 1996. Photocatalytic oxidation and subsequent adsorption characteristics of humic acids. Water Science Technology, 34 (9), 65-72.

Beger, H., 1937. Die Eisenbakterien in Wasserversorgungsanlagen und ihre praktische Bedeutung. Das Gas-und Wasseerfach, 80, 886-889, 908-911.

Boogerd, F. C., de Vrind, J.P.M., 1987. Manganese Oxidation by *Leptothrix discophora*. Journal of Bacteriology, 169 (2), 489-494.

Bowen, H.J.M., 1979. Environmental Chemistry of the Elements. London: Academic Press.

Bradford, M.M. 1976. A rapid and sensitive method for the quantitation of microgram quantities of protein utilizing the principle of protein-dye binding. Analytical Biochemistry, 72 (1-2), 248-254.

Brigante, M., Zanini, G., Avena, M., 2007. On the dissolution kinetics of humic acid particles Effects of pH, temperature and $Ca^{2+}$ concentration. Colloids and Surfaces A: Physicochemical Engineering Aspects, 294 (1-3), 64-70.

Bromfield, S. M. 1956. Oxidation of manganese by soil microorganisms. Australian Journal Biological Sciences, 9 (2), 238-252.

Bromfield, S.M., and David, D.J., 1976. Sorption and Oxidation of Manganous Ions and Reduction of Manganese Oxide by Cell-Suspensions of a Manganese Oxidizing Bacterium. Soil Biology & Biochemistry, 8 (1), 37-43.

Brouwers G.J., de Vrind, J.P.M., Corstjens, P.L.A.M., Cornelis, P., Baysse, C., DeJong, E.W.D.V, 1999. CumA, a Gene Encoding a Multicopper Oxidase, is Involved in $Mn^{2+}$-Oxidation in *Pseudomonas putida* GB-1. Applied Environmental Microbiology, 65 (4), 1762–1768.

Brouwers, G.J., Vijgenboom, E., Corstjens, P.L.A.M., de Vrind, J.P.M., and de Vrind-de Jong, E.W., 2000. Bacterial $Mn^{2+}$ Oxidizing Systems and Multicopper Oxidases: An Overview and of Mechanism and Functions. Geomicrobiology Journal, 17 (1), 1-24.

Butterfield, P.W., Camper, A.K., Biederman, J.A., Bargmeyer, A.M., 2002. Minimizing biofilm in the presence of iron oxides and humic substances. Water Research, 36 (15), 3898-3910.

Caiazza, N.C., Lies, D.P., Newman, D.K., 2007. Phototrophic Fe(II) Oxidation Promotes Organic Carbon Acquisition by *Rhodobacter capsulatus* SB1003. Applied Environmental Microbiology, 73 (19), 6150.

Carraro, E., Bugliosi, E.H., Meucci, L., Baiocchi., Gilli, G., 2000. Biological drinking water treatment processes, with special reference to mutagenicity, Water Research, 34 (11), 3042-3054.

Cerrato, J.M., Falkinham III, J.O., Dietrich, A.M., Knocke, W.R., McKinney, C.W., and Pruden, A., 2010. Manganese-oxidizing and –reducing microorganisms isolated from biofilms in chlorinated drinking water systems. Water Research, 44 (13), 3935-3945.

Chapnick, S.D., Moore, W.S., Nealson, K.H., 1982. Microbially Mediated Manganese Oxidation in a Fresh-Water. Limnology and Oceanography, 27 (6), 1004-1014.

Chin, Y.P., and Gschwend, P.M. The Abundance, Distribution, and Configuration of Porewater Organic Colloids in Recent Sediments. Geochimica et Cosmochimica Acta, 55 (5), 1309-1317.

Chin, Y.-P., Aiken, G. R., Danielsen, K. M., 1997. Binding of Pyrene to Aquatic and Commercial Humic Substances: The Role of Molecular Weight and Aromaticity, Environmental Science and Technology, 31 (6), 1630-1635.

Chirwa, E.M.N., 2000. Modeling Chromium(VI) Reduction In Pure and Coculture Biofilm Reactors. Ph.D. Thesis. University of Kentucky, Lexington, KY.

Choi, H., Silverstein, J. 2007. Effluent recirculation to improve perchlorate reduction in a fixed film bioreactor. Biotechnology and Bioengineering, 98 (1), 132-140.

Chowdhury, S., 2012. Heterotrophic bacteria in drinking water distribution system: a review, Environmental Monitoring and Assessment, 184 (10), 6087-6137.

Chudoba, J., Cech, J.S., Chudona P., 1985. The Effect of Aeration Tank Configuration on Nitrification Kinetics. Journal Water Pollution Control Federation, 57 (11), 1078-1083.

Clement, B.G., Luther, G.W., Tebo, B.M., 2009. Rapid, oxygen-dependent microbial Mn(II) oxidation kinetics at sub-micromolar oxygen concentrations in the Black Sea suboxic zone. Geochimica et Cosmochimica Acta, 73 (7), 1878-1889.

Colthurst J.M., Singer, P.C., 1982. Removing Trihalomethane Precursors By Permanganate Oxidation and Manganese-Dioxide Adsorption. Journal American Water Works Association, 74 (2), 78-83.

Cox, P.A., 1995. The Elements on Earth: Inorganic Chemistry in the Environment, New York: Oxford University Press, 287 pp.

Cristiano, E., Hu, Y.J., Siegfried, M., Kaplan, D., Nitsche, H., 2011. A Comparison of Point of Zero Charge Measurement Methodology. Clays and Clay Minerals, 59 (2), 107-115.

Czekalla, C., Mevius, W., Hanert, H., 1985. Quantitative Removal of Iron and Manganese By Microorganisms in Rapid Sand Filters (In Situ Investigations). Water Supply, 3, Berlin 'B', 111-123.

Dang, J.S., Harvey, D.M., Jobbagy, A., Grady, C.P.L. Jr., 1989. Evaluation of biodegradation kinetics with respirometric data. Research Journal Water Pollution Control Federation, 61 (11-12), 1711-1721.

Das, B.K., Roy, A., Koschorreck, M., Mandal, S.M., Wendt-Potthoff, K., Bhattacharya, J., 2009. Occurrence and role of algae and fungi in acid mine drainage environment with special reference to metals and sulfate immobilization. Water Research, 43 (4), 883-894.

Dastidar, A., 2010. Arsenite Oxidation by Pure Cultures of *Thiomonas Arsenivorans* strain B6 in Bioreactor Systems. Ph.D. Thesis. University of Kentucky, Lexington, KY.

De Haan, H., 1974. Effect of a Fulvic Acid Fraction on the growth of a Pseudomonas from Tjeukemeer. Freshwater Biology, 4 (3), 301-310.

DePalma, S. R. 1993. Manganese oxidation by *Pseudomonas putida*. Ph.D. Thesis. Harvard University, Cambridge, Mass.

Dollhopf, M.E., Nealson, K.H., Simon, D.M., Luther, G.W., 2000. Kinetics of Fe(III) and Mn(IV) reduction by the Black Sea strain of *Shewanella putrefaciens* using in situ solid state voltammetric Au/Hg electrodes. Marine Chemistry, 70 (3), 171-180.

Donlan, R.M., Costerton, J.W., 2002. Biofilms: Survival Mechanisms of Clinically Relevant Microorganisms. Clinical Microbiology Reviews, 15 (2), 167-193.

EC-Official Journal of the European Communities Council Directive, Drinking water quality intended for human consumption, Brussels, Belgium, 98/83/EC 330, 32-54, 1998.

Edzwald, J. (ed.), 2010. Water Quality and Treatment: A Handbook of Community Water Supplies, 6th Ed., McGraw-Hill, Inc., New York, NY, 1696 p.

Ehrlich, H. L., Newman, D.K., 2008. Geomicrobiology of Manganese. In: Geomicrobiology, 5th edition. Boca Raton, FL: CRC Press. 628.

Eisenthal, R., Cornish-Bowden, A. 1974. The direct linear plot: A new graphical procedure for estimating enzyme kinetic parameters. Biochemical Journal, 139 (3), 715-720.

Ellis,T.G., Barbeau, D.S., Smets, B.F., Grady, C.P.L., 1996. Respirometric technique for determination of extant kinetic parameters describing biodegradation. Water Environment Research, 68 (5), 917-926.

Emerson, S., Kalhorn, S., Jacobs, L., Tebo, B.M., Nealson, K.H., Rosson, R.A., 1982. Environmental Oxidation Rate of Manganese(II) – Bacterial Catalysis. Geochimica et Cosmochimica Acta, 46 (6), 1073-1079.

Falamin, A.A., Pinevich, A.V., 2006. Isolation and Characterization of a Unicellular Manganese-Oxidizing Bacterium from a Freshwater Lake in Northwestern Russia. Microbiology, 75 (2), 180-185.

Flemming, H.-C., Wingender, J., 2002. Extracellular polymeric substances: structure, ecological functions, technical relevance, p. 1223-1231. In G. Bitton (ed.), Encyclopedia of environmental microbiology, Vol. 3. ,Wiley, New York, NY.

Flemming, H.-C., Neu, T.R., Wozniak, D.J., 2007. The EPS Matrix: The "house of biofilm cells." Journal Bacteriology, 189 (22), 7945–7947.

Fogler H.S. ,1999. Elements of chemical reaction engineering, 3rd Ed., Prentice-Hall, Upper Saddle River, N.J.

Gabelich, C.J., Gerringer, F.W., Lee, C.C., Knocke, W.R., 2006. Sequential Manganese Desorption and Sequestration in Anthracite Coal and Silica Sand Filter Media. Journal American Water Works Association, 98 (5), 116-127.

Gagnon, G.A., Huck, P.M., 2001. Removal of easily biodegradable organic compounds by drinking water biofilms: Analysis of kinetics and mass transfer. Water Research, 35 (10), 2554-2564.

Gantzer, P.A., Bryant, L.D., and Little, J.C., 2009. Controlling soluble iron and manganese in a water-supply reservoir using hypolimnetic oxygenation. Water Research, 43 (5), 1285-1294.

Geszvain, K., Butterfield, C., Davis, R.E., Madison, A.S., Lee, S-W., Parker, D.L., Soldatova, A., Spiro, T.G., Luther III, G.W., Tebo, B.M., 2012. The molecular biogeochemistry of manganese(II) oxidation. Biochemical Society Transactions, 40, part 6, 1244-1248.

Ghernaout, D., Ghernaout, B., Wahib, M.N. 2011. Embodying the chemical water treatment in the green chemistry - A review. Desalination, 271 (1-3), 1-10.

Ghiorse, W.C., Hirsch, P., 1979. Ultrastructural-Study of Iron and Manganese Deposition Associated With Extracellular Polymers of *Pedomicrobium*-Like Budding Bacteria. Archives of Microbiology, 123 (3), 213-226.

Goodman, M.F., Keener, S., Guidotti, S., Branscomb, E.W., 1983. On the enzymatic basis for mutagenesis by manganese. Journal Biological Chemistry, 258 (6), 3469-3475.

Gorisch, H., Rupp, M., 1989. Quinoprotein ethanol dehydrogenase from *Pseudomonas*. Antonie Van Leeuwenhoek, 56 (1), 35-45.

Gounot, A.M., 1994. Microbial Oxidation and Reduction of Manganese: Consequences in Groundwater and Applications. FEMS Microbiology Reviews, 14 (4), 39-350.

Grady, C.P.L Jr., Smets, B.F., Barbeau, D.S., 1996. Variability in kinetic parameter estimates: A review of possible causes and a proposed terminology. Water Research, 30 (3), 742-748.

Grasso, D., Chin, Y-P., Weber, W.J. Jr., 1990. Structural and Behavioral Characteristics of a Commercial Humic Acid and Natural Dissolved Aquatic Organic Matter, Chemosphere, 21 (10-11), 1181-1197.

Guggenberger, G., Kaiser, K., 2003. Dissolved organic matter in soil: challenging the paradigm of sorptive preservation. Geoderma, 113 (3-4), 293-310.

Gu, B.H., Schmitt, J.,Chen, Z.H., Liang, L.Y. McCarthy, J.F., 1994. Adsorption and Desorption of Natural Organic-Matter on Iron-Oxide-Mechanisms and Models. Environmental Science and Technology, 28 (1) 38-46.

Gu, B.H., Schmitt, J., Chen, Z.H., Liang, L.Y. , McCarthy, J.F., 1995. Adsorption and Desorption of Different Organic-Matter Fractions on Iron-Oxide. Geochimica et Cosmochimica Acta, 59 (2), 219-229.

Hastings D., Emerson S. 1986. Oxidation of manganese by spores of a marine Bacillus: kinetic and thermodynamic considerations. Geochimica et Cosmochimica Acta, 50 (8) 1819–1824.

Hem, John D. Study and Interpretation of the Chemical Characteristics of Natural Water, 3rd ed. Alexandria, VA: Department of the Interior, U.S. Geological Survey, Water-Supply Paper 2254,1985.

Hodge, J.E., Hofreiter, B.T., 1962. Determination of reducing sugars and carbohydrates. In: Methods in Carbohydrate Chemistry 1, Vol. 1, 380-394. R.L. Whistler, M.L. Wolfrom, eds. Academic Press, London.

Hope, C.K., Bott, T.R., 2004. Laboratory Modelling of Manganese Biofiltration using Biofilms of *Leptothrix discophora*. Water Research, 38 (7), 1853-1861.

Hutchinson, D.H., Robinson, C.W., 1988. Kinetics of the simultaneous batch degradation of p-cresol and phenol by *Pseudomonas putida*. Applied Microbiology Biotechnology, 29 (6), 599–604.

Jennings, P.A., 1975. A mathematical model for biological activity in expanded bed adsorption columns. Ph.D Thesis. University of Illinois, Urbana, IL.

Jensen, J.N., 2001. Approach to steady state in completely mixed flow reactors. Journal Environmental Engineering- American Society Civil Engineers, 127 (1), 13-18.

Johnson, A.H., Stokes, J.L., 1966. Manganese Oxidation by *Sphaerotilus discophorus*. Journal of Bacteriology, 91 (4),1543-1547.

Jung, W.K., Schweisfurth, R., 1976. Manganoxydierende Bacterien III. Wachstum und Manganoxydation bei *Pseudomonas manganoxidans*. Zeitshrift fur Allgemeine Mikrobiologie, 16 (8), 587–597.

Jung, W. K., Schweisfurth, R., 1979. Manganese oxidation by an intracellular protein of a *Pseudomonas* species. Zeitschrift fur Allgemeine Mikrobiologie, 19 (2), 107-115

Katsoyiannis, I.A., Zouboulis, A.I., 2004. Biological Treatment of Mn(II) and Fe(II) Containing Groundwater: Kinetic Considerations and Product Characterization. Water Research, 38 (7), 1922–1932.

Kepkay P., Nealson, K.H., 1987. Growth of a Manganese Oxidizing Pseudomonas sp. in Continuous Culture. Archives of Microbiology, 148 (1), 63–67.

Kieber, D.J., McDaniel, J., Mopper, K., 1989. Photochemical Source of Biological Substrates in Sea-Water-Implications For Carbon Cycling. Nature, 341, 6243, 637-639.

Kim, J.I., Buckau, G., L.I., G.H., Duschner, H., Psarros, N., 1990. Characterization of Humic and Fulvic Acids From Gorleben Groundwater. Fresenius Journal of Analytical Chemistry, 338 (3), 245-252.

Kjelleberg, S., Humphrey, B.A., Marshall, K.C., 1983. Initial Phases of Starvation and Activity of Bacteria at Surfaces. Applied and Environmental Microbiology, 46 (5), 978-984.

Knightes, C.D., Peters, C.A., 2000. Statistical analysis of nonlinear parameter estimation for Monod biodegradation kinetics using bivariate data. Biotechnology and Bioengineering, 69 (2), 160-170.

Kohl, P.M., Medlar, S.J., 2006. Occurrence of Manganese in Drinking Water and Manganese Control. American Water Research Foundation and U.S. EPA.

Kohl, P.M., Dixon, D., 2012. Occurrence, Impacts, and Removal of Manganese in Biofiltration Processes. American Water Research Foundation, Denver, CO.

Korth, A., Bedinger, B., Czekalla, C., Wichmann, K., 2002. Biodegradation of NOM in rapid sand filter for removing iron and manganese. Acta Hydrochimica Et Hydrobiologica, 29 (5), 289-295.

Kovarova-Kovar, K., Egli, T., 1998. Microbiology and Molecular Biology Reviews, 62 (3), 646-666.

Krull, E.S., Baldock, J.A., Skjemstad, J.O., 2003. Importance of mechanisms and processes of the stabilisation of soil organic matter for modelling carbon turnover. Functional Plant Biology, 30 (2), 207-222.

Krumbein, W. E., H. J. Altmann. 1973. A new method for the detection and enumeration of manganese oxidizing and reducing microorganisms. Helgolander Wissenschaftliche Meeresuntersuchungen , 25 (2-3) 347-356.

Larsen, E.I., Sly, L.I., McEwan A.G., 1999. Manganese(II) Adsorption and Oxidation by Whole Cells and a Membrane Fraction of *Pedomicrobium* sp. ACM 3067, Archives of Microbiology, 171 (4), 257-264.

Leenheer, J. A., Brown, P. A., Noyes, T. I. In Aquatic Humic Substances: Influence on Fate and Treatment of Pollutants, Suffet, I. H., MacCarthy, P., Eds., Advances in Chemistry Series 219, American Chemical Society: Washington, DC, 1989; pp 25-39.

Leenheer, J. A., Rostad, C.E., Gates, P.M., Furlong, F.T., Ferrer, I., 2001. Molecular Resolution and Fragmentation of Fulvic Acid by Electrospray Ionization/Multistage Tandem Mass Spectrometry. Analytical Chemistry, 73 (7), 1461-1471.

Li, D., Zhang, J., Wang, H., Yang, H., Wang, B., 2005. Operational Performance of a Biological Treatment for Iron and Manganese Removal. Journal of Water Supply: Research and Technology, 54 (1), 15-24.

Liao, W., Christman, R.F., Johnson, J.D., Millington, D.S., Hass, J.R., 1982. Structural Characterization of Aquatic Humic Material. Environmental Science and Technology, 16 (7), 403-410.

Levenspiel, O., Chemical Reaction Engineering, 3$^{rd}$ Ed., Wiley, New York, 688, 1998.

Livingston, A.G., Chase, H.A. 1989. Modeling phenol degradation in a fluidized- bed reactor. American Institute of Chemical Engineers Journal, 35 (12), 1980-1992.

Longsworth, L.G., 1972. Diffusion in Liquids. In Gray, D.W. (ed.), American Institute of Physics Handbook, McGraw-Hill Book Company, New York, NY

Liu , C.X., Zachara, J.M., 2001. Uncertainties of Monod Kinetic parameters nonlinearly estimated from batch experiments, Environmental Science and Technology, 35 (1), 133-141.

Luther, III, G. W. 2005. Manganese(II) oxidation and Mn(IV) reduction in the environment—two one-electron transfer steps versus a single two-electron step. Geomicrobiology Journal, 22 (3-4), 195-203.

MacCarthy, P., 2001. The principles of humic substances. Soil Science, 166 (11), 738-751.

Martin, S.T. Precipitation and Dissolution of Iron and Manganese Oxides: In Environmental Catalysis, ed. V.H. Grassian, 61-82. Boca Raton, FL: CRC Press, 2005.

Marquardt, D., 1963. An Algorithm for Least-Squares Estimation of Nonlinear Parameters. Journal of the Society for Industrial and Applied Mathematics, 11 (2), 431–441.

Maximov, O.B., Shvets, T.V., and Elkin, Y.N., 1977. Permanganate Oxidation of Humic Acids, Geoderma, 19 (1), 63-78.

Monod, J., 1949. The Growth of Bacterial Cultures. Annual Review of Microbiology, 3, 371-394.

Morgan, J.J., Stumm, W., 1964. Journal Colloid Science, 19 (4), 347-359.

Morgan, J.J., 2000. Manganese in natural waters and earth's crust: Its availability to organisms. In Metal Ions in Biological Systems (ed. A. Sigel and H. Sigel), Vol. 37, pp. 1-34, Marcel Dekker USA.

Morgan, J.J., 2005. Kinetics of reaction between $O_2$ and Mn(II) species in aqueous solutions. Geochimica et Cosmochimica Acta, 69 (1), 35-48.

Moran, M.A., Hodson, R.E., 1990. Bacterial production on humic and nonhumic components of dissolved organic carbon. Limnology and Oceanography, 35 (8), 1744-1756.

Morimatsu, K., Eguchi, K., Hamanaka, D., Tanaka, F., Uchino, T., 2012. Effects of Temperature and Nutrient Conditions on Biofilm Formation of *Pseudomonas putida*. Food Science and Technology Research, 18(6), 879-883.

Mouchet, P.C., 1992. From Conventional to Biological Removal of Iron and Manganese in France. Journal American Water Works Association, 84 (4), 158-167.

Murdoch,F., Smith, P.G., 2000. The interaction of a manganese-oxidising bacterium as part of a biofilm growing distribution pipe materials. Water Science and Technology, 41 (4-5), 295-300.

Nealson, K.H., Tebo, B.M. 1980. Surface Enhancement of Bacterial Manganese Oxidation – Implications for Aquatic Environments. Geomicrobiology Journal, 2 (1), 21-37.

Nealson, K.H, Tebo, B.M., Rosson, R.A. 1988. Occurrence and Mechanisms of Microbial Oxidation of Manganese. In Advances in Applied Microbiology, 33, 279-318, Academic Press.

Murray, J.W., Balistrieri, L.S., Paul, B., 1984. The Oxidation State of Manganese in Marine Sediments and Ferromanganese Nodules. Geochimica et Cosmochimica Acta, 48 (6), 1237-1247.

Nealson, K.H., The Manganese-Oxidizing Bacteria, Vol. 1, Part 1, Ch. 3.1.10 in Prokaryotes, 5, 222-231, Springer, 2005.

Nelson Y. M., Lion L. W., Shuler, M. L., Ghiorse W. C., 2002. Effect of oxide formation mechanisms on lead adsorption by biogenic manganese (hydr)oxides, iron (hydr)oxides, and their mixtures. Environmental Science and Technology, 36 (3), 421–425.

Niederer, C., Schwarzenbach, R.P., Goss, K.U., 2007. Elucidating differences in the sorption properties of 10 humic and fulvic acids for polar and nonpolar organic chemicals. Environmental Science and Technology, 41 (19), 6711-6717.

Nguyen, V.T., Shieh, W.K., 1995. Evaluation of intrinsic and inhibition kinetics in biological fluidized bed reactors. Water Research, 29 (11), 2520-2524.

Okazaki, M., Sugita, T.,Shimizu, M., Ohode, Y., Iwamoto, K., De Vrind-De Jong, E.W., De Vrind, J.P.M., Corstjens, P.L.A.M., 1997. Partial Purification and Characterization of Manganese-Oxidizing Factors of *Pseudomonas fluorescens* GB-1. Applied and Environmental Microbiology, 63 (12), 4793-4799.

O'Reilly, S.E., Hochella, M.F., 2003. Lead sorption efficiencies of natural and synthetic Mn and Fe-oxides. Geochimica et Cosmochimica Acta, 67 (23), 4471-4487.

Pacini, V.A., Ingallinella, A.M., and Sanguinetti, G., 2005. Removal and Iron and Manganese using Biological Roughing Flow Filtration Technology. Water Research, 39 (18), 4463-4475.

Paillard, H., Legube, B., Bourbigot, M.M., Lefebvre, E., 1989. Iron and Manganese Removal with Ozonation in the Presence of Humic Substances. Ozone Science & Technology, 11 (1), 93-114.

Parikh, S.J., Chorover, J., 2005. FTIR Spectoscopic Study of Biogenic Mn-Oxide Formation by *Pseudomonas putida* GB-1. Geomicrobiology Journal, 22 (5), 207-218.

Reardon, K.F., Mosteller, D.C., Rogers, J.D.B., 2000. Biodegradation kinetics of benzene, toluene, and phenol as single and mixed substrates for *Pseudomonas putida* F1. Biotechnology and Bioengineering, 69 (4), 385-400.

Riefler, G.R., Ahlfeld, D.P., Smets, B.F. 1998. Respirometric Assay for Biofilm kinetics Estimation: Parameter Identifiability and Retrievability. Biotechnology and Bioengineering, 57 (1), 35-45.

Robinson, J.A., 1985. Determining microbial kinetic parameters using non-linear regression analysis. Advances in Microbial Ecology, 8, 61-114.

Robinson, J.A., Tiedje, J.M., 1983. Nonlinear Estimation of Monod growth Kinetic Parameters from a Single Substrate Depletion Curve. Applied Environmental Microbiology, 45 (5), 1453-1458.

Van Raij, B., Peech, M., 1972. Electrochemical properties of some Oxisols and Alfisols of the tropics. Soil Science Society American Proceedings, 36, 587-593.

Rittmann, B.E., Crawford, L., Tuck, C.K., Namkung, E., 1986. In situ determination of kinetic parameters for biofilms: Isolation and characterization of oligotrophic biofilms. Biotechnology and Bioengineering, 28 (11), 1753-1760.

Rittmann, B.E., McCarty, P.L. 1980b. Evaluation of steady-state biofilm kinetics. Biotechnology and Bioengineering, 22 (11), 2359-2373.

Rittmann, B.E., 1990. Analyzing biofilm processes in biological filtration. Journal American Water Works Association, 82 (12), 62-66.

Rittmann, B.E., McCarty, P.L., 2001. Environmental Biotechnology: Principles and Application. McGraw-Hill, New York.

Routt, J.C., 2004. Lowering DBPs in Combined Systems. Opflow, American Water Works Association, 30 (4), April.

Ruegg, I., Hafner, T., Bucheli-Witschel, M., Egli, T., 2007. Dynamics of benzene and toluene degradation in *Pseudomonas putida* F1 in the presence of the alternative substrate succinate. Engineering in Life Sciences, 7 (4), 331-342, July.

Ruggiero, P., Interesse, F.S., Cassidei, L., Sciacovelli, O., 1980. ¹H NMR spectra of humic and fulvic acids and their peracetic oxidation products, Geochimica et Cosmochimica Acta, 44 (4), 603-609.

Santelli, C.M., Pfister, D.H., Lazarus, D., Sun, L., Burgos, W.D., Hansel, C.M., 2012. Promotion of Mn(II) oxidation and Remediation of Coal Mine Drainage in Passive Treatment Systems by Diverse Fungal and Bacterial Communities. Applied and Environmental Microbiology, 76 (14), 4871-4875.

Saez, P.B., Rittmann, B.E., 1992. Accurate Pseudoanalytical Solution for Steady-State Biofilms. Biotechnology and Bioengineering, 39 (7), 790-793.

Saratovsky. I., Wightman, P.G., Pasten, P.A., Gaillard, J.F, Poeppelmeier, K.R., 2006. Manganese Oxides: Parallels between Abiotic and Biotic Structures. Journal of the American Chemical Society, 128 (34), 11188-11198.

Schnoor, J.L., 1996. Environmental modeling: Fate and transport of pollutants in water, air and soil. New York: John Wiley & Sons.

Schweisfurth, R., 1973. Manganoxydierende Bacterien I. Isolierung und Bestimmung einiger Stamme von Manganbakterien. Zeitshrift fur Allg Mikrobiol., 13, 341–347.

Schlegel, H.G., Bowien, B., 1989. Autotrophic Bacteria, Science Tech Publishers, Madison, Wisconsin, 528 pp.

Schnitzer, M. 1978. Some Observations on Chemistry of Humic Substances, Agrochmica, 22 (3-4), 216-225.

Sehlin, H.M., Lindstrom, E.B., 1992. Oxidation and Reduction of Arsenic by *Sulfolobus-Acidocaldarius* Strain BC. FEMS Microbiology Letters, 93 (1), 87-92.

Shin, H.S., Lim, K.H., 1996. Spectroscopic and elemental Investigation of Microbial Decomposition of Aquatic Fulvic Acid in Biological Process of Drinking Water Treatment. Biodegradation, 7 (4), 287-295.

Shin, H.S., Monsallier, J.M., Choppin, G.R., 1999. Spectroscopic and Chemical Characterization of Molecular Size Fractionated Humic Acid, Talanta, 50 (3), 641-647.

Simkins, S., Alexander, M., 1984. Models for Mineralization Kinetics With The Variables of Substrate Concentration and Population Density. Applied and Environmental Microbiology, 47 (6), 1299-1306.

Singer, P.C., Reckhow, D.A., 2010. Chapter 7, Chemical Oxidation, Water Quality and Treatment: A Handbook of Community Water Supplies, 6th Ed. Edited by James Edzwalk, McGraw-Hill, Inc., New York, NY, 1696 p.

Sly, L.I., Arunpairojana,V., Dixon, D.R., 1993. Biological Removal of Manganese from Water by Immobilized Manganese-Oxidising Bacteria, Water: Journal Australian Water Association, 20 (3), 38-40.

Smets, B.F., Riefler, R.G., Lendenmann, U., Spain, J.C. 1999. Kinetic Analysis of Simultaneous 2, 4-Dinitrotoluene (DNT) and 2, 6-DNT Biodegradation in an Aerobic Fluidized-Bed Biofilm Reactor. Biotechnology and Bioengineering, 63 (6) 642-653.

Soldatova, A.V., Butterfield, C., Oyerinde, O.F., Tebo, B.M., Spiro, T.G., 2012. Multicopper oxidase involvement in both Mn(II) and Mn(III) oxidation during bacterial formation of $MnO_2$. Journal Biological Inorganic Chemistry, 17 (8), 1151-1158.

Sonnenberg, L.B., Johnson, J.D., Christman, R.F. Chemical Degradation of Humic Substances for Structural Characterization, ACS Symposium Series, 219, 3-23.

Spiro, T.G., Bargar, J.R., Sposito, G., Tebo, B.M., 2010. Bacteriogenic Manganese Oxides. Accounts of Chemical Research, 43 (1), 2-9.

Sposito, G. The Surface Chemistry of Soils, Oxford University Press: New York, 1984.

Stone, A.T., Morgan, J.J., 1984. Reduction and Dissolution of Manganese (III) and Manganese (IV) oxides by Organics. Environmental Science and Technology, 18 (6), 450-456.

Stone, A.T., 1987. Reductive Dissolution of Mn(III/IV) Oxides by Substituted Phenols. Environmental Science and Technology, 21 (10), 979-988.

Stumm, W., Morgan, J.J, 1996. Aquatic Chemistry, 3rd Ed., John Wiley & Sons, Inc. 252-424.

Sunda, G.W., Kieber, D.J., 1994. Oxidation of Humic Substances by Manganese Oxides Yields Low-Molecular-Weight Organic Subtrates. Nature, 367, 62-64.

Suttigarn, A., Wang, Y. T., 2005. Arsenite Oxidation by *A. faecalis* O1201. Journal Environmental Engineering, American Society of Civil Engineers, 131 (9), 1293-1301.

Suzuki, T., 1976. Purification and some properties of polyvinyl alcohol-degrading enzyme produced by *Pseudomonas* O-3. Agricultural and Biological Chemistry, 40 (3), 497–504.

Swift, R.S. 1996. Organic matter characterization (chap 35). pp. 1018-1020. In D.L. Sparks et al. (eds) Methods of soil analysis. Part 3. Chemical methods. Soil Science Society of American Book Series: 5. Soil Science Society of America, Madison, WI.

Tan, L., Amy, G.L., 1991. Comparing ozonation and membrane separation for color removal and disinfection by-product control. Journal American Water Works Association, 83 (5), 74-79.

Lo, T., Sudak, R.G, 1992. Removing Color From a Groundwater Source. Journal American Water Works Association, 84 (1), 1–79.

Tebo, B. M., He, L. M., 1999. Microbially Mediated Oxidative Precipitation Reactions. In Mineral-Water Interfacial Reactions Kinetics and Mechanisms (eds. D. L. Sparks and T. J. Grundl), Chap. 20, pp. 393–414. American Chemical Society, Washington, D.C.

Tebo, B. M., Bargar, J.R., Clement, B.G., Dick, G.J., Murray, K.J., Parker, D., Verity, R., Webb, S.M., 2004. Biogenic Manganese Oxides: Properties and mechanisms of Formation. Annual Review of Earth and Planetary Sciences, 32, 287-328.

Tebo, B.M., Edwards, D.B., Sunda, W.G., Kieber, D.J., 1995. Bacterial Manganese Oxidation Leads to the Degradation and Utilization of Natural Organic Matter. Abstract Paper American Chemical Society 209:77 (GEOC).

Tebo, B.M., Johnson, H.A., McCarthy, J.K., Templeton, A.S., 2005. Geomicrobiology of Manganese (II) Oxidation. Trends in Microbiology, 13 (9), 421-428.

Tipping, E., 1981. The Adsorption of aquatic humic substances by iron-oxides. Geochimica et Cosmochimica Acta, 45 (2), 191-199.

Tipping, E., Heaton, M.J., 1983. The adsorption of aquatic humic substances by two oxides of manganese. Geochimica et Cosmochimica Acta, 47 (8), 1393-1397.

Tipping, E., 1984. Temperature-Dependence of Mn(II) Oxidation in Lakewaters – A Test of Biological Involvement. Geochimica et Cosmochimica Acta, 48 (6), 1353-1356.

Toyama, H., Fujii, A., Matsushita, K., Shinagawa, E., Ameyama, M., Adachi, O.3 Distinct Quinoprotein Alcohol Dehydrogenases are Expressed when *Pseudomonas Putida* is Grown on Different Alcohols, Journal of Bacteriology, 177 (9), 2442-2450.

United States Environmental Protection Agency, 1979. National Primary and Secondary Drinking Water Regulations. Final Rule, Federal Register.

United States Environmental Protection Agency, 1998. National Interim Primary Drinking Regulation; Disinfectants and Disinfection By-products Rule. Final Rule Federal Register, United States Government Printing Office, Washington D.C., pp. 69390-69476.

United States Environmental Protection Agency, 2004. Drinking Water Health Advisory for Manganese, U.S. Environmental Protection Agency, Office of Water, Health and Ecological Criteria Division, EPA-822-R-04-003, Washington, DC.

Van Loosdrecht, M.C.M., Lyklema, J., Norde, W., Zehnder, A.J.B., 1990. Influence of interfaces on microbial activity. Microbiology Review, 54 (1), 75-87.

Vermeer, A.W.P., Koopal, L.K., 1998. Adsorption of humic acids to mineral particles. 2. Polydispersity effects with polyelectrolyte adsorption. Langmuir, 14 (15), 4210-4216.

Villalobos, M., Toner, B., Bargar, J., Sposito, G., 2003. Characterization of the Manganese Oxide Produced by *Pseudomonas putida* Strain MnB1. Geochimica et Cosmochimica Acta, 67 (14), 2649-2662.

Waite, T.D., Wrigley, I.C., Szymczak, R., 1988. Photoassisted Dissolution of a Colloidal Manganese Oxide in the Presence of Fulvic Acid. Environmental Science and Technology, 22 (7), 778-785.

Wang, Y. T., Suidan, M. T., Rittmann B. E., 1986. Anaerobic Treatment of Phenol by an Expanded-Bed Anaerobic Reactor. Journal Water Pollution: Control Federation, 58, 227-233.

Wang, Y. T., Suidan, M. T., Rittmann, B. E., 1987. Modeling Biofilm Kinetics for a Low-Loaded Expanded-Bed Anaerobic Reactor. Biotechnology and Bioengineering, 30 (1), 15-21.

Wang, Y.T., Shen, H., 1997. Modeling Cr(VI) Reduction by Pure Bacterial Cultures. Water Research, 31 (4) 727-732.

Wang, Y. T., Suttigarn, A., Dastidar, A., 2009. Arsenite Oxidation by Immobilized Cells of *Alcaligenes faecalis* Strain O1201 in a Fluidized-Bed Reactor. Water Environment Research, 81 (2), 173-177.

Watnick, P.I., Kolter, R., 2000. Biofilm, City of Microbes. Journal of Bacteriology, 182 (10), 2675-2679.

Wilczak A., Knocke, W.R., Hubel, R.E., Aieta, E.M., 1993. Manganese Control During Ozonation of Water Containing Organic-Compounds. Journal of the American Water Works Association, 85 (10), 98-104.

Williamson, K.J., McCarty, P.L., 1976. Verification studies of the biofilm model for bacterial substrate utilization. Journal Water Pollution: Control Federation, 48, 281-289.

Wilson, M.A., Collin, P.J., Malcolm, R.L., Perdue, E.M., Cresswell, P., 1988. Low molecular weight species in humic and fulvic fractions. Organic Geochemistry, 12 (1), 7-12.

Woolschlager, J., Rittman, B.E., 1995. Evaluating what is measured by BDOC and AOC tests. Revue Science de l'Eau 8, pp. 372-385.

World Health Organization, 1971. International Standards for Drinking-Water. 3rd Edition. Geneva.

World Health Organization, 1998. Guidelines for Drinking Water Quality. Geneva, Switzerland.

Yang, H., Li, D., Zhang, J., Hao, R., Li, B., 2004. Design of Biological Filter for Iron and Manganese Removal. Journal of Environmental Science and Health / Part A – Toxic/Hazardous Substances & Environmental Engineering, 39 (6), 1447-1454.

Zhang, J., Lion, L.W., Nelson, Y.M., Shuler, M.L., Ghiorse, W.C., 2001. Kinetics of reaction between $O_2$ and Mn(II) species in aqueous solutions. Geochimica et Cosmochimica Acta, 65 (5), 773-781.

Zhang, S., Huck, P.M., 1996. Parameter estimation for biofilm processes in biological water treatment. Water Research, 30 (2), 456-464.

Zhdanov, A. V., Dubinina, G. A., 1975. *Arthrobacter iderocapsulatus* isolated from lake water. Microbiology, 44 (4), 644-649.

Zhu, I.X., Getting, T., Bruce, D., 2010. Review of biologically active filters in drinking water applications. Journal of American Water Works Association, 102 (12), 67-77.

# VITA

1. Former Project Engineer/Scientist at Nesbitt Engineering, Inc.
2. Current Professional Engineer (KY), License #24239
3. BS, Western Kentucky University; BS, MS, University of Kentucky
4. Michael S. Snyder